Vanadium-Catalyzed Aerobic Oxidation of Diols and Lignin Models/Extracts

by

Christian Díaz-Urrutia

Thesis submitted to the
Faculty of Graduate and Postdoctoral Studies
In partial fulfillment of the requirements for the degree of
Doctor of Philosophy, Chemistry

Center for Catalysis Research and Innovation
Department of Chemistry and Biomolecular Sciences, University of Ottawa

Abstract

As the world moves forward to the development of biorefineries, the interest to replace chemicals and materials derived from petroleum is increasing exponentially. Lignin is a macromolecular by-product derived from the wood pulping industry, mainly used for heating purposes. The development of new processes to produce high value-added lignin products such as multifunctional aromatic chemicals and high-tech carbon materials are required to fulfill the needs for biorenewable feedstocks. Such processes are likely to include selective oxidation catalysis.

The aim of this *Thesis* is to advance the *state-of-the-art* for the oxidation of lignin models and lignin extracts using homogeneous catalysts based on vanadium, an inexpensive and abundant transition metal, using air as the only oxidant. Lignin models containing the most important features of lignin (*e.g.*, β-O-4 and β-1 linkages) were initially used to assess the catalytic potential. Previously reported $(HQ)_2V(O)(O^iPr)$ and (dipic)V(O)(O^iPr) catalysts (dipic = dipicolinate and HQ = 8-oxyquinoline) displayed different selectivity for C-H, C-O and C-C bond cleavage upon varying of the solvent, the lignin model or the catalyst. Moreover, these catalysts cleave the C-H bond of secondary alcohols through a two-electron oxidation process and the C-C bond cleavage of the oxidation product ketone in the presence of exogenous base.

Several amine bis(phenolate) oxovanadium(V) catalysts were synthesized and fully characterized, and demonstrated very good activity for the oxidation of lignin models and the depolymerization of organosolv lignin. These new catalysts overcome the need for added base, display higher reaction rates of oxidation, and improve the selectivity for the disassembly of lignin models. The different selectivities involving C-H *vs.* C-O *vs.* C-C bond cleavage are discussed together with a novel redox-neutral C-C bond cleavage of lignin model 1,2-diphenyl-2-methoxyethanol.

The oxovanadium(V) catalysts, along with a metal-free variant and other transition metal catalysts, were employed to assess their performance for the oxidation and depolymerization of organosolv lignin. Although most catalysts oxidized the lignin extracts, the oxovanadium(V) complexes demonstrated the highest degree of lignin depolymerization as shown by Gel Permeation Chromatography (GPC), quantitative-

Heteronuclear Single Quantum Correlation (q-HSQC) and quantitative ^{31}P NMR spectroscopy of derived phosphite esters.

In a complementary study, oxovanadium(V) catalysts also established their utility for the valorization of cellulose-derived substrates (*e.g.*, diols). Two trialkoxyamine oxovanadium(V) complexes bearing a triethoxyamine and tris[2-(3,5-di-*tert*-butyl-phenoxy)methyl]amine ligand respectively, selectively cleaved the C-C bond in 1,2-diols with excellent rates and using air as the only oxidant. In a stoichiometric investigation of this reaction, it was determined that the transformation proceeds through an unusual direct oxidative two-electron cleavage of diols, affording a non-oxo monometallic V(III) intermediate. DFT calculations support a single-site proton-coupled electron-transfer of the hydroxyl hydrogen to the V oxo orbital.

In summary, this *Thesis* describes new developments in vanadium catalysis such as mechanistic implications and catalyst optimization for the valorization of lignocellulosic biomass utilizing air as an oxidant.

Acknowledgements

I am going to be cliché in this first sentence: Professor Tom Baker's support towards independent thinking and freedom to challenge any possible ideas was fundamental to me in order to create a rich and diverse research environment. Of course, the saying 'work hard, play hard' was redefined by Baker together with my appreciation for *Hawaiian* shirts. I am looking forward to applying these same principles of work and fun in my entire career. Thank you very much Baker for having me in your group and for all your support along the way.

I will miss the countless chemistry discussions, periodical professional visits to *La Maison*, and many other adventures with all the Baker Group and some outsiders, especially Steve Maguire, Nicole Hunter, Graham Lee, Mehdi Mostajeran, Hassan Kalviri, Nick Andrella and Alex Sicard. Thank you Jenny Daccache for the great job performed at the lab during the last two years. Although, there are two people that deserve an honorable mention: Uttam Das and Kaitie Giffin. Correcting papers and scholarship applications, and endless advice are a few examples of their amazing support. Uttam, I am glad we shared the office space and the lab during three years and became very good friends. I hope to continue working with you in many other plans in the near future. Kaitie, I cannot describe in this page how happy you make me feel inside and outside the lab, *thank you.*

I would like to express my tremendous gratitude to my family for all their support and to withstand all my absences from birthdays, graduations and some holidays, and especially to my brothers Sebastián and Fabián.

I want to especially give thanks to Tito Scaiano for his tremendous support in helping me come to Ottawa for the first time and for welcoming me in his research lab in 2010. Thank you also to Eric Ye and Glenn Facey for the excellent assistance with the NMR facilities, Charles-Oneil Crites for the GPC, Veroniqué Chen for 2D NMR, Roxanne Clément for the high throughput experiments, Ammar Saleem for HPLC-MS and Baburam Sedai for Copper catalysts. I would like to particularly acknowledge Susan Hanson for introducing me to the oxovanadium chemistry. Thanks to Alexandre Martinez who hosted me in his lab at ENS Lyon, and Dawei Zhang for his hospitality and help. Likewise to Carine Michel and Paul Fleurat-Lessard for their enormous help in improving my papers with their meticulous DFT work.

Table of Contents

Abbreviations

Ac Acetyl, -C(O)CH_3

atm Atmosphere (1 atm = 14.7 psi)

Ar Aryl

Bn Benzyl, -CH_2Ph

ca. *circa*, approximately

Cat. Catalyst

Conv. Conversion

cf. Compare

DAD Diode array detector

Deg Degrees (^{o})

DEPT Distortionless enhancement by polarization transfer

DIBALH Diisobutylaluminium hydride, $C_{16}H_{38}Al_2$

DIPA Diisopropylamine, $C_6H_{15}N$

Dipic dipicolinic acid

DFT Density functional theory

DME 1,2-Dimethoxyethane

DMF Dimethylformamide, $(CH_3)_2NCOH$

DMSO Dimethylsulfoxide, $(CH_3)_2SO$

ESI Electrospray Ionization

Equiv. Equivalents

Et Ethyl, -C_2H_5

FT Fourier transform

GC-FID Gas chromatography flame ionization detection

GC-MS Gas chromatography mass spectrometry

GPC Gel permeation chromatography

HMQC Heteronuclear multiple-quantum coherence

q-HSQC Quantitative heteronuclear single quantum coherence

HRMS High resolution mass spectrometry

HQ 8-Hydroxyquinoline

HPLC High performance liquid chromatography

Hz Hertz (s^{-1})

i.e. It is

^{i}Pr Isopropyl, -$CH(CH_3)_2$

IR Infrared

IS Internal standard

KIE Kinetic isotope effect

Me Methyl, -CH_3

Mes Mesityl, 2,4,6-trimethylphenyl

n.d. Not detected

NEt_3 Triethylamine, $N(CH_2CH_3)_3$

NMR Nuclear magnetic resonance

OAc Acetate, CH_3CO_2-

OTf Trifluoromethanesulfonate, -OSO_2CF_3

PDI Polydispersity index

Ph Phenyl, -C_6H_5

ppm Parts per million

pyr Pyridine, C_5H_5N

^{t}Bu Tert-butyl, -CMe_3

TEMPO 2,2,6,6-Tetramethylpiperidine-1-oxyl, $(CH_2)_3(CMe_2)_2NO$

THF Tetrahydrofuran, C_4H_8O

TMS Tetramethylsilane, $SiMe_4$

TMDP 2-Chloro-4,4,5,5-tetramethyl-1,3,2-dioxaphospholane, $C_6H_{12}ClO_2P$

TOF Turnover frequency

TON Turnover number

Tol Toluene

TS Transition state

VHPOs Vanadium haloperoxidases

UHP Ultra high purity

List of Schemes

List of Tables

List of Figures

List of Compounds

Oxovanadium(V) Complexes

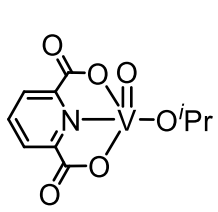

OV1

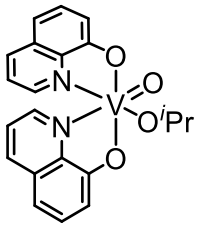

OV2

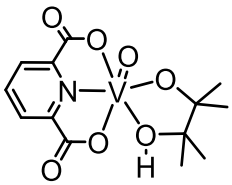

OV3

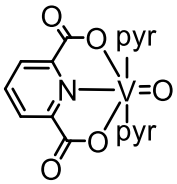

OV4

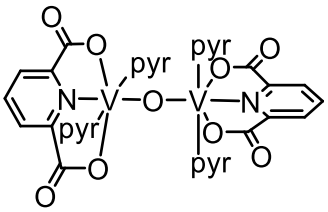

OV5

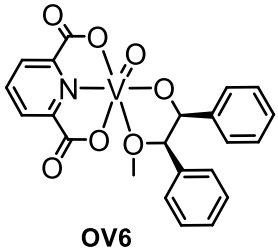

OV6

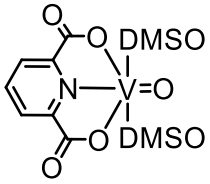

OV7

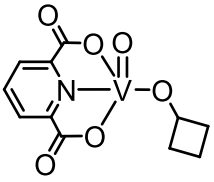

OV8

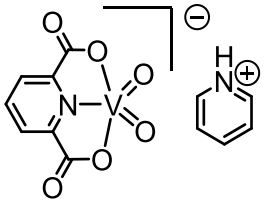

OV9

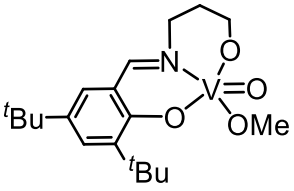

OVS

Other Homogeneous Catalysts for Disassembly of Lignin

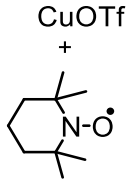

Cu*

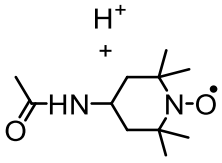

MFH

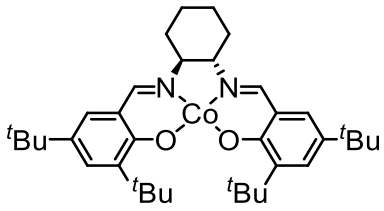

CoL

Amino Bis(phenolate)Ligands (PL) and Oxovanadium(V) Complexes (AP)

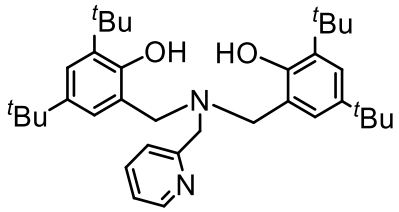

PL1

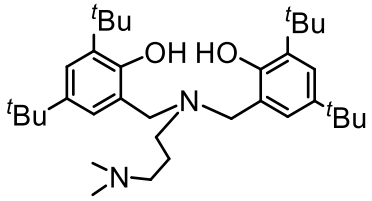

PL2

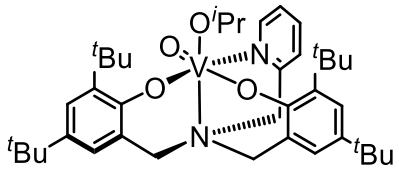

AP1

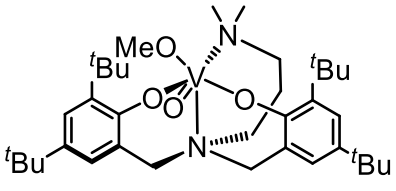

AP2

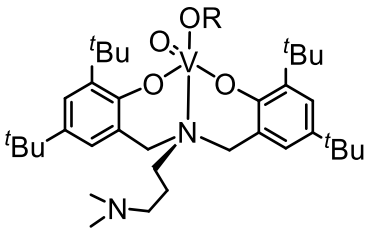

R = ^{i}Pr (**AP3**), ^{t}Bu (**AP4**), CyBu (**AP5**)

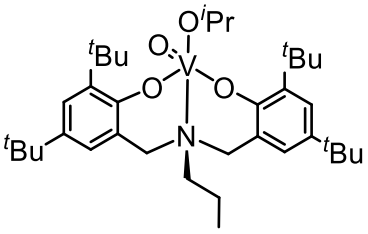

AP6

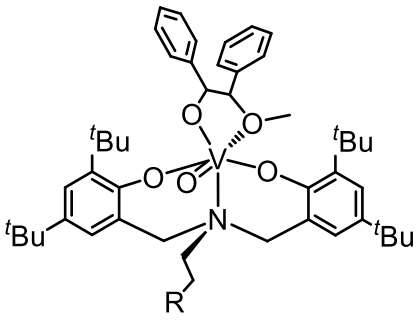

R = $CH_2N(CH_3)_2$ (**AP7**), CH_3 (**AP8**)

Trialkoxyamine and Hemicarcerand Vanadium Complexes

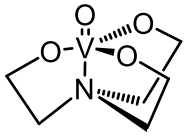

TA1

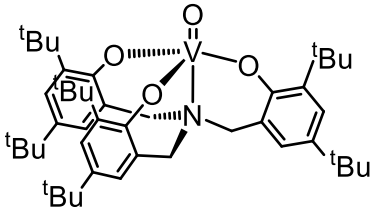

TA2

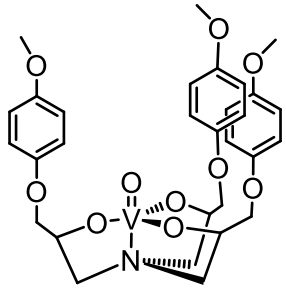

TA3

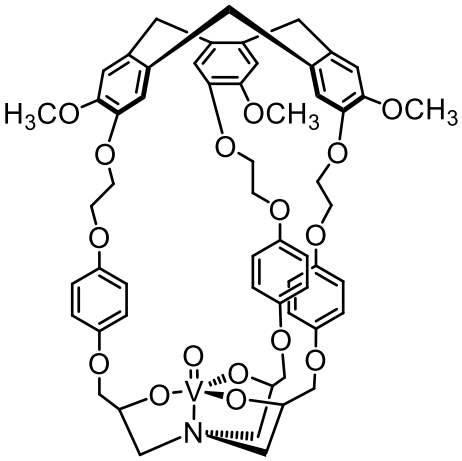

TA4

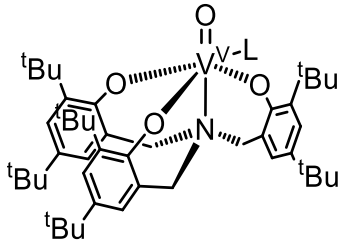

L = pyr (**TA5**), DMSO (**TA6**)

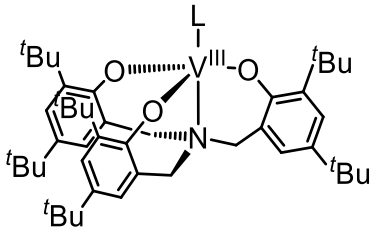

L = H_2O (**TA7**), CH_3CN (**TA8**), DME (**TA9**)

Lignin Model Compounds (LM) and Building Blocks of Lignin Models (BBLM)

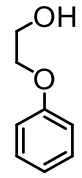

LM1

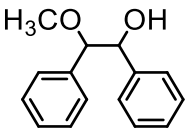

LM2

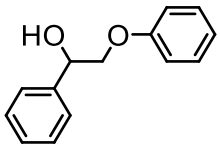

LM3

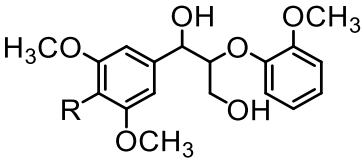

R = H (**LM4**), OH (**LM5**)

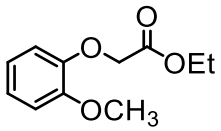

BBLM1

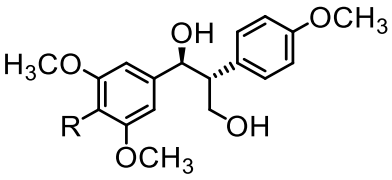

R = H (**LM6**), OH (**LM7**)

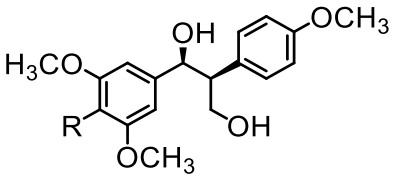

R = H (**LM8**), OH (**LM9**)

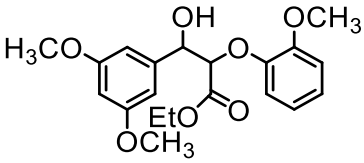

BBLM2

Cellulose Model (Polyalcohols) Compounds

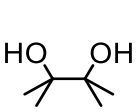

pinacol

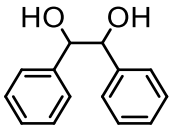

1,2-Diphenyl-1,2-ethanediol
(hydrobenzoin)

Oxidation Products of the Disassembly of Lignin Model Compounds

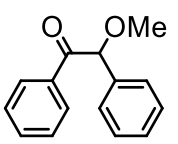

OP1

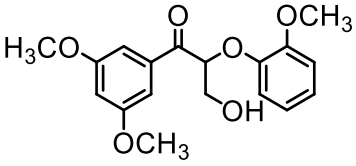

OP2

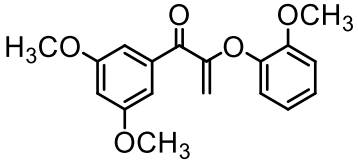

OP3

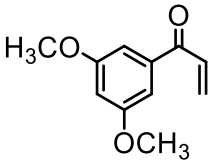

OP4

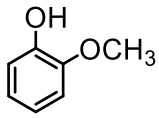

OP5

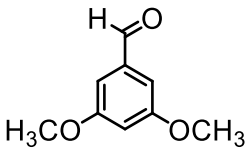

OP6

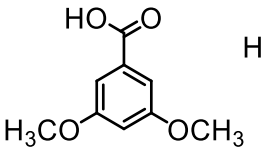

OP8

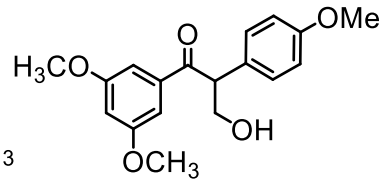

OP9

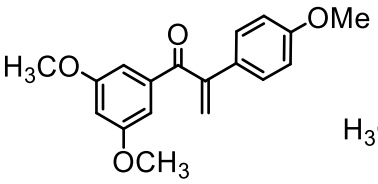

OP10

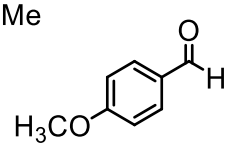

OP11

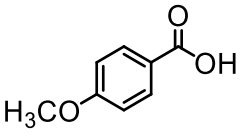

OP12

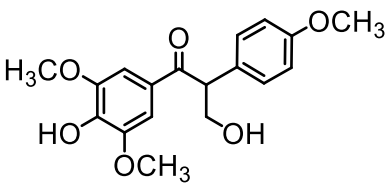

OP13

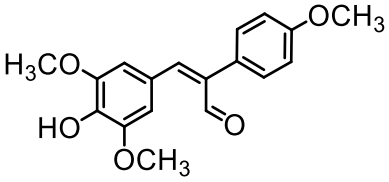

OP17

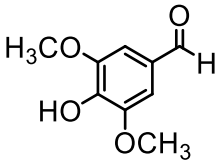

OP15

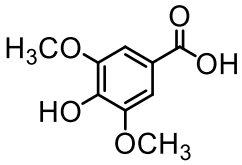

OP16

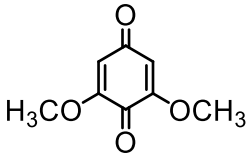

OP14

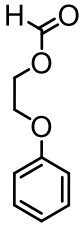

OP18

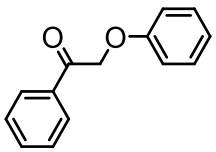

OP19

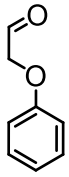

OP20

List of Contributions

Publication resulting from the chapters of this thesis:

7) **Díaz-Urrutia, C.**; Dawei Zhang, Martinez, A.; Baker, R.T. Hemicarcerand vanadium catalysts for selective C-C bond cleavage of lignin models **2016**, *manuscript in preparation*.

6) **Díaz-Urrutia, C.**; Daccache, J.; Michel, C.; Fleurat-Lessard, P.; Korobkov, I.; Baker, R.T. Highly active oxovanadium catalysts for oxidative C-C bond cleavage of lignin models and oxidation of organosolv lignin **2016**, *submitted*.

5) **Díaz-Urrutia, C.**; Michel, C.; Fleurat-Lessard, P.; I.; Korobkov, I.; Martinez, A.; Baker, R.T. Aerobic oxidative C-C bond cleavage of 1,2-diols by trialkoxyamine oxovanadium(V) catalysts: Unprecedented direct two-electron oxidation, **2016**, *submitted*.

4) **Díaz-Urrutia, C.**; Chen, W-C.; Crites, C-O.; Daccache, J.; Korobkov, I.; Baker, R. T. Towards lignin valorization: Comparing homogeneous catalysts for the aerobic oxidation and depolymerisation of organosolv lignin, *RSC Advances* **2015**, *5*, 70502–70511.

3) **Díaz-Urrutia, C.**; Sedai, B.; Leckett, K. C. Baker, R. T.; Hanson, S. K. Selective aerobic oxidation of phenoxyethanol lignin models, *ACS Sustainable Chemistry & Engineering* **2016**, *submitted*.

2) Sedai, B.; **Díaz-Urrutia, C.**; Baker, R. T.; Wu, R.; Silks, L. A.; Hanson, S. K. Aerobic oxidation of β-1 lignin model compounds with copper and oxovanadium catalysts. *ACS Catalysis* **2013**, *3*, 3111–3122.

1) Sedai, B.; **Díaz-Urrutia, C.**; Baker, R. T.; Wu, R.; Silks, L. A.; Hanson, S. K. Comparison of copper and vanadium homogeneous catalysts for aerobic oxidation of lignin models. *ACS Catalysis* **2011**, *1*, 794–804.

Publication resulting from the work not presented in this thesis:

2) Hurisso, B. B.; Ambrose, K.; **Díaz-Urrutia, C.**; Baker, R. T.; Singer, R. D. Oxidation of lignin with ionic liquid tagged VO(salen) catalyst in ionic liquids using microwave irradiation, *Green Chemistry* **2016**, *submitted*.

1) **Díaz-Urrutia, C**.; Hurriso, B. Gauthier, P. M. P. Sedai, B.; Singer, R. D.; Baker, R. T. Oxidation of lignin-derived bio-oils with oxovanadium complexes and ionic liquid catalysts, *Journal of Molecular Catalysis A: Chemical* **2016**, *423*, 414–422.

Contribution Statement

The majority of the hypothesis and the subsequent experimental work was done by me in close mentorship with Professor Baker. All the work presented in this Thesis is or is in the process of being published in six independent peer-reviewed articles with me as a first or second author. Not included in this *Thesis* is the work I did for the valorization of lignin-derived bio-oils in collaboration with Professor Robert Singer (St Mary's University, Halifax). The catalytic oxidation and the depolymerization of several bio-oils using homogeneous oxovanadium catalysts was reported and will be published in two independent manuscripts.

The study of the oxidation of β-O-4 and β-1 lignin models using $(HQ)_2V(O)(O^iPr)$ and (dipic)V(O)(O^iPr) catalysts (*Chapter 2*) was carried out in collaboration with Dr. Susan Hanson (Los Alamos National Laboratories, New Mexico). The experimental work was performed by me together with Dr. Baburam Sedai (former post-doc of the Baker Group).

The oxidation of phenoxyethanol lignin models (*Chapter 3*) was led by me in collaboration with Dr. Susan Hanson, Dr. Baburam Sedai and Kyle Leckett (Summer Undergraduate Student of the Baker Group).

The design, synthesis and reactivity studies of the new amine bis(phenolate) oxovanadium(V) catalysts (*Chapter 4*) were entirely performed by me in collaboration with Jennifer Daccache (current Honours Student of the Baker Group).

The experimental work and the experiment designs for the valorization of lignin extracts (*Chapter 5*) were done by me. The NMR experiments and GPC analysis were performed with assistance from Veroniqué Chen (former MSc of Baker Lab) and Dr. Charles-Oneil Crites (Scaiano Lab).

The selective aerobic oxidative C-C bond cleavage of 1,2-diols (*Chapter 6*) was completely designed and carried out by me. The hemicarcerand oxovanadium complexes were kindly provided by Professor Alexandre Martinez (École Normale Supérieure de Lyon, France). The theoretical calculations were performed by Dr. Serge Gorelsky. Detailed DFT calculations are currently in progress in an ongoing collaboration with Dr. Carine Michel and Dr. Paul Fleurat-Lessard (ENS Lyon).

Chapter 1: Introduction

1.1 Biorefineries and the Bioeconomy

Serious weather-related disasters have become more frequent as Climate Change rapidly progresses, causing important economic impacts.[1] Recently, the United Nations Climate Change Conference (COP 21) set the guidelines to reduce CO_2 emissions and phase out fossil fuels in the near future.[2] Lower investment attractiveness, high variability of oil prices and higher costs due to potential carbon taxes, will eventually reduce the profitability of the petrochemical industry.[3] In this context, biomass is a striking alternative for the replacement of fuels, chemicals and materials.[4] As of 2012, the contribution of bioenergy to the total energy consumption of the European Union was 8.7%, representing 62% of the total renewable energy production.[5] In order to increase the revenues that justify the infrastructure for large scale biorefineries, similar to what occurs in current petrochemical refineries, production of specialty chemicals and materials from biomass is needed. For example, petrochemicals account for only 7-8% of crude oil but they provide nearly 50% of the profits for the industry, with sales over $435 billion in the US.[6]

The most important non-edible component of biomass is lignocellulose, accounting for nearly 90% of the total plant biomass production worldwide.[7] Lignocellulose is composed primarily of hemicellulose, cellulose, and lignin. The latter is the most abundant aromatic-containing macromolecule in Nature.[7] Despite the large global production of lignin from both the pulp and paper and bioethanol industries (over 50 million metric tons annually) most is currently used on site as a source of heat and electrical power.[8] Only a small portion of lignin is used for low-value applications such as dispersants and binding agents. Furthermore, the upgrading of hemicellulose and cellulose to high value-added sugar-derived compounds such as 5-hydroxymethylfurfural, levulinic acid and γ-valerolactone among others,[9] has gained increasing attention for the replacement of non-renewable petro-based chemicals and materials.

In the last few decades, interest for the production of cellulose-derived products has progressively shifted from competing food sources such as corn and sugar cane to

agriculture and forest industry waste products. Some industrial examples include the new Dupont facilities in Iowa for the conversion of agriculture residue (*e.g.*, corn stover, sugarcane bagasse, empty fruit bunch, etc.) into bio-ethanol for fuel production; and Renmatix who is using supercritical water to produce different high value-added sugars from cellulose waste products. Industrial bio-catalysis (*e.g.*, microorganisms) is also established with examples from Genomatica and Gevo, producing 1,2-propanediol, isobutanol and ethanol along with other high value-added products. Chemical processing of agricultural and several sugar-containing materials for the production of levulinic acid and other C6 molecules is being pursued by Rennovia and Segetis. BioAmber, both in the US and Canada, specializes in the production of succinic acid and 1,4-butanediol through enzymatic and chemical pathways. On the other hand, industrial examples of lignin valorization to high value-added products are still scarce. Spero Energy in Indiana converts lignin into complex aromatic compounds for flavor, fragrance, and pharmaceutical uses and Borregaard in Norway produces a variety of lignin-based chemicals such as vanillin and lignin-based materials used as dispersants and emulsions.

1.2 Lignocellulosic Biomass

1.2.1 Structure and Composition

Lignocellulose contains primarily hemicellulose, cellulose and lignin. Hemicellulose is a series of short and highly cross-linked macromolecules composed of pentoses (D-xylose and L-arabinose) and hexoses (D-mannose, D-galactose and D-glucose) that provide the structural strength between cellulose and lignin.[10] Cellulose is a linear homo-polysaccharide consisting of anhydrous glucose units, the major component of lignocellulose biomass at about 45 wt.% depending on the type of wood (*e.g.*, softwoods commonly contain higher amounts of cellulose).[11] In contrast, lignin arises from the ran-

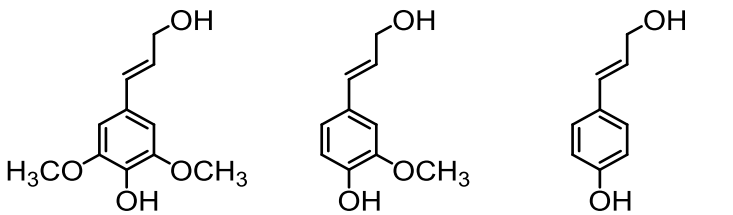

sinapyl alcohol coniferyl alcohol *p*-coumaryl alcohol

Figure 1.1. Structure of monolignols.

dom radical phenol coupling of the three monolignols in plants (Figure 1.1).[12] The composition of lignin varies greatly depending on the species of tree and growing conditions,[12] presenting a significant challenge towards its effective valorization.

Although lignin is not a regular polymer, monolignol coupling produces new C-C and C-O bonds, producing a variety of linkages, several of which are depicted in Figure 1.2.[13]

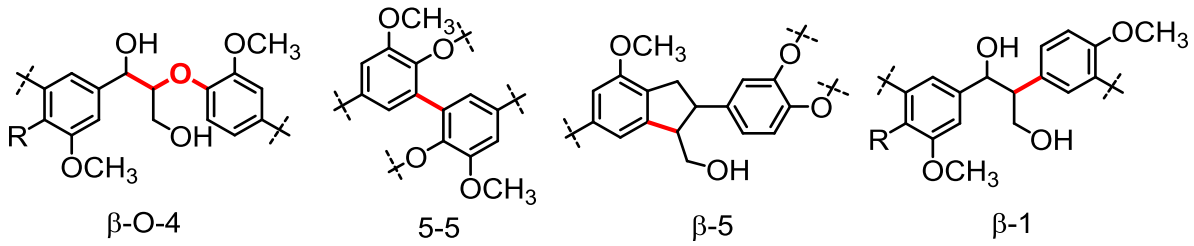

Figure 1.2. Most important linkages of lignin in decreasing order of abundance in softwood (left to right), where R = OH, H or lignin.

Most abundant is the β-O-4 linkage making up ca. 50% of total linkages in both softwood and hardwood.[13]

The structural irregularity and poor solubility of lignin macromolecules in organic solvents makes detailed characterization difficult, requiring use of multiple analytical techniques. Gel permeation chromatography (GPC) is important to estimate molecular weight and polydispersity index.[14a] 2D ^{1}H-^{13}C NMR spectroscopy has been employed for qualitative and quantitative characterization of lignin linkages and structures[14b] and ^{31}P NMR spectroscopy[14c] for characterization of lignin O-H linkages through derived phosphite esters. Gas- and high-pressure liquid chromatography coupled with mass spectrometry (GC-MS, HPLC-MS) as well as more advanced MS techniques, allow for quantification of monomers, dimers and some higher molecular weight fragments.[14d]

1.2.2 Lignin Extracts

Industrially, lignin can be extracted from wood using different techniques which have a large impact on their properties. Each method will produce a lignin extract with a different composition, structure and potential applications. Future biorefineries will need to strike a compromise between the amount of energy needed and the quality of the lignin produced to facilitate the upgrading to chemicals and materials.

Commercially available lignin is mainly produced as a by-product of the pulp and paper industry.[15] The most important chemical process is the production of Kraft lignin, where large amounts of sodium hydroxide and sodium sulfide cleave the ester bonds between cellulose and lignin, producing a black liquor rich in lignin.[16] Kraft lignin is then precipitated by lowering the pH of the black liquor, affording a highly modified and hydrophobic lignin with lower molecular weight compared with the native material. Currently, the majority of the Kraft lignin generated in the pulp and paper industry is used as fuel for heating in the paper-making process.

The second most important lignin extract, derived from the paper industry as well, are lignosulfonates which are isolated from the sulfite pulping liquor (calcium and magnesium sulfites).[17] Lignosulfonates contain sulfonate groups that provide higher solubility (compared with unmodified lignin) in polar solvents and higher molecular weights in comparison with Kraft lignin. As a result, lignosulfonates are used as plasticizers in concrete, dispersants for pesticides and oil drilling muds, dust suppressors on roads and as a key ingredient in plasteboard.

The solid-liquid extraction of wood pellets using different organic solvents (*e.g.,* mixtures of alcohols and water) affords organosolv lignin.[18] The extracts are obtained in higher purity, without sulfur and hemicellulose compared with Kraft lignin and lignosulfonates, ideal for valorization to chemicals. However, the difficulties with solvent recovery and lower yields have increased the costs, making this process less sustainable for an integrated biorefinery.

The exponential increase of renewable sugar-based chemicals derived from enzymatic hydrolysis of wood have increased the availability of solid cellulolytic enzyme lignin.[19] This lignin contains significant carbohydrate impurities and exhibits higher molecular weights compared with both Kraft lignin and lignosulfonates. The main problem arises from the cross-linked structure between hemicellulose and lignin. However, the low cost of enzymatic lignin, considered a waste product in the sugar platform, makes it a promising source for upgrading to fine chemicals and materials.

1.2.3 Lignin Model Compounds and Polyalcohols

As mentioned in previous sections, the high heterogeneity of lignin has diminished the studies for the disassembly and valorization of real lignin extracts. As a result, many

investigations use lignin models in order to assess catalyst activity and selectivity. This section is not intended to cover all lignin models described in the literature, but will be focused exclusively on the lignin models used throughout this Thesis.

The most popular lignin model compounds are based on the β-O-4 linkage, considering that this structure predominates in both softwood- and hardwood lignins.[13] The simplest lignin models are 2-phenoxyethanol (**LM1**), 1,2-diphenyl-2-methoxyethanol (**LM2**) and 1-phenyl-2-phenoxy-ethanol (**LM3**)[20] depicted in Figure 1.3. The first two compounds are

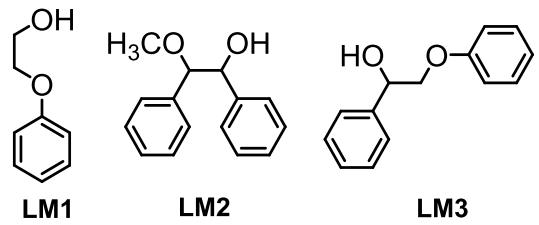

Figure 1.3. Simple lignin model compounds.

commercially available, facilitating the experimental workload. More complex lignin models containing the β-aryl glycerol moiety with primary and secondary alcohols, such as non-phenolic β-aryl glycerol model 1-(3,5-dimethoxyphenyl)-2-(2-ethoxyphenoxy)-propane-1,3-diol (**LM4**)[21] and phenolic β-aryl glycerol model 1-(4-hydroxy-3,5-dimethoxyphenyl)-2-(2-methoxyphenoxy)-propane-1,3-diol (**LM5**)[22] are depicted in Figure 1.4.

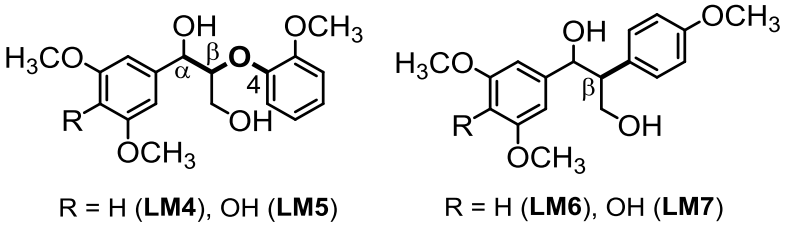

Figure 1.4. Complex lignin model compounds containing the β-O-4 (left) and β-1 (right) linkages, respectively.

Another variation of lignin models contains the β-1 linkage that constitutes 7-9% of lignin linkages in different type of woods.[13] For example, Figure 1.4 depicts non-phenolic β-1 lignin model 1-(3,5-dimethoxyphenyl)-2-(4-methoxyphenyl)-propane-1,3-diol (**LM6**)[23] and phenolic β-1 lignin model 1-(4-hydroxy-3,5-dimethoxyphenyl)-2-(4-methoxyphenyl)-propane-1,3-diol (**LM7**).[24] Lignin models containing β-aryl glycerol and β-1 moieties

require several synthetic steps and separations (*e.g.*, **LM4** has two chiral centers giving two different diastereoisomers) for their synthesis.

On the other hand, diols are important models for cellulose-derived polyalcohols with a simpler structure that facilitates the analysis and catalyst optimization.[25] Pinacol and hydrobenzoin (1,2-diphenyl-1,2-ethanediol) are particularly interesting due to their commercial availability and diverse reactivity toward C-C bond cleavage and benzylic hydrogen abstraction affording acetone and benzoin (2-hydroxy-2-phenylacetophenone), respectively (Figure 1.5).

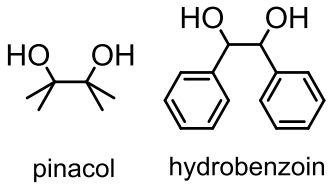

Figure 1.5. Diol models for cellulose valorization.

1.3 Valorization of Lignin

The interest in lignin research has increased drastically over the last decade as depicted in Figure 1.6. The graph shows the number of publications (*e.g.*, papers, reviews, patents,

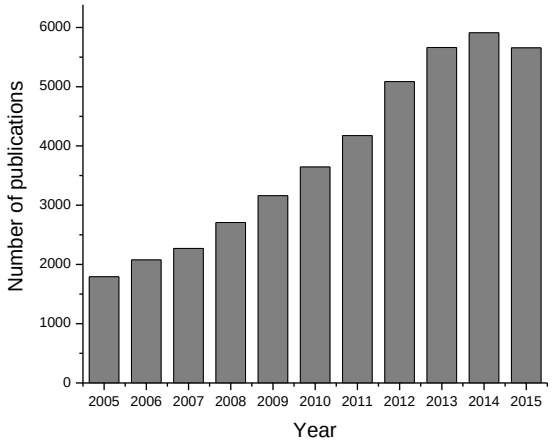

Figure 1.6. Number of publications per year with the entry 'lignin'. The slight decrease for 2015 might be due to old databases (data from SciFinder®).

etc.) containing the word "lignin". As introduced in the previous sections, finding an effective method, or combination of methods for the valorization of lignin is a key factor for biorefinery economic viability.

In order to build a renewable resource economy, stoichiometric amounts of reagents as well as toxic and expensive processes must be avoided. In this context, catalysis science provides an incredible opportunity to overcome these problems.[25] The techniques for depolymerization of lignin depend on the nature of the catalysts (*e.g.,* heterogeneous or homogeneous). Heterogeneous catalysts have been used for reductive and oxidative approaches,[27] with different degrees of success for the valorization of lignin. Despite the extraordinary expansion in the literature and the recent ground-breaking advances using heterogeneous catalysis, this Thesis will be focused on homogeneous catalysis to facilitate mechanistic studies and selectivity control.

1.3.1 Reductive Homogeneous Methods

The principal reductive method for lignin valorization is the hydrogenolysis of C-O bonds catalyzed by first row transition metals. Hartwig and co-workers demonstrated that $Ni(COD)_2$ (COD = 1,5-cyclooctadiene) and NHC (N-heterocyclic carbene) ligands are able to break the C-O bond of diaryl ethers using 1 bar of H_2 at 120 ^oC, affording high yields of arenes and phenols (Scheme 1.1).[28a] Further investigation of this reaction demonstrated that

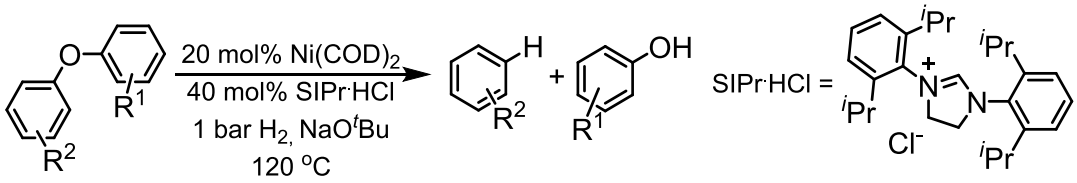

Scheme 1.1. Nickel-catalyzed C-O bond cleavage of aryl ethers.

H_2 gas is not involved in the C-O bond cleavage. Instead, an oxidative addition of the aryl C-O bond followed by β-H elimination occurs, and formaldehyde-assisted reductive elimination of the aryl-H bond initiates the C-O bond scission.[29] Later, Hartwig and co-workers showed that the $Ni(COD)_2$ precursor in the presence of strong bases produces stable nanoparticles suitable for the catalytic hydrogenolysis of aryl ethers using 1 bar of H_2.[28b]

A similar example where the state of the catalyst is unclear was reported by Wang and co-workers. The reductive C-O bond cleavage of aryl ethers using 20 mol% $Fe(acac)_3$ (acac = acetylacetonate) and stoichiometric amounts of $LiAlH_4$ and NaO^tBu affords phenols and phenylethanol, or acetophenone if the source of hydride is H_2 gas.[30] The selectivity for the C-O bond cleavage of **LM3** is low (*ca.* 41%) and the catalyst is likely heterogeneous in nature since the mercury test completely poisoned the reaction.

More expensive homogeneous transition metals catalysts such as Ru and Ir, and less practical methods for valorization of lignin, have also been extensively studied. Ruthenium catalysts (*e.g.,* $RuH_2(CO)(PPh_3)_3$ with Xantphos ligands) reported by Ellman and co-workers follow a redox-neutral, tandem dehydrogenation/reductive ether C-O cleavage of β-aryl ethers such as **LM3** to afford acetophenone and phenol (Scheme 1.2; Xantphos = 9,9-dimethyl-4,5-bis(di-tert-butylphosphino)xanthene).[31] James and co-workers expanded

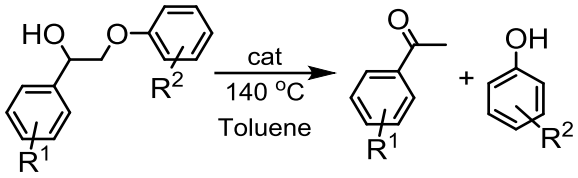

Scheme 1.2. Redox-neutral tandem dehydrogenation/reductive ether cleavage of β-aryl ethers. 1 mol% $RuH_2(CO)(PPh_3)_3$ and Xantphos (Ellman); 5 mol% $RuH_2(CO)(PPh_3)_3$(Xantphos) (James); 5 mol% [Ru(COD)(methylallyl)$_2$] and Triphos (Leitner); 5 mol% $RuCl_2(PPh_3)_3$ + 25 mol% K-*t*-amylate and EtOAc (Plietker).

the substrate scope to β-aryl glycerol lignin models.[32] The cleavage does not require addition of hydrogen gas which constitutes a clear advantage compared with the nickel systems. A highly efficient C-O bond cleavage of β-aryl ethers using [Ru(COD)(methylallyl)$_2$], triphos [1,1,1-tris(diphenylphosphinomethyl)ethane] and trimethylenemethane was later developed by Leitner and co-workers.[33] The above Ru catalysts likely cleave the C-O bond of β-aryl ethers following an intramolecular hydrogen transfer process under redox neutral conditions.[34] Plietker and co-workers were able to break the C-O bond of β-aryl ethers and couple the products with two hydrogen-transfer processes of dearyloxylation and subsequent dehydrative α-alkylation using primary

alcohols to generate different alkylated products based on lignin models, using $RuCl_2(PPh_3)_3$ as their catalyst.[35]

Ruthenium catalysts were also used for the depolymerization of real lignin extracts. A modest degree of depolymerization was achieved using $RuCl_2(PPh_3)_3$ for the ethanol organosolv lignin, affording small molecular weight fractions and changes in solubility.[36] It is important to note that most of the reductive methods for depolymerization of real lignin extracts are achieved using heterogeneous catalysts.[27] Alternatively, iridium homogeneous catalysts reported by Goldman and co-workers based on a (PCP)Ir platform (PCP = pincer bisphosphine ligand) for the dehydroaryloxylation of C-O bonds in alkyl aryl ethers afford phenols and olefins using relatively low temperatures (150 - 200 ^oC) and low catalyst loadings (2 mol%).[37]

1.3.2 Oxidative Homogeneous Methods

Oxidation catalysis is the preferred technique chosen by Nature for degradation of lignin (*e.g.*, manganese peroxidases).[38] Oxidative cleavage of lignin also offers several advantages compared to the reductive methodologies previously discussed. The reactions are more robust as they do not require an inert atmosphere, lower pressures are needed and they use inexpensive oxidants such as peroxides or simple air. Oxidation of lignin can be divided in three different groups: metal-free systems, first row transition metal catalysts and second or third row transition metal catalysts.

Firstly, it important to mention that back in the 1940's and later in 1980's two different oxidation methods were established as analytical techniques for the quantification and identification of lignin. The hydrolysis of lignin using CuO and strong bases yields several methoxylated phenols,[39] and the oxidative cleavage of lignin using the alkaline nitrobenzene method produces aldehydes and aromatic carboxylic acids in quantitative yields,[40] respectively. Drawbacks of these methods are the stoichiometric amounts of reagents and poor yields and conversions.

Stahl and co-workers developed a metal-free organocatalytic system for the oxidation and depolymerization of aspen lignin (typical hardwood lignin), employing 4-acetamido-TEMPO under acidic conditions. Two-dimensional NMR data revealed that all guaiacyl [4-(2-methoxyphenol)] and syringyl [4-(2,6-dimethoxyphenol)] units of lignin were transformed, establishing that the β-O-4 linkages were oxidized to aryl ketone-containing

β-ether units though C-H bond cleavage (Scheme 1.3).[41a] Subsequently, a redox-neutral cleavage of the C-O bond through the addition of a superstoichiometric amount of buffer formate/formic acid afforded small molecular weight fractions and syringyl and guaiacyl-derived diketones.[41b]

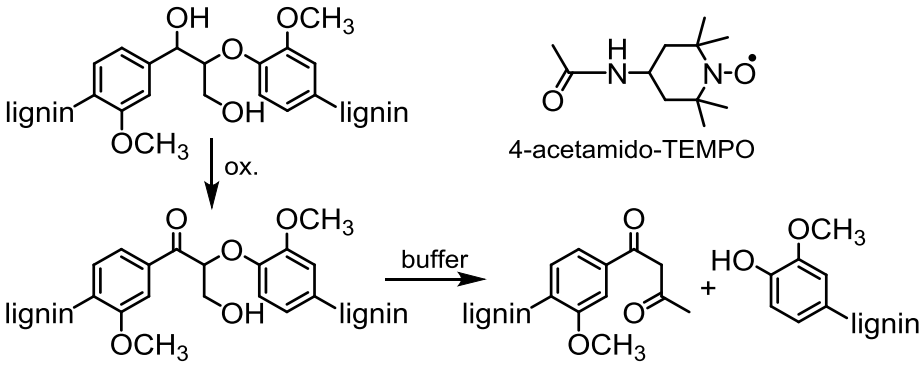

Scheme 1.3. Metal-free systems for depolymerization of lignin.[41] Oxidation: 4 wt. % 4-acetamido-TEMPO, 1.5:1 HNO_3/HCl, 2 atm O_2, 48 h, 65 ^oC; C-O bond cleavage: 3 equiv. HCOOH/HCOONa, 110 ^oC, 24 h.

First row transition metal-catalyzed oxidations of lignin models and lignin extracts are based on inexpensive Cu, Co, Fe and V catalysts. There is a vast amount of literature concerning the Cu/TEMPO catalyst (TEMPO = 2,2,6,6-tetramethylpiperidine-1-oxyl) and related systems with different nitroxyl radicals for the oxidation of primary and secondary alcohols.[42] However, little has been disclosed about the oxidation of lignin models or real lignin extracts using copper catalysts. Baker and co-workers used Cu(I)/TEMPO with 2,6-lutidine as a solvent and co-ligand for the selective C-C bond cleavage of aryl ethers, β-aryl glycerol and β-1 lignin models (Scheme 1.4).[23,43] The catalyst is powerful for the cleavage

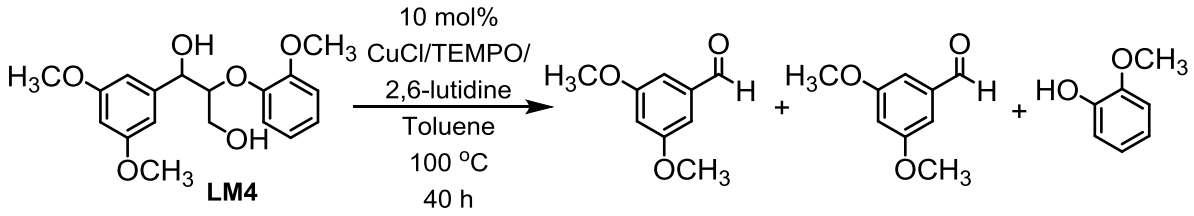

Scheme 1.4. Cu(I)/TEMPO/2,6-lutidine catalyst for the C-C bond cleavage of β-aryl glycerol lignin models.

of C-C bonds, including C_{aryl}-C_{alkyl} or C_{alkyl}-C_{alkyl} depending on the model compound, but the atom economy is poor. Despite the rich chemistry exhibited by the Cu(I)/TEMPO/2,6-

lutidine catalyst, it is not capable of decreasing the molecular weight of ethanol organosolv lignin.[43d]

Bozell and co-workers designed several Co-Schiff base catalysts for the aerobic oxidation of *para*-substituted phenols to the corresponding benzoquinones.[44a] Later, using a modified version of the Co-Schiff base catalyst, they were able to cleave the C_{aryl}-C_{alkyl} bond in phenolic β-aryl glycerol lignin models, affording benzoquinones (Scheme 1.5). The

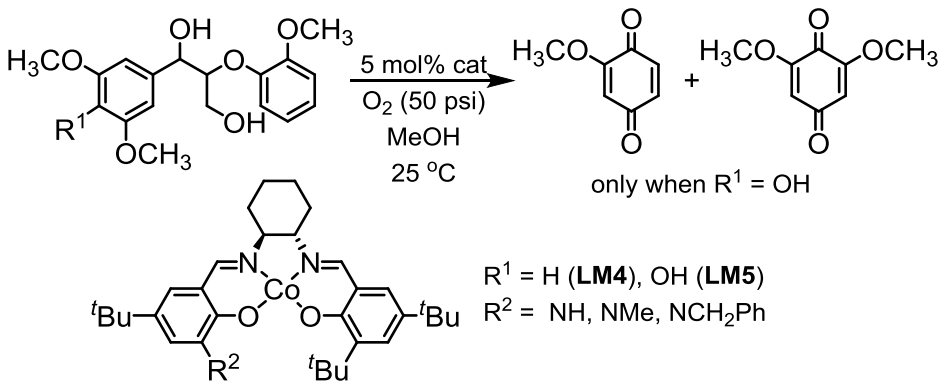

Scheme 1.5. Co-Schiff base catalyst for the selective C_{aryl}-C_{alkyl} bond cleavage.[44] If R^1 = H, only the C-H bond cleavage is observed.

oxidation of organosolv lignin affords various quinones, representing 3.5% of the initial weight of lignin.[39b]

The oxidation of hydrocarbons using Fe catalysts (*e.g.*, Fe-TAML [tetraamido tetracyclic ligands] complexes with peroxides) normally produces CO_2.[45] The challenge for Fe catalysts in terms of lignin oxidation is to modulate the reactivity to obtain higher yields and good atom economy for the depolymerization of lignin. Iron-(TAML)Li catalysts reported by Andrioletti and co-workers[46a] and a related patent from Collins[46b] (Figure 1.7)

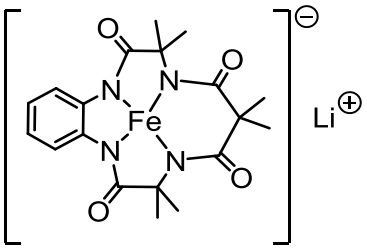

Figure 1.7. Fe(TAML)Li for lignin disassembly.

displayed a mixed reactivity towards β-aryl ether lignin models. Using 1 mol% of catalyst under mild conditions (25 °C, 1 h) but with 2 equiv. of a sacrificial oxidant, diacetoxy

iodobenzene, they were able to form C-H bond cleavage products (ketones), and C-C bond cleavage products (benzaldehydes and benzoic acids). However, a radical re-polymerization of the guaiacyl side of the lignin model might decrease the yield of these reactions.

In a more recent example of iron-catalyzed reactions, Bolm and co-workers described a radical cleavage of β-aryl glycerol lignin models, producing a mixture of C-C and C-O bond cleavage products, methoxyphenols and benzaldehydes, respectively.[47] The combination of Fe-DABCO (DABCO = 1,4-diazabicyclo[2.2.2]octane) and DMSO generates methyl radicals which are the active catalytic species. The depolymerization of organosolv lignin was also assessed, affording contradictory results. On one hand, the disappearance of the principal structures of lignin (*e.g.,* β-O-4 linkages) indicates that the bond cleavage is occurring in real lignin extracts as observed by 2D NMR. However, the poor reduction in the molecular weight of lignin observed by GPC might reveal a radical re-polymerization to high molecular weight structures.

Manganese catalysts bearing TACN (1,4,7-triaza-cyclononane) ligands have been widely used together with peroxides for the oxidation of substituted phenyl ethanol (Figure 1.8).[48] Catalytic oxidation of β-O-4 or more complex lignin models have not yet been repo-

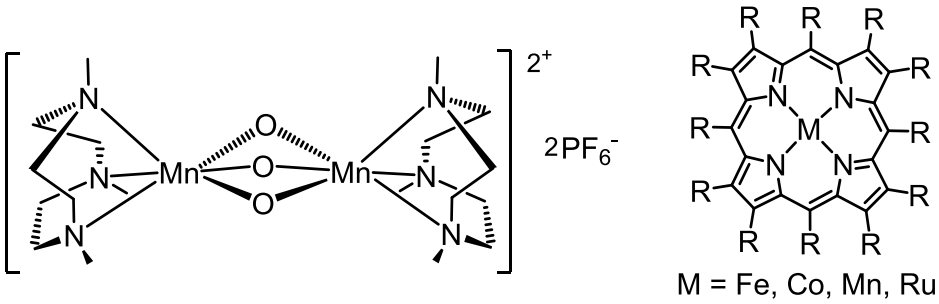

Figure 1.8. Mn-TACN and metallo-deuteroporphyrins.

rted. Ying and co-workers have reported several catalysts based on metallo-deuteroporphyrins using Fe, Cu, Mn and Ru for the selective oxidation of β-aryl ether lignin models using superstoichiometric amounts of oxidants.[49] The conversions are quantitative but the atom economy is very low with only *ca.* 9% carbon balance for one aryl ring of the lignin model. They were also able to oxidize enzymolysis lignin (similar to solid cellulolytic enzyme lignin) into depolymerized products including up to 33 wt.% of a soluble portion that contained well-defined aromatic monomers.

Second and third row transition metal catalysts such as Re[50a] and Mo[50b] have also been reported for the oxidative disassembly of lignin. Among these examples, Kühn and co-workers disclosed an elegant methyltrioxorhenium (MTO) catalytic system for the selective C-O bond cleavage of β-aryl ether lignin models.[51] The cleavage generates phenols and aldehydes using 5 mol% $MeReO_3$ catalyst under mild conditions (110 ^oC, 4 h). Unfortunately, the oxidation of β-aryl glycerol lignin models yielded a high number of undesired products, decreasing the yields of C-O bond products considerably.

1.3.3 Other Homogeneous Methods

Toste and co-workers reported an unusual non-oxidative C-O bond cleavage of β-aryl glycerol ethers using oxovanadium(V) catalysts bearing tridentate Schiff base ligands (Scheme 1.6).[52] The C-O bond cleavage of lignin models affords aryl enones and phenols

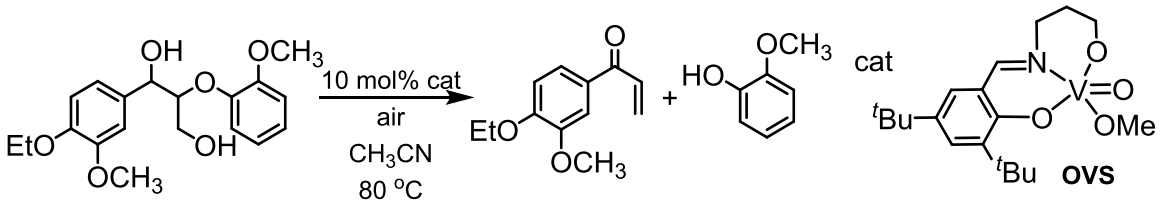

Scheme 1.6. Non-oxidative C-O bond cleavage reported by Toste and co-workers.

in higher conversions and yields under aerobic conditions compared to reductive catalysts. Moreover, the reaction even proceeds under nitrogen, albeit at a slower rate. The authors proposed a one-electron mechanism with formation of an aryloxy radical and a V(IV) intermediate which is re-oxidized back to V(V) by the aryloxy radical. This catalytic system was applied to organosolv lignin, showing the formation of enones by 2D NMR but resulting in a minimal decrease in the relative molecular weight.[52b]

Several photocatalytic methods have been reported using visible light to trigger bond cleavage in lignin models. Son and co-workers were able to selectively break C-C bonds of β-aryl glycerol ethers using visible light (λ > 420 nm) and oxovanadium(V) catalysts beari-

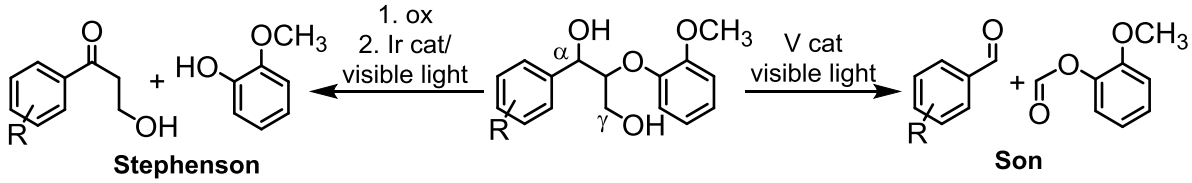

Scheme 1.7. Stephenson and Son photocatalytic systems for C-O and C-C bond cleavage, respectively

ng similar ligands as the ones reported by Toste (Scheme 1.7, right).[53] The experients were carried out at room temperature (24 h), affording phenylformate and benzaldehyde using 10 mol% catalyst loading. Stephenson and co-workers developed a two-step method for the selective C-O bond cleavage of β-aryl glycerol ethers (Scheme 1.7, left).[54] First, a selective oxidation of the α- or γ-alcohol using metal free organocatalysts (*e.g.*, 4-acetamido-TEMPO) was performed, followed by a photocatalytic cleavage of the reduced ketone using 1 mol% of $[Ir(ppy)_2(dtbbpy)]PF_6$ (ppy = 2-(2-pyridyl)phenyl, dtbbpy = 4,4′-di-tert-butyl-2,2′-bipyridine) and visible light to afford phenol and β-hydroxyphenyl ketone. However, the photocatalyst needs 3 equiv. of diisopropylethylamine and 3 equiv. of formic acid for a batch reaction.

A ruthenium-catalyzed selective C-C bond cleavage of β-aryl glycerol ether lignin models was reported by Leitner and co-workers.[55] In this example, using 5 mol% of $RuHCl(PPh_3)_3$ and the triphos ligand, a dehydrogenation-initiated retro-aldol reaction cleaves the C-C bonds using high temperatures (160 ^oC) and short reaction times (4 h), affording similar products as the system described by Son (Scheme 1.7, right). The difference between Leitner's catalyst compared to the previous reductive ruthenium catalysts in section 1.3.1. is the absence of reductive C-O bond cleavage (using H_2).

A tandem process using acid catalysis and different chemical derivatizations was proposed by de Vries and co-workers.[56] The C-O bond cleavage of β-aryl glycerol ethers using 20 mol% triflic acid afforded benzylacetaldehydes which are captured by the reaction with either diols, catalytic hydrogenation/dehydration or decarbonylation to produce acetals, primary alcohol/alkanes or methyl aromatics, respectively. This procedure was applied to organosolv lignin, affording 5 wt.% of acetals after treatment with diols.

The majority of the above reported procedures (including reductive and oxidative methods) require high catalyst loadings (*e.g.*, 5 - 20 mol%), long reaction times (*e.g.*, 24 - 48 h), superstoichiometric amounts of reagents (*e.g.*, formate/formic acid systems or molecular hydrogen gas) or expensive transition metal catalysts (*e.g.*, the current prices for ruthenium and vanadium in January 2016 are 1,350 and 13.2 USD/Kg, respectively)[57] making these methodologies impractical for application in a future biorefinery where the amounts of lignin treated will probably be tens of metric tons per day.

1.4 Oxovanadium(V) Catalysts

1.4.1 First Generation of Oxovanadium(V) Catalysts

The discovery of vanadium-dependent enzymes such as haloperoxidases and nitrogenases, and their role in different biological catalytic processes, attracted broad scientific attention in the last century.[58] Inspired by Nature, the development of bio-inorganic vanadium metal catalysts for several oxidative transformations flourished.

Early work by Mimoun in the 1980s with oxovanadium(V) peroxo complexes demonstrated their ability to hydroxylate aromatic hydrocarbons to phenols and alkanes to alcohols and ketones. The mechanisms of these reactions are closely related to the enzyme cytochrome P_{450} monooxygenases.[59] Later, Thorn and co-workers reported that phosphatovanadium(V) complexes can readily exchange with alcohols to produce the corresponding alkoxide-coordinated oxovanadium complexes (Scheme 1.8).[60]

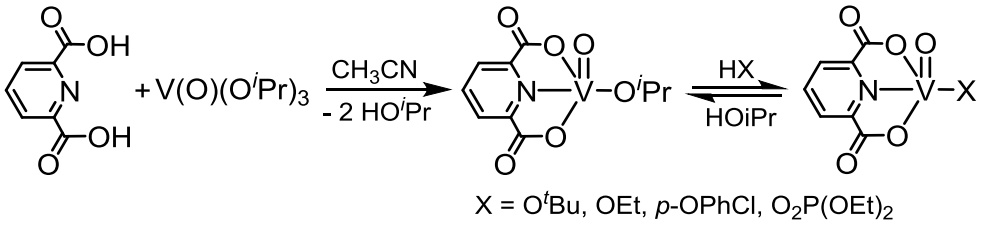

Scheme 1.8. Thorn's vanadium complexes.

In the late 2000s, Baker and Hanson started to extensively study the oxovanadium(V) isopropoxide complexes **OV1** and **OV2** for their applications in alcohol oxidation and lignin model disassembly (Figure 1.9).[61] Vanadium complexes bearing the tridentate dipic-

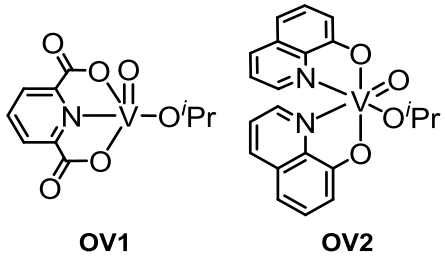

Figure 1.9. First generation of oxovanadium(V) catalysts.

olinate and the bidentate 8-oxyquinoline ligands can be synthesized in high yields from V(O)(O^{i}Pr)$_3$ and the respective ligands under moisture-free conditions, or using V(O)(acac)$_2$ as a source of vanadium in air.

1.4.2 Oxidative Bond Cleavage of Pinacol and β-O-4 Lignin Models

In order to assess the potential for C-C bond cleavage in 1,2-diols and β-O-4 lignin models, several chelated vanadium complexes were synthesized. The reaction of **OV1** and pinacol at room temperature in acetonitrile affords the chelated pinacolato oxovanadium(V) complex **OV3**. The **OV3** complex reacts slowly (*ca.* 7 days) at 25 ^{o}C in the presence of pyridine under anaerobic conditions, affording the C-C bond cleavage product acetone and bis(pyridine) oxovanadium(IV) complex **OV4** (Scheme 1.9).[62a,b] The reaction times can be

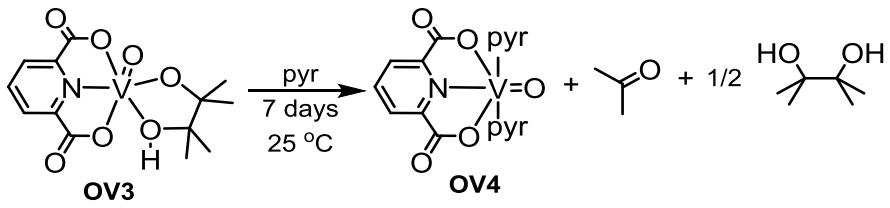

Scheme 1.9. Pyridine triggers the C-C bond cleavage of the chelated **OV3** complex.

as short as 48 h if the temperature is increased to 100 ^{o}C to reach 100% conversion. The reaction is formally a one-electron oxidation of the substrate considering that one metal center was reduced to an oxovanadium(IV) complex. The catalytic activity of **OV1** for the C-C bond cleavage of pinacol was studied using 5 mol% catalyst in 1-methyl-2-pyrrolidinone as a solvent (100 ^{o}C, 3 days, air) affording 97% conversion, which translates to 19 turnovers. Control experiments showed that pinacol is stable in a hot solution of pyridine (100 ^{o}C) for several weeks. Anaerobic reaction of the oxovanadium(IV) complex **OV4** with pinacol using harsher conditions (48 h, 100 ^{o}C) affords the C-C bond cleavage product, acetone, and a μ-oxo bimetallic vanadium(III) complex **OV5** (Scheme 1.10).[62a,b] Note that this reaction involves O atom transfer from vanadium to form water.

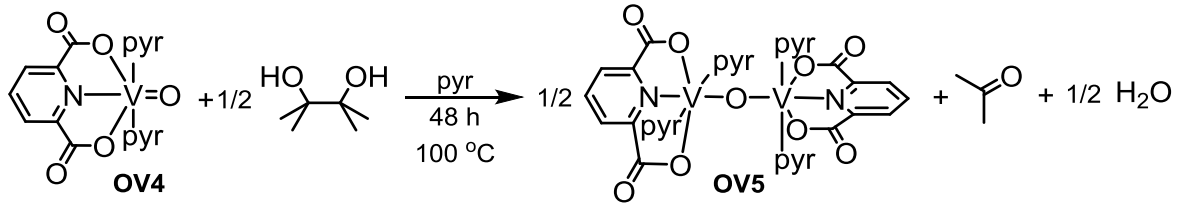

Scheme 1.10. Bis(pyridine) oxovanadium(V) **OV4** induces the C-C bond cleavage of pinacol.

The reactivity of the oxovanadium(V) complexes was then studied with a simple 1,2-hydroxyether lignin model, 1-methoxy-1-phenyl-2-propanol (**LM2**, Scheme 1.11). The

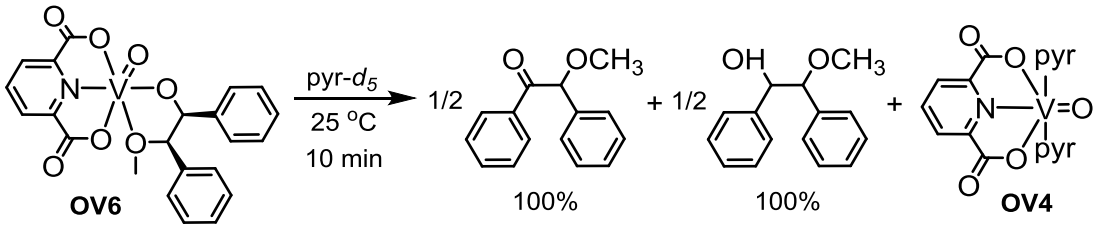

Scheme 1.11. C-H bond cleavage of chelated complex **OV6** in pyr-d_5.

reaction of **OV1** with **LM2** forms a chelated vanadium(V) complex **OV6**. Dissolution of this complex in pyridine rapidly affords the C-H bond cleavage product ketone and **OV4.**[62c] In contrast, when the chelated complex **OV6** is dissolved in wet dimethylsulfoxide (DMSO), only 30% of the reaction leads to the ketone with the rest giving a mixture of the C-C and C-H bond cleavage products, benzaldehyde and methanol.[62c] In this case the oxovanadium(IV) product **OV7** has two molecules of DMSO coordinated *trans* to each other (Scheme 1.12).

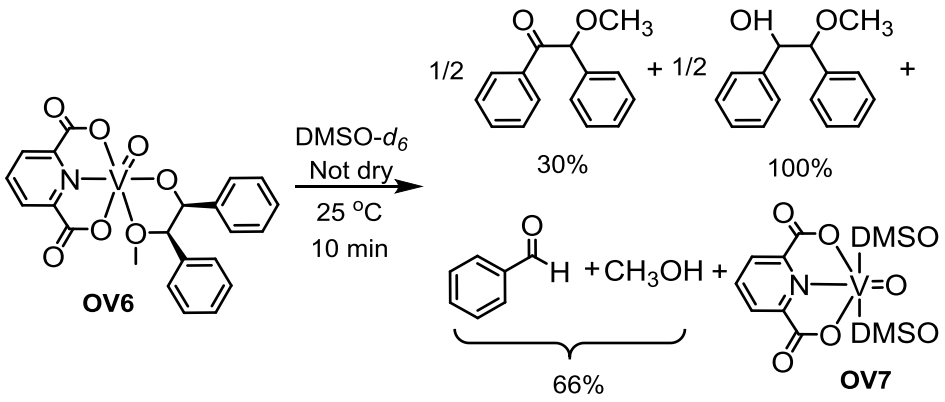

Scheme 1.12. C-C bond cleavage of chelated complex **OV6** in 'wet' DMSO-d_6.

The mechanism of this C-C/C-H bond cleavage is still unknown and a radical pathway has not been ruled out. Addition of 9,10-dihydroanthracene afforded less than 1% of anthracene with no change in the reaction rate. However, the chelated complex **OV6** reacts directly with BHT (2,6-di-*tert*-butyl-4-methylphenol) and PPh_3 to give many uncharacterized products. Nonetheless, the difference in reactivity for the C-H and C-C bond cleavage in pyridine and DMSO, respectively, allows for solvent-dependent selectivity control.[62c,e,g]

The aerobic catalytic reactions of additional lignin models were also investigated using **OV1**. The oxidation of **LM1** afforded 20% conversion (10 mol% **OV1**, DMSO-d_6, 100 °C,

7 days) with an 18% yield of phenol and 6% formic acid.[62c] The β-O-4 lignin model **LM2** afforded 94% conversion using the same conditions as above but in 20 h of reaction time, yielding 73% benzaldehyde, 69% methanol, 13% ketone, 5% benzoic acid and 5% methyl benzoate. In contrast, when pyridine-d_5 is used as a solvent, the aerobic catalytic oxidation of **LM2** takes place over 6 days giving 99% conversion with 9% yield of benzaldehyde, 6% methanol, 9% ketone, 85% benzoic acid and 84% methyl benzoate. This clearly demonstrates the solvent dependence of the product distribution using vanadium catalyst **OV1**.

1.4.3 Base-Assisted Redox Deprotonation

Inspired by the important role played by pyridine in the C-C bond cleavage of pinacol, the C-H bond cleavage of isopropoxide in **OV1** was examined in detail. Dissolving **OV1** in pyridine-d_5 gives an immediate reaction affording C-H bond cleavage product acetone and vanadium (IV) complex **OV4** (Scheme 1.13). This reaction can be described as a two-

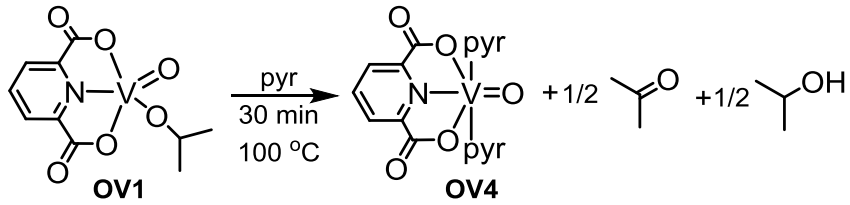

Scheme 1.13. C-H bond cleavage of isopropoxide mediated by pyridine.

electron oxidation of the substrate.[62a,b] Radical clocks such as cyclobutanol are a good indicator for one- vs. two-electron oxidation pathways. Cyclobutanoxide oxovanadium(V) complex **OV8** was prepared by dissolving **OV1** in a concentrated solution of cyclobutanol. Thermolysis of **OV8** in pyridine-d_5 (100 °C, 30 min) produced 93% yield of cyclobutanone indicative of a two-electron pathway (Scheme 1.14).[62a,b] In contrast, one-electron pathways

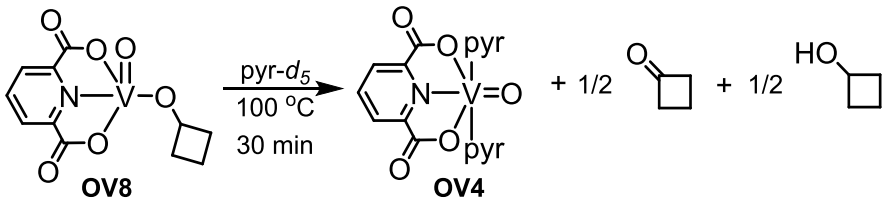

Scheme 1.14. Oxidation of cyclobutanoxide complex in pyridine-d_5.

that predominate using VO_2^+ in $HClO_4$ give ring-opened products such as 4-hydroxybutyraldehyde or butyraldehyde.

The catalytic properties of the oxovanadium(V) complexes **OV1** and **OV2** were examined for a series of primary and secondary benzylic, allylic and propargylic alcohols.[62d] The reaction produced the corresponding aldehydes or ketones in excellent yields using 2 mol% **OV2** and 10 mol% NEt_3 (60 - 100 ^oC, 24 h, air). However, unactivated alcohols such as 2-butanol and 1-butanol gave yields less than *ca.* 5%. To understand the catalytic properties of **OV1** and its implication in the oxidation of alcohol and lignin models, the vanadium(III) complex **OV5** was exposed to air in pyridine, affording vanadium(IV) complex **OV4** in 1 h at room temperature.[62a,b] Furthermore, the oxidation of **OV4** to V(V) in air at room temperature only occurs at very low yield. The vanadium(IV) complex **OV4** is slowly re-oxidized with only 50% yield to a dioxo vanadium(V) complex **OV9** after 4 days at 100 ^oC (Scheme 1.15). The dioxo complex can

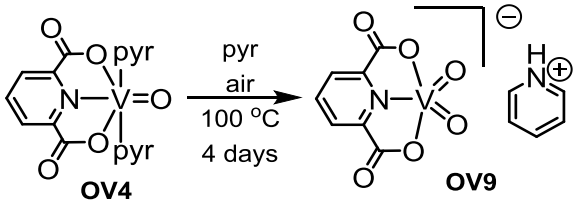

Scheme 1.15. Re-oxidation of bis(pyridine) oxovanadium(IV) in air.

be independently synthesized by dissolving **OV1** in a wet solution of pyridine. In an attempt to explain the role of the dioxo vanadium(V) complex **OV9** in the catalytic oxidation of alcohols, **OV9** was reacted with μ-oxo bimetallic vanadium(III) complex **OV5** in pyridine at room temperature, producing two moles of vanadium(IV) complex **OV4** and 0.5 molecules of water (Scheme 1.16).[62a,b]

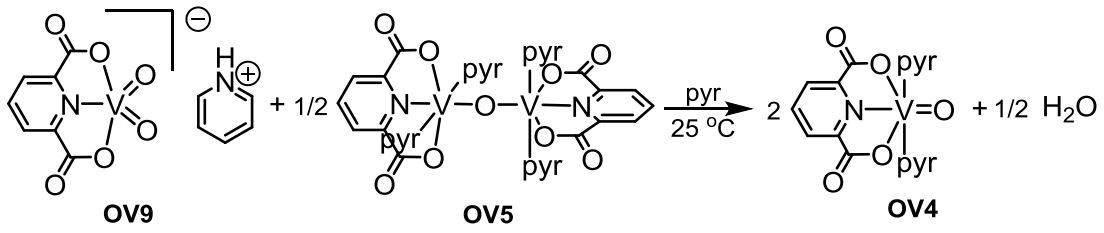

Scheme 1.16. Conproportionation of dioxo vanadium(V) **OV9** and V(III) **OV5**.

The catalytic cycle for the oxidation of alcohols using oxovanadium(V) complexes **OV1** and **OV2** is depicted in Scheme 1.17. An initial slow step for the C-H bond cleavage of the

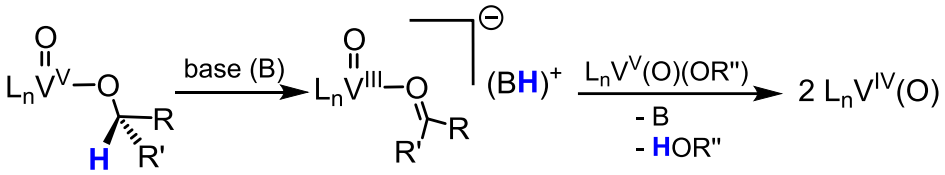

Scheme 1.17. Base-assisted redox deprotonation (BARD) where R = benzylic, allylic and propargylic.

α-H produces a vanadium(III) product following a two-electron oxidation pathway. Then a rapid conproportionation of the V(III) product with another equivalent of vanadium(V) complex produced two moles of vanadium(IV) which is subsequently reoxidized to V(V). Although, as explained above, the oxidation of the **OV4** product back to **OV1** or dioxo vanadium(V) complex **OV9**, is very slow.

1.5 Conclusions

Lignocellulose biomass is an attractive source for the production of biorenewable chemicals and materials. Catalysis science, especially homogeneous methods, has emerged as one of the most promising tools for the valorization of lignocellulose biomass. However, the efficiency of many catalytic systems depends greatly on high catalyst loadings and harsh reaction conditions. In this context, oxovanadium catalysts using air as the only oxidant offer an inexpensive and practical methodology for an integrated biorefinery.

Chapter 2 of this *Thesis* explores an expanded substrate scope for the aerobic oxidation of β-O-4 and β-1 lignin model compounds. Interesting bond cleavage selectivity and the significant role of base will also be discussed, followed by the study of simpler lignin model compounds (*e.g.*, phenoxyethanol) in *Chapter 3*. Based on these findings, *Chapter 4* shows the synthesis, characterization and the reactivity of new oxovanadium complexes bearing N-donor appended bis(2-phenol-methyl)amine ligands. Futhermore, *Chapter 5* presents a systematic study of the oxidation and depolymerization of organosolv lignin using the oxovanadium complexes along with several reported oxidation catalysts. In the pursuit of the valorization of cellulose biomass, *Chapter 6* discusses the novel reactivity of

trialkoxyamine oxovanadium catalysts for the selective aerobic oxidative cleavage of 1,2-diols.

1.6 References

(1) a) Smith, A., Matthews, J. *Nat. Hazards* **2015**, *77*, 1829-1851; b) Solomon, S.; Plattner, G. K.; Knutti, R.; Friedlingstein, P. *Proc. Natl. Acad. Sci.* **2009**, *106*, 1704–1709.
(2) United Nations Framework Convention on Climate Change. (2015). Adoption of the Paris Agreement. Proposal by the President, Paris Climate Change Conference. Paris, France: United Nations.
(3) University of British Columbia. (2015). Fossil Fuel Divestment: Reviewing Arguments, Implications & Policy Opportunities. Vancouver, BC: Ritchie, J.; Dowlatabadi, H. Edited by Dr. Tom Pedersen, PICS Executive Director; Robyn Meyer, PICS Senior Communications Officer & Ami Kingdon, PICS Science Writer.
(4) a) Huber, G. W.; Iborra, S.; Corma, A. *Chem. Rev.* **2006**, *106*, 4044–4098; b) Besson, M.; Gallezot, P.; Pinel, C. *Chem. Rev.* **2014**, *114*, 1827–1870; c) Zhou, C-H.; Xia, X.; Lin, C-X.; Tong, D-S.; Beltramini, J. *Chem. Soc. Rev.* **2011**, *40*, 5588–5617.
(5) a) European Commission. (2010) Energy 2020: A strategy for competitive, sustainable and secure energy. Brussels, Belgium; b) European Commission. (2014) A policy framework for climate and energy in the period from 2020 to 2030. Brussels, Belgium.
(6) Guide to the Business of Chemistry 2006, American Chemistry Council: Arlington, 2006.
(7) a) Calvo-Flores, F. G.; Dobado, J. A. *ChemSusChem* **2010**, *3*, 1227−1235; b) Kuhad R. C.; Singh A. *Crit. Rev. Biotechnol.* **1993**, *13*, 151–172.
(8) Werpy, T.; Petersen, G. In Top Value-Added Chemicals from Biomass - Results of Screening for Potential Candidates from Sugars and Synthesis Gas; Eds.; U.S. Department of Energy: Washington, DC, 2004, Vol. 1
(9) The National Non-Food Crops Centre. (2011). Renewable Chemicals Factsheet: Lignin. London, UK: Higson, A.; Smith, C.
(10) a) Kuhad, R. C.; Singh, A.; Ericksson, K. E. *Adv. Biochem. Eng. Biotechnol.* **1997**, *57*, 45–125; b) Reddy, N.; Yang, Y. *Trend. Biotechnol*. **2005**, *23*, 22–27; c) Li, B. Z.; Balan, V.; Yuan, Y. J.; Dale, B. E. *Bioresour. Technol.* **2010**, *101*, 1285–1292.
(11) a) Ralph, J.; Lundquist, K.; Brunow, G.; Lu, F.; Kim, H.; Schatz, P. F.; Marita, J. M.; Hatfield, R. D.; Ralph, S. A.; Christensen, J. H.; Boerjan, W. *Phytochem. Rev.* **2004**, *3*, 29–60; b) Boerjan, W.; Ralph, J.; Baucher, M. *Annu. Rev. Plant Biol.* **2003**, *54*, 519–546.
(12) Manara, P.; Zabaniotou, A.; Vanderghem, C.; Richel, A. *Catal. Today* **2014**, *223*, 25−34.
(13) a) Adler, E. *Wood Sci. Technol.* **1977**, *11*, 169–218; b) Evtuguin, D. V.; Neto, C. P.; Silva, A. M. S.; Domingues, P. M.; Amado, F. M. L.; Robert, D.; Faix, O. *J. Agric. Food Chem.* **2001**, *49*, 4252−4261; c) Sakakibara, A. In *Wood and Cellulose Chemistry*; Hon, D. N.-S., Shiraishi, N.; Marcel Dekker Inc.: New York, 1991.
(14) a) Stewart, J. J.; Kadla, J. F.; Mansfield, S. D. *Holzforschung* **2006**, *60*, 111–122; b) Heikkinen, S.; Toikka, M. M.; Karhunen, P. T.; Kilpeläinen, I. A. *J. Am. Chem. Soc.* **2003**, *125*, 4362–4367; c) Pu, Y.; Cao, S.; Ragauskas, A. J. *Energy Environ. Sci.* **2011**, *4*, 3154-3166; d) Morreel, K.; Oana Dima, O.; Hoon Kim, H.; Lu, F.; Niculaes, C.; Vanholme, R.; Dauwe, R.; Goeminne, G.; Inzé, D.; Messens, E.; Ralph, J.; Boerjan, W. *Plant Physiol.* **2010**, *153*, 1464–1478.
(15) Bajpai, P. (2013). Biorefinery in the Pulp and Paper Industry. London, UK: Academic Press.

(16) a) Chakar, F. S.; Ragauskas, A. J. *Ind. Crops Prod.* **2004**, *20*, 131–141; b) Xiao, B.; Sun, X. F.; Sun, R. C. *Polym. Degrad. Stab.* **2001**, *74*, 307−319.
(17) Lin, S. Y.; Lin, I. S. In Ullmann's Encyclopedia of Industrial Chemistry; 5th ed.; VCH: Weinheim, Germany, 1990; Vol. 15, p 305.
(18) a) Scholze, B.; Hanser, C.; Meier, D. *J. Anal. Appl. Pyrolysis* **2001**, *387*, 58–59; b) El Hage, R.; Brosse, N.; Chrusciel, L.; Sanchez, C.; Sannigrahi, P.; Ragauskas, A. *Polym. Degrad. Stab.* **2009**, *94*, 1632−1638.
(19) a) Abdulkhani, A.; Karimi, A.; Mirshokraie, A.; Hamzeh, Y.; Marlin, N.; Mortha, G. *J. Appl. Polym. Sci.* **2010**, *118*, 469−479; b) Holtman, K. M.; Chang, H. M.; Kadla, J. F. *J. Agric. Food Chem.* **2004**, *52*, 720−726.
(20) a) Preti, L.; Attanasi, O. A.; Caselli, E.; Favi, G.; Ori, C.; Davoli, P.; Felluga, F.; Prati, F. *Eur. J. Org. Chem.* **2010,** *22*, 4312–4320; b) Corrie, J. E. T.; Lunazzi, L. *J. Chem. Soc., Perkin Trans.* **1993**, *2*, 1299–1304.
(21) Cho, D. W.; Parthasarathi, R.; Pimentel, A. S.; Maestas, G. D.; Park, H. J.; Yoon, U. C.; Dunaway-Mariano, D.; Gnanakaran, S.; Langan, P.; Mariano, P. S. *J. Org. Chem.* **2010**, *75*, 6549–6562.
(22) Pardini, V. L.; Smith, C. Z.; Utley, J. H. P.; Vargas, R. R.; Viertler, H. *J. Org. Chem.* **1991**, *56*, 7305–7313.
(23) Sedai, B.; Díaz-Urrutia, C; Baker, R. T.; Wu, R.; Silks, L. A. P.; Hanson, S. K. *ACS Catal.* **2013**, *3*, 3111–3122.
(24) Reddy, G. V. B.; Sridhar, M.; Gold, M. H. *Eur. J. Biochem*. **2003**, *270*, 284−292.
(25) a) Kusserow, B.; Schimpf, S.; Claus, P. *Adv. Synth. Catal.* **2003**, *345*, 289−299; b) Castoldi, M. C. M.; Camara, L. D. T.; Aranda, D. A. G. *React. Kinet. Catal. Lett.* **2009**, *98*, 83−89; c) Román-Leshkov, Y.; Barrett, C. J.; Liu, Z. Y.; Dumesic, J. A. *Nature* **2007**, *447*, 982−985.
(26) a) Trost, B. M. *Science* **1991**, *254*, 1471–1477; b) Trost, B. M. *Angew. Chem. Int. Ed. Eng.* **1995**, *34*, 259–281.
(27) a) Corma, A. Iborra, S. Velty, A. *Chem. Rev.* **2007**, *107*, 2411–2502; b) Zakzeski, J.; Bruijnincx, P. C. A.; Jongerius, A. L.; Weckhuysen, B. M. *Chem. Rev.* **2010**, *110*, 3552–3599; c) Li, C.; Zhao, X.; Wang, A.; Huber, G. W.; Zhang, T. *Chem. Rev.* **2015**, *115*, 11559−11624; d) M. P. Pandey and C. S. Kim, *Chem. Eng. Technol.* **2010**, *34*, 29–41; e) Deuss, P. J.; Barta, K. *Coord. Chem. Rev.* **2016**, *306*, 510–532.
(28) a) Sergeev, A. G.; Hartwig, J. F. *Science* **2011**, *332*, 439–443; b) Sergeev, A. G.; Webb, J. D.; Hartwig, J. F. *J. Am. Chem. Soc.* **2012**, *134*, 20226–20229.
(29) Kelley, P.; Lin, S.; Edouard, G.; Day, M.W.; Agapie, T. *J. Am. Chem. Soc.* **2012**, *134*, 5480–5483.
(30) Ren, Y.; Yan, M.; Wang, J.; Zhang, Z. C.; Yao, K. *Angew. Chem. Int. Ed.* **2013**, *52*, 12674 –12678.
(31) Nichols, J. M.; Bishop, L. M.; Bergman, R. G.; Ellman, J. A. *J. Am. Chem. Soc.* **2010**, *132*, 12554–12555.
(32) Wu, A.; Patrick, B. O.; Chung, E.; James, B. R. *Dalton Trans.* **2012**, *41*, 11093–11106.
(33) vom Stein, T.; Weigand, T.; Merkens, C.; Klankermayer, J.; Leitner, W. *ChemCatChem* **2013**, *5*, 439–441.

(34) a) Bähn, S.; Imm, S.; Neubert, L.; Zhang, M.; Neumann, H.; Beller, M. *ChemCatChem* **2011**, *3*, 1853 –1864; b) J. Moran, M. J. Krische, *Pure Appl. Chem.* **2012**, *84*, 1729– 1739.
(35) Weickmann, D.; Plietker, B. *ChemCatChem* **2013**, *5*, 2170–2173.
(36) Nagy, M.; David, K.; Britovsek, G. J. P.; Ragauskas, A. J. *Holzforschung* **2009**, *63*, 513–520.
(37) Haibach, M. C.; Lease, N.; Goldman, A. S. *Angew. Chem. Int. Ed.* **2014**, *53*, 10160–10163.
(38) a) Gasser, C. A.; Hommes, G.; Schäffer, A.; Corvini, P. F-X. *Appl. Microbiol. Biotechnol.* **2012**, *95*, 1115–1134; b) Hofrichter, M. *Enzyme Microb. Technol.* **2002**, *30*, 454–466.
(39) a) Hedges, J. I.; Ertel, J. R. *Anal. Chem.* **1982**, *54*, 174–178; b) Hedges, J. I.; Mann, D. C. *Geochim. Cosmochim. Acta* **1979**, *43*, 1809–1818.
(40) a) Wacek, A.; Kratzl, K. *J. Polym. Sci.* **1948**, *3*, 539–548; b) Chang, H.-M.; Allan, G.G. In Lignins - Occurrence, Formation, Structure and Reactions. K.V. Sarkanen and C.H. Ludwig, Eds. John Wiley and Sons, NY, 1971; pp. 433–485; c) Schultz, T. P.; Templeton, M. C. *Holzforschung* **1986**, *40*, 93–97.
(41) a) Rahimi, A.; Azarpira, A.; Kim, H.; Ralph, J.; Stahl, S.S. *J. Am. Chem. Soc.* **2013**, *135*, 6415–6418; b) Rahimi, A.; Ulbrich, A.; Coon, J. J.; Stahl, S. S. *Nature* **2014**, *515*, 249–252.
(42) a) Sheldon, R. A.; Arends, I. W. C. E. *J. Mol. Catal. A: Chem.* **2006**, *251*, 200–214; b) Ryland, B. L.; Stahl, S. S. *Angew. Chem. Int. Ed.* **2014**, *53*, 8824–8838.
(43) a) Sedai, B.; Baker, R. T. *Adv. Synth. Catal.* **2014**, *356*, 3563–3570; b) Sedai, B.; Díaz-Urrutia, C; Baker, R. T.; Wu, R.; Silks, L. A. P.; Hanson, S. K. *ACS Catal.* **2011**, *1*, 794–804; c) Díaz-Urrutia, C.; Sedai, B.; Leckert, K.; Baker, R. T.; Hanson, S. K. *ACS Sustainable Chem. Eng. **2016**, submitted;* d) Díaz-Urrutia, C.; Chen, W-C.; Crites, C.-O.; Daccache, J.; Korobkov, I.; Baker, R. T. *RSC Adv.* **2015**, *5*, 70502–70511.
(44) a) Bozell, J. J.; Hames, B. R.; Dimmel, D. R. *J. Org. Chem.* **1995**, *60*, 2398−2404; b) Biannic, B.; Bozell, J. J. *Org. Lett.* **2013**, *15*, 2730–2733.
(45) Collins, T. J. *Acc. Chem. Res.* **2002**, *35*, 782–790.
(46) a) Napoly, F.; Jean-Gérard, L.; Goux-Henry, C.; Draye, M.; Andrioletti, B. *Eur. J. Org. Chem.* **2014**, 781–787; T. J. Collins, C P. Horwitz, U. S. Patent 6,241,779, issue date: June 5, **2001**.
(47) Mottweiler, J.; Rinesch, T.; Besson, C.; Buendia, J.; Bolm, C. *Green Chem.* **2015**, *17*, 5001–5008.
(48) a) Alves, V.; Capanema, E.; Chen, C-L.; Gratzl, J. *J. Mol. Catal. A: Chem.* **2003**, *206*, 37–51; b) Zucca, P.; Mocci, G.; Rescigno, A.; Sanjust, E. *J. Mol. Catal. A: Chem.* **2007**, *278*, 220–227; c) Cui, Y.; Chen, C-L.; Gratzl, J. S.; Patt, R. *J. Mol. Catal. A: Chem.* **1999**, *144*, 411–417.
(49) Zhu, C.; Ding, W.; Shen, T.; Tang, C.; Sun, C.; Xu, S.; Chen, Y.; Wu, J.; Ying, H. *ChemSusChem* **2015**, *8*, 1768–1778.
(50) a) Lange, H.; Decina, S.; Crestini, C. *Eur. Polym. J.* **2013**, *49*, 1151−1173; b) Oasmaa, A; Johansson, A. *Energy Fuels* **1993**, *7*, 426–9.
(51) Harms, R. G.; Markovit, I. E. I.; Drees, M.; Herrmann, W. A.; Cokoja, M.; Kühn, F. E. *ChemSusChem* **2014**, *7*, 429–434.

(52) a) Son, S.; Toste, F. D. *Angew. Chem. Int. Ed.* **2010**, *49*, 3791–3794; b) Chan, J. M. W.; Bauer, S.; Sorek, H.; Sreekumar, S.; Wang, K.; Toste, F. D. *ACS Catal.* **2013**, *3*, 1369–1377.
(53) Gazi, S.; Ng, W. K. H.; Ganguly, R.; Moeljadi, A. M. P.; Hirao, H.; Soo, H. S. *Chem. Sci.* **2015**, *6*, 7130–7142.
(54) Nguyen, J. D.; Matsuura, B. S.; Stephenson, C. R. J. *J. Am. Chem. Soc.* **2014**, *136*, 1218−1221.
(55) vom Stein, T.; Hartog, T.; Buendia, J.; Stoychev, S.; Mottweiler, J.; Bolm, C.; Klankermayer, J.; Leitner, W. *Angew. Chem. Int. Ed.* **2015**, *54*, 5859–5863.
(56) Deuss, P. J.; Scott, M.; Tran, F.; Westwood, N. J.; de Vries, J. G.; Barta, K. *J. Am. Chem. Soc.* **2015**, *137*, 7456–7467.
(57) InfoMine Home Page. http://www.infomine.com/investment (accessed January 9, 2015)
(58) a) Richards, R. L. Vanadium: Inorganic and Coordination Chemistry. In *Encyclopedia of Inorganic Chemistry;* Scott, R. A., Ed.; Wiley: New York, 2006; b) Ligtenbarg, A. G. J.; Hage, R.; Feringa, B. L. *Coord. Chem. Rev.* **2003**, *237*, 89–101; c) Amadio, E.; Di Lorenzo, R.; Zonta, C.; Licini, G. *Coord. Chem. Rev.* **2015**, *301*, 147–162.
(59) a) Mimoun, H.; Mignard, M.; Brechot, P.; Saussine, L. *J. Am. Chem. Soc.* **1986**, *108*, 3711–3718; b) Mimoun, H.; Saussine, L.; Daire, E.; Postel, M.; Fischer, J.; Weiss, R. *J. Am. Chem. Soc.* **1983**, *105*, 3101–3110; c) Mimoun, H.; Chaumette, P.; Mignard, M.; Saussine, L.; Fischer, J.; Weiss, R. *Nou*v. *J. Chim.* **1983**, *7*, 467–475.
(60) Thorn, D. L.; Harlow, R. L.; Herron, N. *Inorg. Chem.* **1996**, *35*, 547–548.
(61) Hanson, S. K.; Baker, R. T. *Acc. Chem. Res.* **2015**, *48*, 2037−2048.
(62) a) Hanson, S. K.; Baker, R. T.; Gordon, J. C.; Scott, B. L.; Sutton, A. D.; Thorn, D. L. *J. Am. Chem. Soc.* **2009**, *131*, 428−429; b) Hanson, S. K.; Baker, R. T.; Gordon, J. C.; Scott, B. L.; Silks, L. A. P.; Thorn, D. L. *J. Am. Chem. Soc.* **2010**, *132*, 17804–17816; c) Hanson, S. K.; Baker, R. T.; Gordon, J. C.; Scott, B. L.; Thorn, D. L. *Inorg. Chem.* **2010**, *49*, 5611−5618; d) Hanson, S. K.; Wu, R.; Silks, L. A. P. *Org. Lett.* **2011**, *13*, 1908–1911; e) Hanson, S. K.; Wu, R.; Silks, L. A. P. *Angew. Chem. Int. Ed.* **2012**, *51*, 3410−3413; f) Wigington, B. N.; Drummond, M. L.; Cundari, T. R.; Thorn, D. L.; Hanson, S. K.; Scott, S. L. *Chem. Eur. J.* **2012**, *18*, 14981–14988; g) Zhang, G.; Scott, B. L.; Wu, R.; Silks, L. A. P.; Hanson, S. K. *Inorg. Chem.* **2012**, *51*, 7354−7361.

Chapter 2: Selective Aerobic Oxidation of β-O-4 and β-1 Lignin Model Compounds Using Vanadium Catalysts

This chapter has been partially published in: a) Sedai, B.; Díaz-Urrutia, C.; Baker, R. T.; Wu, R.; Silks, L. A.; Hanson, S. K. ACS Catal. ***2011****, 1, 794–804; b) Sedai, B.; Díaz-Urrutia, C.; Baker, R. T.; Wu, R.; Silks, L. A.; Hanson, S. K. ACS Catal.* ***2013****, 3, 3111–3122.*

2.1 Introduction

Lignin valorization requires efficient catalytic systems (*e.g.*, low catalyst loadings, inexpensive metals and ligands) with superior selectivity for the production of high value-added chemicals and materials. The study of lignin depolymerization has been facilitated by the use of lignin model compounds containing the most predominant β-O-4 and β-1 linkages (Figure 2.1) accounting for nearly 50% and 9% in different type of woods, respectively.[1] As discussed in *Chapter 1*, several approaches for the disassembly of lignin models have been utilized such as reductive and oxidative methods using both homogeneous and heterogeneous catalysts (see section 1.3 for more details). However, in order to use air as the terminal oxidant, inexpensive first row transition metal catalysts offer a promising approach.

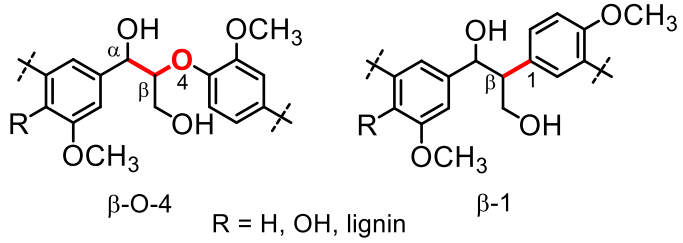

Figure 2.1. Phenolic and non-phenolic β-O-4 and β-1 linkages in lignin.

Previously, Hanson and Baker successfully developed several oxovanadium(V) catalysts (Figure 2.2), together with the addition of exogenous base, for the selective cleavage of C-H, C-O and C-C bonds, respectively, in lignin model compounds such as **LM1**, **LM2** and **LM3** (Figure 2.2).[2] One of the most important observations about the performance of catalyst **OV1** is the solvent dependence for the selective bond cleavage of **LM2**.[2c] In basic solvents such as pyridine, **OV1** affords predominately C-H bond cleavage to give the ketone product. In contrast, using less basic solvents like DMSO, catalyst **OV1** gives a mixture of C-C and C-H bond cleavage products (see section 1.4.2 for more details).

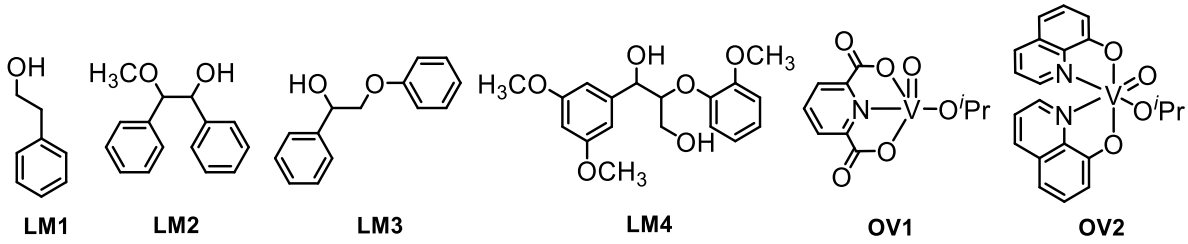

Figure 2.2. Simple and complex β-O-4 lignin models, and oxovanadium(V) catalysts.

Inspired by the diverse reactivity of oxovanadium catalysts, the aim of this *Chapter* is to expand the substrate scope with simple and complex β-O-4 (**LM2** and **LM4**, Figure 2.2) and β-1 lignin models (**LM6-9**, Figure 2.3) using 5- and 6-coordinate oxovanadium(V) catalysts **OV1** and **OV2**, respectively. Synthesis of lignin model compounds, mechanistic implications, as well as catalyst optimization and product distribution will also be discussed.

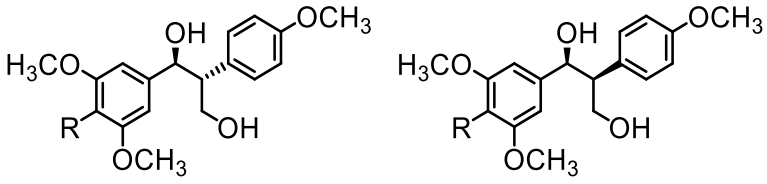

Figure 2.3. Phenolic and non-phenolic β-1 lignin models.

2.2 Material and Methods

2.2.1 General Considerations

Unless specified otherwise, all reactions were carried out in the presence of air. Triethylamine (Et_3N), dimethylsulfoxide (DMSO), dichloromethane (DCM), tetrahydrofuran (THF), ethyl acetate (EtOAc), hexane, toluene, 3,5-dimethoxy-benzaldehyde and 2-methoxyphenol were purchased from Sigma Aldrich or Fisher Scientific and used without further purifications. *n*-Butyllithium, diisopropylamine and ethyl bromoacetate were purchased from Sigma Aldrich and stored under air-free conditions. Acetonitrile, methanol (HPLC grade chromasolv©), were purchased from Sigma Aldrich or Alfa Aesar. All other reagents were used as received. Toluene was dried on columns of activated alumina using a J. C. Meyer solvent purification system. Deuterated solvents were purchased from Cambridge Isotope Laboratories and pyridine-d_5 was dried over CaH_2. ^{1}H, ^{13}C, and ^{51}V NMR spectra were obtained at room temperature on a Bruker AV300 MHz or AV400 MHz spectrometer, with chemical shifts (δ) referenced to the residual solvent signal or externally to $V(O)Cl_3$ (0 ppm). GC-MS analysis was performed using a Hewlett-Packard 6890 GC system equipped with a Hewlett-Packard 5973 mass selective detector. HPLC-MS analyses were conducted on a Dionex Ultimate 3000 Liquid Chromatograph coupled with an Applied Biosystem API2000 triple quadrupole mass spectrometer (LCMS delay 0.27 min), using a reversed-phase gradient column (RSLC PA2 2.2 μm 120 Å, 2.1 x 150 mm) and 0.5% acetic acid in H_2O, acetonitrile/methanol as mobile phases. The analysis employed a DAD UV-vis (Diode Array) detector or the mass spectrometer (Q1MS) with electrospray ionization (ESI-MS) in positive mode (ion spray voltage: 5000.0 V, TEM: 400.0 ºC, declustering potential: 11.00 V and focusing potential: 300.0 V). The oxovanadium complexes **OV1**,[3] **OV2**[2d] and **OVS,**[4] ^{13}C-labeled **LM4**-$^{13}C_2$[5a] and the β-1 lignin models **LM6-7**[5b] were prepared using published procedures.

2.2.2 Synthesis of 1,2-Diphenyl-2-methoxyethanol LM2

Despite the commercial availability of the lignin model compound **LM2**, most of the suppliers provide a contaminated sample containing traces of benzaldehyde and benzoic acid. **LM2** was prepared following the published procedure.[2c] Additionally, **LM2** can be

synthesized by reducing benzoin methyl ether, affording high yields from inexpensive starting materials. In a 500 mL round-bottom flask, benzoin methyl ether (8.00 g, 35.3 mmol) was dissolved in 250 mL of dry methanol. The mixture was treated with small portions of $NaBH_4$ (667 mg, 17.6 mmol) cooling with a cold water bath and then stirring for 1 h. The solution turned colourless indicating completion of the reaction. A saturated solution of NH_4Cl (20 mL) followed by 50 mL of DCM was then added. The organic layer was extracted, washed with water, dried with $MgSO_4$ and concentrated on a rotary evaporator to give a white powder. The crude white product was recrystallized in hot ethanol to give 6.57 g (82%) of 1,2-diphenyl-2-methoxyethanol. Integration of the benzylic protons in the ^1H NMR spectrum showed that the product was a mixture of 85:15 *erythro* (R,S + S,R): *threo* (R,R + S,S) diastereomers as observed in a previous related synthesis.[2c] ^1H (300 MHz, $CDCl_3$): δ 7.33-7.23 (ov m, 6H, Ar, *erythro* isomer), 7.23-7.12 (ov m, 5H, Ar, *erythro* + *threo* isomer), 7.08-6.99 (ov m, 6H, Ar, *threo* isomer), 4.91 (d, 1H, *J* = 5.5 Hz, CH *erythro* isomer), 4.67 (d, 1H, *J* = 8.4 Hz, CH *threo* isomer), 4.36 (d, 1H, *J* = 5.5 Hz, CH *erythro* isomer), 4.15 (d, 1H, *J* = 8.4 Hz, CH *threo* isomer), 3.48 (s, 3H, OCH_3, *erythro* isomer), 3.33 (s, 3H, OCH_3, *threo* isomer).

2.2.3 Synthesis of 1-(3,5-Dimethoxyphenyl)-2-(2-methoxyphenoxy)propane-1,3-diol LM4

The synthesis of the building block of lignin model ethyl 2-(2-methoxyphenoxy)-acetate (**BBLM1**) was carried out in a 250 mL single necked round-bottom flask. 2-Methoxyphenol (6.207 g, 50.00 mmol), K_2CO_3 (7.602 g, 55.00 mmol), and ethyl bromoacetate (8.872 g, 52.50 mmol) were suspended in dry acetone (100 mL) and the reaction mixture was stirred overnight. Examination of the solution by ^1H NMR spectroscopy indicated partial completion. Refluxing for an additional 24 h gave rise to a complete reaction. The reaction solvent was removed and the residue was purified by flash column chromatography using 10% ether/hexanes (v/v) to give 10.575 g (100%) of a colourless oil.

Initial attempts to prepare the diastereomers of ethyl 3-hydroxy-3-(3,5-dimethoxyphenyl)-2-(2-methoxyphenoxy)-propanoate (**BBLM2**) using a previously published procedure did not give appreciable yields of this compound.[6] However, using an alternate procedure reported by Son and Toste afforded the aldol product in high yield.[4] A THF solution (30 mL) of diisopropyl amine (3.1 mL, 22 mmol) was cooled to 0 ^oC under

nitrogen, and *n*-butyllithium (8.8 mL of a 2.5 M solution in hexanes, 22 mmol) was added dropwise. The mixture was stirred at 0 ^{o}C for 20 min and then chilled to -78 ^{o}C. A solution of ethyl 2-(2-methoxyphenoxy)-acetate in THF (20 mL) was added dropwise *via* cannula, followed by dropwise cannula addition of a solution of 3,5-dimethoxybenzaldehyde (3.32 g, 20.0 mmol) in THF (10 mL). The mixture was stirred at -78 ^{o}C for 1.5 h. A saturated aqueous solution of NH_4Cl (10 mL) was then added, the solution was allowed to warm to room temperature, and the solution was extracted with ethyl acetate (3 x 20 mL). The extracts were combined, the solvent was removed under vacuum, and the residue was purified by silica gel flash chromatography (25% EtOAc/hexanes) to give 0.557 g of a first fraction and 6.818 g (90%) of a second fraction that contained the product, a mixture of the *threo* and *erythro* isomers which was a colourless syrup. The major diastereomer is assigned as the *erythro* form based on comparison with the closely related compounds *erythro*- and *threo*-ethyl 3-hydroxy-3-(3,4-dimethoxyphenyl)-2-(2-methoxyphenoxy)-propanoate.[6]

The synthesis of 1-(3,5-Dimethoxyphenyl)-2-(2-methoxyphenoxy)propane-1,3-diol **LM4** was carried out by dissolving the mixture of diastereomers of ethyl 3-hydroxy-3-(3,4-dimethoxyphenyl)-2-(2-methoxyphenoxy)-propanoate (3.78 g, 10.0 mmol), in a THF/water mixture (33 mL/11 mL). To this was added solid $NaBH_4$ (1.89 g, 50.0 mmol)[4] at ambient temperature, and the reaction mixture was stirred overnight, until thin layer chromatography (TLC) analysis indicated the absence of starting material. The mixture was then extracted with ethyl acetate (3 x 20 mL) and dried over Na_2SO_4. Filtration followed by removal of the solvent under vacuum gave rise to the crude material. Purification by silica gel flash chromatography using 60% ethyl acetate/hexane afforded 2.924 g (87%) of the diol diastereomers (4:1) as a colourless syrup. The major diastereomer is assigned as the *erythro* isomer, based on comparison of the ^{1}H and ^{13}C NMR data with the closely related reported compounds *erythro*- and *threo*-(1-(3,4-dimethoxyphenyl)-2-(2-methoxy-phenoxy)propane-1,3-diol[6] and (1R*,2S*)-1-(4-ethoxy3-methoxyphenyl)-2-(2-methoxy-phenoxy)propane-1,3-diol.[4] ^{1}H NMR (400 MHz, $CDCl_3$): δ 7.12-6.88 (m, 6H, aryl), 6.61 (d, 2H, *J* = 2.0 Hz, aryl of minor diastereomer), 6.55 (d, 2H, *J* = 2.0 Hz, aryl of major diastereomer), 6.40 (t, 1H, *J* = 2.0 Hz, aryl of minor diastereomer), 6.37 (t, 1H, *J* = 2.0 Hz, aryl of major diastereomer), 4.98-4.95 (br m, 1H, OH), 4.20-4.17 (m, 1H, CHOH of major

diastereomer), 4.08-4.04 (m, 1H, CHOH of minor diastereomer), 3.94-3.64 (m, 3H, CH_2OH and CHOAr), 3.88 (s, 3H, -OCH_3 of minor diastereomer), 3.86 (s, 3H, -OCH_3 of major diastereomer), 3.77 (s, 6H, -OCH_3 of minor diastereomer), 3.76 (s, 6H, -OCH_3 of major diastereomer), 3.54 (br s, 1H, -OH of minor diastereomer), 2.96 (br s, 1H, -OH of major diastereomer). $^{13}C\{^1H\}$ NMR (100 MHz, $CDCl_3$), major diastereomer: δ 161.0, 151.7, 146.9, 142.6, 124.3, 121.8, 121.0, 112.3, 104.2, 99.8, 87.2, 73.0, 60.8, 55.5; minor diastereomer: δ 161.0, 151.3, 147.8, 142.3, 124.2, 121.8, 121.0, 112.3, 105.1, 100.4, 89.1, 74.3, 61.3, 56.0. HRMS (EI): m/z calcd for $C_{18}H_{23}O_6$ $[M+H]^+$: 335.1495, found: 335.1504.

2.2.4 Oxidation of Benzoin Methyl Ether OP1 Using OV1 in Air

In an NMR tube, the oxidation product benzoin methyl ether **OP1** (32 mg, 0.14 mmol) and **OV1** (5.0 mg, 0.014 mmol) were dissolved in pyr-d_5 (1 mL) containing dimethylsulfone (8 mM) as an internal standard. An initial spectrum was recorded, and then the reaction mixture was transferred to a 50 mL round-bottom flask. The flask was equipped with a stir bar and an air condenser and heated at 100 ºC for 48 h. The mixture was then cooled to room temperature and transferred to an NMR tube. Integration of the ^1H NMR spectrum against the internal standard revealed that *ca.* 96% of the starting material had been consumed. The products of the reaction consisted of benzoic acid (90%), methyl benzoate (90%), and benzil (<10%). The identity of the products was confirmed by comparison with commercial samples of the authentic compounds.

2.2.5 Oxidation of OP1 in Air with No Catalyst

In an NMR tube, benzoin methyl ether **OP1** (43 mg, 0.19 mmol) was dissolved in pyr-d_5 (0.9 mL) containing dimethylsulfone (7 mM) as an internal standard. An initial ^1H NMR spectrum was recorded, and then the solution was transferred to a 50 mL round-bottom flask equipped with a stir bar and an air condenser. The reaction was heated at 100 ºC for 48 h, cooled to room temperature, and the reaction mixture transferred to an NMR tube. Integration against the internal standard revealed that 43% of the starting material had been consumed, affording benzoic acid (39%), methyl benzoate (34%), benzil (8%), and methanol. Trace benzaldehyde (1% or less) was also present in the spectrum.

2.2.6. General Procedure for the Catalytic Oxidation of β-O-4 and β-1 Lignin Model

The desired lignin model was dissolved in 1 mL of the appropriate solvent (pyr-d_5, DMSO-d_6 or toluene) containing dimethylsulfone (3 mM) or 1,3,5-trimethylbenzene (6 μL) as an internal standard. An initial spectrum was recorded, and then the solution was transferred under air to a 50 mL round-bottom flask containing the catalyst. The flask was equipped with a reflux condenser and stir bar, and the reaction was heated at 100 °C for 48 h. The reaction was cooled to room temperature, the solution was transferred to an NMR tube, and a final NMR spectrum was recorded. Yields were determined by integration against the internal standard and calculated from an average of two runs of this type. Yields are expressed as a percentage of the theoretical maximum based on the initial amount of substrate.

2.3 Results

2.3.1 Catalytic Oxidation of Simple β-O-4 Lignin Model Compounds

Previous work investigating the catalytic oxidation of 1,2-diphenyl-2-methoxyethanol **LM2** with air and **OV1** (10 mol%) in pyridine found that initial alcohol oxidation to the oxidation product ketone benzoin methyl ether **OP1** (45% overall yield at 56% conversion) was followed by C-C bond cleavage and further oxidation to benzoic acid (85%) and methyl benzoate (84%).[2c] Benzaldehyde (9%), methanol (6%), benzil (<5%), and benzoin (<5%) were formed as minor products in the reaction.[2c] The viability of **OP1** as an intermediate in the formation of benzoic acid and methyl benzoate was confirmed by a subsequent experiment involving oxidation of **OP1** with air using **OV1** (10 mol%) in pyridine-d_5. After 48 h at 100 °C, 96% conversion of **OP1** was observed, affording benzoic acid (90%) and methyl benzoate (90%) as the major products (Scheme 2.1). Benzil was

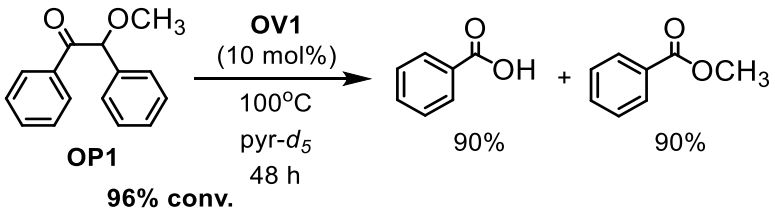

Scheme 2.1. Aerobic oxidation of benzoin methyl ether **OP1** with catalyst **OV1**.

also detected as a minor product in this reaction (*ca.* 6%), but neither benzaldehyde nor methanol were detected (^{1}H NMR spectroscopy). Compound **OP1** is also subject to aerobic oxidation under air with no added catalyst, albeit at a slower rate. In a control experiment, compound **OP1** was heated under air in pyr-d_5 with no catalyst. After 48 h at 100 ^{o}C, 43% conversion was observed, with the major products consisting of benzoic acid (39%), methyl benzoate (34%), benzil (8%), and methanol.

2.3.2 Catalytic Oxidation of Complex β-O-4 Lignin Model Compounds

A variety of compounds have been studied as models for the β-O-4 linkage.[7-25] The lignin model compound 1-(3,5-dimethoxyphenyl)-2-(2-methoxyphenoxy)propane-1,3-diol-[2,3-$^{13}C_2$] **LM4**-$^{13}C_2$ was selected as a synthetic target as it was anticipated that incorporation of ^{13}C labels into the positions β- and γ- to the benzylic alcohol group could help identify reaction products derived from the β- and γ-carbons. Previous studies of lignin model compound oxidations suggest that it is often difficult to determine the oxidation products that result from this portion of the molecule.[20,21] Hammel and co-workers have demonstrated that selective labeling (^{14}C and ^{13}C) of the substrate facilitated product analysis in the enzymatic oxidation.[19,21] Compound **LM4**-$^{13}C_2$ is similar to previously reported lignin model compounds,[4,6,26] and was prepared as a 4:1 mixture of diastereomers (*erythro*: *threo*) in three steps from ethyl bromo-[1,2-$^{13}C_2$]-acetate, following a reported version published elsewhere.[5] The major diastereomer is assigned as the *erythro* isomer, based on comparison of the ^{1}H and ^{13}C NMR data with the closely related reported compounds *erythro*- and *threo*-1-(3,4-dimethoxyphenyl)-2-(2-methoxyphenoxy)propane-

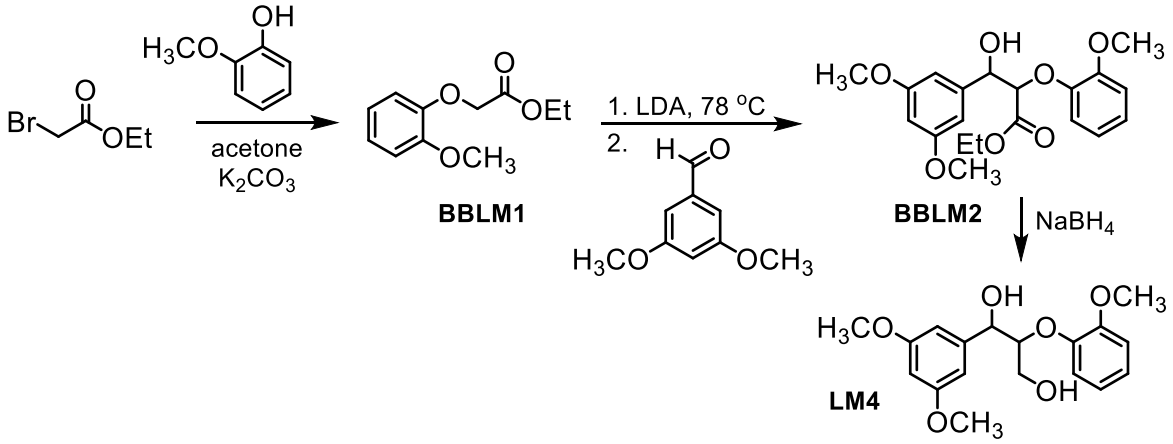

Scheme 2.2. Synthesis of unlabeled β-aryl glycerol lignin model **LM4**.

1,3-diol[6] and (1R*,2S*)-1-(4-ethoxy-3-methoxyphenyl)-2-(2-methoxyphenoxy)propane-1,3-diol.[4] An identical procedure was used for the preparation of a diastereomeric mixture of the unlabeled analogue **LM4** (Scheme 2.2, see section 2.2.3 for experimental details). The structural assignment for **LM4** and **LM4**-$^{13}C_2$ was confirmed by ^{1}H and ^{13}C NMR spectroscopy and high resolution mass spectroscopy (HRMS).

Vanadium complexes **OV1** and $V^{V}(O)(O^{i}Pr)_3$ were tested as catalysts for the aerobic oxidation of **LM4**-$^{13}C_2$. When lignin model **LM4**-$^{13}C_2$ was heated under air with **OV1** (10 mol%) in DMSO-d_6 solvent at 100 ^{o}C for 48 h, complete conversion of the starting material was observed. Examination of the ^{1}H and ^{13}C NMR spectra of the reaction mixture[5a] revealed the formation of a mixture of products, including ketone **OP2**-$^{13}C_2$ (65%), dehydrated ketone **OP3**-$^{13}C_2$ (5%), alkene **OP4**-$^{13}C_2$ (14%), 3,5-dimethoxybenzaldehyde (**OP6**) (2%), formic acid-$^{13}C_1$ (**OP7**-$^{13}C_1$) (4%), and 3,5 dimethoxybenzoic acid (**OP8**) (11%) (Scheme 2.3). Consideration of the yields of the products derived from the 3,5-

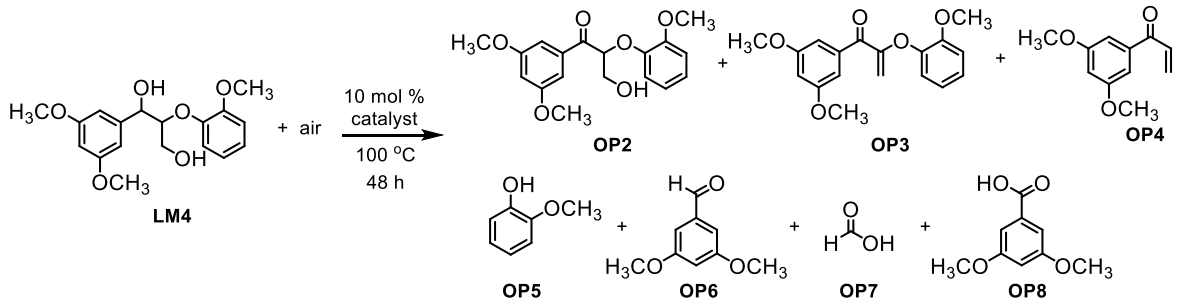

	Solvent[a]	Conv.(%)	**OP2**	**OP3**	**OP4**	**OP5**	**OP5**	**OP7**	**OP8**
OV1	DMSO-d_6	> 95	65	5	14	n.d.[b]	2	11	4
OV1	pyr-d_5	*ca.* 85	27	14	29	n.d.	4	6	< 1
$V(O)(O^{i}Pr)_3$	DMSO-d_6	*ca.* 75	39	ND	16	n.d.	7	7	12

[a]100 °C, 48 h; [b]n.d.= not detected

Scheme 2.3. Catalytic oxidation of β-O-4 lignin models using **OV1**.

dimethoxyarene ring (**OP2**, **OP3**, **OP4**, **OP6**, and **OP8**) shows that the carbon balance is about 95% for this portion of the original lignin model compound.[27] The mass balance for the remainder of the molecule is not as good; formic acid-$^{13}C_1$ is formed as a co-product, most likely arising from a deeper oxidation of the labeled β- and γ-carbons. 2-Methoxyphenol (**OP5**) was also detected as a product by GC-MS, but it was not possible to quantify by ^{1}H NMR because of overlap with resonances from the other products. Carbon

dioxide-$^{13}C_1$ could also potentially be formed as a product; this would be difficult to detect under the reaction conditions (air).

The identity of the products was confirmed by carrying out the reaction on a larger scale; ketone **OP2**-$^{13}C_2$, dehydrated ketone **OP3**-$^{13}C_2$, and alkene **OP4**-$^{13}C_2$ were isolated and characterized by ^{1}H and ^{13}C NMR spectroscopy and HRMS.[28] Ketone **OP2**-$^{13}C_2$ displays resonances in the $^{13}C\{^1H\}$ NMR spectrum ($CDCl_3$) at 84.7 and 63.7 ppm ($^1J_{C\text{-}C}$ = 38 Hz), as well as a characteristic resonance in the ^{1}H NMR spectrum for the proton on the labeled carbon adjacent to the ketone, which appears as a multiplet at 5.42 ppm with $^1J_{C\text{-}H}$ = 148 Hz. The $^{13}C\{^1H\}$ NMR spectrum of dehydrated ketone **OP3**-$^{13}C_2$ shows signals at 157.7 and 101.5 ppm ($^1J_{C\text{-}C}$ = 82 Hz), while the ^{1}H NMR spectrum shows signals for the olefinic protons at 5.25 ($^1J_{C\text{-}H}$ = 165 Hz) and 4.79 ($^1J_{C\text{-}H}$ = 160 Hz) ppm. Alkene **OP4**-$^{13}C_2$ shows ^{13}C NMR resonances at 132.6 and 130.4 ppm ($^1J_{C\text{-}C}$ = 69 Hz). The vinylic protons on **OP4**-$^{13}C_2$ appear as complex multiplets centered at 7.11, 6.45, and 5.93 ppm. Alkene **OP4** is the product of a C-O bond cleavage reaction analogous to that previously reported by Son and Toste (Scheme 2.4).[4] To determine whether ketone **OP2**-$^{13}C_2$ was an interme-

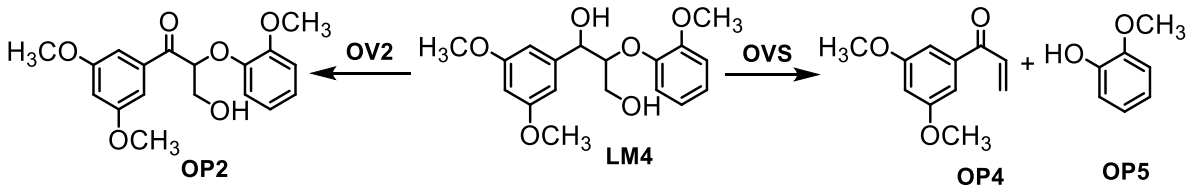

Scheme 2.4. Salen-vanadium catalyst **OVS** affords different selectivity compared with oxovanadium catalysts **OV1** and **OV2**.

diate in the formation of any of the other products, the oxidation of an isolated sample of **OP2**-$^{13}C_2$ with air was tested using **OV1** (10 mol%) in DMSO-d_6 solvent at 100 ^{o}C. After 48 h, examination of the ^{1}H and ^{13}C NMR spectra of the reaction mixture[5a] showed that approximately 40% of the ketone had been consumed, affording dehydrated ketone **OP3**-$^{13}C_2$ (14%), 3,5-dimethoxybenzoic acid (19%) and formic acid-$^{13}C_1$ (7%) (Scheme 2.5). 2-Methoxyphenol was also detected as a product by GC-MS. In a control experiment in the absence of the vanadium catalyst, where the ketone **OP2**-$^{13}C_2$ was heated under air in DMSO-d_6 at 100 ^{o}C for 48 h, no reaction occurred.

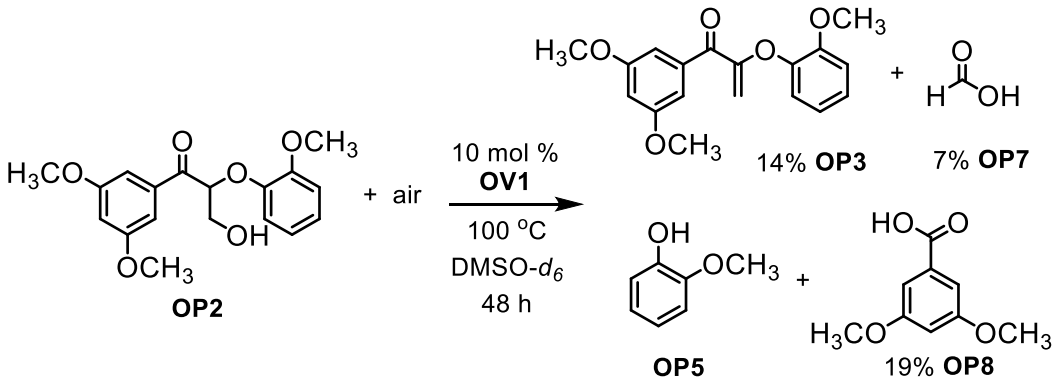

Scheme 2.5. Oxidation of ketone intermediate **OP2** using **OV1**.

Compared to the dipicolinate vanadium complex **OV1**, $V^{V}(O)(O^{i}Pr)_3$ was a somewhat slower catalyst for the aerobic oxidation of **LM4**-$^{13}C_2$.When a solution of **LM4**-$^{13}C_2$ and $V^{V}(O)(O^{i}Pr)_3$ (10 mol%) was heated under air in DMSO-d_6 solvent at 100 °C for 48 h, approximately 75% of the starting material was consumed, as judged by integration of the ^{1}H NMR resonances against an internal standard (Scheme 2.3). The primary products of the oxidation were the ketone **OP2**-$^{13}C_2$ (39%), the alkene product **OP4**-$^{13}C_2$ (16%), 3,5-dimethoxybenzoic acid (12%), 3,5-dimethoxybenzaldehyde (7%), and formic acid-$^{13}C_1$ (7%).

Carrying out the oxidation of **LM4**-$^{13}C_2$ with the dipicolinate vanadium complex **OV1** in a different solvent (pyr-d_5) had a significant impact on the product distribution, increasing the yields of the alkene product **OP4**-$^{13}C_2$ and dehydrated ketone **OP3**-$^{13}C_2$ relative to ketone **OP2**-$^{13}C_2$. Heating **LM4**-$^{13}C_2$ with **OV1** (10 mol%) in pyr-d_5 solvent under air resulted in approximately 85% conversion of the starting material, affording **OP2**-$^{13}C_2$ (27%), **OP3**-$^{13}C_2$ (14%), **OP4**-$^{13}C_2$ (29%), **OP6** (4%), and **OP8** (6%). 2-Methoxyphenol (**OP5**) was also detected in the GC-MS trace of the reaction. Using catalyst **OV1**, a signal corresponding to the *cis*-dioxo vanadium(V) complex $[(dipic)V^{V}(O)_2]^-$ (related compound to **OV9**)[2c] was detected at -518 ppm by ^{51}V NMR at the end of the reactions in both DMSO-d_6 and pyr-d_5 solvent. No signals were observed in the ^{51}V NMR spectrum of the oxidation reaction carried out using $V^{V}(O)(O^{i}Pr)_3$ in DMSO-d_6 solvent.

2.3.3 Catalytic Oxidation of Non-phenolic β-1 Lignin Model Compounds

To identify potential selectivity differences that could arise between β-O-4 and β-1 lignin model compounds, the six-coordinate vanadium complex **OV2** was tested as a

catalyst for the aerobic oxidation of non-phenolic β-1 lignin models **LM6** and **LM8** in pyridine solvent. When **LM6** was heated with 10 mol% of the catalyst under air at 100 °C (pyr-d_5, 48 h), complete conversion of the starting material was observed, as judged by integration of the ^{1}H NMR resonances against an internal standard (Scheme 2.6). The

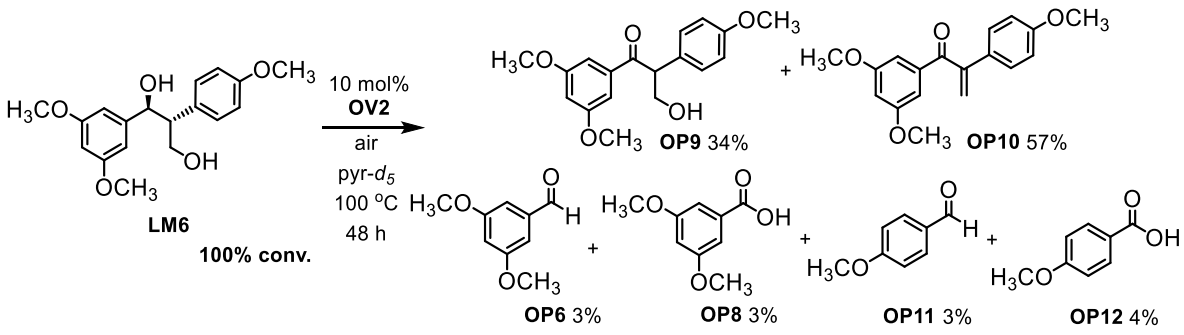

Scheme 2.6. Aerobic oxidation of non-phenolic lignin model **LM6**.

major products of this reaction were the ketone **OP9** (34%) and dehydrated ketone **OP10** (57%). Additional minor products included 3,5-dimethoxybenzaldehyde **OP6**, 4-methoxy benzaldehyde **OP11**, 3,5-dimethoxybenzoic acid **OP8**, and 4-methoxybenzoic acid **OP12**.

The *erythro* isomer (**LM8**) was oxidized more slowly by the vanadium catalyst with only 76% conversion observed after 48 h, affording a similar product distribution with somewhat lower yields of the ketone **OP9** (29%) and dehydrated ketone **OP10** (38%) products (100 °C, pyr-d_5). The identity of the products was confirmed by carrying out the reaction of **LM6** on a larger scale; ketone **OP9** and dehydrated ketone **OP10** were isolated and characterized by ^{1}H and ^{13}C NMR spectroscopy and high-resolution mass spectrometry.

To assess the potential influence of the solvent on the reaction selectivity, the aerobic oxidation of the non-phenolic β-1 lignin model compounds **LM6** and **LM8** was also carried out using DMSO as the solvent and the vanadium complex **OV2**. When the non-phenolic lignin model **LM6** was heated with 10 mol% of catalyst under air at 100 °C (DMSO-d_6, 48 h), 91% conversion of the starting material was observed after 48 h. The major product of this reaction was the ketone **OP9** (66%). Additional minor products included the dehydrated ketone **OP10** (6%), 3,5-dimethoxybenzaldehyde (**OP6**), 4-methoxybenzaldehyde (**OP11**), 3,5-dimethoxybenzoic acid (**OP8**), 4-methoxybenzoic acid (**OP12**), and methanol (Table 2.1).

Table 2.1. Summary of the oxidation of non-phenolic β-1 lignin model using **OV2**.

Substrate	Solvent	Conv. %	Yields (%)					
			OP9	**OP10**	**OP6**	**OP11**	**OP8**	**OP12**
LM6	Pyr-d_5	100	34	57	3	3	3	4
LM6	DMSO-d_6	91	66	6	3	3	4	11
LM8	toluene	100	72	<1	7	2	<1	<1

Toluene was also an effective solvent for the oxidation of the β-1 lignin model compounds. Using **OV2** (10 mol%) as a catalyst in combination with the base promoter NEt_3 (15 mol%), complete conversion of **LM8** was observed after heating in toluene for 48 h (100 °C). The major product of this reaction was the ketone **OP9** (*ca.* 72%), with minor amounts of 3,5-dimethoxybenzaldehyde (*ca.* 7%) and 4-methoxybenzaldehyde (*ca.* 2%) also formed (Scheme 2.7). Overall, changing the solvent from pyridine to toluene did not

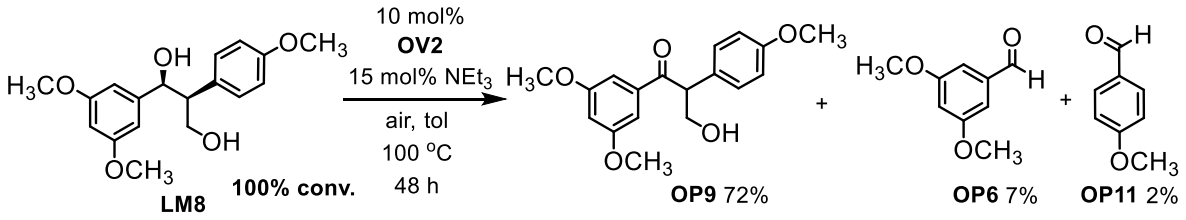

Scheme 2.7. Aerobic oxidation of non-phenolic lignin model **LM8**.

have a dramatic impact on the reaction selectivity in the vanadium-catalyzed oxidation of **LM6** and **LM8**; preferential oxidation at the secondary benzylic alcohol position was observed in both cases.

2.3.4 Catalytic Oxidation of Phenolic β-1 Lignin Model Compounds

Hanson and co-workers previously reported the unusual substrate-dependence of catalyst **OV2** for complex β-aryl glycerol lignin model compounds.[2e] Scheme 2.8 depicts the difference in selectivity for non-phenolic β-aryl glycerol models (**LM4**) where the C-H bond cleavage is the major product (ketone). Under similar conditions, the aerobic oxidation of the phenolic β-aryl glycerol model (**LM5**) gives C_{aryl}-C_{alkyl} bond cleavage affording benzoquinone and acrolein derivative as major products.

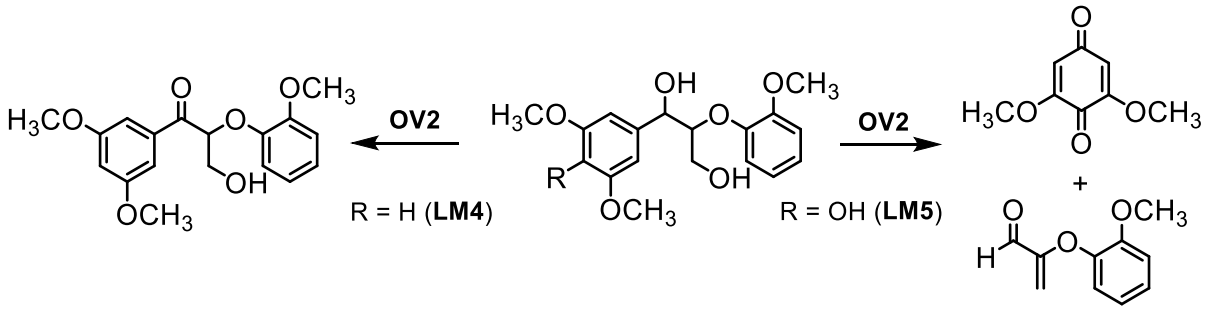

Scheme 2.8. Different selectivity was observed using **OV2** for phenolic (**LM5**) and non-phenolic (**LM4**) lignin models.

Consequently, **OV2** was tested as a catalyst for the aerobic oxidation of the phenolic β-1 lignin model compounds **LM7** and **LM9**. When compound **LM7** was heated with 10 mol% of the catalyst under air in pyridine at 100 °C, complete consumption of the starting material was observed (Scheme 2.9). The major products of this reaction were the ketone

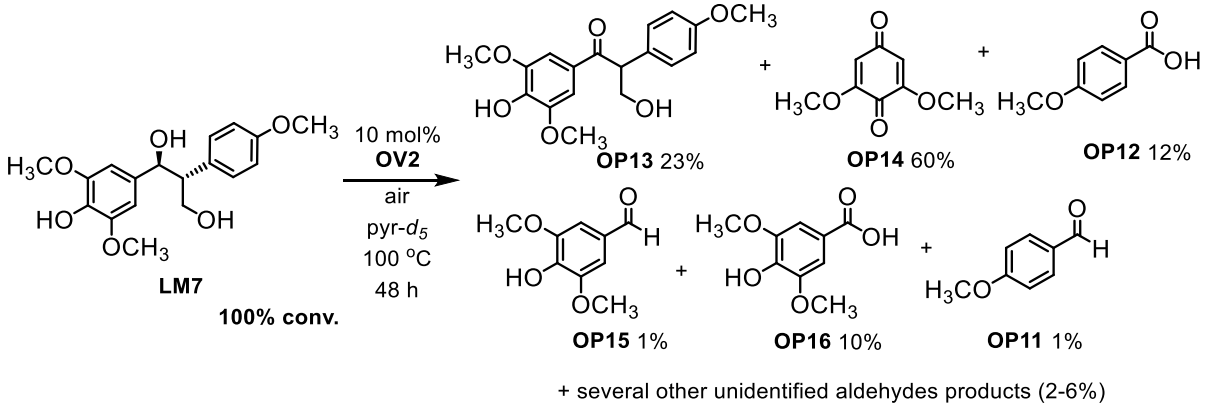

Scheme 2.9. Aerobic oxidation of phenolic lignin model **LM7**.

OP13 (23%) and 2,6-dimethoxybenzoquinone (**OP14**, 60%). In addition, multiple minor products formed, including 4-hydroxy-3,5-dimethoxybenzoic acid (**OP16**), 4-hydroxy-3,5-dimethoxybenzaldehyde (**OP15**), 4-methoxybenzoic acid (**OP12**), 4-methoxy-benzaldehyde (**OP11**), and several unidentified aldehyde species (1−12% yields, see Scheme 2.9). In the catalytic aerobic oxidation of the *erythro* isomer **LM9** using **OV2**, complete conversion of the starting material was also observed, affording the ketone **OP13** (7%), 2,6-dimethoxybenzoquinone (**OP14**, 43%), and minor amounts of the corresponding carboxylic acid and aldehyde products. The identity of ketone **OP13** was confirmed by

isolation from a larger scale reaction mixture; compound **OP13** was characterized by ^{1}H and ^{13}C NMR spectroscopy and HRMS analysis. In control experiments conducted under identical conditions with no added catalyst, no reaction of **LM7** was observed.

In the reactions of the phenolic lignin model compounds **LM7** and **LM9**, an incomplete mass balance was obtained; however, no additional major products were evident in the ^{1}H NMR spectrum of the reaction mixture which could account for all of the missing material, and the reaction mixture was a dark brown color with some solid material formed. An incomplete mass balance in the oxidation of lignin model compounds has been noted in previous reports and has been attributed to polymerization or other reactions of radical intermediates.[29] To evaluate this idea, the aerobic oxidation of 2,6-dimethoxyphenol was carried out using the vanadium complex **OV2** (5 mol%) as a catalyst with added base (NEt_3, 10 mol%). After 24 h of heating at 80 °C, more than 98% of the 2,6-dimethoxyphenol had reacted, affording a dark brown solid. No soluble organic products were detected in the ^{1}H NMR spectrum of an aliquot of the reaction mixture ($CDCl_3$), consistent with polymerization or other reactions to afford intractable solid products.[29]

Given the range of selectivities observed in the aerobic oxidation of the β-1 lignin model compounds, we tested the 5-coordinate vanadium complex **OV1** as a catalyst for the aerobic oxidation of the phenolic β-1 lignin model **LM9**. On heating **LM9** with 10 mol% of the catalyst under air (100 °C, 48 h, pyr-d_5), complete conversion of the starting material was observed (^{1}H NMR spectroscopy). The formation of a new aldehyde product **OP17** (44%) was detected (Scheme 2.10). Compound **OP17** was identified by carrying out a

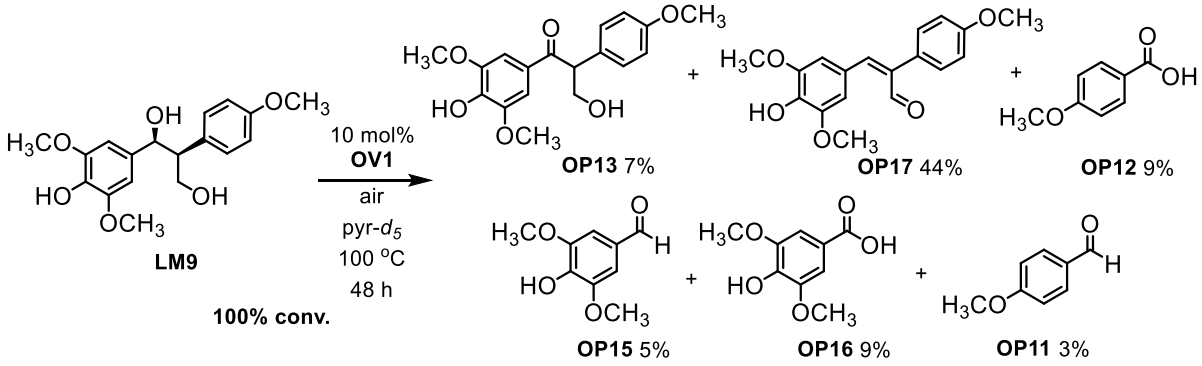

Scheme 2.10. Aerobic oxidation of phenolic lignin model **LM9**.

reaction on a larger scale, isolating the product, and characterizing it by ^{1}H and ^{13}C NMR spectroscopy and HRMS. Other minor products of the reaction included the ketone **OP13**, 4-hydroxy-3,5-dimethoxybenzoic acid (**OP16**), 4-hydroxy-3,5-dimethoxybenzaldehyde (**OP15**), 4-methoxybenzoic acid (**OP12**), and 4-methoxybenzaldehyde (**OP11**). The formation of aldehyde **OP17** was unanticipated; compound **OP17** was not observed as a product with the vanadium catalyst **OV2**, and its mechanism of formation is unclear at this time. Aldehyde **OP17** apparently results from oxidation of the primary alcohol and dehydration of the secondary alcohol in **LM9**. The product distributions from each of the vanadium-catalyzed oxidations of the phenolic β-1 model compound are shown in Table 2.2.

Table 2.2. Summary of the oxidation of phenolic β-1 lignin model using **OV1** and **OV2**.

Cat	Substrate[a]	Conv. %	Yields (%)						
			OP13	**OP14**	**OP15**	**OP11**	**OP16**	**OP12**	**OP17**
OV2	**LM7**	100	23	60	1	1	10	12	0
OV1	**LM9**	100	7	<2	5	3	9	9	44

[a]solvent: pyr-d_5

2.3.5 Competitive Oxidation of β-O-4 and β-1 Lignin Model Compounds

Internal competition experiments were carried out to assess the relative reactivities of the vanadium catalyst with β-O-4 and β-1 lignin model compounds. A 1:1 mixture of **LM8** and the β-O-4 lignin model compound **LM4** was heated under air with the vanadium precatalyst **OV2** (10 mol %) in pyr-d_5 solvent. After 24 h, *ca.* 50% conversion of **LM4** and *ca.* 43% conversion of **LM8** were observed (Scheme 2.11). The products of this reaction were a mixture of ketone **OP2** (*ca.* 27%, derived from **LM4**) and ketone **OP9** (*ca.* 16%, derived from **LM8**). 3,5-Dimethoxybenzaldehyde (**OP6**, 5%) and 4-methoxybenzaldehyde (**OP11**, 1%) were also observed as minor products. The predominant selectivity of the vanadium catalyst for oxidation of the secondary benzylic alcohol was maintained, and the β-O-4 lignin model compound reacted only slightly faster than the β-1.

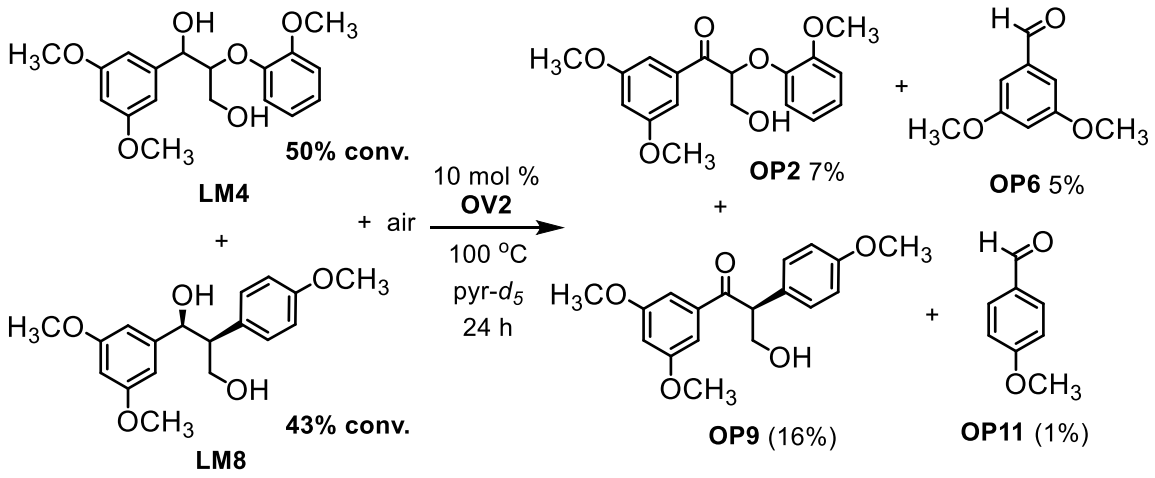

Scheme 2.11. Aerobic oxidation of a mixture of 1:1 β-O-4 (**LM4**) and β-1 (**LM8**) lignin models using **OV2**.

2.4 Discussion

For vanadium, a one-electron pathway involving a vanadium(IV) intermediate is proposed for the oxidative dimerization of phenols to binaphthols.[30] Limberg favored a hydrogen atom transfer pathway for a metavanadate-cinnamic acid catalyst for alcohol oxidation,[31] and work by Toste and Chen proposed a hydride transfer pathway for several vanadium-catalyzed alcohol oxidation reactions.[32]

Extensive previous work has involved using arylglycerol β-aryl ether compounds similar to **LM4** to model the β-O-4 linkage in lignin.[7-25] A variety of techniques have been explored for the oxidation of arylglycerol β-aryl ether compounds, including enzymatic oxidation (lignin peroxidase or manganese-dependent peroxidase and H_2O_2),[20-22,25] stoichiometric one-electron oxidation (using reagents like cerium ammonium nitrate or potassium-12-tungstocobalt(III)ate),[4,6,22,26,33] single electron transfer sensitized photochemical oxidation,[6] electrochemical oxidation,[29] and transition metal catalyzed oxidations.[4,2a,34,35] In general, stoichiometric one-electron oxidants react with the lignin model compound (similar to **LM4**) to form a radical cation which undergoes oxidative cleavage of the C_α-C_β bond, generating veratryl aldehyde as the major product.[6,22,26,33] In contrast to the reactivity documented for single electron transfer oxidants, aerobic oxidation of lignin model **LM4** using dipicolinate vanadium catalyst **OV1** in DMSO-d_6 or pyr-d_5 afforded ketone **OP2**, dehydrated ketone **OP3**, and alkene **OP4** as the major

products. Alkene product **OP4** is the result of a non-oxidative C-O bond cleavage reaction analogous to that recently described by Son and Toste for a closely related arylglycerol β-aryl ether lignin model.[4] Unlike the reported Schiff base vanadium(V) catalyst for which the non-oxidative C-O bond cleavage pathway is predominant,[4] dipicolinate vanadium complex **OV1** affords mostly ketone **OP2** and dehydrated ketone **OP3**. The two vanadium catalysts are also distinct in that **OV1** catalyzes oxidative C_α-C_β bond cleavage in ketone **OP2** (affording 3,5-dimethoxybenzoic acid and formic acid), whereas the Schiff base catalyst reported by Toste did not react with the analogous ketone under the catalytic conditions.[4]

In the oxidation of **LM6** and **LM8**, the dominant pathway of the vanadium-catalyzed reaction is the oxidation of the secondary benzylic alcohol, affording ketone products (*ca.* 90%). Products arising from C−C bond cleavage were formed in lower yields (<10%). This selectivity for oxidation of the secondary benzylic alcohol parallels that observed in the oxidation of the analogous non-phenolic β-O-4 lignin model compound by the vanadium complex **OV2**, which afforded primarily ketone products (Scheme 2.5). Previous kinetic and computational studies of the oxyquinolinate vanadium system suggest that oxidation proceeds through a two-electron, base-assisted pathway.[2f] The observed selectivity for oxidation at the secondary benzylic alcohol of **LM6** is consistent with such a mechanism.

For the vanadium-catalyzed oxidations, the incorporation of a phenolic group into the substrate had a significant impact on the reaction selectivity. Although the non-phenolic lignin model compound **LM6** was oxidized at the secondary alcohol position to give ketone products, the phenolic model compound **LM7** underwent C_{aryl}-C_α bond cleavage to generate the 2,6-dimethoxybenzoquinone product. A similar trend was previously noted in the oxidation of phenolic and non-phenolic β-O-4 lignin model compounds using the vanadium catalyst **OV2**.[2e] The formation of quinone products upon oxidation of phenolic β-O-4, β-1, and β-5 model compounds has also been observed by Crestini and co-workers,[9] and Bozell and co-workers,[36] who reported several cobalt-catalyzed reactions. In the cobalt systems, the C_{aryl}-C_α bond cleavage was proposed to proceed through a radical pathway involving a cobalt-superoxo intermediate.[37,38]

2.5 Conclusions

The reactivity of the oxovanadium complexes **OV1** and **OV2** has been studied for the aerobic oxidation of lignin model compounds bearing β-O-4 and β-1 linkages. The vanadium complexes catalyzed the aerobic oxidation of lignin model compounds under mild conditions. A different pattern was observed for dipicolinate vanadium catalyst **OV1**, which reacted with ketone benzoin methyl ether **LM2** and β-aryl glycerol lignin model **LM4** to break the C-H bond, generating **OP1** and **OP2** (respectively) as initial products. Both **OP1** and **OP2** were subject to further oxidation under the reaction conditions, affording benzoic acid and 3,5-dimethoxybenzoic acid as final products. Similarly, with non-phenolic β-1 lignin model **LM6** and **LM8** the vanadium catalyst **OV2** affords primarily ketone products. The products observed in the vanadium-catalyzed reaction are more consistent with a two-electron oxidation pathway, in line with previous studies of the reactivity of **OV2**. The vanadium complex **OV2** also yielded products of C_{aryl}-C_{α} bond cleavage, 2,6-dimethoxybenzoquinone and 4-methoxybenzoic acid. The incorporation of the phenolic group had a detrimental impact on the selectivity for the formation of monomeric products, with lower product yields and some formation of solids detected for the vanadium catalysts.[38]

A major challenge in the production of more valuable chemicals and fuels from lignin is the complex, irregular nature of the polymer. New ways to control the selectivity of chemical transformations within lignin could significantly improve our ability to harness this renewable resource. Homogeneous catalysts are attractive candidates for the aerobic oxidation of lignin, offering the potential for tuning the metal and ligand framework to direct the reaction toward specific linkages or toward a desired product. As described above, the observation that vanadium catalysts display different reactivity toward different lignin models highlights the viability of using homogeneous catalysts to control selectivity in the reactions of lignin.

2.6 References

(1) a) Adler, E. *Wood Sci. Technol.* **1977**, *11*, 169–218; b) Evtuguin, D. V.; Neto, C. P.; Silva, A. M. S.; Domingues, P. M.; Amado, F. M. L.; Robert, D.; Faix, O. *J. Agric. Food Chem.* **2001**, *49*, 4252−4261; c) Sakakibara, A. in *Wood and Cellulose Chemistry*; Hon, D. N.-S., Shiraishi, N.; Marcel Dekker Inc.: New York, 1991.
(2) a) Hanson, S. K.; Baker, R. T.; Gordon, J. C.; Scott, B. L.; Sutton, A. D.; Thorn, D. L. *J. Am. Chem. Soc.* **2009**, *131*, 428−429; b) Hanson, S. K.; Baker, R. T.; Gordon, J. C.; Scott, B. L.; Silks, L. A. P.; Thorn, D. L. *J. Am. Chem. Soc.* **2010**, *132*, 17804–17816; c) Hanson, S. K.; Baker, R. T.; Gordon, J. C.; Scott, B. L.; Thorn, D. L. *Inorg. Chem.* **2010**, *49*, 5611−5618; d) Hanson, S. K.; Wu, R.; Silks, L. A. P. *Org. Lett.* **2011**, *13*, 1908–1911; e) Hanson, S. K.; Wu, R.; Silks, L. A. P. *Angew. Chem. Int. Ed.* **2012**, *51*, 3410−3413; f) Wigington, B. N.; Drummond, M. L.; Cundari, T. R.; Thorn, D. L.; Hanson, S. K.; Scott, S. L. *Chem. Eur. J.* **2012**, *18*, 14981–14988; g) Zhang, G.; Scott, B. L.; Wu, R.; Silks, L. A. P.; Hanson, S. K. *Inorg. Chem.* **2012**, *51*, 7354−7361.
(3) Thorn, D. L.; Harlow, R. L.; Herron, N. *Inorg. Chem.* **1996**, *35*, 547-548.
(4) Son, S.; Toste, F. D. *Angew. Chem. Int. Ed.* **2010**, *49*, 3791–3794.
(5) a) Sedai, B.; Díaz-Urrutia, C.; Baker, R. T.; Wu, R.; Silks, L. A.; Hanson, S. K. *ACS Catal.* **2011**, *1*, 794–804; b) Sedai, B.; Díaz-Urrutia, C.; Baker, R. T.; Wu, R.; Silks, L. A.; Hanson, S. K. *ACS Catal.* **2013**, *3*, 3111–3122.
(6) Cho, D. W.; Parthasarathi, R.; Pimentel, A. S.; Maestas, G. D.; Park, H. J.; Yoon, U. C.; Dunaway-Mariano, D.; Gnanakaran, S.; Langan, P.; Mariano, P. S. *J. Org. Chem.* **2010**, *75*, 6549–6562.
(7) Hammel, K. E.; Tardone, P. J.; Moen, M. A.; Price, L. A. *Biochem. Biophys.* **1989**, *270*, 404–409.
(8) Crestini, C.; Pro, P.; Neri, V.; Saladino, R. *Bioorg. Med. Chem.* **2005**, *13*, 2569–2578.
(9) a) Crestini, C.; Crucianelli, M.; Orlandi, M.; Saladino, R. *Catal. Today* **2010**, *156*, 8–22; b)
Lange, H.; Decina, S.; Crestini, C. *Eur. Polym. J.* **2013**, *49*, 1151−1173.
(10) Crestini, C.; Caponi, M. C.; Argyropoulos, D. S.; Saladino, R. *Bioorg. Med. Chem.* **2006**, 14, 5292–5302.
(11) Makhotkina, O. A.; Preis, S. V.; Parkhomchuk, E. V. *Appl. Catal., B* **2008**, *84*, 821–826.
(12) Deng, H.; Lin, L.; Sun, Y.; Pang, C.; Zhuang, J.; Ouyang, P.; Li, Z.; Liu, S. *Catal. Lett.* **2008**, *126*, 106–111.
(13) Crestini, C.; Pastorini, A.; Tagliatesta, P. J. *Mol. Catal. A: Chem.* **2004**, *208*, 195–202.
(14) Chen, C. L.; Capanema, E. A.; Gracz, H. S. J. *Agric. Food Chem.* **2003**, *51*, 6223–6232.
(15) Alves, V.; Capanema, E.; Chen, C. L.; Gratzl, J. J. *Mol. Catal. A: Chem.* **2003**, *206*, 37–51.
(16) Cui, F.; Dolphin, D. *Bioorg. Med. Chem.* **1995**, *3*, 471–477.
(17) Cui, F.; Wijesekera, T.; Dolphin, D.; Farrell, R.; Skerker, P. *J. Biotechnol.* **1993**, *30*, 15–26.
(18) Robinson, M.; Wright, L. J. *J. Wood Chem. Technol.* **2000**, *20*, 357–373.
(19) Jensen, K. A.; Bao, W.; Kawai, S.; Srebotnik, E.; Hammel, K. E. *Appl. Environ. Microbiol.* **1996**, *62*, 3679–3686.

(20) Tien, M.; Kirk, T. K. *Proc. Natl. Acad. Sci.* **1984**, *81*, 2280–2284.
(21) Hammel, K. E.; Mozuch, M. D.; Jensen, K. A.; Kersten, P. *J. Biochemistry* **1994**, *33*, 13349–13354.
(22) Bohlin, C.; Persson, P.; Gorton, L.; Lundquist, K.; Jonsson, L. J. *J. Mol. Catal. B: Enzym.* **2005**, *35*, 100–107.
(23) Ahvonen, T.; Brunow, G.; Kristersson, P.; Lundquist, K. *Acta. Chem. Scand. B* **1983**, *37*, 845–849.
(24) Ibrahim, W.; Lundquist, K. *Acta Chem. Scand.* **1994**, *48*, 149–151.
(25) Tuor, U.; Wariishi, H.; Schoemaker, H. E.; Gold, M. H. *Biochemistry* **1992**, *31*, 4986–4995.
(26) Bohlin, C.; Andersson, P. O.; Lundquist, K.; Jonsson, L. J. *J. Mol. Catal. B: Enzym.* **2007**, *45*, 21–26.
(27) The error on yields determined by ^{1}H NMR integration is estimated at 5-10%.
(28) See reference 5 for ^{1}H and ^{13}C NMR spectra of the isolated products.
(29) (a) Pardini, V. L.; Smith, C. Z.; Utley, J. H. P.; Vargas, R. R.; Viertler, H. *J. Org. Chem.* **1991**, *56*, 7305−7313; (b) Pardini, V. L.; Vargas, R. R.; Viertler, H. *Tetrahedron* **1992**, *48*, 7221−7228.
(30) a) Barhate, N. B.; Chen, C. T. *Org. Lett.* **2002**, *4*, 2529–2532; b) Guo, Q. X.; Wu, Z. J.; Luo, Z. B.; Liu, Q. Z.; Ye, J. L.; Luo, S. W.; Cun, L. F.; Gong, L. Z. *J. Am. Chem. Soc.* **2007**, *129*, 13927–13938.
(31) Ohde, C.; Limberg, C. *Chem. Eur. J.* **2010**, *16*, 6892–6899.
(32) a) Radosevich, A. T.; Musich, C.; Toste, F. D. *J. Am. Chem. Soc.* **2005**, *127*, 1090–1091; b) Pawar, V. D.; Bettigeri, S.; Weng, S. S.; Kao, J. Q.; Chen, C. T. *J. Am. Chem. Soc.* **2006**, *128*, 6308–6309; c) Weng, S. S.; Shen, M. W.; Kao, J. Q.; Munot, Y. S.; Chen, C. T. *Proc. Natl. Acad. Sci.* **2006**, *103*, 3522–3527; d) Chen, C. T.; Kao, J. Q.; Salunke, S. B.; Lin, Y. H. *Org. Lett.* **2011**, *13*, 26–29.
(33) Baciocchi, E.; Fabbri, C.; Lanzalunga, O. *J. Org. Chem.* **2003**, *68*, 9061–9069.
(34) DiCosimo, R.; Szabo, H. C. *J. Org. Chem.* **1988**, *53*, 1673–1679.
(35) Partenheimer, W. *Adv. Synth. Catal.* **2009**, *351*, 456–466.
(36) (a) Bozell, J. J.; Hames, B. R.; Dimmel, D. R. *J. Org. Chem.* **1995**, 60, 2398−2404. (b) Cedeno, D.; Bozell, J. J. *Tetrahedron Lett.* **2012**, *53*, 2380−2383. (c) Biannic, B.; Bozell, J. J. *Org. Lett.* **2013**, *15*, 2730−2733.
(37) Zombeck, A.; Drago, R. S.; Corden, B. B.; Gaul, J. H. *J. Am. Chem. Soc.* **1981**, **103**, 7580−7585.
(38) Higher yields of quinone products (up to 86%) have been obtained from syringyl β-O-4 models using Co-salen complexes in the presence of a bulky amine that can be employed at room temperature (see reference 36b)

Chapter 3: Aerobic Oxidation of 2-Phenoxyethanol Lignin Model Compounds Using Vanadium Catalysts

This chapter has been partially published in: Díaz-Urrutia, C.; Sedai, B.; Leckett, K. C. Baker, R. T.; Hanson, S. K. ACS Sustainable Chem. Eng. ***2016****, submitted.*

3.1 Introduction

As discussed previously, an effective depolymerization of lignin requires an exhaustive study of the reactivity of the different linkages of lignin. One promising approach involves the use of homogeneous transition metal catalysts for relatively low temperature (<150 °C) oxidative cleavage of the β-O-4 linkage (Figure 1),[1] the most prevalent feature (*ca.* 55%) in

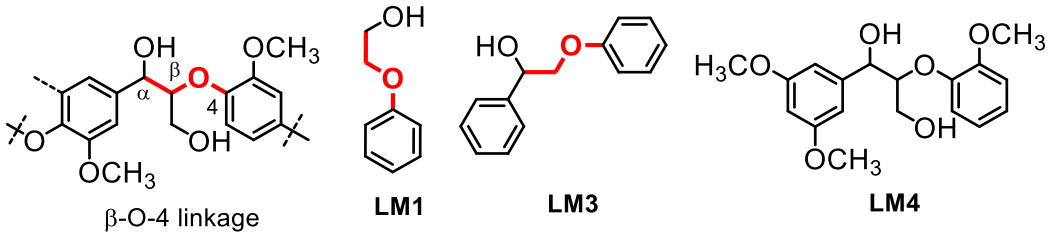

Figure 3.1. Phenoxyethanol lignin models **LM1** and **LM3**.

the lignin structure.[2] Lignin model compounds provide an opportunity to understand and compare the reactivity and selectivity of different catalysts.

In previous work, our group compared the aerobic oxidation of **LM4** using copper and vanadium homogeneous catalysts in pyridine solvent.[3] Both the oxovanadium complex **OV1** (Figure 3.2) and CuCl/TEMPO/pyridine (**Cu***) catalyzed the aerobic oxidation of complex lignin models bearing β-O-4 and β-1 linkages, but with dramatically different selectivities. While use of **OV1** led to cleavage of the benzylic C-H bond of **LM1** to afford the corresponding ketone as the major product, catalyst **Cu*** afforded predominantly aldehyde product (arising from C_α-C_β bond fission).[3] In contrast, using the oxovanadium

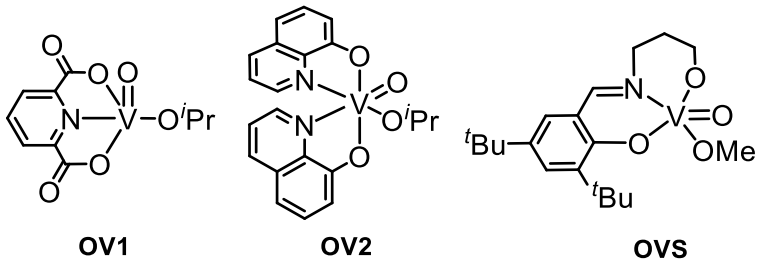

Figure 3.2. 5- and 6-coordinate oxovanadium(V) catalysts, and salen-vanadium catalyst.

complex **OVS** with a salen-type ligand, Son and Toste showed that oxidation of a substrate similar to **LM4** proceeded predominantly *via* C-O bond cleavage, affording phenol and α,β-unsaturated enone products.[4]

In addition to arylglycerol β-aryl ether compounds, other types of readily synthesized 1,2-hydroxyether compounds have been used to model the β-O-4 linkage. For instance, Bergman and co-workers reported that a ruthenium xantphos complex catalyzed C-O bond cleavage in the simple lignin model 1-phenyl-2-phenoxyethanol **LM3** (Figure 3.1) *via* an internal transfer hydrogenation reaction.[5] However, recent work by James and co-workers showed that different products were formed using the same ruthenium xantphos catalyst with more complex arylglycerol β-aryl ether lignin model compounds such as **LM4**.[6] See *Chapter 1*: *Introduction*, for more details about reductive approaches for lignin disassembly.

Chapter 2 examined the reactivity of complex lignin models (β-O-4 and β-1 linkages) using catalysts **OV1** and **OV2** finding new product distributions and interesting selectivities. Given the potential reactivity differences between simple and more complex lignin model compounds, *Chapter 3* revisits the reactivity of vanadium catalysts with the simple lignin model compounds 2-phenoxyethanol **LM1** and 1-phenyl-2-phenoxyethanol **LM3**. Previous work using five-coordinate oxovanadium catalyst precursor **OV1**[7] has been extended to include six-coordinate bis(oxyquinolate) complex **OV2**.[8] The influence of phenyl substitution on the backbone of the lignin model has been explored, and several unusual new reaction products have been identified, shedding further light on the fundamental modes of reactivity of earth-abundant metal catalysts in the aerobic oxidation of lignin model compounds.

3.2 Materials and Methods

3.2.1 General Considerations

Unless specified otherwise, all reactions were carried out under argon or nitrogen using Schlenk techniques. Acetonitrile, methanol (HPLC grade chromasolv©), were purchased from Sigma Aldrich or Alfa Aesar. All other reagents were used as received. Toluene was dried on columns of activated alumina using a J. C. Meyer solvent purification system. Methylene chloride (CH_2Cl_2) was dried over activated alumina. Deuterated solvents were purchased from Cambridge Isotope Laboratories. ^{1}H, $^{13}C\{^{1}H\}$ and ^{51}V NMR spectra were obtained at room temperature on Bruker AVANCE 400 or 300 MHz spectrometers, with chemical shifts referenced to the residual solvent signal (^{1}H and ^{13}C) or externally to $VOCl_3$ (0 ppm, ^{51}V). GC-MS analysis was performed using a Hewlett Packard 6890 GC system equipped with a Hewlett Packard 5973 mass selective detector. HPLC-MS analyses were performed on a Dionex Ultimate 3000 liquid chromatograph and an Applied Biosystem API2000 triple quadrupole mass spectrometer, using a reversed-phase gradient column (RSLC PA2 2.2 μm 120 Å, 2.1 x 150 mm). High resolution mass spectra (HRMS) were obtained by the John L. Holmes Mass Spectrometry Facility, University of Ottawa. The complexes **OV1**,[9] **OV2**[8b] and **OVS**[4] were prepared using published procedures. The yields and conversions of the catalytic oxidations are an average of at least two independent experiments.

3.2.2 Synthesis of 1-Phenyl-2-Phenoxyethanol LM3

1-Phenyl-2-phenoxyethanol was synthesized using a modified version of a previously published procedure.[10] 2-Phenoxyacetophenone (531 mg, 2.50 mmol) was dissolved in methanol (25 mL), and then reduced by slow addition of $NaBH_4$ (47.3 mg, 1.25 mmol). The mixture was stirred at room temperature for 1 h, and then the reaction was quenched by addition of 50 mL of saturated NH_4Cl. The product was extracted with 100 mL of CH_2Cl_2, washed with water, dried over $MgSO_4$, and evaporated to dryness under reduced pressure, affording a yellow solid. Yield: 445 mg (83%). ^{1}H NMR (400 MHz, $CDCl_3$): δ 7.37 (m, 7H, Ph), 6.95 (m, 2H, Ph), 5.14 (ddd, 1H, *J* = 9, 3, 2.5 Hz, C*H*), 4.12 (dd, 1H, *J* = 10, 3 Hz, CH_2), 4.01 (dd, 1H, *J* = 10, 9 Hz, CH_2), 2.77 (d, 1H, *J* = 2.5 Hz, O*H*); $^{13}C\{^{1}H\}$

NMR (100 MHz, $CDCl_3$): δ 158.4, 139.6, 129.6, 128.6, 128.2, 126.3, 121.3, 114.7, 73.3, 72.6.

3.2.3 Synthesis of 2-Phenoxyacetaldehyde OP20

2-Phenoxyacetaldehyde was prepared following a modified version of a published procedure.[11] A solution of methyl phenoxyacetate (500 mg, 2.99 mmol) in CH_2Cl_2 was cooled to -78 ^oC and treated with DIBALH (3.6 mL of 1.0 M solution in THF, 3.6 mmol). The reaction mixture was kept at -78 ^oC for 1 h and then quenched by addition of methanol (0.1 mL), followed by addition of CH_2Cl_2 (25 mL). The reaction mixture was washed with aqueous 1 M HCl (5 mL) and brine (5 mL), and then the organic phase was dried under vacuum. The crude compound was purified by column chromatography (eluting with 50:50 hexanes/ethyl acetate), yielding 245 mg (59%). ^1H NMR (300 MHz, $CDCl_3$): δ 9.87 (s, 1H, O=C*H*), 7.31 (m, 2H, Ph), 7.03 (m, Ph), 6.91 (m, 2H, Ph), 4.57 (s, 2H, CH_2); $^{13}C\{^1H\}$ NMR (100 MHz, $CDCl_3$): δ 199.5, 157.6, 129.8, 122.0, 114.6, 72.6.

3.2.4 Synthesis of 2-Phenoxyacetophenone OP19

2-Phenoxyacetophenone was synthesized using a modified version of a previously published procedure.[12] 2-Bromoacetophenone (2.00 g, 0.010 mol), phenol (1.42 g, 0.015 mol) and K_2CO_3 (2.08 g, 0.015 mol) were suspended in DMF (20 mL) in a 100 mL round-bottom flask. The solution was stirred for 24 h, and then the reaction was diluted with water (20 mL). The product was extracted four times with a 3:1 diethyl ether:pentane solution (4 x 20 mL). The organic layers were combined and washed with 3 M NaOH (2 x 20 mL), dried over $MgSO_4$, and then evaporated to dryness under reduced pressure affording 0.83 g (38%) of 2-phenoxyacetophenone **OP19**. ^1H NMR (400 MHz, $CDCl_3$): δ 8.01 (m, 2H, Ph), 7.26 (m, 1H, Ph), 7.51 (m, 2H, Ph), 7.29 (m, 2H, Ph), 6.95 (ov m, 3H, Ph), 5.28 (s, 2H, CH_2); $^{13}C\{^1H\}$ NMR (100 MHz, $CDCl_3$): δ 194.7, 158.2, 134.7, 134.0, 129.7, 129.0, 128.3, 121.8, 115.0, 71.0.

3.2.5 Catalytic Oxidation of 2-Phenoxyethanol LM1 Using OV2

In an NMR tube, 2-phenoxyethanol (68 mg, 0.49 mmol) and the internal standard hexamethylbenzene (12 mg, 0.07 mmol) were dissolved in pyr-d_5 (0.9 mL). Initial ^1H and inverse-gated ^{13}C NMR spectra were recorded. To a 50 mL round bottom flask was added **OV2** (20.5 mg, 0.049 mmol). The pyr-d_5 solution was added to the flask, which was

equipped with a stir bar and an air condenser. The mixture was heated at 100 ^{o}C with stirring under air for 48 h, then cooled to room temperature. The solution was transferred to an NMR tube, and ^{1}H and inverse-gated ^{13}C NMR spectra were recorded at the end of the reaction. Integration of the NMR spectra revealed that 69% conversion of the starting material occurred, affording phenol (51%), 2-phenoxyethyl-1-formate **OP18** (18%), and formic acid (3%). The formate ester was isolated by preparative scale TLC using a 7:3 mixture of hexanes:ethyl acetate. ^{1}H NMR for **OP18** (400 MHz, $CDCl_3$): 8.14 (s, 1H, O=C*H*), 7.31 (t, 2H, *J* = 7.6 Hz, Ph), 6.99 (t, 1H, *J* = 7.6 Hz, Ph), 6.93 (d, 2H, *J* = 7.6 Hz, Ph), 4.54 (t, 2H, *J* = 4.8 Hz, CH_2), 4.22 (t, 2H, *J* = 4.8 Hz, CH_2); ^{13}C{^{1}H} NMR for **OP18** (100 MHz, $CDCl_3$): 161.0, 129.8, 121.6, 114.8, 105.2, 65.8, 62.5; HRMS (EI) for **OP18**: *m/z* calcd for $C_9H_{10}NO_3$ $[M]^+$: 166.0630, found: 166.0621.

3.2.6 Catalytic Oxidation of 1-Phenyl-2-phenoxyethanol LM3 Using OV2

In an NMR tube, 1-phenyl-2-phenoxyethanol (41 mg, 0.19 mmol) and the internal standard hexamethylbenzene (6.8 mg, 0.042 mmol) were dissolved in pyr-d_5 (0.8 mL). Initial NMR spectra were recorded, and then the solution was transferred to a 25 mL round bottom flask containing **OV2** (7.8 mg, 0.019 mmol). The reaction was heated under air with stirring at 100 ^{o}C for 48 h, using an air condenser. The reaction mixture was cooled to room temperature and the solution was transferred to an NMR tube. ^{1}H and inverse-gated ^{13}C NMR spectra were recorded. Integration of the NMR spectra against the internal standard revealed that 58% conversion occurred, affording benzoic acid (46%), phenol (45%), 2-phenoxyacetophenone (16%), and formic acid (2%).

3.2.7 Catalytic Oxidation of 2-Phenoxyacetophenone OP19 Using OV2 in DMSO-d_6

In an NMR tube, 2-phenoxyacetophenone (20 mg, 0.093 mmol) and **OV2** (3.9 mg, 0.94 μmol) were dissolved in DMSO-d_6 (1 mL) containing dimethylsulfone (5 mM) as an internal standard. An initial ^{1}H NMR spectrum was recorded, and then the sample was transferred to a thick-walled 50 mL Schlenk tube equipped with Teflon stopcock. The mixture was heated at 100 ^{o}C with constant stirring. The reaction was monitored periodically by NMR over the course of 7 days. At the end of the reaction, integration of the ^{1}H NMR spectra against the internal standard revealed that 75% conversion of starting material had occurred, affording benzoic acid (51%), phenol (46%), and formic acid (37%).

3.2.8 Catalytic Oxidation of 2-Phenoxyacetophenone OP19 Using OV2 in pyr-d_5

In an NMR tube, 2-phenoxyacetophenone (22 mg, 0.10 mmol) was dissolved in pyr-d_5 (0.9 mL) containing dimethylsulfone added as an internal standard. An initial ^{1}H NMR spectrum was recorded, and then the reaction mixture was transferred to a 50 mL round bottom flask containing **OV2** (4 mg, 0.01 mmol). The flask was equipped with a stir bar and an air condenser, and then the reaction mixture was heated at 100 ^{o}C under air with stirring for 48 h. The reaction mixture was cooled to room temperature, and the solution was transferred to an NMR tube. Integration of the ^{1}H and inverse-gated ^{13}C NMR spectra revealed that 70% of the starting material was consumed, affording benzoic acid (60%), phenol (70%), and formic acid (2%).

3.2.9 Catalytic Oxidation of LM3 Using OVS

In a 25 mL Schlenk flask, 2-phenyl-1-phenoxyethanol (20 mg, 0.093 mmol) and 1 mol% **OVS** (0.362 mg, 9.34x10^{-4} mmol) were dissolved in 1 mL of toluene. The reaction was heated to 105 ^{o}C, with constant stirring for 18 h. The reaction mixture changed color to dark-red (a control experiment with only catalyst in toluene does not change color). At the end of the reaction the Schlenk flask was cooled down to room temperature and the solvent was removed under vacuum and replaced by 0.8 mL of $CDCl_3$ containing 1,3,5-trimethylbenzene (6.0 uL, 0.043 mmol) as an internal standard. The reaction mixture was transferred to a NMR tube and a ^{1}H NMR was recorded. Integration against the internal standard revealed 97% conversion of the starting material had occurred, affording 2-phenoxyacetophenone (3%), acetophenone (30%), phenol (40%).

3.2.10 Catalytic Oxidation 2-Phenoxyacetophenone OP19 Using OVS

In a 25 mL Schlenk tube 2-phenoxyacetophenone (20 mg, 0.093 mmol) and 1 mol% **OVS** (0.360 mg, 9.30x10^{-4} mmol) were dissolved in 1 mL of toluene. The reaction was heated to 105 ^{o}C with constant stirring for 18 h. At the end of the reaction, the solution turned light green. The Schlenk flask was then cooled to room temperature and the solvent was removed under vacuum. 0.8 mL of $CDCl_3$ was added to the residue together with 1,3,5-trimethylbenzene (6.0 uL, 0.043 mmol) as an internal standard. The reaction mixture was transferred to a NMR tube and a ^{1}H NMR spectrum was recorded. Integration against the internal standard revealed 98% conversion of the starting material had occurred,

affording benzaldehyde (5%), benzoic acid (72%), formic acid (9%) and several unidentified aldehyde and formate peaks (*ca.* 6%).

3.2.11 Control Reaction of 2-Phenoxyacetaldehyde OP20 in DMSO-d_6

In an NMR tube, 2-phenoxy-acetaldehyde (34 mg, 0.25 mmol) was dissolved in DMSO-d_6 (1 mL) containing 1,3,5-tri-*tert*-butylbenzene (5 mM) as an internal standard. An initial ^{1}H NMR spectrum was recorded, and then the sample was transferred to a thick-walled 50 mL Schlenk tube equipped with a Teflon stopcock. The mixture was heated at 100 ^{o}C with constant stirring. After 48 h, complete conversion of the starting material was observed by ^{1}H NMR affording formic acid, phenol, and several unidentified aldehyde and formate products.

3.3 Results

In previous work using oxovanadium catalyst **OV1** in air, 95% conversion was obtained for the oxidation of substrate **LM3** (100 ^{o}C, 7 days in DMSO-d_6) to benzoic acid (81%), phenol (77%), formic acid (46%) and 2-phenoxy-acetophenone (9%).[7] Substrate **LM1** was more sluggish to react, affording just 20% conversion to phenol, formic acid, and unidentified products under the same conditions (Scheme 3.1). These experiments showed

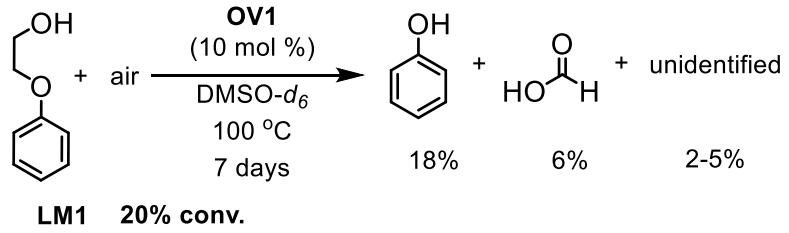

Scheme 3.1. Previously reported aerobic oxidation of **LM1** using **OV1**.[7]

that simple lignin models **LM1** and **LM3** were oxidized more slowly than the complex lignin model **LM4**[3] (see *Chapter 2*). In subsequent work, more active versions of both vanadium and copper catalysts have been developed. For example, the 6-coordinate oxovanadium complex **OV2** showed improved oxidation performance over **OV1** in aerobic alcohol oxidation reactions.[8] Thus, optimized system **OV2** was used to examine in more detail the aerobic oxidation of simple lignin models **LM1** and **LM3**.

3.3.1 Oxidation of 2-Phenoxyethanol LM1

When a pyr-d_5 solution of **LM1** was heated under air with the vanadium catalyst **OV2** (10 mol%), 69% conversion was observed after 48 h at 100 °C. The major products of this reaction were phenol, formic acid and the formylated substrate 2-phenoxyethyl-1-formate **OP18** (Scheme 3.2). No other products were detected in the reaction mixture by ^{1}H NMR

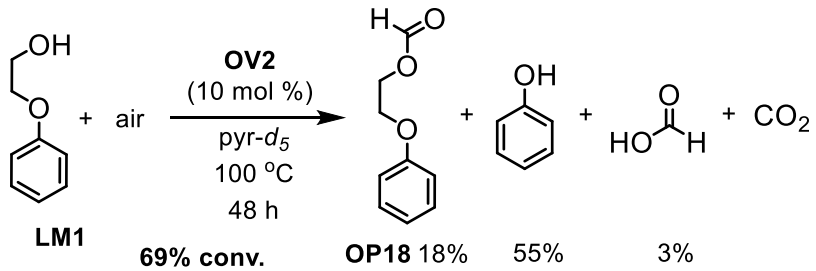

Scheme 3.2. Aerobic oxidation of **LM1** using **OVS**.

spectroscopy, suggesting that formation of phenol is accompanied by oxidation of the C_2H_4 backbone to give formic acid and CO_2. In a separate experiment, the ability of **OV2** (10 mol%) to catalyze the oxidation of formic acid to CO_2 was investigated; after 48 h of heating under air (100 °C, pyr-d_5 solvent), 23% of the formic acid was consumed. The possible role of 2-phenoxyacetaldehyde **OP20** as an intermediate in this reaction[13] could not be rigorously confirmed, as control experiments heating independently prepared[11] **OP20** in DMSO-d_6 (with an internal standard) for 24 h at 100 °C showed that **OP20** decomposed thermally to afford phenol, formic acid and several unidentified products.

3.3.2 Oxidation of 1-Phenyl-2-Phenoxyethanol LM3

Using 10 mol% oxovanadium complex **OV2**, substrate **LM3** was oxidized somewhat more slowly than **LM1**, with 58% conversion obtained after 48 h (100 °C, pyr-d_5). The slower oxidation of **LM3** is consistent with previous studies which showed that oxidation of sterically hindered secondary benzylic alcohols is slower than that of primary alcohols using **OV2**.[8b] The major products of the reaction were benzoic acid, phenol and the ketone 2-phenoxyacetophenone **OP19**, along with a small amount of formic acid (Scheme 3.3). The identity of ketone **OP19** was confirmed by comparison with an independently prepared sample.[12] The ketone is likely an intermediate in the formation of the benzoic acid and phenol co-products using catalysts **OV1** and **OV2**. Indeed, heating an isolated sample of the ketone **OP19** with **OV2** (10 mol%) in pyr-d_5 solvent (48 h, 100 °C) afforded a similar

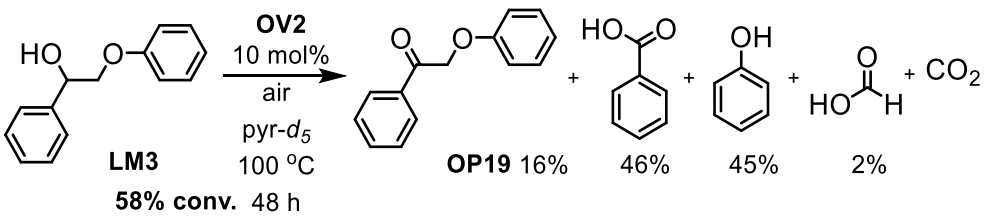

Scheme 3.3. Aerobic oxidation of **LM3** using **OV2**.

mixture of benzoic acid, phenol and formic acid with 70% overall conversion (Scheme 3.4).

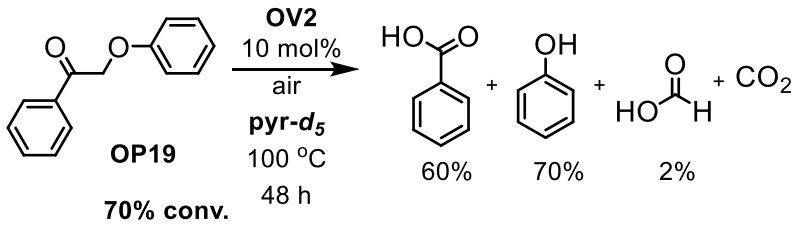

Scheme 3.4. Aerobic oxidation of **OP19** using **OV2**.

Additional experiments showed lower conversions of **OP19** using catalyst **OV2** (10 mol%) in DMSO-d_6 compared with those in pyr-d_5 (Scheme 3.5) as observed previously

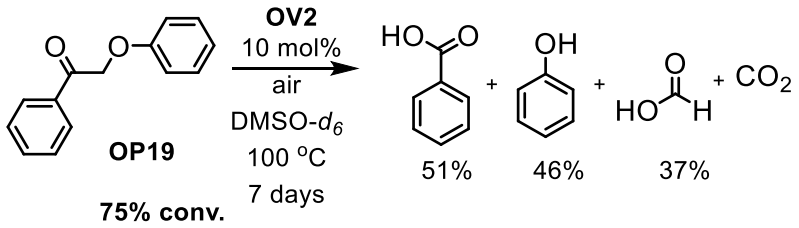

Scheme 3.5. Aerobic oxidation of **OP19** using **OV2** after 7 days.

using catalyst **OV1** and substrate **LM1**.[7] The oxidation of formic acid to CO_2 in DMSO-d_6, however, was observed to a lesser extent (*vs.* pyr-d_5).

As discussed in previous paragraphs, the salen-vanadium catalyst **OVS** is highly selective for the C-O bond cleavage of arylglycerol β-aryl ether.[4] Here, the ability of the **OVS** catalyst was tested to determine if its reactivity for complex lignin models translates to simple phenoxyethanol lignin models. The aerobic oxidation of **LM3** using only 1 mol% **OVS** afforded 97% conversion (105 °C, toluene, 18 h) with C-O bond cleavage products, acetophenone (30%) and phenol (40%) (Scheme 3.6). While the activity of the salen-vanadium catalyst is evident when comparing the conversions for **LM3** (58% for **OV2**

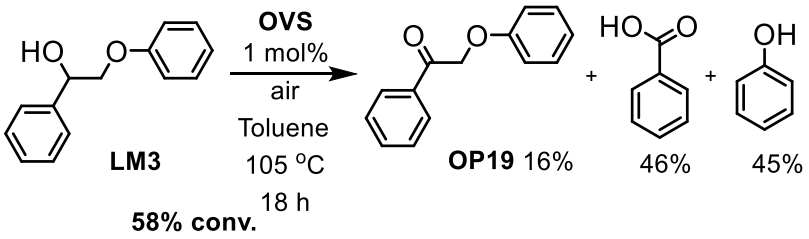

Scheme 3.6. Aerobic oxidation of **LM3** using **OVS**.

versus 97% for **OVS**), the yield is lower with less than 50% yield of products. Intrigued by the different reacivity of **OVS** for the oxidation of **LM3**, the aerobic oxidation of the ketone 2-phenoxyacetophenone was also studied. Using only 1 mol% **OVS**, 98% conversion (105 °C, toluene, 18 h) of 2-phenoxyacetophenone was observed affording benzoic acid, benzaldehyde, formic acid and several unidentified peaks corresponding to aldehydes and formate products (Scheme 3.7).

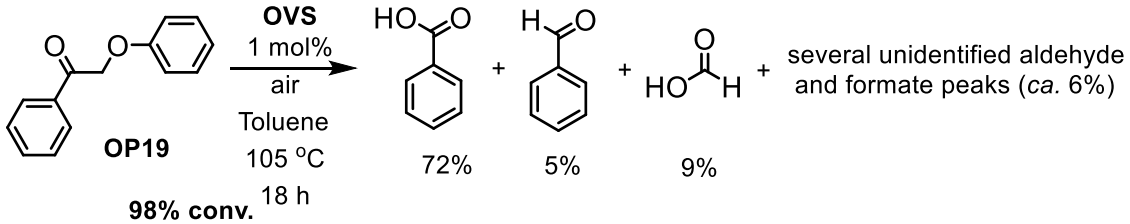

Scheme 3.7. Aerobic oxidation of ketone using **OVS**.

3.4 Discussion

In previous work involving the oxidation of the complex lignin model compound **LM4** using vanadium catalyst **OV1**[3] (see *Chapter 2*), it was found that the predominant reaction in the basic solvent pyridine is oxidation of the secondary alcohol[7] (Scheme 3.8), presumably by a 2e- base-assisted process as elucidated for alcohol oxidation using catalysts **OV1** and **OV2**.[14] Subsequent oxidation of the resulting ketone **OP2** and dehydrated ketone **OP3** was also promoted by base to give a mixture of guaiacol (2-methoxyphenol, **OP5**), aldehyde (2,6-dimethoxybenzaldehyde, **OP6**), carboxylic acid (2,6-dimethoxybenzoic acid, **OP8**), and formic acid **OP7**.

With simple models **LM1** and **LM3** and using oxovanadium catalyst **OV2**, initial oxidation of the alcohol likely also predominates, although the intermediacy of aldehyde **OP20** derived from substrate **LM1** is difficult to confirm given its thermal decomposition

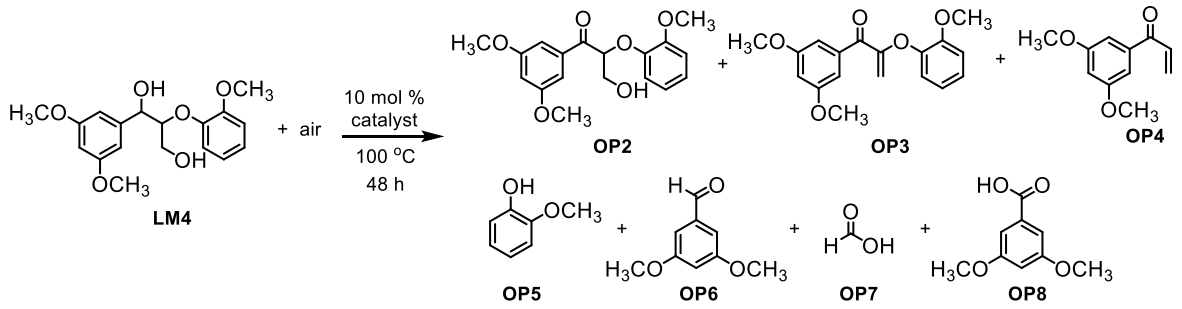

	Solvent[a]	Conv.(%)	**OP2**	**OP3**	**OP4**	**OP5**	**OP5**	**OP7**	**OP8**
OV1	DMSO-d_6	> 95	65	5	14	n.d.[b]	2	11	4
OV1	pyr-d_5	*ca.* 85	27	14	29	n.d.	4	6	< 1

[a]100 °C, 48 h; [b]n.d. = not detected

Scheme 3.8. Catalytic oxidation of β-O-4 lignin model **LM4** with **OV1** (see *Chapter 2*).

to phenol and formic acid. Vanadium catalyst **OV2** also promotes the formylation of **LM1** to **OP18**, which is much more slowly oxidized under the reaction conditions. With substrate **LM3,** the more stable ketone **OP19** undergoes clean conversion to benzoic acid, phenol, and formic acid using the vanadium catalyst **OV2** with no evidence for substrate formylation. In spite of the formylation side-product from primary alcohol substrate **LM1**, the performance of vanadium catalyst **OV2** is clearly superior to that of the previously reported vanadium catalyst **OV1**. Similar conversion of **LM1** (10 mol% cat, 100 °C, DMSO-d_6) to useful products (69 % using **OV2** *vs.* 20 % with **OV1**) was achieved in 2 days using **OV2** (*vs.* 7 days for **OV1**).[7] Previous studies suggest that the higher turnover rates observed using more electron-rich **OV2** (*vs.* **OV1**) can be attributed to the ease of V^V catalyst regeneration by air.[7,14] With secondary alcohol substrate **LM3**, however, the two catalyst precursors showed similar performance, presumably due to the increased steric demands of six-coordinate complex **OV2**.

While the aerobic oxidation of **LM3** using **OVS** is faster than with **OV1** or **OV2** catalysts (*e.g.,* 1 mol% *versus* 10 mol%), the yields for the C-O bond cleavage products are not as high as those for the C-C bond cleavage products using catalysts **OV1** or **OV2**. The amount of oxidation product (ketone 2-phenoxyacetophenone) is low for catalyst **OVS**, and the independent oxidation of the ketone afforded a complex mixture with benzoic acid as the major product (72% yield), confirming that it is not an intermediate to the C-O bond

cleavage products. Jones and co-workers reported several salen-vanadium catalysts with different substituents on the aromatic ring (Figure 3.3).[15] The conversions and yields for

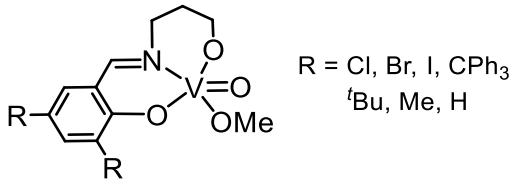

Figure 3.3. Salen-vanadium for C-O bond cleavage of **LM3** reported by Jones and co-workers.[15]

the aerobic oxidation of **LM3** using 5 mol% catalyst loadings (DMSO-d_6, 100 ^{o}C, 4 days) increased with the bulkiness of the aromatic substituents. However, the amount of oxidation product (2-phenoxyacetophenone) also increased.

3.5 Conclusions

To date, efficient aerobic C-C bond cleavage of simple phenoxyethanol lignin models **LM1** and **LM3** under mild conditions remains a challenge. Examples of C-C/C-O bond cleavage of **LM3** using microwaves,[16] silanes[17] or base-catalyzed[18] reactions (to name a few), require superstoichiometric amounts of reagents and harsh conditions (see *Chapter 1* for more details). Here, it was demonstrated the ability of catalysts **OV2** and **OVS** to oxidize simple lignin models **LM1** and **LM3** through C-C and C-O bond cleavage, respectively. The reactivity of **OV2** is consistent with previous results in complex lignin models such as **LM4**. Overall, the different selectivities observed in the vanadium and salen-vanadium reactions are consistent with fundamental differences in oxidation mechanisms enabled by the two different ligand scaffolds.

3.6 References

(1) Zakzeski, J.; Bruijnincx, P. C. A.; Jongerius, A. L.; Weckhuysen, B. M. *Chem. Rev.* **2010**, *110*, 3552–3599.
(2) a) Adler, E. *Wood Sci. Technol.* **1977**, *11*, 169–218; b) Evtuguin, D. V.; Neto, C. P.; Silva, A. M. S.; Domingues, P. M.; Amado, F. M. L.; Robert, D.; Faix, O. *J. Agric. Food Chem.* **2001**, *49*, 4252−4261; c) Sakakibara, A. In *Wood and Cellulose Chemistry*; Hon, D. N.-S., Shiraishi, N.; Marcel Dekker Inc.: New York, 1991; d) Reale, S.; Di Tullio, A.; Spreti, N.; De Angelis, F. *Mass Spectrom. Rev.* **2004**, *23*, 87–126.
(3) a) Sedai, B.; Díaz-Urrutia, C.; Baker, R. T.; Wu, R.; Silks, L. A. P.; Hanson, S. K. *ACS Catal.* **2011**, *1*, 794–804; b) Sedai, B.; Díaz-Urrutia, C; Baker, R. T.; Wu, R.; Silks, L. A. P.; Hanson, S. K. *ACS Catal.* **2013**, *3*, 3111–3122.
(4) Son, S.; Toste, F. D. *Angew. Chem. Int. Ed.* **2010**, *49*, 3791–3794.
(5) Nichols, J. M.; Bishop, L. M.; Bergman, R. G.; Ellman, J. A. *J. Am. Chem. Soc.* **2010**, *132*, 12554–12555.
(6) Wu, A.; Patrick, B. O.; Chung, E.; James, B. R. *Dalton Trans.* **2012**, *41*, 11093–11106; b) Wu, A.; Patrick, B. O.; James, B. R. *Inorg. Chem. Comm.* **2012**, *24*, 11–15.
(7) Hanson, S. K.; Baker, R. T.; Gordon, J. C.; Scott, B. L.; Thorn, D. L. *Inorg. Chem.* **2010**, *49*, 5611–5618.
(8) a) Hanson, S. K.; Wu, R.; Silks, L. A. *Angew. Chem. Int. Ed.* **2012**, *51*, 3410-3413; b) Hanson, S. K.; Wu, R.; Silks, L. A. P. *Org. Lett.* **2011**, *13*, 1908–1911; c) Zhang, G.; Scott, B. L.; Wu, R.; Silks, L. A. P.; Hanson, S. K. *Inorg. Chem.* **2012**, *51*, 7354−7361.
(9) Thorn, D. L.; Harlow, R. L.; Herron, N. *Inorg. Chem.* **1996**, *35*, 547–548.
(10) Eagon, S.; Ball-Jones, N.; Haddenham, D.; Saavedra, J.; DeLieto, C.; Buckman, M.; Singaram, B. *Tetrahedron Lett.* **2010**, *51*, 6418–6421.
(11) Preti, L.; Attanasi, O. A.; Caselli, E.; Favi, G.; Ori, C.; Davoli, P.; Felluga, F.; Prati, F. Eur. *J. Org. Chem.* **2010**, *22*, 4312–4320.
(12) Bu, X.; Jing, H.; Wang, L.; Chang, T.; Jin, L.; Liang, Y. *J. Mol. Catal. A-Chem.* **2006**, *259*, 121–124.
(13) Stoichiometric reaction of complex **OV1** with substrate **LM1** in pyridine for 10 min at 100 °C afforded 0.5 equivalents each of **LM1** and 2-phenoxyacetaldehyde **OP20** (reference 7).
(14) a) Hanson, S. K.; Baker, R. T.; Gordon, J. C.; Scott, B. L.; Silks, L. A.; Thorn, D. L. *J. Am. Chem. Soc.* **2010**, *132*, 17804–17816; b) Wigington, B. N.; Drummond, M. L.; Cundari, T. R.; Thorn, D. L.; Hanson, S. K.; Scott, S. L. A. *Chem. Eur. J.* **2012**, *18*, 14981–14988.
(15) Parker, H. J.; Chuck, C. J.; Woodman, T.; Jones, M. D. *Catal. Today* **2016**, *269*, 40–47.
(16) Pan, J.; Fu, J.; Lu, X.; *Energy Fuels* **2015**, *29*, 4503−4509.
(17) Feghali, E.; Cantat, T. *Chem. Commun.*, **2014**, *50*, 862–865.
(18) Xu, H.; Yu, B.; Zhang, H.; Zhao, Y.; Yang, Z.; Xu, J.; Han, B.; Liu, Z. *Chem. Commun.* **2015**, *51*, 12212–12215.

Chapter 4: Second Generation Oxovanadium Catalysts: New Amine Bis(phenolate) Oxovanadium(V) Complexes for Disassembly of Lignin Models

This chapter has been partially published in: a) Díaz-Urrutia, C.; Chen, W-C.; Crites, C-O.; Daccache, J.; Korobkov, I.; Baker, R. T. RSC Adv. ***2015****, 5, 70502-70511; b) Díaz-Urrutia, C.; Daccache, J.; Michel, C.; Fleurat-Lessard, P.; Korobkov, I.; Baker, R. T.* ***2016****, submitted.*

4.1 Introduction

Efficient conversion of lignocellulosic biomass into valuable chemicals and materials presents a daunting challenge for catalysis science.[1] While industrial catalysts have been optimized for the selective functionalization of petroleum-derived hydrocarbons, biomass feedstocks typically contain an oxygen linkage to nearly every carbon. One approach to developing new catalysts for selective transformation of biomass to chemicals and materials aims to take advantage of the ligating properties of the C-O bonds that could serve as directing groups or allow for intramolecular redox processes (Figure 4.1). Many efforts have been made for the catalytic reductive or oxidative C-O and/or C-C bond cleavage of lignin using precious metals such as Re,[2] Ru[3] or Pd[4]; however, a future biorefinery economy requires inexpensive catalysts.

Several first-row transition metal catalysts for lignin model and real lignin disassembly have been reported (for more details see *Chapter 1*). Examples include the hydrogenolysis of C-O bonds using Ni and super-stoichiometric amounts of strong bases[5] and vanadium

salen catalysts which break the C-O bond of β-aryl glycerol lignin models affording olefin and phenol through an anaerobic radical process.[6a] However, the depolymerization of organosolv lignin using vanadium salen complexes showed no significant reduction in the molecular weight.[6b] A related system using photocatalysis afforded C-C bond cleavage of lignin models.[7] Cobalt salen catalysts for the aerobic oxidation of phenolic lignin models were reported to afford a mixture of C-O and C-C bond cleavage products.[8] Our group has demonstrated the selective C-C bond cleavage of β-O-4 lignin models using a Cu(I)/TEMPO catalyst.[9] Nonetheless, the need for high catalyst loadings, long reaction times and high temperatures are a drawback for industrial applications of these methods.

Chapters 2 and *3* showed that oxovanadium(V) complexes, **OV1** and **OV2** with added base effect the selective catalytic oxidation of benzylic secondary alcohols in lignin model compounds (Scheme 4.1).[10] Moreover, these same catalysts induce the selective C_α-C_β bond cleavage of the resulting ketone intermediate in the presence of base, thus proving useful for lignin depolymerization (see *Chapter 5*). However, the large catalyst loadings, low turnover numbers (TON) and the need for co-additives, are driving the development of new catalytic systems.

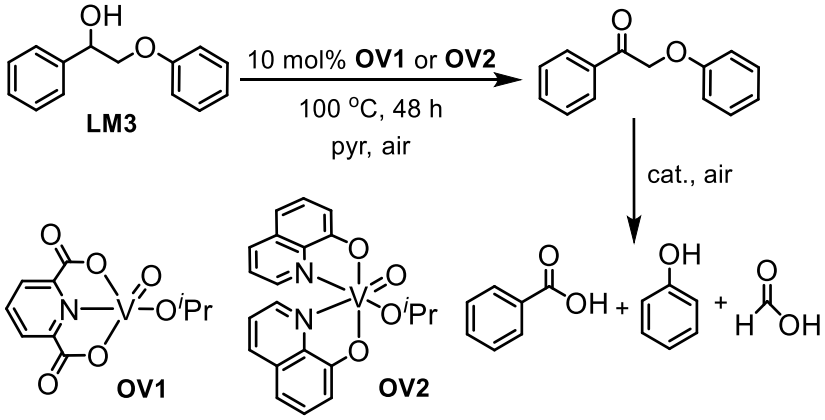

Scheme 4.1. Oxovanadium(V) catalysts **OV1** and **OV2** for the selective oxidation of 1-phenyl-2-phenoxyethanol.[10b]

This *Chapter* describes the preparation of new oxovanadium(V) catalysts incorporating a pendant base in the ligand scaffold to increase the oxidation rates through an intramolecular deprotonation of the secondary alcohol and their catalytic activity for the oxidative C-C and C-O bond cleavage of lignin models. The incorporation of the pendant

base in the ligand scaffold and the potential bifunctionality of the catalysts will also be discussed.

4.2 Materials and Methods

4.2.1 General Considerations

Unless specified otherwise all reactions were carried out under dry nitrogen atmosphere using glovebox or Schlenk techniques. Acetonitrile (CH_3CN), toluene, diethylether (Et_2O) and dichloromethane (DCM) were purchased from Sigma Aldrich or Alfa Aesar. Toluene and diethylether were dried on columns of activated alumina using a J. C. Meyer solvent purification system. Acetonitrile and dichloromethane were dried refluxing over CaH_2, distilling and stirring over activated alumina. Benzoin methyl ether was purchased from Sigma Aldrich and used without further purification. Deuterated acetonitrile (CD_3CN), chloroform ($CDCl_3$), benzene (C_6D_6), toluene (toluene-*d*$_8$) and dimethylsulfoxide (DMSO-*d*$_6$) solvents were purchased from Cambridge Isotope Laboratories and dried following the previous procedures. All other reagents were used as received. ^{1}H, $^{2}H\{^{1}H\}$, $^{13}C\{^{1}H\}$, ^{51}V and 2D NMR spectra were obtained at room temperature on Bruker AVANCE 300 MHz, 400 MHz or 500 MHz spectrometers, with chemical shifts referenced to the residual solvent signal (^{1}H and ^{13}C), externally to $VOCl_3$ (0 ppm, ^{51}V) or internally adding one drop of $CDCl_3$ (7.26 ppm, ^{2}H). For ^{1}H NMR the residual internal solvent peaks are C_6D_6 (δ 7.16), CD_3CN (δ 1.94) and $CDCl_3$ (δ 7.26). For $^{13}C\{^{1}H\}$ residual internal solvent peaks are C_6D_6 (δ 128.06), CD_3CN (δ 1.32, 118.26), toluene-*d*$_8$ (δ 2.08, 6.97, 7.01 and 7.09), DMSO-*d*$_6$ (δ 2.50) and $CDCl_3$ (δ 77.16). IR spectra were obtained on a Thermo Nicolet NEXUS 670 FTIR spectrometer. Mass spectra were recorded on an AB Sciex Q1MS mass spectrometer with electrospray ionization (ESI-MS) in positive mode (ion spray voltage: 5000.0 V, TEM: 400 ºC, declustering potential: 11.00 V and focusing potential: 300.0 V) with samples prepared to *ca.* 0.05 mg/mL in acetonitrile. Elemental analysis was performed at the Laboratoire d'Analyse Élémentaire de l'Université de Montréal and the G.G. Hatch Stable Isotope Laboratory at the University of Ottawa. Turnover numbers (TON) were calculated as the maximum moles of substrate consumed over the amount -in moles- of the catalysts used. Turnover frequencies (TOF) were calculated based on the total TON divided by the total reaction time in hours (h^{-1}). 1-Phenyl-2-methoxyethanol **LM3**[10a] and

arylglycerol β-aryl ether **LM4**[10e] models were prepared according to the published procedures. Oxovanadium complexes **OV1**[11], **OV2**[10f] and **AP6**[12] were also synthesized according to the published literature.

4.2.2 X-ray Crystallography

Data collection results for compounds **AP1** (CCDC reference number 1062663), **AP3**, **AP2**, **AP4** and **AP7** represent the best data sets obtained in several trials for each sample. The crystals were mounted on thin glass fibers using paraffin oil. Prior to data collection crystals were cooled to 200 K. Data were collected on a Bruker AXS SMART single crystal diffractometer equipped with a sealed Mo tube source (wavelength 0.71073 Å) APEX II CCD detector. Raw data collection and processing were performed with APEX II software package from BRUKER AXS.[13] Diffraction data for all samples were collected with a sequence of 0.3° ω scans at 0, 120, and 240° in φ. Initial unit cell parameters were determined from 60 data frames with 0.3° ω scan each collected at the different sections of the Ewald sphere. Semi-empirical absorption corrections based on equivalent reflections were applied.[14] Systematic absences in the diffraction data-set and unit-cell parameters were consistent with triclinic **P**-*1* for compound **AP3**, monoclinic **P***2₁/c* (№14) for compound **AP7**, **C***2/c* (№15) for compound **AP4** and orthorombic **P***ca2₁* (№29) for compound **AP2**. Systematic absences in the diffraction data-set and unit-cell parameters were consistent with monoclinic **P***2₁/c* (№14) for compound **AP1.** Solutions in the centrosymmetric space groups for all compounds yielded chemically reasonable and computationally stable results of refinement. The structures were solved by direct methods, completed with difference Fourier synthesis, and refined with full-matrix least-squares procedures based on F^2.

The asymmetric unit of the structural model for compound **AP1** consists of one molecule of target compound located on the inversion center and one fully occupied molecule of acetonitrile crystallization solvent located on the general position of the symmetry group.

Diffraction data for the crystal of complex **AP2** were collected to 0.75Å resolution; however, due to small crystal size and weak diffraction, it was discovered that both R(int) and R(sigma) exceeded 35% for the data below 1.00Å resolution. Based on R(sigma) value, data were truncated to 0.95Å resolution for refinement. Structure of compound **AP2** reveals one target molecule situated on a general position of the symmetry group. In the

final refinement stage, thermal motion parameters for the ^{t}Bu fragment based at C(23) suggested a rotational disorder not related to the symmetry elements. Disorder was successfully modeled; however, the set of geometrical (SADI) and thermal motion (SIMU, RIGU) restraints were applied to achieve acceptable fragment geometries and thermal motion values. Disordered fragment occupancies were refined initially. However these values were fixed at the latest stages of the refinement and acceptable thermal motion parameters were achieved with occupancies split at 65% : 35% ratio.

The asymmetric unit of the **AP4** structure contains two independent molecules of the target species. Both molecules are located on the general positions of the symmetry group. Thermal motion parameters for two different ^{t}Bu fragments based at C(23) and C(75) strongly suggested a rotational disorder not related to the symmetry elements. Disorder was successfully modeled; however the set of geometrical (SADI) and thermal motion (EADP) restrains were applied to achieve acceptable fragments geometries and thermal motion values. Disordered fragment occupancies were refined initially. However for both ^{t}Bu moieties occupancy values were fixed at the latest stages of the refinement at 50% : 50% ratio. In addition to the rotational disorder of ^{t}Bu groups, thermal parameters of the two carbon atoms C(72) and C(74) of the amino moiety based on C(70) carbon suggested positional disorder not related to symmetry elements. Positions of both carbon atoms were split in two and occupational factors were successfully refined to 50% : 50% ratio. A set of geometry restraints (SADI) was used to maintain acceptable fragment geometry.

Diffraction data for the crystal of the complex **AP7** were collected to 0.75Å resolution, however, due to small crystal size and weak diffraction, it was discovered that both R(int) and R(sigma) exceeded 35% for the data below 1.00Å resolution. Based on R(sigma) value, data were truncated to 0.95Å resolution for refinement. Initial refinement of the structural model for **AP7** suggested the presence of two non-merohedrally twinned domains in the mounted crystal. Two independent orientation matrices were found using CELL_NOW software.[15] The data set was re-integrated with two independent orientation matrices and consecutive model refinement was performed using HKLF5 reflection data file. Twinning domain ratio coefficient (BASF) was refined to 0.25788. The structural model for this compound contains one target molecule and two molecules of

dichloromethane crystallization solvent. All three fragments are located on general positions.

For all four compounds all hydrogen atom positions were calculated based on the geometry of the related non-hydrogen atoms. All hydrogen atoms were treated as idealized contributions during the refinement. All scattering factors are contained in several versions of the SHELXTL program library, with the latest version used being v.6.12.[16]

Table 4.1. Crystallographic data for amine bis(phenolate) oxovanadium complexes **AP1-4** and **AP7**.

	AP1	**AP2**	**AP3**	**AP4**	**AP7**
formula	$C_{76}H_{106}N_6O_7V_2$	$C_{36}H_{60}N_2O_4V$	$C_{38}H_{63}N_2O_4V$	$C_{78}H_{129}N_4O_8V_2$	$C_{52}H_{75}C_{14}N_2O_5V$
fw	1371.54	635.80	662.84	1352.72	1000.88
a (Å)	14.6421(4)	19.1260(12)	9.7974(4)	35.4027(8)	10.429(2)
b (Å)	17.5486(4)	14.6400(8)	10.4615(4)	11.0685(2)	19.157(4)
c (Å)	15.7326(4)	12.8206(8)	21.2065(8)	41.4319(9)	26.765(5)
α (deg)	90	90	97.0544(18)	90	90
β (deg)	113.6928(11)	90	101.0376(18)	90.8045 (11)	92.776(6)
γ (deg)	90	90	107.5275(18)	90	90
crystal system	monoclinic	orthorhombic	triclinic	monoclinic	Monoclinic
Space group	P 21/n	P c a 21	P-1	C 2/c	P 21/c
V ($Å^3$)	3701.74(16)	3589.8(4)	1996.14(14)	16233.7(6)	5340.8(18)
D_c (g cm^{-1})	1.182	1.176	1.103	1.107	1.245
μ (mm^{-1})	0.307	0.314	0.285	0.282	0.431
Z	2	4	2	8	4
F(000)	1412.0	1380.0	720.0	5880.0	2128.0
T/K	200.0	200	200	200	200
R_1 [I>2σ(I)]	0.0369(8127)	0.0443	0.0515	0.0621	0.0769
wR_1 [I>2σ(I)]	0.1030(9146)	0.1002	0.1425	0.1632	0.2049

4.2.3 Synthesis of PL1 Ligand

PL1 was synthesized following the published procedure.[17] A solution of 2,4-di-*tert*-butylphenol (5.00 g, 24.2 mmol) and 2-(aminomethyl)pyridine (1.80 mL, 23.9 mmol) in methanol was heated to reflux for 18 h and then the flask was cooled at -5 ^{o}C for 8 h. The yellow viscous solid was triturated in cold methanol yielding a white solid that was then filtered and dried (2.30 g, 30% yield). ^{1}H NMR (400 MHz, $CDCl_3$): δ 10.56 (s, 2H, Ar-O*H*), 8.70 (d, 1H, *J* = 4.5 Hz, pyr), 7.70 (t, 1H, *J* = 7.6, 1.0 Hz, pyr), 7.29 (t, 1H, *J* = 6.0 Hz, pyr), 7.24 (d, 2H, *J* = 2.3 Hz, Ar-*H*), 7.14 (d, 1H, *J* = 7.6 Hz, pyr), 6.94 (d, 2H, *J* = 2.3 Hz, Ar-*H*), 3.86 (ov br, 2H, CH_2), 3.82 (ov br, 2H, CH_2), 1.41 (s, 18H, ^{t}Bu), 1.30 (s, 18H, ^{t}Bu); ^{13}C{^{1}H} NMR (75.5 MHz, $CDCl_3$): δ 154.0, 148.3, 140.6, 137.4, 136.5, 125.3, 123.6, 122.6, 121.4, 56.9, 55.5, 35.2, 34.3, 31.8, 29.8.

4.2.4 Synthesis of PL2 Ligand

PL2 was synthesized following the published procedure.[17] A solution of 2,4-di-*tert*-butylphenol (4.12 g, 20.0 mmol), *N*,*N*-dimethyl-1,3-propanediamine (1.26 mL, 10.0 mmol) in methanol (5 mL) was stirred and refluxed for 24 h. The mixture was cooled at -5 ^{o}C for 18 h and then the supernatant solution was decanted. The supernatant was removed and the resulting oil was dissolved in CH_3CN. The sample was cooled down at -5 ^{o}C for 2 hours. Some white precipitate was observed in the flask, together with a yellow solution. The flask was cooled down overnight at -5 ^{o}C for 48 h affording a white precipitate. The white solid was filtered, washed with cold acetonitrile and dried to give 1.81 g (36% yield). ^{1}H NMR (300 MHz, $CDCl_3$): δ 7.21 (d, 2H, *J* = 2.5 Hz, Ar-*H*), 6.89 (d, 2H, *J* = 2.5 Hz, Ar-*H*), 3.57 (s, 4H, CH_2), 2.61 (t, 2H, *J* = 6.0 Hz, CH_2), 2.50 (br, 2H, CH_2), 2.39 (s, 6H, N(CH_3)$_2$), 1.82 (br, 2H, Ar-O*H*), 1.42 (s, 18H, ^{t}Bu), 1.29 (s, 18H, ^{t}Bu); ^{13}C{^{1}H} NMR (75.5 MHz, $CDCl_3$): δ 153.4, 140.4, 136.0, 125.3, 123.4, 121.4, 58.7, 57.6, 55.2, 45.8, 35.1, 34.2, 31.8, 29.7, 23.0.

4.2.5 Synthesis of AP1

In a 20 mL scintillation vial a solution of **PL1** (420 mg, 0.771 mmol) in 3 mL of CH_2Cl_2 was added dropwise to a solution of V(O)(O^{i}Pr)$_3$ (207 mg, 0.849 mmol) in 1 mL of CH_2Cl_2. A rapid change of colour was observed from light green to dark purple. The reaction was stirred under nitrogen for 18 hours, then the solvent was removed under

vacuum and replaced by acetonitrile. The mixture was placed at -35 ^{o}C for 18 h and the dark purple precipitate was washed with cold acetonitrile. The purple filtrate was placed at -35 ^{o}C for 2 hours and then filtered again through Celite, resulting in a separation of both isomers. The *trans* isomer was isolated as a dark purple solid (184 mg, 40% yield) by evaporating the acetonitrile filtrate. **AP1a**: ^{1}H NMR (300 MHz, CD_3CN): δ 8.97 (d, 1H, *J* = 5.8 Hz, Ar), 7.49 (td, 1H, J = 7.7, 1.7 Hz, Ar), 7.09 (ov m, 3H, Ar), 7.03 (ov m, 2H, Ar), 6.69 (d, 1H, *J* = 7.7 Hz, Ar), 5.42 (sept, 1H, *J* = 6.0 Hz, V-OCH) 4.46 (d, 2H, *J* = 12 Hz, Ar–CH2), 3.77 (s, 2H, pyr-CH_2), 3.45 (d, 2H, *J* = 12 Hz, Ar-CH_2), 1.36 (d, 6H, *J* = 6.0 Hz, $(CH_3)_2$), 1.31 (s, 18H, ^{t}Bu), 1.24 (s, 18H, ^{t}Bu); $^{13}C\{^{1}H\}$ NMR (75.5 MHz, CD_3CN): δ 156.5, 156.5, 152.2, 141.7, 139.1, 125.2, 124.9, 122.5, 62.1, 55.6, 34.6, 33.9, 30.8, 29.3; ^{51}V NMR (78.9 MHz, CD_3CN): -473.9 ppm (s); IR (NaCl plate): $\nu_{V=O}$ = 918 cm^{-1}. The *cis* isomer was isolated as a brown solid (92 mg, 18% yield) from filtration of the cold solution of the isomer mixture. **AP1b**: ^{1}H NMR (300 MHz, CD_3CN): δ 8.55 (d, 1H, *J* = 5.0 Hz, Ar), 7.41 (td, 1H, *J* = 7.7, 1.7 Hz, Ar), 7.05 (d, 2H, *J* = 2.5 Hz, Ar), 7.03 (d, 2H, *J* = 2.5 Hz, Ar), 6.99 (ov m, 1H, Ar), 6.77 (d, 1H, *J* = 7.7 Hz, Ar), 5.97 (sept, 1H, *J* = 6.0 Hz, V-OCH), 4.69 (d, 2H, *J* = 13 Hz, Ar-CH_2), 3.91 (s, 2H, pyr-CH_2), 3.84 (d, 2H, *J* = 13.4 Hz, Ar-CH_2), 1.64 (d, 6H, *J* = 6.0 Hz, $(CH_3)_2$), 1.26 (s, 18H, ^{t}Bu), 1.23 (s, 18H, ^{t}Bu). Due to rapid isomerization, the ^{13}C NMR spectrum for **AP1b** was not obtained. ^{51}V NMR (78.9 MHz, CD_3CN): -514.1 ppm (s); IR (NaCl plate): $\nu_{V=O}$ = 960 cm^{-1}; Anal. Calcd. for $C_{39}H_{57}O_4N_2V$: C 70.04 H 8.59 N 4.19; Found: C 69.98 H 8.60 N 4.26.

4.2.6 Synthesis of AP2

In a 20 mL scintillation vial, complex **AP3** (100 mg, 0.150 mmol) and 0.5 mL of methanol were dissolved in 1 mL of acetonitrile. The reaction mixture was stirred for 20 min and then the solvent was reduced under vacuum to afford a pale brown solid. The solid was recrystallized using a mixture of 1:1:1 (v/v) Et_2O/CH_3CN/hexanes at -35 ^{o}C affording pale orange crystals. The solid was filtered and washed with cold acetonitrile to afford 20 mg (21 % yield). For the major isomer: ^{1}H NMR (300 MHz, C_6D_6): δ 7.55 (d, 2H, *J* = 2.5 Hz, Ar), 6.99 (d, 2H, *J* = 2.5 Hz, Ar), 5.21 (s, 3H, V-OC*H*$_3$), 4.47 (br d, 2H, *J* = 14 Hz, Ar-C*H*$_2$), 3.47 (d, 2H, *J* = 14 Hz, Ar-C*H*$_2$), 2.63 (t, 2H, *J* = 6.5 Hz, VNC*H*$_2$CH$_2$CH$_2$), 1.91 (s, 6H, N(C*H*$_3$)$_2$), 1.78 (m, 3H, CH$_2$C*H*$_2$CH$_2$), 1.66 (s, 18H, ^{t}Bu), 1.38 (s, 18H, ^{t}Bu), 1.23 (t, 2H, *J* = 6.5 Hz, VNCH$_2$CH$_2$C*H*$_2$); $^{13}C\{^{1}H\}$ NMR (75.5 MHz, C_6D_6): δ 162.3, 143.0, 142.3,

135.8, 124.3, 123.8, 123.4, 123.1, 122.5, 73.2, 62.0, 58.5, 46.6, 35.5, 34.5, 32.0, 30.4; ^{51}V NMR (78.9 MHz, C_6D_6): δ -501.7 (br); IR (NaCl plate): $\nu_{V=O}$ = 1063 cm^{-1}. For the minor isomer: ^{51}V NMR (78.9 MHz, C_6D_6): δ -475.0 (ov br); IR (NaCl plate): $\nu_{V=O}$ = 996 cm^{-1}. Anal. Calcd. for $C_{36}H_{59}O_4N_2V$: C 68.11 H 9.37 N 4.41; Found: C 68.14 H 9.37 N 4.38.

4.2.7 Synthesis of AP3

In a 20 mL scintillation vial a solution of **PL2** (271 mg, 0.503 mmol) in 3 mL of DCM was added dropwise to a solution of V(O)(O^{i}Pr)$_3$ (136 mg, 0.550 mmol) in DCM. The resulting dark red solution was stirred for 18 hours, and then the solvent was removed under vacuum and replaced with 5 mL of acetonitrile. The mixture was cooled down at -35 ^{o}C for 24 h, and the resulting red solid was filtered, washed with cold acetonitrile and dried to give 298 mg (89% yield). X-ray quality crystals were prepared using a concentrated solution of 3:1 (v/v) DCM/acetonitrile. Two isomers are observed by ^{1}H NMR in a 1:0.2 ratio. For the major isomer: ^{1}H NMR (300 MHz, C_6D_6): δ 7.51 (ov d, 2H, *J* = 2.5 Hz, Ar), 6.95 (d, 2H, *J* = 2.5 Hz, Ar), 5.93 (sept, 1H, *J* = 6.0 Hz, V-OC*H*), 4.90 (d, 2H, *J* = 15 Hz, Ar-C*H*$_2$), 3.46 (d, 2H, *J* = 15 Hz, Ar-C*H*$_2$), 2.90 (m, 2H, VNC*H*$_2$CH$_2$CH$_2$), 1.65 (s, 6H, N(C*H*$_3$)$_2$), 1.63 (ov d, 6H, *J* = 6.0 Hz, O^{i}Pr), 1.60 (s, 18H, ^{t}Bu), 1.51 (t, 2H, *J* = 6.5 Hz, VNCH$_2$CH$_2$C*H*$_2$), 1.37 (s, 18H, ^{t}Bu), 1.29 (ov m, 2H, VNCH$_2$CH$_2$C*H*$_2$); ^{13}C{^{1}H} NMR (75.5 MHz, CD_3CN): δ 143.7, 125.1, 124.2, 122.5, 60.5, 57.8, 45.3, 35.6, 35.0, 31.8, 50.2, 30.1, 19.1; ^{51}V NMR (78.9 MHz, C_6D_6): -567.2 (s); IR (NaCl plate): $\nu_{V=O}$ = 977 cm^{-1}. For the minor isomer: ^{1}H NMR (300 MHz, C_6D_6): δ 6.88 (d, 2H, *J* = 2.5 Hz, Ar), 6.26 (sept, 1H, *J* = 6.0 Hz, V-OC*H*), 3.61 (br s, 4H, Ar-C*H*$_2$), 3.13 (m, 2H, VNC*H*$_2$CH$_2$CH$_2$), 1.85 (s, 6H, N(C*H*$_3$)$_2$); ^{51}V NMR (78.9 MHz, C_6D_6): -516.1 (br); IR (NaCl plate): $\nu_{V=O}$ = 916 cm^{-1}; For the mixture of both isomers: Anal. Calcd. for $C_{38}H_{63}O_4N_2V$: C 68.85 H 9.58 N 4.23; Found: C 69.75 H 9.46 N 4.06.

4.2.8 Synthesis of AP4

In a 20 mL scintillation vial complex **AP3** (150 mg, 0.230 mmol) and 2 mL of HO^{t}Bu were dissolved in 0.5 mL of DCM. The reaction mixture was stirred for 30 min at room temperature and then the solvent was removed under vacuum and replaced by 0.5 mL of CH_3CN. After overnight cooling at -35 ^{o}C, a dark brown solid was isolated, washed with cold acetonitrile and dried. The crude compound was dissolved in 1:1 (v/v)

DCM/acetonitrile and cooled down at -35 ^{o}C yielding 33 mg of a dark red solid (22% yield). X-ray quality crystals were prepared using a concentrated solution of 3:1 (v/v) DCM/acetonitrile. ^{1}H and ^{51}V NMR spectra show a mixture of two isomers in a 1:0.3 ratio. For the major isomer: ^{1}H NMR (300 MHz, C_6D_6): δ 7.50 (ov d, 2H, *J* = 2.5 Hz, Ar), 6.94 (d, 2H, *J* = 2.5 Hz, Ar), 5.03 (d, 2H, *J* = 15 Hz, Ar-C*H*$_2$), 3.43 (d, 2H, *J* = 15 Hz, Ar-C*H*$_2$), 2.91 (m, 2H, VNC*H*$_2$CH$_2$CH$_2$), 1.80 (s, 9H, V-O^{t}Bu), 1.59 (ov s, 18H, ^{t}Bu), 1.58 (s, 6H, N(C*H*$_3$)$_2$), 1.52 (t, 2H, *J* = 6.5 Hz, VNCH$_2$CH$_2$C*H*$_2$), 1.36 (ov s, 18H, ^{t}Bu), 1.26 (ov m, 2H, VNCH$_2$CH$_2$C*H*$_2$); ^{13}C{^{1}H} NMR (75.5 MHz, C_6D_6): δ 145.5, 124.5, 124.1, 123.8, 122.7, 122.2, 60.3, 56.9, 45.3, 44.8, 35.4, 34.5, 32.1, 31.9, 30.29; ^{51}V NMR (78.9 MHz, C_6D_6): δ -590.6; IR (NaCl plate): $\nu_{V=O}$ = 954 cm^{-1}. For the minor isomer: ^{1}H NMR (300 MHz, C_6D_6): δ 7.48 (ov d, 2H, *J* = 2.5 Hz, Ar), 6.85 (br d, 2H, *J* =2.5 Hz, Ar), 3.68 (br s, 2H, Ar-C*H*$_2$), 3.57 (m, 2H, Ar-C*H*$_2$), 3.22 (m, 2H, VNC*H*$_2$CH$_2$CH$_2$); ^{51}V NMR (78.9 MHz, C_6D_6): δ -563.5 (br); IR (NaCl plate): $\nu_{V=O}$ = 985 cm^{-1}.

4.2.9 Synthesis of AP5

In a 20 mL scintillation vial, complex **AP3** (100 mg, 0.151 mmol) and cyclobutanol (44 mg, 0.60 mmol) were dissolved in 3 mL of DCM and stirred at room temperature for 1 h. The solvent was removed under vacuum and 2 mL of 3:1 (v/v) DCM/acetonitrile was added. The flask was cooled down at -35 ^{o}C for 18 h and the resulting solid was filtered, washed with cold acetonitrile and dried to give 72 mg of a brown powder (70%). For the major isomer: ^{1}H NMR (300 MHz, C_6D_6): δ 7.53 (d, 2H, *J* = 2.3 Hz, Ar), 6.95 (d, 2H, *J* = 2.3 Hz, Ar), 6.16 (q, 1H, *J* = 7.6 Hz, OCy), 4.80 (d, 2H, *J* = 15 Hz, Ar-C*H*$_2$), 3.47 (d, 2H, *J* = 15 Hz, Ar-C*H*$_2$), 2.87 (m, 2H, VNCH$_2$C*H*$_2$CH$_2$), 2.60 (m, 4H, Cy), 1.65 (s, 6H, N(C*H*$_3$)$_2$), 1.62 (s, 18H, ^{t}Bu), 1.55 (t, 2H, *J* = 6.7 Hz, VNCH$_2$CH$_2$C*H*$_2$),1.37 (s, 18H, ^{t}Bu), 1.28 (ov br, 2H, Cy); ^{13}C{^{1}H} NMR (75.5 MHz, C_6D_6): δ 160.2, 142.7, 136.3, 123.9, 123.7, 121.8, 87.5, 60.7, 57.1, 46.8, 45.2, 36.7, 35.4, 34.5, 31.9, 30.2; ^{51}V NMR (78.9 MHz, C_6D_6): δ -546.6 (s); IR (NaCl plate): $\nu_{V=O}$ = 989 cm^{-1}. For the minor isomer: ^{1}H NMR (300 MHz, C_6D_6): δ 6.91 (d, 2H, *J* = 2.5 Hz, Ar), 6.36 (q, 1H, *J* = 7.3 Hz, OCy), 3.63 (d br, 2H, Ar-C*H*$_2$), 3.07 (br, 2H, VNCH$_2$C*H*$_2$CH$_2$), 1.90 (s, 6H, N(C*H*$_3$)$_2$); ^{51}V NMR (78.9 MHz, C_6D_6): δ - 497.1 (br); IR (NaCl plate): $\nu_{V=O}$ = 962 cm^{-1}.

4.2.10 Synthesis of AP7

In a 20 mL scintillation vial, complex **AP3** (85 mg, 0.13 mmol) and 1,2-diphenyl-2-methoxyethanol **LM2** (138 mg, 0.603 mmol) were dissolved in 3 mL of DCM. The reaction mixture was stirred for 1 h at room temperature. The solvent was removed under vacuum and the resulting brown solid was recrystallized from 3:1 (v/v) CH_3CN/DCM at -35 ^oC to afford 67 mg of a brown solid (63% yield). Recrystallization from 3:1 (v/v) DCM/CH_3CN at -35 ^oC afforded dark-blue crystals suitable for X-ray crystallography. ^1H NMR (300 MHz, C_6D_6): δ 7.73 (d, 1H, *J* = 2.3 Hz, Ar), 7.64 (d, 1H, *J* = 2.3 Hz, Ar), 7.42 (m, 2H, Ar-**LM2**), 7.22 (d, 1H, *J* = 2.3 Hz, Ar), 7.12 (m ov, 4H, Ar-**LM2**), 7.05 (ov m, 1H, Ar), 6.97 (ov m, 4H, Ar-**LM2**), 6.69 (d, 1H, *J* = 9.2 Hz, VOCH), 4.79 (d, 1H, *J* = 9.2 Hz, MeOCH), 4.08 (d, 1H, *J* = 12 Hz, ArC*H*H), 3.92 (d, 1H, *J* = 12 Hz, ArCH*H*), 3.32 (d, 1H, *J* = 12 Hz, ArC*H*H), 3.22 (s, 3H, OCH_3) 3.18 (d, 1H, *J* = 12 Hz, ArC*H*H), 1.96 (s, 9H, ^{t}Bu), 1.89 (s, 6H, N(CH_3)$_2$), 1.70 (s, 9H, ^{t}Bu), 1.63 (ov m, 2H, VNC$H_2CH_2CH_2$), 1.57 (m ov, 2H, $VNCH_2CH_2CH_2$), 1.43 (s, 9H, ^{t}Bu), 1.42 (s, 9H, ^{t}Bu) 1.37 (m ov, 2H, $VNCH_2CH_2CH_2$); Notice that dichloromethane is strongly included in the crystal lattice of **AP7** appears as an impurity in the ^1H NMR spectrum (δ 4.26). Due to slow decomposition of **AP7** at room temperature, an overnight carbon NMR spectrum was recorded at 268 K: $^{13}C\{^1H\}$ NMR (Toluene-d_8, 75.5 MHz, 268.15 K): δ 165.9, 164.5, 142.3, 141.8, 141.3, 138.2, 137.4, 136.3, 135.4, 124.5, 124.3, 124.2, 123.8, 122.8, 122.7, 94.2, 91.3, 57.7, 57.6, 57.4, 56.7, 53.3, 52.4, 45.4, 35.7, 35.2, 34.5, 32.0, 31.9, 30.8, 30.5, 18.8; ^{51}V NMR (78.9 MHz, C_6D_6): δ -419.7 (br, $\Delta\nu_{1/2}$ = 640 Hz); (NaCl plate): $\nu_{V=O}$ = 994 cm^{-1}; ES-MS: Calcd. $C_{50}H_{71}N_2O_5V$ *m/z* 831.488 ([M+H^+]), found 831.598.

4.2.11 Synthesis of AP8

In a 20 mL scintillation vial, complex **AP6** (100 mg, 0.161 mmol) and 1,2-diphenyl-2-methoxyethanol **LM2** (173 mg, 0.785 mmol) were dissolved in 3 mL of DCM. The reaction mixture was stirred at room temperature for 1 h and then the solvent was removed under vacuum. Recrystallization using a minimum amount of 3:1 (v/v) acetonitrile/DCM at -35 ^oC afforded 45 mg of a black solid (35% yield). ^1H NMR (300 MHz, C_6D_6): δ 7.73 (d, 1H, *J* = 2.4 Hz, Ar), 7.64 (d, 1H, *J* = 2.4 Hz, Ar), 7.43 (ov m, 3H, Ar-**LM2**), 7.19 (ov d, 2H, *J* = 2.4 Hz, Ar-**LM2**), 7.13 (ov d, 2H, *J* = 7.5 Hz, Ar-**LM2**), 7.08 (ov d, 1H, *J* = 2.4 Hz, Ar-**LM2**), 6.98 (ov m, 2H, Ar-**LM2**), 6.97 (ov d, 1H, *J* = 2.4 Hz, Ar), 6.70 (d, 1H, *J* =

9.2 Hz, $VOCH_2$), 4.81 (d, 1H, *J* = 9.2 Hz, MeOCH), 4.08 (d, 1H, *J* = 12 Hz, ArCH*H*), 3.91 (d, 1H, *J* = 12 Hz, ArC*H*H), 3.29 (d, 1H, *J* = 12 Hz, ArCH*H*), 3.23 (s, 3H, OMe), 3.17 (d, 1H, J = 12 Hz, ArCH*H*), 1.97 (s, 9H, ^{t}Bu), 1.71 (s, 9H, ^{t}Bu), 1.42 (s, 18H, ^{t}Bu), 1.36 (d, 1H, *J* = 5.4 Hz, CH*H*), 0.58 (s, 2H, CH*H*), 0.35 (t, 3H, *J* = 7.4 Hz, CH_3), 0.29 (s, 1H, C*H*H); Notice that dichloromethane is strongly included in the crystal lattice of **AP8** and appears as an impurity in the ^{1}H NMR spectrum (δ 4.26); ^{51}V NMR (78.9 MHz, C_6D_6): δ -418 (br, $\Delta\nu_{1/2}$ = 600 Hz).

4.2.12 Synthesis of LM3-$^2H_1$

In a 100 mL round-bottom flask, a solution of 2-phenoxyacetophenone (530 mg, 2.50 mmol) in 25 mL of methanol was treated with small portions of $NaBD_4$ (52 mg, 1.3 mmol) over a 5 min period, cooling with an ice bath. The reaction mixture was stirred at room temperature for 1h and then a saturated solution of NH_4Cl (25 mL) followed by CH_2Cl_2 (25 mL) were added. The organic layer was extracted with CH_2Cl_2 (3 x 25 mL), washed with water, dried in $MgSO_4$ and concentrated in the rotary evaporator to afford a white powder. Recrystallization with hot ethanol afforded 436 mg (81% yield) of 1-phenyl-2-methoxy(1-^{2}H)ethanol. ^{1}H NMR (300 MHz, $CDCl_3$): δ 7.49 - 7.27 (m, 7H, Ar), 6.98 (t, 1H, *J* = 7.4 Hz, Ar), 6.93 (d, 2H, *J* = 7.4 Hz, Ar), 4.12 (d, 1H, *J* = 9.6 Hz, C*H*$_2$), 4.02 (d, 1H, *J* = 9.6 Hz, C*H*$_2$), 2.13 (br, 1H, O*H*); ^{2}H{^{1}H} NMR (46.1 MHz, $CHCl_3$): δ 5.13 (br); ^{13}C{^{1}H} (75.5 MHz, $CDCl_3$): δ 158.5, 139.7, 129.7, 128.7, 128.3, 126.4, 121.4, 114.8, 73.3, 72.3 (t, *J* = 22 Hz, *C*DOH); Anal. Calcd. for $C_{14}H_{13}DO_2$: C 78.11 H 7.02; Found: C 78.09 H 6.84.

4.2.13 General Procedure for Oxidative Catalytic Cleavage of Lignin Models

In an NMR tube, the lignin model (25 mg) and desired amount of vanadium catalyst were dissolved in 1 mL of deuterated solvent containing 6.6 mM of dimethylsulfone or 6.6 mM 1,3,5-tri-*tert*-butylbenzene as an internal standard. An initial ^{1}H NMR spectrum was recorded and the sample was transferred to a sealed 25 mL Schlenk tube. After suitable reaction time the sample was cooled to room temperature and transferred to an NMR tube for analysis. An alternative procedure using non-deuterated solvents for the catalytic reaction required removing the solvent by vacuum and replacing it by $CDCl_3$. ^{1}H NMR integration against the internal standard revealed the conversions and yields for each reaction. Control experiments were performed in the absence of catalyst using the same

conditions described above. Control experiments using 1,2-diphenyl-2-methoxyethanol **LM2** in toluene heated at 105 ^{o}C for 20 h afforded 1% conversion with less than 1% yield of benzaldehyde. Similar results were obtained for 1-phenyl-2-phenoxyethanol **LM3**. Yields are expressed as a percentage of the theoretical maximum in moles based on the initial amount of substrate.

4.3 Results and Discussion

4.3.1 Synthesis of Oxovanadium Complexes

N-donor appended bis(2-phenol-methyl)amine ligands were targeted for this study due to their ease of preparation and inexpensive cost. N,N-bis(3,5-di-*tert*-butyl-2-phenol)-N-(dimethylaminopropyl)amine **PL1** and N,N-bis(3,5-di-*tert*-butyl-2-phenol)-N-(methyl-pyridine)amine **PL2** were prepared in a one-pot synthesis from commercially available reagents through Mannich condensations.[17] Complexes **AP1**[18] and **AP3** were prepared following similar procedures (Figure 4.1), using stoichiometric amounts of V(O)(O^{i}Pr)$_3$

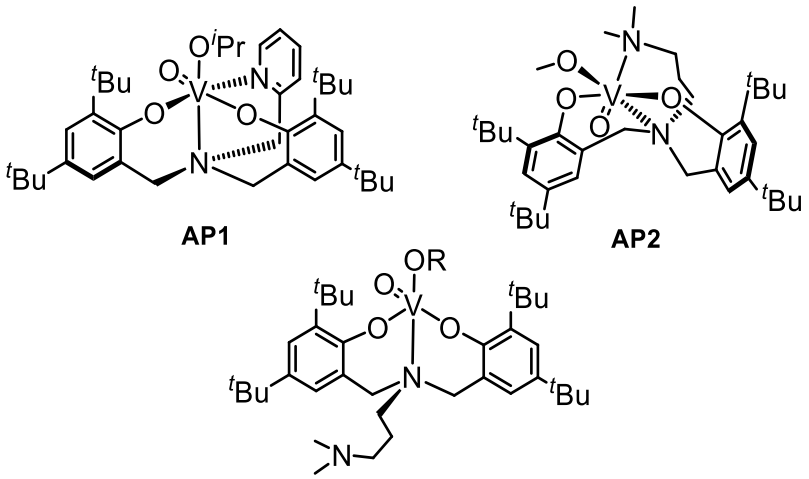

Figure 4.1. New amine bis(phenolate) oxovanadium(V) complexes.

and the corresponding ligand in a concentrated solution of DCM. Several oxovanadium(V) complexes [**PL2**(V^{V}(O)(X))] bearing different alkoxides [X = OMe (**AP2**), O^{t}Bu (**AP4**) and OCyBu (**AP5**)] were synthesized by dissolving complex **AP3** in a concentrated solution of the desired alcohol.

Complexes **AP1** and **AP3** display two different isomers in solution corresponding to the oxo group being *cis* or *trans* to the central nitrogen of the ligand respectively. For complex

AP1, the two different isomers (**AP1a** and **AP1b**) were isolated after several solvent extractions.[18] The *cis* complex **AP1b** rapidly isomerizes in solution to the more stable *trans* isomer **AP1a**.[18] The ^{1}H NMR resonances of the methylene bridges of the phenolate arms are shown as diastereotopic AX protons (*e.g.*, for major isomer of **AP3**: 4.90 and 3.46 ppm, $^{2}J_{H\text{-}H}$ = 15 Hz). In structurally related complexes,[19] the ^{51}V NMR chemical shift tends to lower field as the electronegativity of the X ligand increases (*cf.* -473.9 ppm for **AP1** *vs.* -590.6 ppm for **AP4**). Variable temperature ^{1}H NMR spectra (-15 ^{o}C to 25 ^{o}C) in CD_3CN of complex **AP3** shows that the isomerization occurs on the NMR time scale (see Figure A4). Characteristic methylene peaks for the minor isomer are broad until they disappear as the signals for the major isomer increase. This differs from previous observations where interconversion at high temperatures does not occur.[19a] The isopropoxide methine signal of the major isomer of both complexes **AP1** and **AP3** appears as a *septet* by ^{1}H NMR in CD_3CN at δ 5.42 and 5.93, respectively, shifting downfield as the ligand becomes more electron-donating.[10c] For example, the chemical shift of the methine proton in catalyst **OV2** appears at δ 6.18 in CD_3CN, indicating a comparable electron-donating character for the amine bis(phenoxide) ligands.

The crystal structures of **AP1**, **AP2-4** were obtained from a concentrated solution of CH_3CN/DCM at -35 ^{o}C. As discussed previously, the solution NMR spectrum of **AP1** showed a distinct isopropoxide signals for each isomer; however the solid-state structure indicates a bridging *μ*-oxo bimetallic oxovanadium complex (Figure 4.2). The isopropoxide group in **AP1** presumably undergoes rapid hydrolysis with a quantitative amount of water to form the bimetallic compound depicted in the ORTEP representation. Indeed, conducting the recrystallization under meticulously dry conditions produced the same crystals. Interestingly, the size of the alkoxide plays an important role in determining the coordination number of complexes **AP2** to **AP5**. The propylamine side arm coordinates to V in the methoxide complex **AP2**, giving a pseudooctahedral vanadium center (Figure 4.3, top). With larger alkoxides such as -O^{i}Pr, -O^{t}Bu and -OCyBu the amine side-arm remains uncoordinated (in complexes **AP3**, **AP4** and **AP5** respectively), resulting in a square pyramidal, five-coordinate vanadium center (Figure 4.3, bottom). The structure dependence on the size of the -X groups is in agreement with the hemilabile character of the tethered amine base.[20]

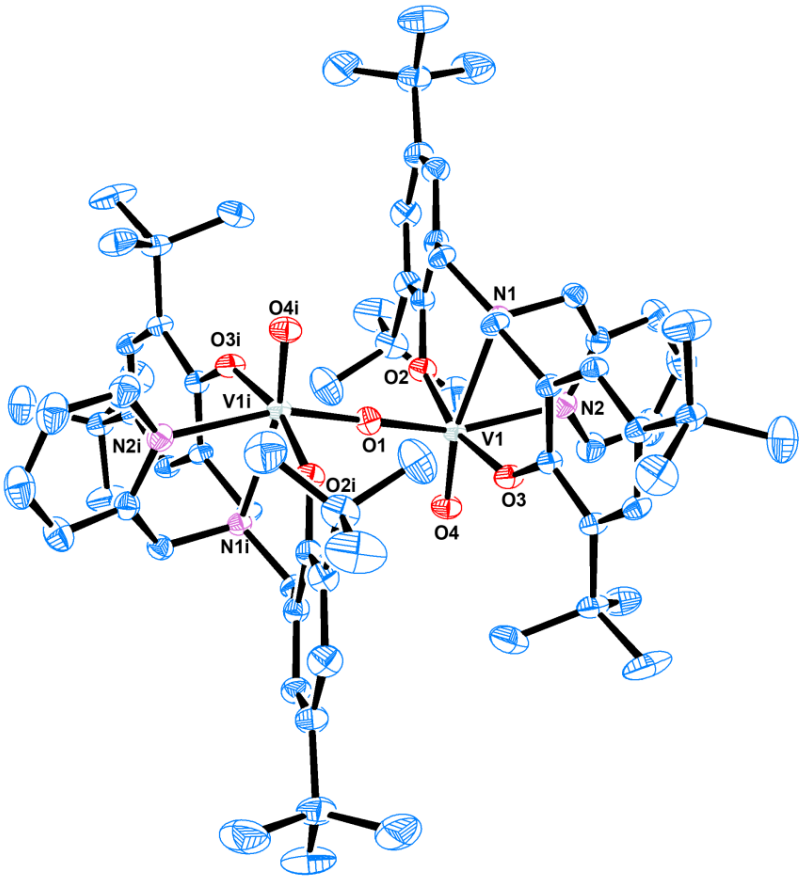

Figure 4.2. ORTEP representation for **AP1**. Thermal ellipsoids set at 50% probability, hydrogen atoms are omitted for clarity. Selected bond lengths (Å) and bond angles (deg) are displayed in Table 4.2 and Table 4.3, respectively.

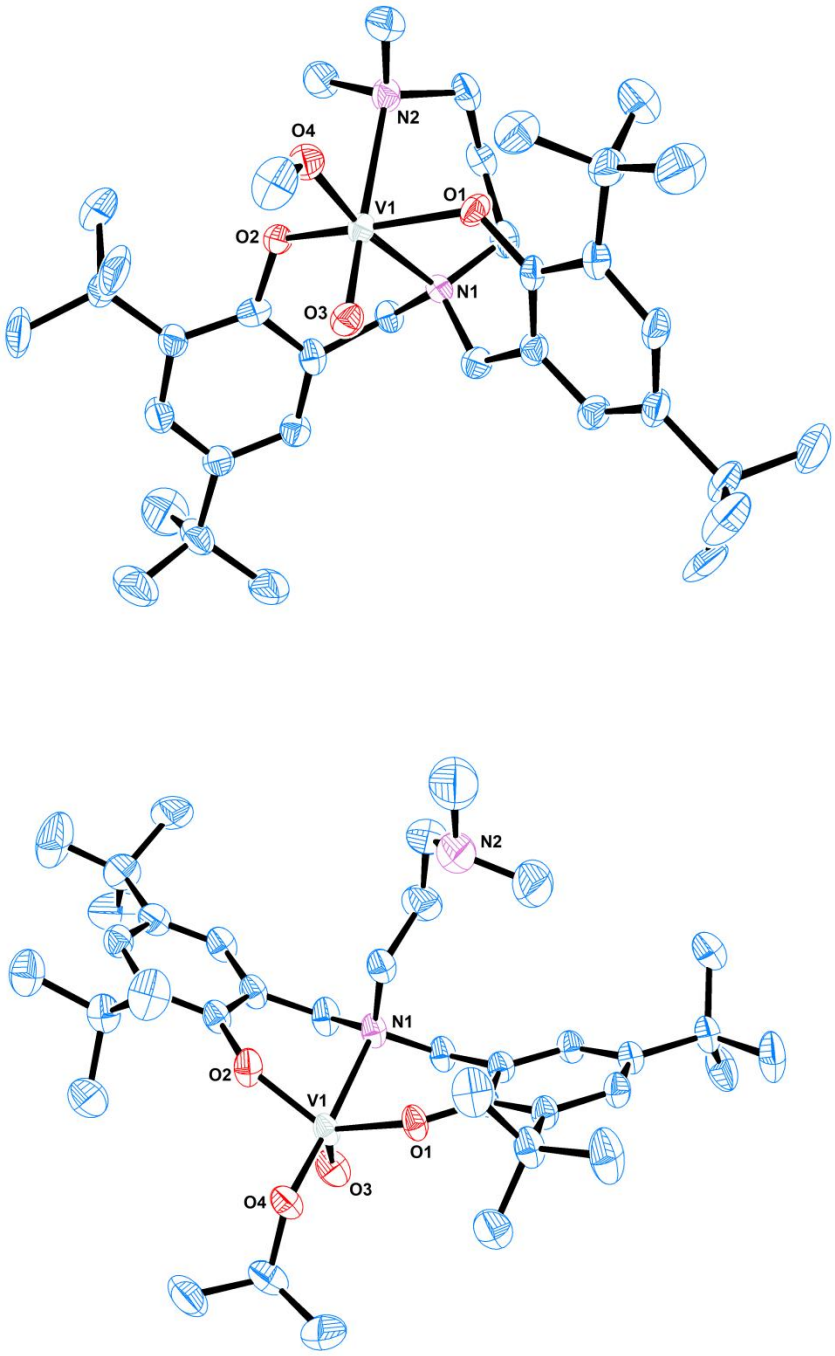

Figure 4.3. ORTEP representations for **AP2** (top) and **AP3** (bottom). Thermal ellipsoids set at 50% probability, hydrogen atoms are omitted for clarity. Selected bond lengths (Å) and bond angles (deg) are displayed in Table 4.2 and Table 4.3, respectively.

Table 4.2. Selected bond lengths (Å) for compounds **AP1**, **AP2**, **AP3, AP4** and **AP7**.

	Bond Lengths (Å)				
	AP1	**AP2**	**AP3**	**AP4**	**AP7**
V1-O1	1.7912(2)	1.888(3)	1.8276(12)	1.8390(14)	1.868(9)
V1-O2	1.8703(9)	1.887(3)	1.8250(14)	1.8251(15)	1.866(9)
V1-O3	1.8533(9)	1.591(3)	1.5883(15)	1.5854(16)	1.582(9)
V1-O4	1.6159(9)	1.782(4)	1.7671(13)	1.7693(14)	1.820(8)
V1-O5	N/A	N/A	N/A	N/A	2.520
V1-N1	2.3582(10)	2.310(4)	2.2813(16)	2.2694(16)	2.319(10)
V1-N2	2.2213(11)	2.466(5)	N/A	N/A	N/A

Table 4.3. Selected bond angles (deg) for compounds **AP1**, **AP2**, **AP3, AP4** and **AP7**.

	Bond Angles (deg)				
	AP1	**AP2**	**AP3**	**AP4**	**AP7**
N1-V1-O4	165.76(4)	170.47(17)	172.19(6)	168.66(7)	171.8(4)
N2-V1-O3	160.52(3)	178.20(18)	N/A	N/A	N/A
N1-V1-O3	83.16(4)	90.32(17)	86.96(7)	87.66(7)	88.6(4)
N1-V1-O2	84.60(4)	82.86(15)	80.26(6)	80.36(6)	82.1(4)
N1-V1-O1	87.70(3)	76.56(15)	80.32(5)	80.47(6)	83.2(4)
O1-V1-O2	165.04(4)	155.26(17)	126.77(7)	129.75(7)	147.6(4)

Complexes **AP3-5** are air stable in the solid state for several weeks. In contrast, complex **AP3** decomposes in a solution of $CDCl_3$ exposed to air at room temperature after 3 days. Analysis of the decomposition products by ^{1}H and ^{51}V NMR spectroscopy shows signals corresponding with V(IV) complexes and several free ligand fragments.

4.3.2 Reactivity Studies

Initially, the auto-oxidation of the isopropoxide moiety to acetone was examined stoichiometrically using the new amine bis(phenolate) oxovanadium(V) complexes. Complex **AP1** was heated under an inert atmosphere in C_6D_6 for 3 days at 80 ^{o}C (Scheme 4.2a). The thermolysis of **AP1** yielded less than 5% acetone. In contrast, vanadium complex **OV1** in pyr-d_5 rapidly afforded a 50% yield of acetone in 30 min at 100 ^{o}C(Scheme 4.2b).[10g] The aerobic thermolysis of **AP1** under air (CD_3CN, 80 ^{o}C, 18 h, Schlenk flask connected to a water condenser open to air) afforded 50% isopropanol and

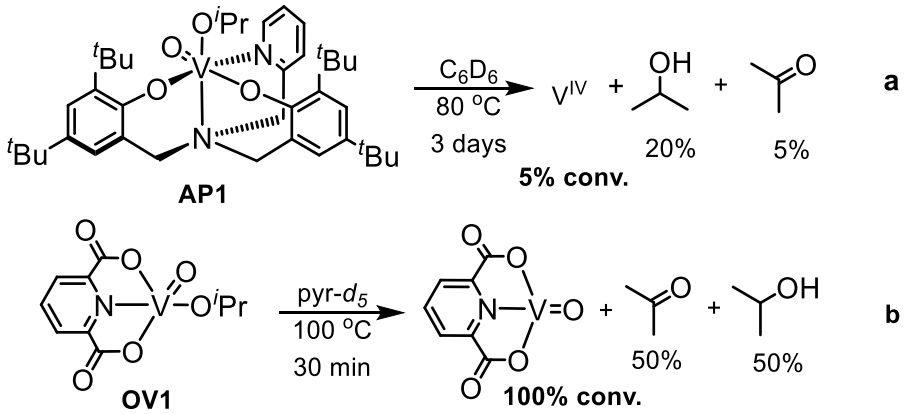

Scheme 4.2. Comparison of the anaerobic thermolysis of **OV1** and **AP1** to afford acetone.

10% acetone accompanied by full decomposition of the catalyst as observed by ^{1}H and ^{51}V NMR spectroscopy. Similarly to the base-assisted redox deprotonation mechanism displayed by **OV1** and **OV2** (see *Chapter 1*, section 1.4.3),[21] complex **AP1** bearing a pendant pyridine base could potentially facilitate the intramolecular deprotonation of the isopropoxide α-hydrogen (Scheme 4.3).

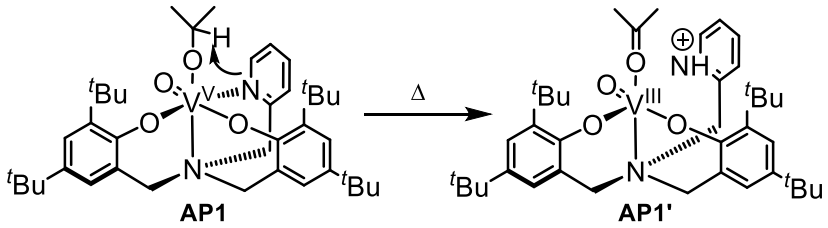

Scheme 4.3. Proposed intramolecular deprotonation of isopropoxide using the pendant base of Vanadium(V) complex **AP1**.

On the other hand, the anaerobic thermolysis (nitrogen atmosphere) of metal complex **AP3** (C_6D_6, 80 °C, 18 h) gave 20% conversion with 10% yield of isopropanol and 5% of acetone. Additional heating for 36 h afforded total decomposition of the vanadium complex. Despite the lower yields of acetone, the stability and robustness of **AP3** could result in better activity for the application in real lignin substrates (see *Chapter 5*). Vanadium complex **AP5** was synthesized from **AP3** and cyclobutanol in order to study the C-H bond cleavage mechanism. Cyclobutanol has previously been used as a radical clock to distinguish between one- and two-electron oxidation pathways.[22] Complex **AP5** was heated under nitrogen to 80 °C (C_6D_6) for up to 22 h but no decomposition products were

observed, and only a small amount of decomposition occurred after 36 h, in agreement with the observations for the anaerobic thermolysis of **AP1** and **AP3**.

Of course our interest in the amine bis(phenolate) oxovanadium complexes resides beyond the oxidation of alcohols. In order to assess the selectivity for bond cleavage in hydroxyethers, lignin model 1,2-diphenyl-2-methoxyethanol **LM2** was studied. Vanadium complex **AP3** was dissolved in DCM with an excess of **LM2** at room temperature (Scheme 4.4). The solution was stirred for 1 h and the solvent was removed under vacuum. Recryst-

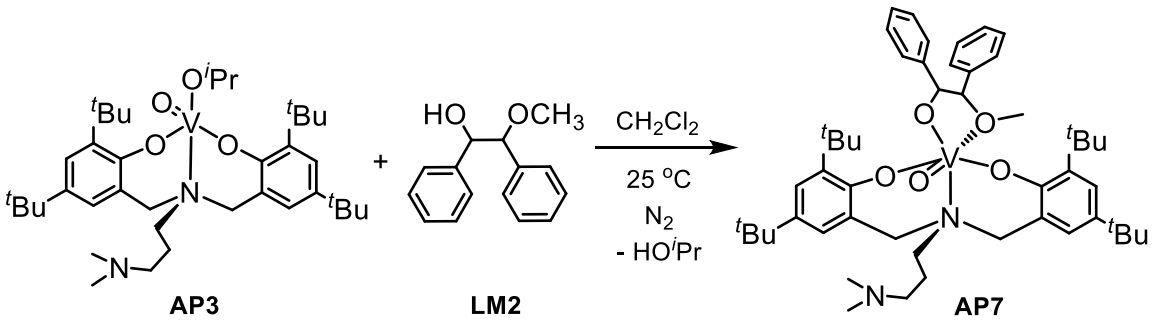

Scheme 4.4. Reaction of **AP3** with lignin model **LM2** to form the Vanadium complex **AP7**.

allization from a mixture of DCM/CH_3CN afforded **AP7** in 63% yield. The ^1H NMR spectrum of **AP7** revealed that all methylene phenolate bridges and methine protons are diastereotopic and magnetically inequivalent. The crystal structure of **AP7** shows a pseudo-octahedral geometry about the vanadium centre with a long V-OMe bond distance of 2.520 Å as depicted in Figure 4.4. The bond lengths for the metal centre to both oxygens of the hydroxyether are longer for **AP7** compared with a similar vanadium(V) complex formed with catalyst **OV1**.[10h] The crystal structure again supports the hemilabile nature of the propyl-dimethylamine backbone [-$N(CH_2)_3N(CH_3)_2$] as the dimethylamino nitrogen is not coordinated to the vanadium centre in **AP7**.[20]

The anaerobic thermolysis of **AP7** in toluene-d_8 (100 °C) affords 98% conversion and 80% yield of benzaldehyde in only 2 h, which is comparatively faster and more reactive than similar reactions using **AP1** or **AP3** (Scheme 4.5). The aldehyde is generated from the C-C bond cleavage of the **LM3** fragment (similar results were obtained using C_6D_6). Analysis of the reaction mixture by ^{51}V NMR spectroscopy revealed complete consumption of **AP7** and two new signals at -505.5 and -536.0 ppm in a 1:0.23 ratio, corresponding to two new V(V) products. As depicted in Scheme 4.5, the ester moiety was

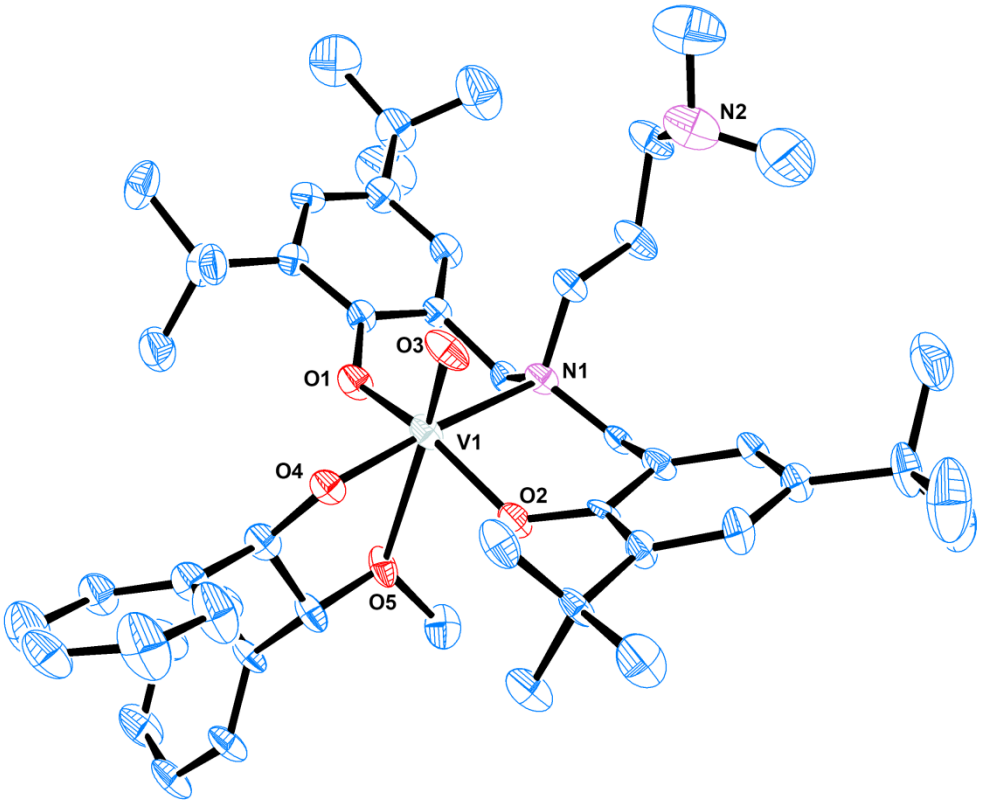

Figure 4.4. ORTEP representation for **AP7**. Thermal ellipsoids set at 50% probability, hydrogen atoms and solvent molecules are omitted for clarity. Selected bond lengths (Å) for **AP7**: V1-O5= 2.520 Å, V1-O1= 1.582(9), V1-O4= 1.820(8); in comparison to the reported metal complex **OV1**[10h]: V1-O5= 2.438(2), V1-O1= 1.576(2), V1-O4= 1.784(2). Selected bond lengths (Å) and bond angles (deg) for **AP7** are displayed in Table 4.2 and Table 4.3, respectively.

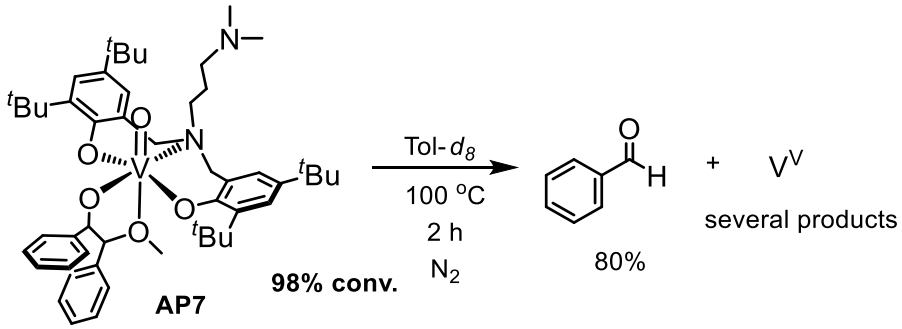

Scheme 4.5. Anaerobic thermolysis of **AP7**.

not identified as a free organic molecule but instead, the fragment might be coordinated to afford an organometallic vanadium(V) complex. An exchange reaction between a fluoroalkoxy ligand (-OCH_2CF_3) and the alkyl fragment of the Lewis acid $B(C_6F_5)_3$ has

been reported by Donnadieu and co-workers.[23] Upon heating the above described reaction mixture in air, the V(V) signals disappear and several paramagnetic species grow in, as observed by ^{1}H NMR spectroscopy. Guastine and co-workers reported that organometallic $V^{III}(Mes)_3(THF)$ [Mes = 2,4,6-$Me_3C_6H_2$] reacts cleanly with oxygen transfer reagents (*e.g.*, styrene oxide) to form the corresponding oxovanadium(V) complex.[24] The V(V) products of the thermolysis of **AP7** could also rapidly react with moisture to regenerate the catalytically active species. Currently, further investigations of this reaction and the full characterization of the V(V) complexes are ongoing.

In order to understand the role of the pendant dimethylamine moiety in this transformation, **AP8** was synthesized from the reaction of the lignin model **LM2** and **AP6**[12], affording an oxovanadium complex bearing a similar ligand scaffold (propyl backbone) as **AP3**, but importantly excluding the dimethylamino donor (Scheme 4.6). Pre-

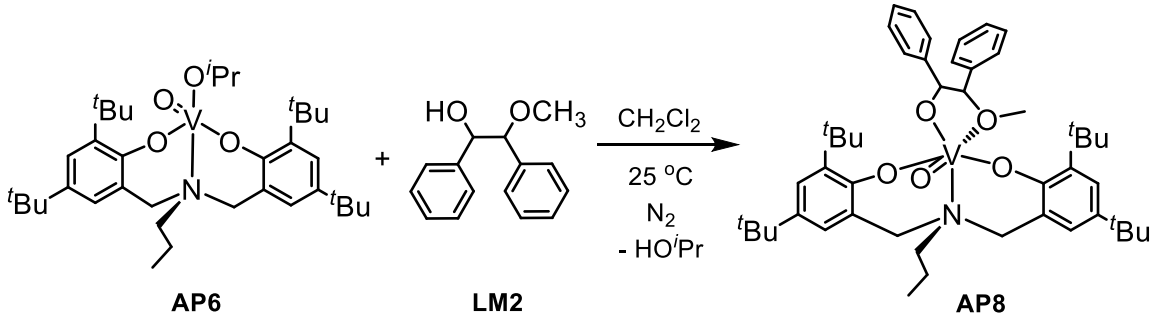

AP6 **LM2** **AP8**

Scheme 4.6. Synthesis of **AP8** from **AP6** and lignin model **LM2**.

liminary results for the thermolysis of **AP8** (C_6D_6, 80 °C) show that formation of benzaldehyde occurs at a lower rate (< 20% conversion, *versus* 98% in **AP7**) compared to the reaction of **AP7**. After prolonged thermolysis of **AP8** for 18 h, the NMR spectra revealed a quantitative yield of benzaldehyde with no signals for V(V) compounds. Formation of the V(V) complexes might thus be facilitated by the dimethylamino backbone of **AP7**.

Scheme 4.7 shows the proposed mechanism for the C-C bond cleavage of **LM2** using **AP1** or **AP3**. Initially, the chelated compound **AP7** is formed through ligand exchange of the alcohol with the catalyst (**AP1,3**). At high temperatures **AP7** releases one equivalent of benzaldehyde (reaction depicted in Scheme 4.5) generating the benzylic radical intermediate (**a**) with the vanadium center in oxidation state +4. A rapid rearrangement of

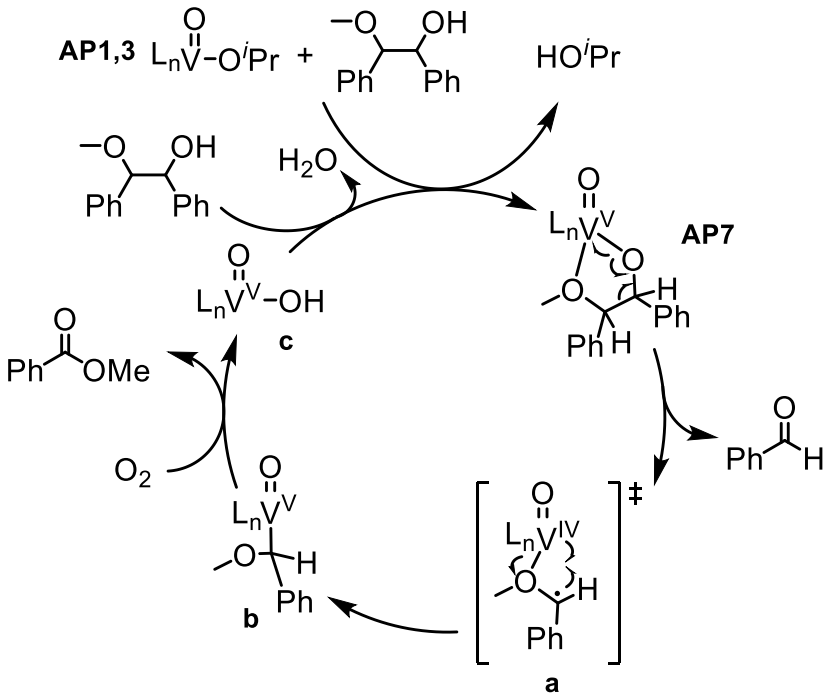

Scheme 4.7. Proposed mechanism for the C-C bond cleavage of **LM2** using amine bisphenolate catalysts.

(**a**) affords the organometallic vanadium(V) complex (**b**) which upon exposure to oxygen produces methylbenzoate and oxovanadium(V) hydroxylate (**c**) that could react with another molecule of **LM2** producing water and closing the catalytic cycle.

4.3.3 Catalytic Aerobic Oxidation of 1,2-Diphenyl-2-methoxyethanol Lignin Model LM2

Previously, the catalytic aerobic oxidation of 1,2-diphenyl-2-methoxyethanol **LM2** was carried out using 10 mol% catalyst **OV1**, affording 99% conversion after 6 days (pyr-d_5, 100 ^{o}C, air).[10h] Catalyst **AP1** reached 100% conversion of **LM2** after only 8 hours (1 mol%, toluene, 105 ^{o}C, air) (Table 4.4, entry 2). Moreover, catalyst **AP3** afforded 76%

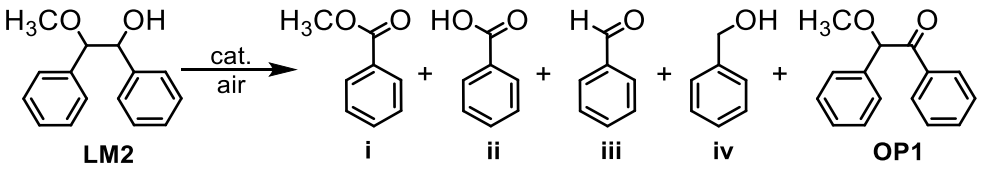

Scheme 4.8. Aerobic oxidation of **LM2** using amine bis(phenolate) oxovanadium catalysts (see Table 4.4 for yields and conversions).

Table 4.4. Catalytic oxidation of **LM2** (see Scheme 4.8).[a]

Entry	Cat. (mol%)	Time (h)	Conv. (%)[b]	**i** (%)	**ii** (%)	**iii** (%)	**iv** (%)	**OP1** (%)	TON[d]
1	**AP1** (1)	6	58	42	n.d.[c]	67	n.d.	12	58
2	**AP1** (1)	8	100	64	n.d.	100	n.d.	12	100
3	**AP1** (1)	18	100	25	76	25	39	0	100
4	**AP1** (0.2)	18	100	25	51	35	58	7	1,000
5	**AP1** (0.01)	18	100	7	47	50	65	27	10,000
6	**AP3** (1)	3	76	12	6	26	22	6	76
7	**AP3** (1)	6	100	8	27	4	30	5	100
8	**AP3** (0.1)	18	100	7	120[e]	27	63	27	1,000
9	**AP6** (0.1)	18	98	18	67	27	76	9	980

[a]Conditions= toluene, 105 ^{o}C under atmospheric pressure of air; [b]Yields are expressed as a percentage of the theoretical maximum in moles based on the initial amount of substrate; [c]n.d, no detected; [d]Turnover numbers are calculated as the maximum moles of substrate consumed over the amount -in moles- of the catalysts used; [e]yields higher than 100% are possible due the interconversion of aldehyde and ester to benzoic acid.

conversion in just 3 hours using 1 mol% of catalyst loading. Comparing catalyst **AP1** and **AP3** (1 mol%), the latter is faster for the oxidation of **LM2** (58% *versus* 100% conversion, respectively) as observed in Table 4.4, entries 1 and 7. Using catalyst **AP1** at longer reaction times (18 h) and low catalyst loading (0.01 mol%), it is possible to obtain TON as high as 10,000 with higher yields of benzaldehyde, benzoic acid and benzyl alcohol (Table 4.4, entry 5). Control experiments using catalysts **AP1** or **AP3** in toluene (105 ^{o}C, 24 h) showed no oxidation of the solvent to benzaldehyde or benzoic acid, eliminating the possibility of toluene auto-oxidation to benzaldehyde.

Oxidation of **LM2** and **LM3** using catalysts **OV1** and **OV2** follows a stepwise process; cleavage of the C-H bond of the hydroxyether (alcohol oxidation) to produce a ketone intermediate (such as **OP1**) which subsequently undergoes a C-C or C-O bond cleavage (depending on the solvent employed) to afford phenol and benzoic acid (see *Chapters 2* and *3*).[10a,h] New amine bis(phenolate) oxovanadium catalysts do not proceed through a stepwise process where the ketone intermediate is generated, but instead catalysts **AP1** and **AP3** cleave the substrate directly. Catalyst **AP1** is more efficient for the aerobic oxidation

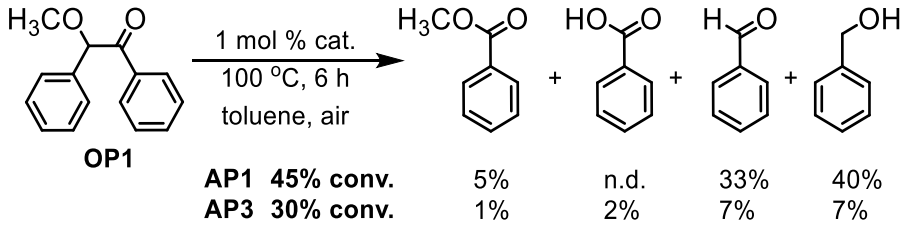

Scheme 4.9. Aerobic oxidation of **OP1** with catalyst **AP1** and **AP3**.

of **OP1** compared with catalysts **AP3** as depicted in Scheme 4.9. Catalyst **AP3** cleaves the C-H bond of **LM2**, affording small amounts of **OP1**. In contrast, catalyst **AP1** catalyzes two different pathways: direct C-C bond cleavage of the substrate to afford methyl benzoate and benzaldehyde and C-H bond cleavage to afford the ketone product **OP1**.

Interestingly, catalysts **AP1** and **AP3** produce high yields of benzyl alcohol at longer reaction times (*ca.* 18 h). A variation of a Cannizzaro[25] and Tishchenko[26] reaction explains the formation of benzyl alcohol under these conditions (Scheme 4.10a). The formation of

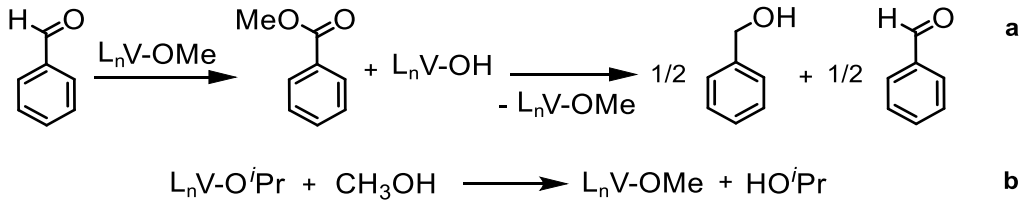

Scheme 4.10. Cannizzaro[25] and Tishchenko[26] reactions for the formation of benzyl alcohol, where L_n is **PL1** or **PL2**.

the active specie L_nV-OMe from the reaction of the catalyst (**AP1** or **AP3**) with methanol is depicted in Scheme 4.10b. Catalyst **AP1** seems to proceed faster for the production of benzyl alcohol, in both the aerobic oxidation of hydroxyether **LM2** and ketone **OP1**. Control experiments for the aerobic oxidation of benzaldehyde using 0.1 mol% of **AP1** (toluene, 105 °C, 18 h) showed 74% conversion with a 30% yield of benzoic acid and a 10% yield of benzyl alcohol. Similarly, methyl benzoate was treated with 10 mol% **AP1** (toluene, 105 °C, 18 h) to afford 79% conversion with 12% benzoic acid, 5% benzaldehyde and 7% benzyl alcohol. As expected, no reaction was observed for the control experiment using 10 mol% **AP1** and benzoic acid (toluene, 105 °C, 18 h). Using ^{1}H NMR spectroscopy, the reaction of 1 mol% **AP3** and **LM2** was monitored every 15 min for 5 hours (toluene-d_8, 90 °C). The formation of benzoic acid, methyl benzoate and

benzaldehyde in the first 100 min is similar, however the amount of acid increases drastically at the expense of the other two compounds in the last 2 hours of the reaction.

In order to understand the role of the pendant base in these reactions, **AP6** was tested (Table 4.4, entry 9). The oxidation of **LM2** (0.1 mol% of **AP6)** afforded 98% conversion with similar product distribution as **AP3** but with a lower yield of benzoic acid. The role of the dimethylamino backbone is not yet known with certainty but the lower conversion achieved by **AP6** (98%) in 18 h indicates the maximum performance of this catalyst.

4.3.4 Catalytic Aerobic Oxidation of Phenoxyethanol Lignin Model LM3

The oxidation of **LM3** with 1 mol% catalyst loading (toluene, 18 h, 100 ºC) afforded 28% conversion for catalyst **AP1** and 56% conversion for **AP3** (Scheme 4.11 and Table 4.5). The oxidation of **LM3** follows the same trend in rates as the oxidation of lignin model

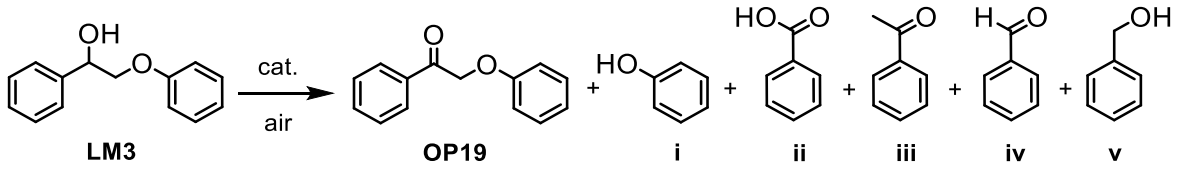

Scheme 4.11. Aerobic oxidation of **LM3** with amine bis(phenolate) oxovanadium catalysts.

Table 4.5. Catalytic oxidation of phenoxyethanol lignin model **LM3** (see Scheme 4.11).

Entry	Cat. (mol%)	time (h)	Conv. (%)[a]	**i** (%)	**ii** (%)	**iii** (%)	**iv** (%)	**v** (%)	**OP19** (%)	TON[c]
1	**AP1** (1)	18	28	2	37	<1	18	59	65	28
2	**AP1** (0.1)	18	0	n.d.[b]	n.d.	n.d.	n.d.	n.d.	n.d.	0
3	**AP3** (1)	18	56	30	n.d.	27	n.d.	n.d.	20	56
4	**AP3** (5)	18	72	10	n.d.	10	n.d.	n.d.	26	14

[a]Yields are expressed as a percentage of the theoretical maximum in moles based on the initial amount of substrate; [b]n.d, no detected; [c]Turnover numbers are calculated as the maximum moles of substrate consumed over the amount -in moles- of the catalysts used.

LM2 observed in previous sections. The oxidation of lignin model **LM3** using catalyst **AP1** produces higher amounts of benzyl alcohol, presumably through the Cannizzaro reaction compared with catalyst **AP3**, showing the same trends as those observed in the oxidation of lignin model **LM2** (Table 4.5, entries 1 and 3). Nonetheless, hydroxyether substrates such as **LM3** are more difficult to degrade compared with hydroxyether

substrate **LM2** (see *Chapter 2* and *Chapter 3*). Lower catalyst loadings of **AP1** or **AP3** (0.1 mol%) are not effective for the oxidation of lignin model **LM3**.

Aerobic oxidation of the ketone product **OP19** afforded high conversion and yields using 1 mol% **AP3** (Scheme 4.12); however **AP1** gave only 1% conversion. *Chapter 3*

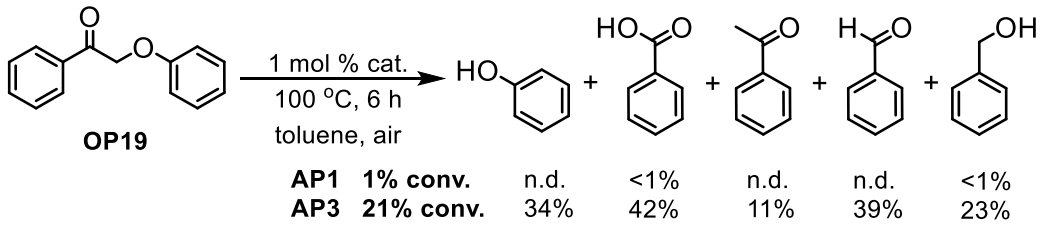

Scheme 4.12. Catalytic oxidation of ketone **OP19** using amine bis(phenolate) oxovanadium catalysts.

explored the reactivity of **OV2** for the oxidation of **OP19**, affording 70% conversion with yields of 60% benzoic acid, 70% phenol and 2% formic acid using 10 mol% catalyst, and after 48 h of reaction time (100 °C, pyr-d_5).[10a] These observations demonstrate the greater activity of **AP3** for the oxidation of **LM3** and its ketone product **OP19**. Interestingly, the aerobic oxidation of lignin model **LM3** or ketone **OP19** using 1 mol% **AP6** in toluene (18 h, 105 °C) gave no reaction.

Preliminary experiments using labeled substrate **LM3-^{2}H$_1$** (1 mol% **AP1**, toluene, 105 °C) shows <1% conversion after 18 h and approximately 3% conversion at 36 h. This might indicate that the C-H and C-O bond cleavages occur at the benzylic position. Further experiments are under investigation in order to calculate the kinetic parameters.

Considering all the above observations, the aerobic oxidation of lignin model **LM3** occurs through three different pathways using the amine bis(phenolate) oxovanadium catalysts as depicted in Scheme 4.13. With catalyst **AP1**, C-H bond cleavage (Scheme 4.13b) and direct C-C bond cleavage are preferred (Scheme 4.13a), while catalyst **AP3** affords C-O bond cleavage (Scheme 4.13c). Smith and co-workers proposed an alternative route for the C-O bond cleavage of lignin model **LM3** using a titanium(IV)-enolate where the coordinated hydroxyether is cleaved to acetophenone through protonolysis using mild acids [HNEt$_3$]X (X = OTf, BPh$_4$).[27] This system is only stoichiometric since the aryloxy fragment does not undergo ligand exchange to regenerate the enolate. For instance, catalysts **AP1** and **AP3** could follow a similar pathway, where the coordinated phenolate

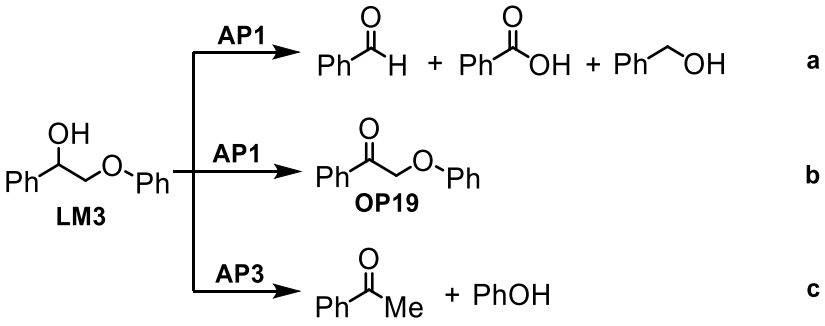

Scheme 4.13. Catalyst **AP1** promotes the C-C and C-H bond cleavage while catalyst **AP3** promotes the C-O bond cleavage in lignin model **LM3** (note that the ketone **OP19** leads to other products).

undergoes C-O bond cleavage. A competitive pathway might afford the C-H bond cleavage product, inhibiting the formation of the product ketone **OP19**.

4.3.5 Catalytic Aerobic Oxidation of β-Aryl Glycerol Lignin Models LM4

Related oxovanadium(V) catalysts bearing bis(phenol)pyridine ligands displayed low performance for the oxidation of β-aryl glycerol lignin models such as **LM4**.[10c] Fast decomposition of the ligand scaffold was observed by the oxidation of the benzylic positions. For example, 84% conversion of the lignin model **LM4** was obtained after prolonged reaction times (48 h, toluene, 100 ^{o}C, air) with large catalyst loadings (*ca.* 10 mol%). New amine bis(phenolate) oxovanadium catalysts **AP1** and **AP3** afforded high conversions (Scheme 4.14 and Table 4.6) using low catalyst loadings (0.1 -1 mol%). This high performance represents a clear advance compared with previous reports for vanadium homogeneous catalysts in terms of reaction times and catalyst loadings.[28] However, the function of the pendant base is still uncertain since 1 mol% catalyst **AP6** gave slightly lower conversion and yields as **AP3** (Table 4.6, entry 2 and 4).

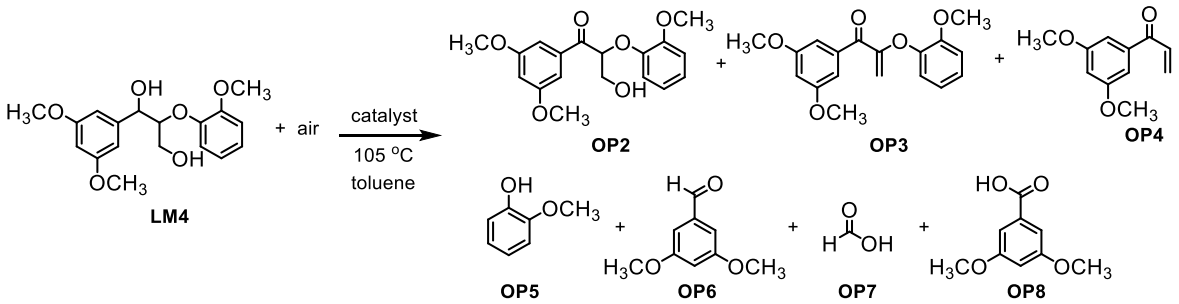

Scheme 4.14. Catalytic oxidation of **LM4** using amine bis(phenolate) oxovanadium catalysts.

Table 4.6. Catalytic oxidation of β-aryl glycerol lignin models **LM4** (see Scheme 4.14).

Entry	Cat. (mol%)	time (h)	Conv. (%)[a]	**OP2** (%)	**OP3** (%)	**OP4** (%)	**OP5** (%)	**OP6** (%)	**OP8** (%)	TON[c]
1	**AP1** (1)	18	30	17	n.d.	4	n.d.	<1	3	31
2	**AP3** (1)	18	90	35	<1	16	n.d	12	10	90
3	**AP3** (0.1)	18	23	4	n.d.	3	n.d.	1	1	23
4	**AP6** (1)	18	73	31	<1	7	n.d.	4	5	73

[a]Yields are expressed as a percentage of the theoretical maximum in moles based on the initial amount of substrate; [b]n.d, no detected; [c]Turnover numbers are calculated as the maximum moles of substrate consumed over the amount -in moles- of the catalysts used.

4.4 Conclusions

The second generation of oxovanadium(V) catalysts **AP1-5** were fully characterized and studied for the aerobic oxidation of lignin models. The new catalysts were synthesized from inexpensive and commercially available precursors in two steps. Amine bis(phenolate) oxovanadium(V) catalysts demonstrated a higher performance for the oxidation of lignin models **LM2**, **LM3** and **LM4** compared with previously reported **OV1** and **OV2** catalysts. Higher conversion and yields are achieved with catalyst loadings as low as 0.01 mol%, without the need for co-additives (*e.g.*, exogenous base) representing one of the best homogeneous systems known to date.

Catalysts **AP1** and **AP3** produce benzyl alcohol from benzaldehyde and methyl benzoate thought Cannizzaro[26] and Tishchenko[26] reactions. The role of the pendant base (pyridine for **AP1** and dimethylamino for **AP3**) is still unknown. Nevertheless, the performance of catalyst **AP3** *versus* **AP6** is higher for all lignin models analyzed in this *Chapter*.

Full characterization of the V(V) complexes derived from thermolysis of **AP7** (and related metal complex **AP8**) and their role in the mechanism for the oxidation of lignin models is currently under investigation. Considering the greater reactivity of the amine bis(phenolate) oxovanadium(V) catalysts (*e.g.*, low catalyst loadings and short reaction times) for the disassembly of lignin models, their potential application for the depolymerization of organosolv lignin will be discussed in *Chapter 5*.

4.5 References

(1) a) Corma, A.; Iborra, S.; Velty, A. *Chem. Rev.* **2007**, *107*, 2411−2502; b) Deuss, P. J.; Barta, K.; de Vries, J. G. *Catal. Sci. Technol.* **2014**, *4*, 1174−1196.
(2) a) Zhou, X.; Mitra, J.; Rauchfuss, T. B. *ChemSusChem* **2014**, *7*, 1623–1626; b) Galvin, V. M.; Sawadjoon, S.; Rohde, V.; Dawange, M.; Samec S. M. J. *ChemCatChem* **2014**, 179–184; c) Parsell, T. H.; Owen, B. C.; Klein, I.; Jarrell, T. M.; Marcum, C. L.; Haupert, L. J.; Amundson, L. M.; Kenttämaa, H. I.; Ribeiro, F.; Miller, J. T.; Abu-Omar, M. M. *Chem. Sci.* **2013**, *4*, 806–813; d) Lohr, T. L.; Li, Z.; Marks, T. J. *ACS Catal.* **2015**, *5*, 7004–7007.
(3) a) Wu, A.; Patrick, B. O.; Chung, E.; James, B. R. *Dalton Trans.* **2012**, *41*, 11093–11106; b) vom Stein, T.; den Hartog, T.; Buendia, J.; Stoychev, S.; Mottweiler, J.; Bolm, C.; Klankermayer, J.; Leitner, W. *Angew. Chem. Int. Ed.* **2015**, *54*, 5859–5863; c) Nichols, J. M.; Bishop, L. M.; Bergman, R. G.; Ellman, J. A. *J. Am. Chem. Soc.* **2010**, *132*, 12554–12555; d) Nagy, M.; David, K.; Britovsek, G. J. P.; Ragauskas, A. J. *Holzforschung* **2009**, *63*, 513–520.
(4) a) Harms, R. G.; Markovits, I. I. E.; Drees, M.; Herrmann, W. A.; Cokoja, M.; Kühn, F. E. *ChemSusChem* **2014**, *7*, 429–434; b) Crestini, C.; Caponi, M. C.; Argyropoulos, D. S.; Saladino, R. *Bioorg. Med. Chem.* **2006**, *14*, 5292–5302.
(5) Sergeev, A. G.; Hartwig, J. F. *Science* **2011**, *332*, 439–443.
(6) a) Son, S.; Toste, F. D. *Angew. Chem. Int. Ed.* **2010**, *49*, 3791–3794; b) Chan, J. M. W.; Bauer, S.; Sorek, H.; Sreekumar, S.; Wang, K.; Toste, F. D. *ACS Catal.* **2013**, *3*, 1369–1377.
(7) Gazi, S.; Ng, W. K. H.; Ganguly, R.; Moeljadi, A. M. P.; Hirao, H.; Soo, H. S. *Chem. Sci.* **2015**, *6*, 7130-7142.
(8) a) Biannic, B.; Bozell, J. J. *Org. Lett.* **2013**, *15*, 2730–2733; b) Bozell, J. J.; Hames, B. R.; Dimmel, D. R. *J. Org. Chem.* **1995**, *60*, 2398−2404.
(9) Sedai, B.; Baker, R. T. *Adv. Synth. Catal.* **2014**, *356*, 3563–3574.
(10) a) Díaz-Urrutia, C.; Sedai, B.; Leckert, K.; Baker, R. T.; Hanson, S. K. *ACS Sustainable Chem. Eng.* **2016**, *submitted*; b) Sedai, B.; Díaz-Urrutia, C.; Baker, R. T.; Wu, R.; Silks, L. A.; Hanson, S. K. *ACS Catal.* **2013**, *3*, 3111–3122; c) Zhang, G.; Scott, B. L.; Wu, R.; Silks, L. A. P. ; Hanson, S. K. *Inorg. Chem.* **2012**, *51*, 7354–7361; d) Hanson, S. K.; Wu, R.; Silks, L. A. P. *Angew. Chem. Int. Ed.* **2012**, *51*, 3410−3413; e) Sedai, B.; Díaz-Urrutia, C.; Baker, R. T.; Wu, R.; Silks, L. A. P.; Hanson, S. K. *ACS Catal.* **2011**, *1*, 794−804; f) Hanson, S. K.; Wu, R.; Silks, L. A. P. *Org. Lett.* **2011**, *13*, 1908–1911; g) Hanson, S. K.; Baker, R. T.; Gordon, J. C.; Scott, B. L.; Silks L. A. P.; Thorn, D. L. *J. Am. Chem. Soc.* **2010**, *132*, 17804–17816; h) Hanson, S. K.; Baker, R. T.; Gordon, J. C.; Scott, B. L.; Thorn, D. L. *Inorg. Chem.* **2010**, *49*, 5611−5618; i) Hanson, S. K.; Baker, R. T.; Gordon, J. C.; Scott, B. L.; Sutton, A. D.; Thorn, D. L. *J. Am. Chem. Soc.* **2009**, *131*, 428−429.
(11) Thorn, D. L.; Harlow, R. L.; Herron, N. *Inorg. Chem.* **1996**, *35*, 547−548.
(12) Lorber, C.; Despagnet-Ayoub, E.; Vendier, L.; Arbaoui, A.; Redshaw, C. *Catal. Sci. Technol.* **2011**, *1*, 489–494.
(13) APEX Software Suite v.2010; Bruker AXS: Madison, W. **2005**.
(14) Blessing, R. *Acta Cryst.* **1995**, *A51*, 33−38.
(15) Sheldrick, G. Cell_Now, Bruker-AXS: Madison, WI, **2004.**

(16) Sheldrick, G. M. *Acta Cryst.* **2008**, A64, 112−122.
(17) Tshuva, E. Y.; Goldberg, I.; Kol, M.; Goldschmidt, Z. *Organometallics* **2001**, *20*, 3017–3028.
(18) Díaz-Urrutia, C.; Chen, W-C.; Crites, C.-O.; Daccache, J.; Korobkov, I.; Baker, R. T. *RSC Adv.* **2015**, *5*, 70502–70511.
(19) a) Wolff, F.; Lorber, C.; Choukroun, R.; Donnadieu, B. *Inorg. Chem.* **2003**, *42*, 7839–7845; b) Barroso, S.; Adão, P.; Madeira, F.; Duarte, M. T.; Pessoa, J. C.; Martins, A. M. *Inorg. Chem.* **2010**, *49*, 7452–7463.
(20) Braunstein, P; Naud, F. *Angew. Chem. Int. Ed.* **2001**, *40*, 680–699.
(21) Wigington, B. N.; Drummond, M. L.; Cundari, T. R.; Thorn, D. L.; Hanson, S. K.; Scott, S. L. *Chem. Eur. J.* **2012**, *18*, 14981–14988.
(22) a) Rocek, J.; Aylward, D. E. *J. Am. Chem. Soc.* **1975**, *97*, 5452–5456; b) Oh, N. Y.; Suh, Y.; Park, M. J.; Seo, M. S.; Kim, J.; Nam, W. *Angew. Chem. Int. Ed.* **2005**, *44*, 4235–4239; c) Pestovsky, O.; Bakac, A. *J. Am. Chem. Soc.* **2004**, *126*, 13757–13764; d) Chandler, W. D.; Wang, Z.; Lee, D. G. *Can. J. Chem.* **2005**, *83*, 1212–1221; e) Whitesides, G. M.; Sadowski, J. S.; Lilburn, J. *J. Am. Chem. Soc.* **1974**, *96*, 2829–2835.
(23) Wolff, F.; Choukroun, R.; Lorber, C.; Donnadieu, B. *Eur. J. Inorg. Chem.* **2003**, 628–632.
(24) Ruiz, J.; Vivanco, M.; Floriani, C.; Chiesi-Villa, A.; Guastini, C. *J. Chem. Soc., Chem. Commun.* **1991**, 762–764.
(25) (a) Cannizzaro, S. *Justus Liebigs Ann. Chem*. **1853**, *88*, 129–130; (b) For a recent example of Cannizzaro reaction see: Basavaiah, D.; Sharada, D. S.; Veerendhar, A. *Tetrahedron Lett*. **2006**, *47*, 5771–5774.
(26) (a) Tischtschenko, W. J. *Russ. Phys. Chem.* **1906**, *38*, 355, 482; (b) Ogata, Y.; Kawasaki, A.; Kishi, I. *Tetrahedron* **1967**, *23*, 825–830.
(27) Desnoyer, A. N.; Fartel, B.; MacLeod, K. C.; Patrick, B. O.; Smith, K. M. *Organometallics* **2012**, *31*, 7625–7628.
(28) a) Son, S.; Toste, F. D. *Angew. Chem. Int. Ed.* **2010**, *49*, 3791–3794; b) Gazi, S.; Ng, W. K. H.; Ganguly, R.; Moeljadi, A. M. P.; Hirao, H.; Soo, H. S. *Chem. Sci.* **2015**, *6*, 7130–7142.

Chapter 5: Towards Lignin Valorization: Comparing Mono- and Bifunctional Homogeneous Catalysts for the Aerobic Oxidation and Depolymerization of Organosolv Lignin

This chapter has been partially published in: a) Díaz-Urrutia, C.; Chen, W-C.; Crites, C-O.; Daccache, J.; Korobkov, I.; Baker, R. T. RSC Adv. ***2015****, 5, 70502–70511; b) Díaz-Urrutia, C.; Daccache, J.; Michel, C.; Fleurat-Lessard, P.; Korobkov, I.; Baker, R. T.* ***2016****, submitted.*

5.1 Introduction

As a potential source of aromatic chemicals, lignin macromolecules could be attractive if more selective catalytic depolymerization processes could be identified and implemented.[1-15] Our group[16] and others[17-22] have recently demonstrated the utility of oxovanadium and copper complex catalysts for controlling the aerobic oxidation of lignin models, and, in three cases, real lignin extracts. In this work, a number of catalysts are compared for the oxidation of organosolv lignin to assess the degree of depolymerization and nature of the oxidative bond cleavage selectivity and resulting functional group formation.

Due to the structural complexity and variability of lignin, models containing the prominent β-O-4 and/or β-1 linkages have been used for many catalytic studies.[3] Reductive approaches,[23] non-oxidative C-O bond cleavage[17] selective oxidation of C-H bonds[20,22] and

tandem approaches[24,25] have all been employed for the degradation of lignin models (Refer to *Chapter 1* for more details). In previous studies our group[16a-d] and Hanson and co-workers[18,19,26] showed that oxovanadium(V) complexes, **OV1** and **OV2** (Figure 5.1), in the

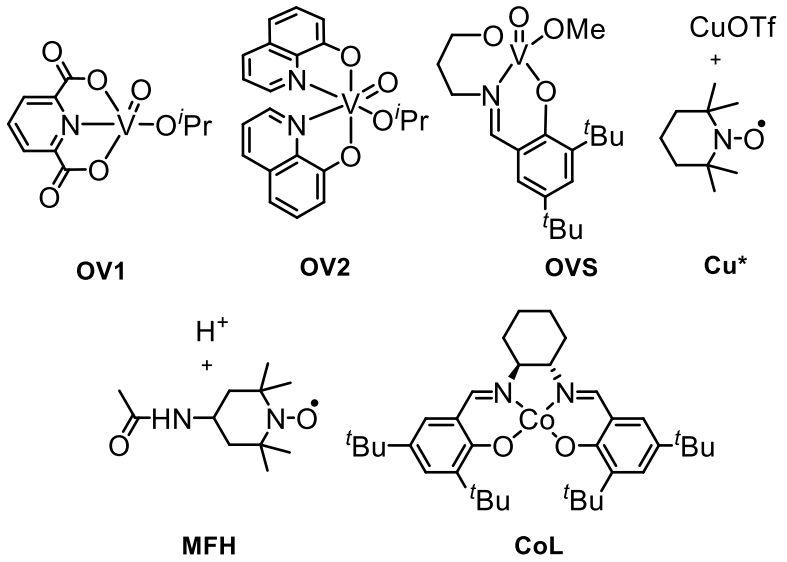

Figure 5.1. Oxovanadium(V) complexes (**OV1**, **OV2** and **OVS**), CuOTf/TEMPO/lutidine (**Cu***), 4-acetamido-TEMPO/acid (**MFH)** and (salen)cobalt(II) (**CoL**) and bifunctional oxovanadium(V) (**AP1**) catalysts for the oxidation of lignin models/extracts (TEMPO = 2,2,6,6-tetramethylpiperidine-1-oxyl; OTf = trifluoromethanesulfonate).

presence of base afford the aryl ketone product *via* a 2e- redox deprotonation pathway (Base-Assisted Redox Deprotonation, BARD). Subsequent cleavage of the C_α-C_β bond in the aryl ketone then gives aldehyde and acid products (see *Chapters 2* and *Chapter 3*). In a complementary reaction, Toste and co-workers showed that complex **OVS** selectively breaks the C_β-O-4 bond to give phenol and ene-one products.[17] In contrast, the Cu catalyst system **Cu*** leads to direct cleavage of the C_α-C_β bond to give primarily the aldehyde product, presumably through a single-electron transfer pathway[16e,21,22] reminiscent of peroxidase enzymes.[27] For the phenolic variants of these lignin models (R = OH), complexes **OV1** and **OV2** (but not **OVS**) catalyze C_{aryl}-C_α bond cleavage, as reported previously using Co Schiff base complex catalyst **CoL** (Figure 5.1).[28,29]

Compared to the model systems described above, extending these studies to lignin extracts is difficult in terms of product analysis and catalyst optimization, due to the heterogeneity of the lignin substrate. To illustrate, Toste and co-workers reported the

decomposition of organosolv lignin (derived from *M. giganteus*) using oxovanadium catalyst **OVS**.[17b] Evidence for depolymerization of the lignin oxidation was provided by GPC and 2D NMR data that showed decreased intensity for correlations involving β-O-4 linkages and formation of enones (products of redox-neutral C-O bond cleavage). Bozell and co-workers used the (salen)cobalt(II) catalyst **CoL** for the aerobic oxidation of organosolv lignin (from tulip poplar) and obtained various quinones, representing 3.5% of the initial weight of lignin.[28] However, the latter two reports do not address the relative molecular weights of the lignin before and after oxidation. Thus, the various studies on catalytic lignin degradation have employed different conditions and taken different approaches to analyze the products. In some cases, the extent of depolymerization was not evaluated, making it difficult or impossible to compare the different approaches/catalysts.

To our knowledge, the methods published by Chornet *et al.*, Song *et al.* and Stahl *et al.* represent the *state-of-the-art* for obtaining valuable aldehyde products from lignin oxidation,[1,9,20] although comparing the various approaches is again challenging due to the different types of analyses applied in each case. The Chornet method utilized Kraft lignin, treated under 1400 kPa (14 atm) of pure oxygen with 135 wt. % NaOH, 5 wt. % $CuSO_4$ and 0.5 wt. % $FeCl_3$ at 160 ^oC for 1 hr, yielding 14 wt. % of aldehydes.[1] Song and co-workers used 5 wt. % $CuSO_4$ supported in ionic liquid using 2500 kPa (25 atm) of pure oxygen at 175 ^oC and reported 30 wt. % yield of aldehydes from commercially-available organosolv lignin.[9] Stahl and co-workers developed a metal-free method for the oxidation of aspen lignin, employing 4-acetamido-TEMPO **MFH** under acidic conditions.[21] The aryl ketone-containing β-ether units are broken using superstoichiometric amounts of buffered formic acid/formate to give up to 50 wt. % of syringyl- and guaiacyl-derived diketones through a redox-neutral C-O bond cleavage.[24]

The requirements for pure oxygen, super-stoichiometric sodium hydroxide and high temperature/pressure are clearly drawbacks as the previous methods also require high temperatures and oxygen pressure.

In pursuit of a milder oxidative degradation of lignin, using air as the oxidant, this *Chapter* report the first comparative studies of catalyzed oxidative lignin depolymerization using oxovanadium(V) catalysts **OV1** and **OV2** and CuOTf/TEMPO/lutidine catalyst **Cu***. In this chapter, previously reported catalysts **OVS**[17a], **MFH**[20] and **CoL**[28] are also studied, as

well as the benchmark method of Chornet,[1] under standardized conditions, insofar as possible. New bifunctional vanadium catalysts **AP1** and **AP3** (Figure 5.2) which incorpora-

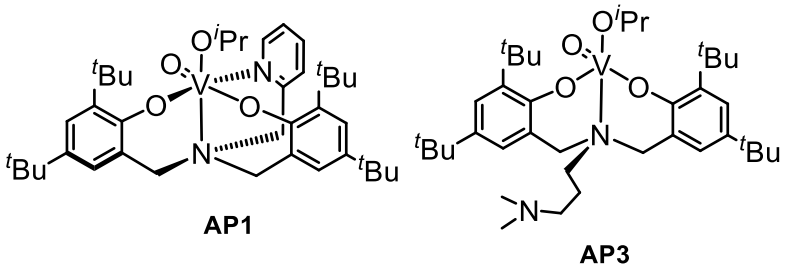

Figure 5.2. Bis(phenolate) oxovanadium(V) catalysts bearing pendant bases.

te a tethered base are also studied (see *Chapter 4* for mechanistic details). The depolymerization is evaluated using GPC, quantitative-HSQC and ^{31}P NMR spectroscopy (after derivatization to phosphite esters).

5.2 Materials and Methods

5.2.1 General Considerations

ACS-grade solvents tetrahydrofuran (THF), *n*-butyl acetate, ethyl acetate (EtOAc), acetonitrile (CH_3CN), dimethylsulfoxide (DMSO), dichloromethane (DCM) and dimethyl formamide (DMF) were purchased from Fisher Scientific. THF HPLC grade Chromasolv™, CuOTf (OTf = trifluoromethanesulfonate), 2,2,6,6-tetramethylpiperidine-1-oxyl (TEMPO), 4-acetamido-2,2,6,6-tetramethylpiperidine-1-oxyl (4-acetamido-TEMPO), (*R,R*)-(−)-*N,N′*-bis(3,5-di-*tert*-butylsalicylidene)-1,2-cyclohexanediamine, 2-chloro-4,4,5,5-tetramethyl-1,3,2-dioxa-phospholane (TMDP), 2,6-lutidine, trimethylamine (Et_3N) and diisopropylamine (DIPA) were purchased from Sigma Aldrich or Alfa Aesar. All other reagents were used as received. Synthetic air (8% oxygen in argon) was purchased from Linde Canada. DCM and CH_3CN were dried refluxing over CaH_2 for 18 h, distilling at reduced pressure followed by filtration with a plug of activated alumina. The dry solvents were stored under activated molecular sieves (4Å). DMSO-d_6, chroloform-*d* ($CDCl_3$) and acetonitrile-d_3 (CD_3CN) were purchased from Cambridge Isotopes Laboratories, Inc. $CDCl_3$ and CD_3CN were dried by refluxing over CaH_2 and distilling at reduced pressure. DMSO-d_6 was dried over activated molecular sieves (4Å). IR spectra were obtained on a Thermo Nicolet NEXUS 670 FTIR spectrometer. Elemental Analysis was performed at the

Laboratoire d'Analyse Élémentaire de l'Université de Montréal. Gel permeation chromatography (GPC) analyses were carried out in an Agilent HPLC-GPC equipped with a DAD (diode array) detector (254.4 nm target wavelength) using 1 mL/min THF at 40 ^{o}C with a guard column and two Waters columns HR-2 and HR-4 connected in series. The analyses were run in duplicate. The instrument was calibrated using polystyrene standard (109,000-162 Da). The single pressure experiments were carried out using a 50 mL Fike™ pressure reactor (Fike Corporation). Screening experiments were performed using the Freeslate high-throughput facilities in the Centre for Catalysis Research and Innovation (CCRI) at the University of Ottawa. The pressure reactor consists of 4 mL borosilicate glass vials and borosilicate glass beads placed in aluminum 24-well plates, fitted with a Teflon™ gasket and Goretex™ gasket and a cover with one-way check valves (common headspace down the rows). The plates were then encased in high-pressure blocks, placed on a 4-position heated orbital shaker system, pressurized manually with synthetic air, and agitated at 400 rpm. Vanadium complexes **OV1**,[16a] **OV2**,[16b] **OVS**[17a] and **CoL**[30] were prepared according to the published methods.

5.2.2 Preparation of Organosolv Lignin

Organosolv lignin (extracted with 1:1 ethanol/water from mixed hardwoods - aspen, maple and birch) was provided by Lignol Energy Corporation. Before use, the organosolv lignin was heated at 150 ^{o}C for 4 h under reduced pressure (*ca.* 10 mTorr) to remove volatiles; the black uniform residue was then used without further purification in all the experiments. The relative amount of major structural units in the oxygenated aliphatic region in organosolv lignin was determined by integrating the H_{α}/C_{α} NMR correlation: 0.67 (β-O-4 **A**), 0.22 (β-5 **B**), 1.0 (β-β **C**) and 0.45 (dibenzodioxocin **D**) (See Figure A52). For the aromatic region, syringyl (**S2/6**), guaicacyl (**G**), oxidized syringyl and guaiacyl (**S''**, **S'**, and **G'**) and, *p*-hydroxyphenyl (**H2/6**) units were detected. The relative ratios of (**S'**+**S''**):**S** and **G'**:**G** were 0.08 and 0.02, respectively. The ^{31}P NMR spectrum of phosphite esters derived from organosolv lignin showed 15.6 mmol of hydroxyl units per gram of lignin distributed as substituted guaiacyl (**C**$_5$, 8.0 mmol g^{-1}), *p*-hydroxyphenyl (**H**, 0.6 mmol g^{-1}), guaiacyl (**G**, 2.7 mmol g^{-1}), aliphatic (**AH**, 3.3 mmol g^{-1}) and carboxylic (**CH**, 1.0 mmol g^{-1}).

5.2.3 NMR Experiments

^{1}H, $^{13}C\{^{1}H\}$, $^{31}P\{^{1}H\}$, ^{51}V and 2D NMR spectra were obtained using a Bruker AVANCE 300 MHz or 500 MHz instrument with chemical shifts (δ) referenced to the residual solvent peak or externally to 85% H_3PO_4 (0 ppm) or $V(O)Cl_3$ (0 ppm). For quantitative ^{1}H-^{13}C HSQC experiments (q-HSQC), the spectra were acquired at room temperature with the Bruker AVANCE 500 MHz spectrometer equipped with Broadband Inverse Probe (BBI) with z-gradient. An aliquot of the reaction mixture (100 mg) was evaporated under reduced pressure and dissolved in 1 mL of DMSO-d_6. A modified version of the method reported by Heikkinen and co-workers was used.[31] All the structural units of the lignin substrate were assigned based on the lignin database and reported literature.[32] The spectral width was set to 12 - 0 ppm and 170 - 0 ppm for ^{1}H and ^{13}C dimensions, respectively. For quantitative data, the recycle delay was set to 5 s. The number of collected points was 2048 for ^{1}H dimension. The number of scans were 88 with 256 increments for a total time of approximately 33 hours. The squared sine, QSINE, function with a sine bell shift of 2 was applied in both dimensions. q-HSQC NMR spectra of the control experiments (no catalysts) in different solvents (EtOAc, *n*-butyl acetate, DMF, MeOH/DMSO and DMSO) showed no real changes in the lignin in the oxygenated aliphatic or aromatic regions.

Quantitative ^{31}P NMR spectroscopy experiments were carried out following the reported procedure.[33] Under nitrogen atmosphere, 25 mg of organosolv lignin or oxidized lignin residue was dissolved in 1.6:1 (v/v) of pyridine/$CDCl_3$ (500 μL) then 50 μL of TMDP was added to the solution. The reaction mixture was stirred for 10 min at room temperature and then transferred to a sealed screw-cap NMR tube. The spectrum was acquired using an inverse-gated decoupling pulse sequence, with a 90^{o} pulse angle, 25 s pulse delay and 256 scans. Chromium(III) tris(acetylacetonate) and cyclohexanol were used as relaxation reagent and internal standard, respectively. The spectrum was calibrated using the internal standard chemical shift at 145.2 ppm. All spectra were processed using TopSpin 3.0.

5.2.4 Procedure for the Catalytic Oxidation of Organosolv Lignin

The catalytic oxidation reactions involving catalysts **OV1**, **OV2**, **Cu*, MFH**, **AP1** (a mixture of isomers **AP1a** and **AP1b** was used) and **AP3** were carried out in a 24-well plate reactor (Freeslate) under 8.2 atm of synthetic air (8% O_2 in Ar), at 100 ^{o}C with constant

stirring (400 rpm). After 18 h, 400 μL aliquots were removed and analyzed by GPC, q-HSQC and ^{31}P NMR spectroscopy. Lignin oxidation/depolymerization reactions utilizing oxovanadium(V) complexes **OV1** and **OV2** were carried out using 10 wt. % catalyst and 10 wt. % base (Et_3N or DIPA). The CuOTf/TEMPO/lutidine catalyst **Cu***, consisted of 10 wt. % CuOTf, 10 wt. % TEMPO and 100 wt. % 2,6-lutidine in DMF, the mixture was then heated at 100 ^oC for 18 h.[16e] For catalysts **OVS**, **MFH** and **CoL**, the reported conditions were used (solvents, temperature and catalyst loading) in order to avoid variability in the catalyst performance, although O_2 pressure in the experiment was lower than that reported for the Co catalyst. For catalysts **AP1** and **AP3**, 1 wt. % or 10 wt. % catalyst in EtOAc or *n*-butylacetate were used for all experiments. The oxovanadium(V) catalyst **OVS** (10 wt. %) was tested in an 8:1 (v/v) EtOAc/THF mixture and heated at 80 ^oC for 24 h in a sealed vial under atmospheric pressure of air. For the metal-free system **MFH**, 5 wt. % of 4-acetamido-TEMPO was used together with 10 wt. % concentrated HNO_3 and 10 wt. % concentrated HCl (37%) in 19:1 (v/v) CH_3CN/H_2O. The reaction mixture was then heated at 65 ^oC using 8.2 atm of synthetic air for 24 h. For catalyst **CoL**, 10 wt % [Co] complex was used, 100 wt. % pyridine in 1:1 (v/v) MeOH/ DMSO, at 100 ^oC with 8.2 atm of synthetic air for 18 h. The Chornet method (135 wt. % NaOH, 5 wt. % $CuSO_4$ and 0.5 wt. % $FeCl_3$ heated at 160 °C with 8.2 atm of synthetic air for 18 h) was modified using THF as solvent instead of water in order to facilitate the GPC analysis (Extraction of the aqueous mixture with organic solvents such as ethyl acetate gave non-representative samples). While the amount of soluble base is reduced, both metal salts dissolved readily under these basic conditions.

5.2.5 GPC Analysis

The GPC instrument was calibrated using polystyrene standards although these have been shown to be of limited value for absolute MW determination of branched macromolecules such as lignin.[34] Thus a qualitative comparison was opted for the data from the control and catalytic reactions, in which the lignin was subjected to identical conditions (solvent, temperature, *etc.*) without some or all components of the catalyst. Average molecular weight (M_w), number average molecular weight (M_n) and polydispersity index (PDI) for the control and the catalytic experiments are reported in Table 5.1 and Table 5.2. For GPC analysis an aliquot of the reaction mixture was

evaporated and dissolved in THF.

5.3 Results and Discussion

5.3.1 GPC Analysis

Control experiments with organosolv lignin substrate and Et_3N yielded a broad peak in the GPC corresponding to a polystyrene MW of *ca.* 870 Da with several lower molecular weight components eluting at longer times (Figure 5.3, Table 5.1). While use of catalyst **1** has a clear effect on reducing the average molecular weight, the best performance was obtained using catalyst **OV2** which gives the largest MW shift and a major increase in the lower molecular weight components (Mw = 758 Da *vs.* Mw = 575 Da). The lower performance of catalyst **OV1** can be explained in part by its reaction with water to form less active dioxo anionic species, as observed in previous studies.[35] Catalysts **OV1** and **OV2** were tested in EtOAc, THF and *n*-butyl acetate as solvents and ethyl acetate was found to be most effective for depolymerization of the organosolv lignin.

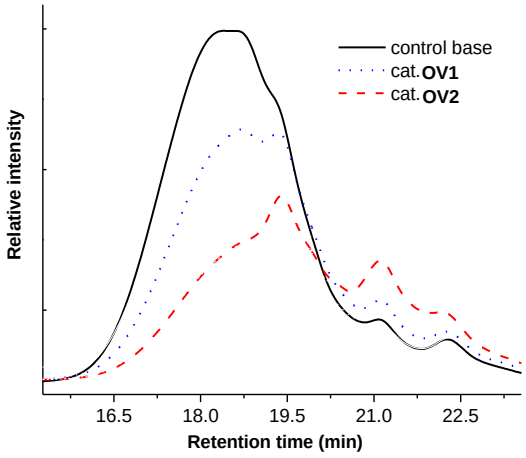

Figure 5.3. GPC data (THF solvent, elution rate: 1 mL/min, 245.5 nm detection) for the catalytic oxidation of organosolv lignin using **OV1** (10 wt. % **OV1** and 10 wt. % Et_3N) and **OV2** (10 wt. % **OV2** and 10 wt. % Et_3N) compared with the control experiment (10 wt% Et_3N). For all runs: solvent = EtOAc; temperature = 100 ^oC; pressure of synthetic air = 8.2 atm; reaction time = 18 h.

Table 5.1. GPC data for different catalyst systems and control experiments (THF solvent, elution rate: 1 mL/min, 254.4 nm detection).

Entry	Experiment	Mw (Da)	Mn (Da)	PDI
1	Organosolv lignin[a]	2526	850	2.97
2	**OV1**[b]	758	429	1.80
3	**OV2**[b]	575	324	1.77
4	Control (no catalyst) for **OV1** and **OV2**[b]	870	525	1.66
5	**OVS**[c]	808	411	1.97
6	Control (no catalyst) for **OVS**[c]	1085	456	2.38
7	**Cu***[d]	413	229	1.80
8	Control in DMF (no Cu)[d]	817	347	2.36
9	Control TEMPO and 2,6-lutidine (no Cu)[d]	493	239	2.06
10	**MFH**[e]	502	330	1.52
11	Control (no 4-acetamido-TEMPO) for **MFH**[e]	606	452	1.34
12	**CoL**[f]	760	242	3.14
14	Control (no catalyst) for **CoL**[f]	723	241	3.00
16	Chornet method[g]	835	445	1.88

[a]For untreated organosolv lignin, M_w = 1606 Da and M_n = 637 Da. [b]10 wt. % catalyst and 10 wt. % Et_3N. For all runs: Solvent = EtOAc; temperature = 100 °C; pressure of synthetic air = 8.2 atm; reaction time = 18 h. [c]10 wt. % catalyst. For all runs: solvent = 8:1 (v/v) EtOAc/THF; temperature = 80 °C; sealed vial under atmospheric pressure of air; reaction time = 18 h. [d]10 wt. % catalyst, 10 wt. % TEMPO and 100 wt. % 2,6-lutidine. For all runs: solvent = DMF; temperature = 100 °C; pressure of synthetic air = 8.2 atm; reaction time = 18 h. [e]5 wt. % 4-acetamido-TEMPO, 10 wt. % HNO_3 (70%) and 10 wt. % HCl (37%). For all runs: solvent = 19:1 (v/v) CH_3CN/H_2O; temperature = 65 °C; pressure of synthetic air = 8.2 atm; reaction time = 24 h. [f]10 wt. % catalyst and 100 wt. % pyridine. For all runs: solvent = 1:1 (v/v) MeOH/DMSO; temperature = 100 °C; pressure of

synthetic air = 8.2 atm; reaction time = 18 h. [g]135 wt. % NaOH, 5 wt. % $CuSO_4$ and 0.5 wt. % $FeCl_3$. For all runs: solvent = THF; temperature = 100 °C; pressure of synthetic air = 8.2 atm; reaction time = 18 h.

The control reaction in DMF solvent led to a more pronounced bimodal distribution and while addition of catalyst system **Cu*** (CuOTf/TEMPO/2,6-lutidine) in DMF effected a modest shift to lower molecular weights, the major difference lies in the significant increase in the amount of the lower molecular weight component eluting at *ca.* 21.25 min (Figure 5.4). However, nearly identical results were obtained when only TEMPO and 2,6-

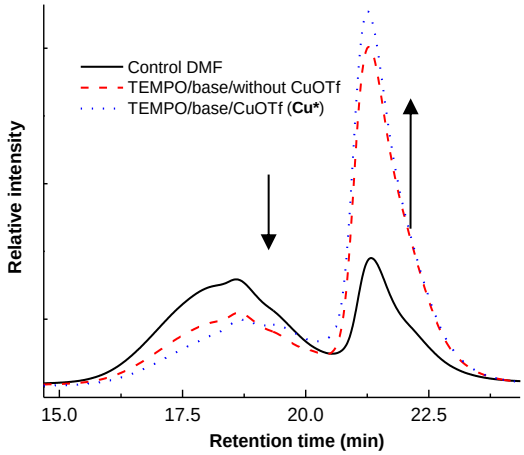

Figure 5.4. GPC data (THF solvent, elution rate: 1 mL/min, 245.5 nm detection) for the catalytic oxidation of organosolv lignin using **Cu*** (10 wt. % CuOTf, 10 wt. % TEMPO and 100 wt. % 2,6-lutidine), compared with the control experiment (no catalyst, TEMPO or base) and an experiment with TEMPO and base only. For all runs: solvent = DMF; temperature = 100 °C; pressure of synthetic air = 8.2 atm; reaction time = 18 h.

lutidine were present (*i.e.*, without CuOTf), suggesting that radical processes, not mediated by the metal, are contributing to the depolymerization process (Table 5.1).

In contrast to the results using catalysts **OV1** and **OV2**, oxovanadium catalyst **OVS** showed the same features and retention times as the control experiment. This catalyst can operate anaerobically, exhibiting a preference for C_{alkyl}-O bond cleavage, and the mechanism is thought to proceed through aryloxy radicals;[17a] perhaps these radicals initiate reactions leading to new polymeric networks, precluding significant molecular weight

reduction for the organosolv lignin used in the present study.

Metal-free catalyst **MFH** and cobalt complex **CoL** showed also no difference in the retention times between the catalytic and control experiments (see Table 5.1). Previous reports showed that catalyst **MFH** oxidizes benzylic C-H bonds in lignin models.[20] Here, the same effect was observed in terms of lack of decrease of the molecular weight on organosolv lignin. The lower lignin depolymerization activity that was observed for catalyst **CoL** (*vs.* previous report using aspen lignin) may be explained by the replacement of 3.4 atm O_2 in the original method with synthetic air (8% O_2 in Ar, 8.2 atm). Catalyst **CoL** is also sensitive to the amount of free phenolic moieties in lignin; lower activity for C_{aryl}-C_{alkyl} bond cleavage has been observed for low phenolic-containing lignin.[28]

The performance of catalyst **OV2** was compared to the benchmark method reported by Chornet and co-workers (Figure 5.5, left).[1] Use of the stronger base (135 wt. % NaOH in

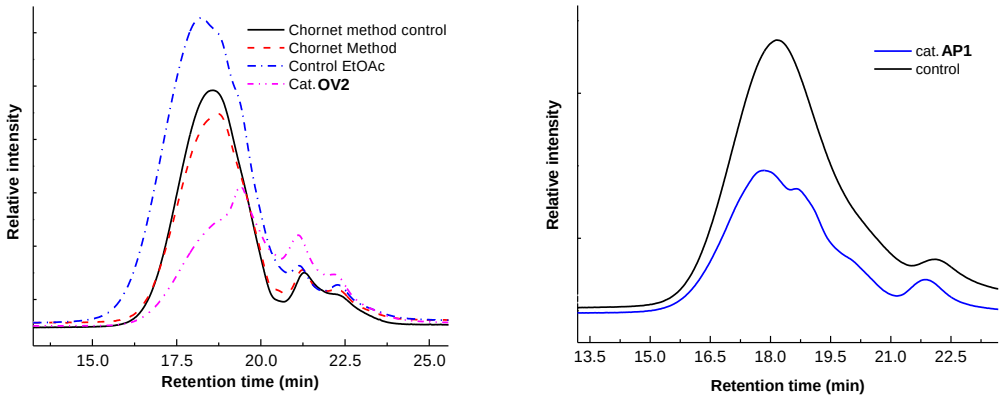

Figure 5.5. GPC data (THF solvent, elution rate: 1 mL/min, 245.5 nm detection) (left) for the catalytic oxidation of organosolv lignin using the Chornet method (THF, 135 wt. % NaOH, 5 wt. % $CuSO_4$ and 0.5 wt. % $FeCl_3$), Chornet control (THF and 135 wt. % NaOH) and catalyst **OV2** (EtOAc, 10 wt. % **OV2**, 10 wt. % Et_3N). (Right) catalytic oxidation of organosolv lignin using **AP1** (EtOAc, 10 wt. % **AP1**) and control (EtOAc). For all runs: temperature = 100 ^oC; pressure of synthetic air = 8.2 atm; reaction time = 18 h.

the Chornet control) gave a narrower MW distribution than heating the lignin in pure EtOAc or with Et_3N in EtOAc (as seen in Figure 5.3). The GPC chromatograms revealed, however, only minimal depolymerization when the Chornet method was used (Cu and Fe salts plus NaOH). Indeed, of the catalysts evaluated in this work, only catalyst **OV2**,

operating under synthetic air pressure, induced a significant decrease in the molecular weight of the organosolv lignin substrate.

As reported previously, oxovanadium catalysts such as **OV1** and **OV2** require base for both the initial alcohol oxidation and the subsequent C-C bond cleavage. In the bifunctional oxovanadium catalyst **AP1**, the incorporated pendant pyridine in the ligand scaffold could serve as the external base. Use of this catalyst, however, showed only minimal decrease in the molecular weight in EtOAc albeit without the need for additives (Figure 5.5, right). In contrast, the treatment of organosolv lignin with 10 wt. % catalyst **AP3** in *n*-butylacetate afforded the highest degree of depolymerisation to date in terms of reducing the molecular weight of lignin (Figure 5.6) in comparison to either homogenous[36] or heterogeneous[37]

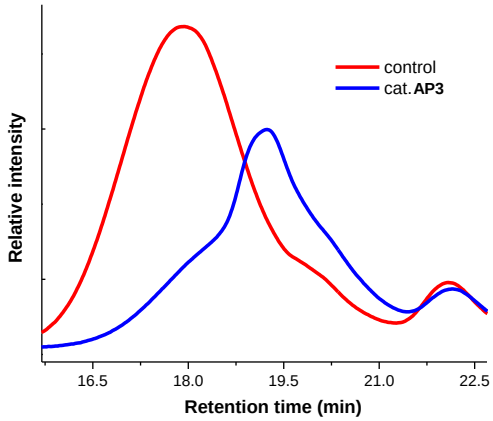

Figure 5.6. GPC data (THF solvent, elution rate: 1 mL/min, 245.5 nm detection) for the oxidation of organosolv lignin using 10 wt. % of **AP3** (*n*-butylacetate) and control experiment with no catalyst. For all runs: temperature = 100 ^{o}C; pressure of synthetic air = 8.2 atm; reaction time = 18 h.

metal catalysts. A large shift to lower molecular weight features (Table 5.2) is observed by GPC. The molecular weight of the residue from the catalytic experiment is almost half that from the control experiment. Note that the MW weight and polydispersity of the control experiment (no base added or catalyst) is comparable to the untreated organosolv lignin.

Table 5.2. GPC data for different amino(bisphenolate) oxovanadium catalysts and control experiments (THF solvent, elution rate: 1 mL/min, 254.4 nm detection).

Entry	Experiment	Mw (Da)	Mn (Da)	PDI
1	Organosolv lignin[a]	2526	850	2.97
2	**AP1**[b]	1110	564	1.96
3	**AP3**[b]	663	351	1.89
4	Control (no catalyst) for **AP1** and **AP3**[b]	1211	549	2.2

For untreated organosolv lignin, M_w = 1606 Da and M_n = 637 Da; [b]10 wt. % catalyst. For all runs: Solvent = *n*-butylacetate; temperature = 100 °C; pressure of synthetic air = 8.2 atm; reaction time = 18 h.

5.3.2 q-HSQC NMR Analysis

The q-HSQC NMR spectroscopic analysis allows for the evaluation of the reactivity of the various linkages (Figure 5.7) in the organosolv lignin when subjected to the different

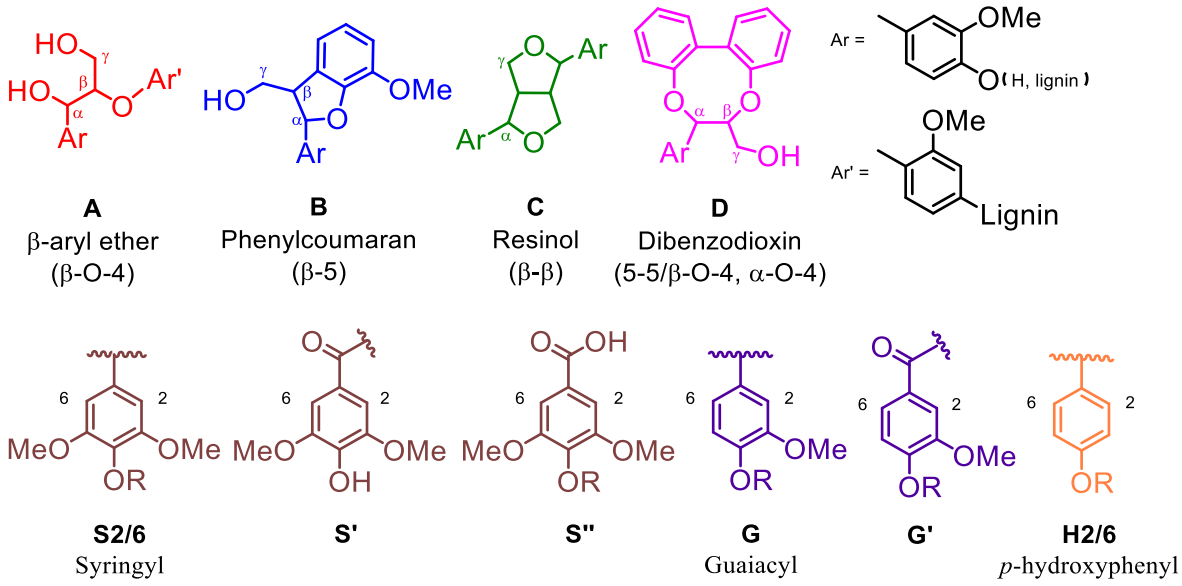

Figure 5.7. Lignin linkages observed by q-HSQC NMR.

homogeneous catalysts. Looking first at the aromatic nucleus, catalytic oxidation of organosolv lignin using catalyst **OV2** (EtOAc, 10 wt. % **OV2** and 10 wt. % Et_3N) converts all of the syringyl units **S** and most of the guaiacyl units **G** to the corresponding carbonyl-containing moieties **S'**, **S''** and **G'**; the **G'2**:**G2** ratio increased to 0.74 from 0.16 in the control (10% base with no catalyst; Figure 5.8). The small amount of hydroxyphenyl units

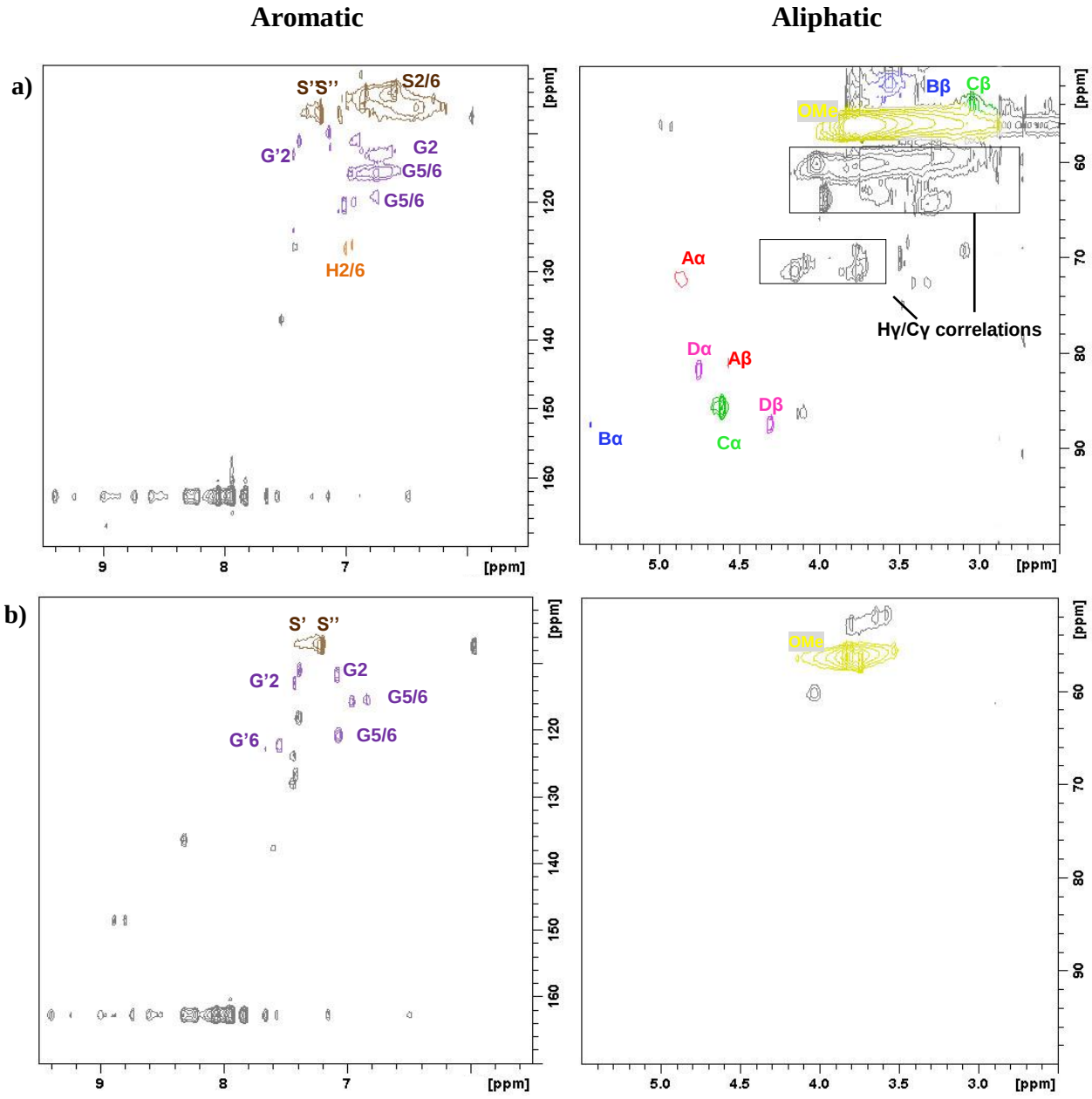

Figure 5.8. q-HSQC NMR spectra of organosolv lignin for: (a) control experiment (no catalyst) and b) catalytic oxidation using 10 wt. % **OV2** and 10 wt. % Et_3N. For all runs: solvent = EtOAc; temperature = 100 ^oC; pressure of synthetic air = 8.2 atm; reaction time = 18 h.

H were also converted.

Further details of the oxidative lignin depolymerization are provided by assessment of the aliphatic linkages. Correlations due to the major structural units **A**-**D** (δ 3.0 to 6.0 ppm in the ^{1}H NMR spectrum) that persisted on heating the organosolv lignin for 18 h with 10 wt. % base all disappeared on treatment with catalyst **OV2** under the same conditions. At shorter reaction times (4 h; Figure A26) correlations due to **A-D** were again absent while those in the aromatic region showed a lower degree of oxidation (**S'** + **S''**: **S2/6** = 0.90 and **G'2:G** = 0.04).

As indicated by the GPC and q-HSQC (Figure A22) data, catalyst **OV1** showed reduced activity (*vs.* **OV2**) for the oxidative depolymerization of organosolv lignin. Previous work showed that reaction of **OV1** with water (aerobic oxidation by-product) gives a less-active anionic dioxovanadium(V) complex.[35] Indeed, the ^{51}V NMR spectrum after the catalytic run revealed a strong signal at -522 ppm due to this complex.[38] Finally, it was noted that use of catalyst **OV2** without base resulted in no change for correlations due to **A-D** in the q-HSQC spectrum, confirming the importance of the BARD pathway for benzylic alcohol oxidation.

On the other hand, the copper catalyst **Cu*** resulted in the breakdown of **A**, **B**, **C** and **D** in addition to **S2/6** being oxidized to mostly **S'** and **S''**, the ratio increased to 0.73 from 0.26 in the control (no catalyst) (Figures 5.9 and A24). However, paramagnetic interference from residual copper (II) species hindered further investigation on this catalyst.

Similar to experiments with copper catalyst **Cu***, results from the Chornet method (paramagnetic Cu and Fe salts) prevented from obtaining noise-free and well-resolved q-HSQC spectra (Figure 5.9c). Filtration through various supports (silica, alumina, Celite) resulted in non-representative samples of the oxidized organosolv lignin. However, the GPC traces showed that the molecular weight was not decreased significantly in either the Chornet control experiment (only base) or the Chornet method (base and metal salts) (Figure 5.5).

Under the modified reaction conditions oxovanadium catalyst **OVS** was only able to oxidize the β-O-4 structural unit **A** in the oxygenated aliphatic region (Figure 5.9b). Correlations corresponding to **H2/6** in the aromatic region disappeared while other structural units remained roughly intact. This is in agreement with the C-O bond cleavage

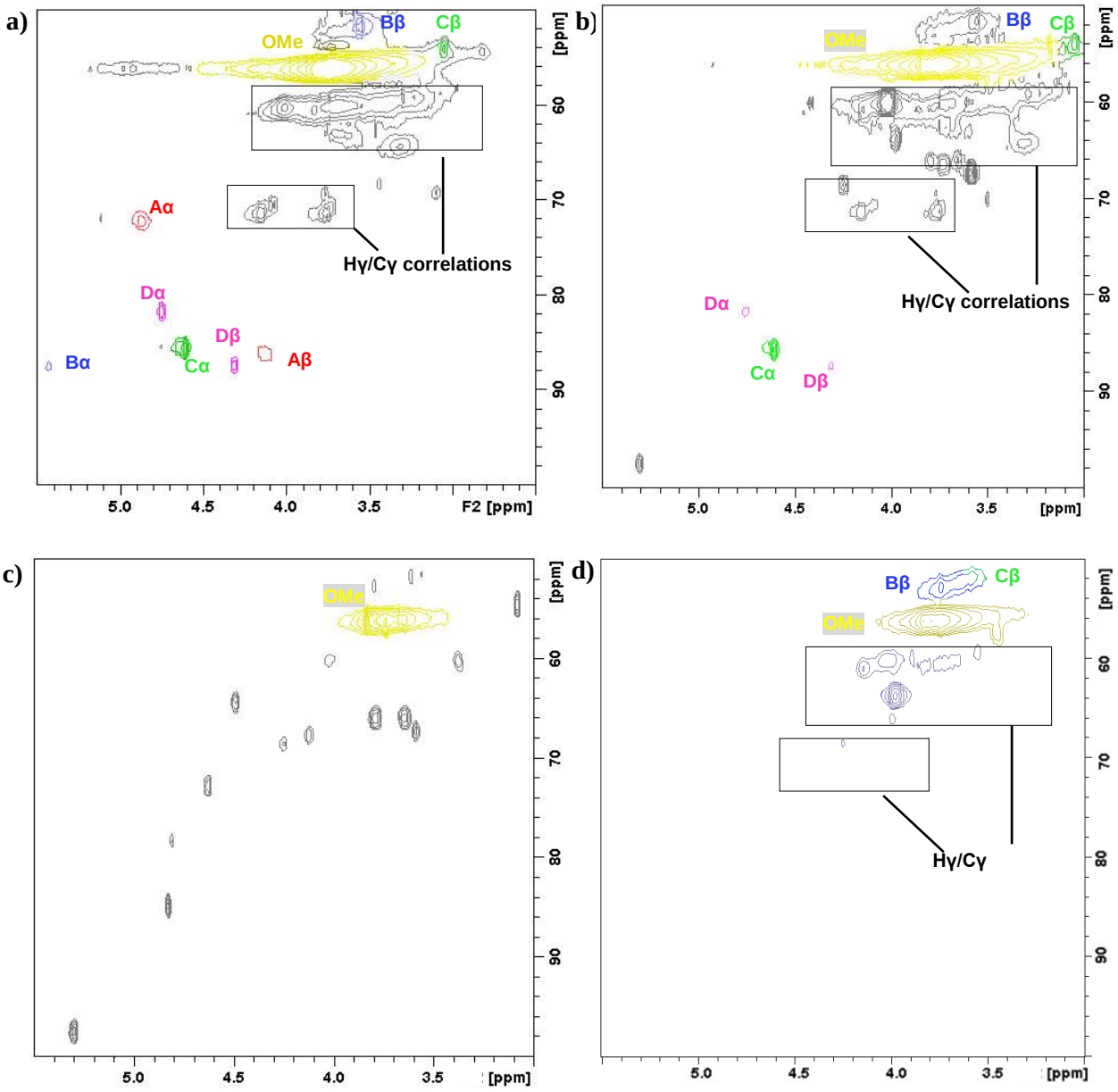

Figure 5.9. q-HSQC aliphatic regions of (a) organosolv lignin and oxidized material using catalysts (b) **OVS**, (c) **Cu*** and (d) **AP1** (see experimental section for reaction conditions).

mechanism proposed for this catalyst.[17]

Metal-free catalyst **MFH** cleaved the major structural units **A**, **B**, **C** and **D,** increasing the oxidized syringyl **S** and guaiacyl **G** units ((**S''** + **S'**)/**S2/6** to 0.82 from 0.76). However, the control experiment (without 4-acetamido-TEMPO) also demonstrated some oxidation of organosolv lignin under the modified conditions (Figure A28). Contrary to previous

reports,[20] the oxidized **A'** units were not observed under the modified reaction conditions.

As suggested by the GPC data, Co catalyst **CoL** was not able to oxidize organosolv lignin at the oxygen concentrations employed in this work (Figure S29). All of the major structural units in the oxygenated aliphatic region remained intact and the aromatic region remained similar to organosolv lignin spectrum. The ratios of **S'' + S' / S2/6** and **G'2 / G2**

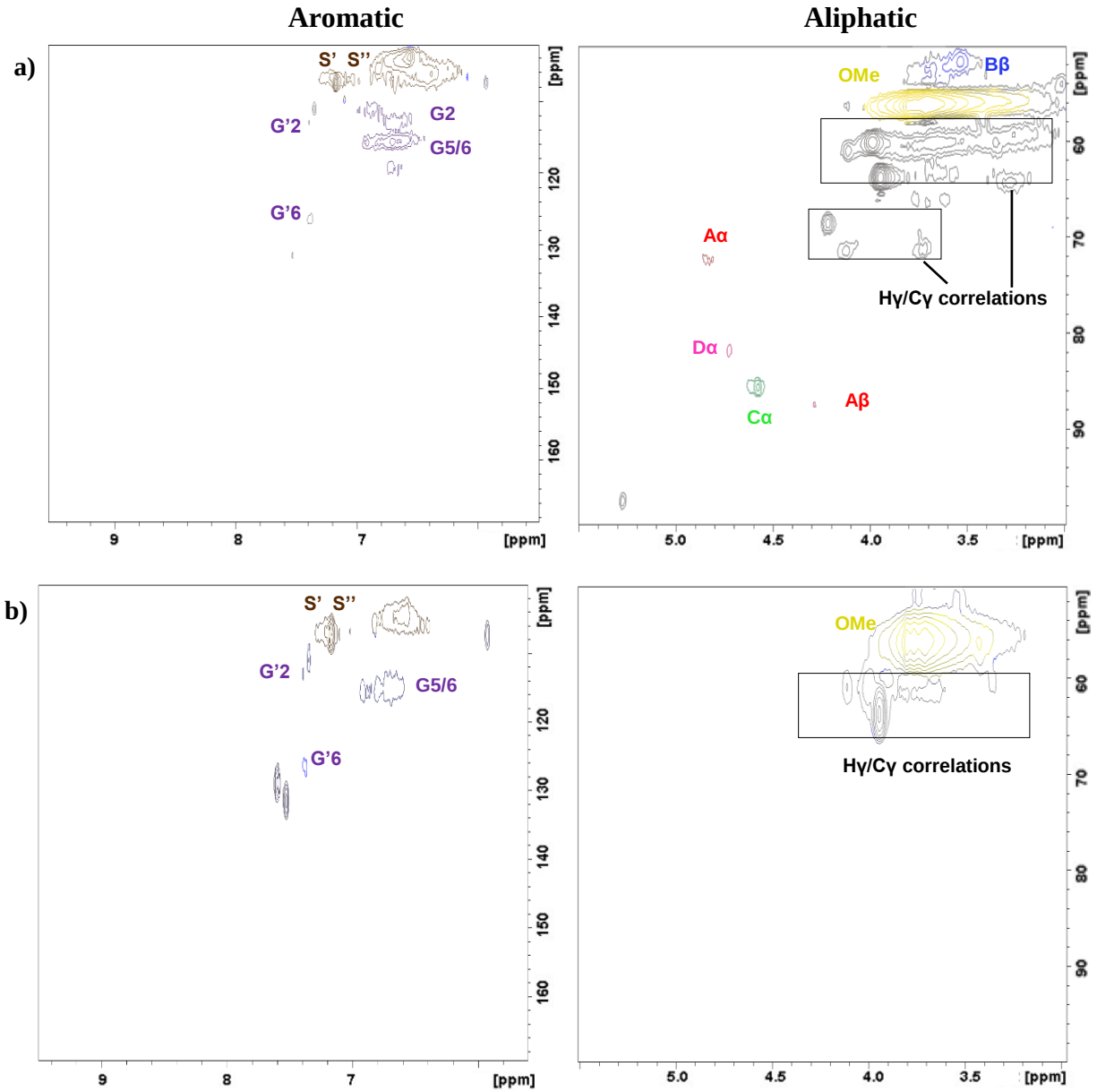

Figure 5.10. q-HSQC NMR spectra of organosolv lignin for **AP3**: (a) 1 wt. % **AP3** and (b) 10 wt. % **AP3**. For all runs: Solvent = *n*-butylacetate; temperature = 100 °C; pressure of synthetic air = 8.2 atm; reaction time = 18 h.

were almost identical to those in the original organosolv lignin: **S''** + **S'** / **S2/6** = 0.09 and, **G'2** / **G2** = 0.02.

Bifunctional oxovanadium catalyst **AP3** showed a large decrease on the major units **A**, **B**, **C** and **D**, and most of the aromatic region when 1 wt. % catalyst is added (Figure 5.10b). The degree of depolymerization shown by **AP3** is comparable to catalyst **OV2** but with no need for addition of external base. In contrast, the addition of just 1 wt. % **AP3** does not show the same extended degree of depolymerization as the higher catalyst loading. However, both concentrations of catalysts are by far more effective compared to all the other methods tested in this study (Figure 5.10b). As demonstrated by GPC, the tethered base in **AP1** increased the performance for C-C and C-O bond cleavage compare with catalysts **OV1** and **OV2**.

5.3.3 Quantitative ^{31}P NMR Spectroscopy

Phosphitylation has been shown to be a useful tool for characterizing the various types of aromatic, aliphatic and carboxylic acid O-H bonds in lignin (Figure 5.11).[33] The control

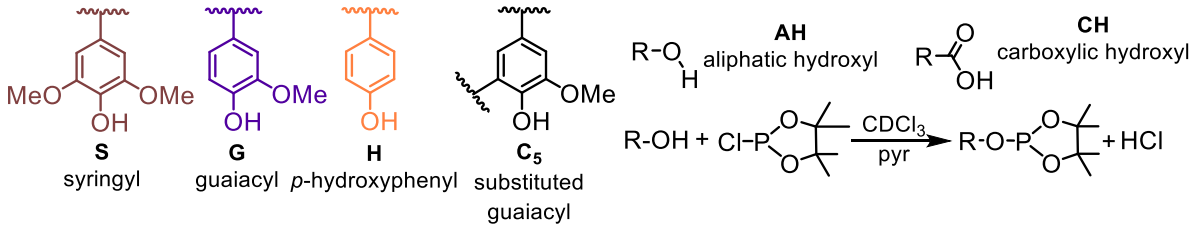

Figure 5.11. Hydroxyl-containing lignin structural units characterized by ^{31}P NMR spectra of derived phosphite esters.

experiment using 10 wt. % base (no catalyst) showed similar composition to the organosolv lignin (Table 5.3). As expected, concentrations of aliphatic and especially phenolic O-H units (but not carboxylic acids) decreased substantially after treatment of the organsolv lignin with catalyst **OV2** + Et_3N. Figure 5.12 displays a typical ^{31}P NMR spectrum for organosolv lignin treated with different conditions. It was observed previously that catalyst **OV2** readily cleaves C_{alkyl}-C_{aryl} bonds in β-O-4[23] and β-1[24] phenolic lignin models.

Catalyst **AP1** showed similar decreased in the lignin linkages as catalyst **OV2**, however, lower activity is observed as expected by the GPC and 2D NMR (see above sections).

Table 5.3. Concentrations (mmol g^{-1} substrate) of lignin-derived phosphite esters as determined by quantitative $^{31}P\{^{1}H\}$ NMR spectroscopy.

$\delta_{(ppm)}$[a]	**G**$_{(139.0\text{-}140.5)}$	**H**$_{(137.5\text{-}138.8)}$	**C$_5$**$_{(141.0\text{-}144.5)}$	**AH**$_{(146.1\text{-}150.0)}$	**CH**$_{(133.6\text{-}136.0)}$
Organosolv lignin	2.68	0.59	8.00	3.29	1.00
Lignin + base control[b,d]	2.25	0.57	6.56	2.08	1.62
Catalyst **OV2**[c,d]	0.31	0.12	0.72	0.36	1.02
Catalyst **AP1**[e]	1.75	0.58	5.04	1.63	1.15

[a]Syringyl units **S** are omitted due to overlap with substituted guaiacyl **C$_5$** units at 142.7 ppm. [b]Control experiment using 10 wt. % Et_3N. [c]Catalytic oxidation using 10 wt. % **OV2** and 10 wt. % Et_3N. [d]For all runs: solvent = EtOAc; temperature = 100 °C; pressure of synthetic air = 8.2 atm; reaction time: 18 h. [e]Catalytic oxidation using 10 wt. % **AP1**.

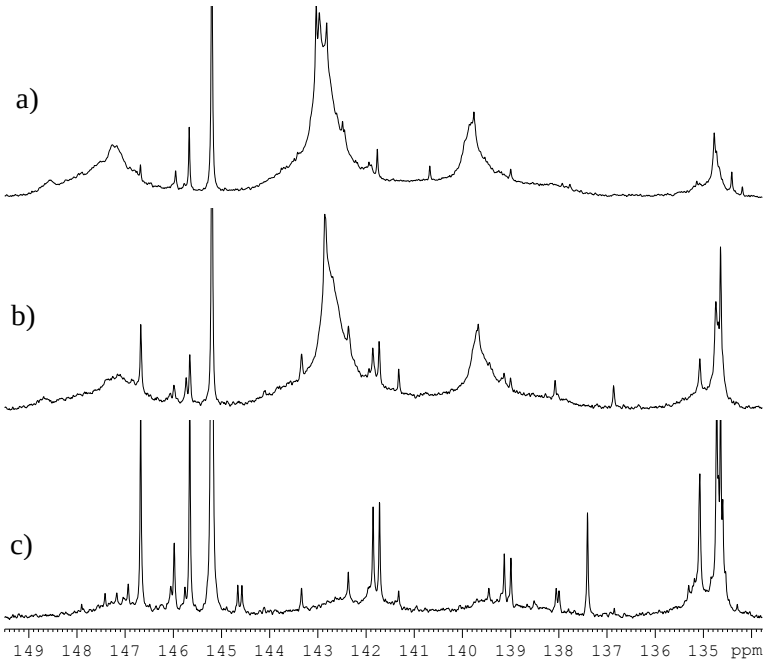

Figure 5.12. Quantitative $^{31}P\{^{1}H\}$ NMR spectra (121 MHz, line broadening 2.5 Hz) of derived phosphite esters from a) organosolv lignin; b) control experiment (base with no catalyst); and c) residue after the catalytic lignin oxidation using 10 wt. % **OV2** and 10 wt. % Et_3N. For all runs: solvent = EtOAc; temperature = 100 °C; pressure of synthetic air = 8.2 atm; reaction time = 18 h.

5.4 Conclusions

Of the catalysts tested in this work, the bis(8-oxy-quinoline) oxovanadium and amine bis(phenolate) oxovanadium catalyst **OV2** and **AP3**, respectively, showed the best activity for depolymerization/oxidation of organosolv lignin, as evidenced by GPC and q-HSQC NMR spectroscopy. A substantial decrease in the molecular weight, quantitative conversion of four common aliphatic linkages, and an increase in oxidized **S** and **G** units, were observed compared to the control experiment. Moreover, significant conversion of phenolic and aliphatic hydroxyls was demonstrated by ^{31}P NMR spectra of derived phosphite esters.

In comparing the performance of several homogeneous catalysts for the aerobic oxidation of organosolv lignin, several additional observations can be made:

1) Whereas copper catalysts **Cu*** exhibit complementary selectivity to oxovanadium catalysts, **OV1** and **OV2** in aerobic oxidation of simple lignin models, the former suffers from poor carbon balance with more complex models which translates to inefficient depolymerization with lignin extracts, likely due to radical recombination. As discussed in section 2.3.4, radical coupling of phenoxyl radicals have been described as the major source of humins and undesirable oligomers using copper, vanadium and alkaline solutions of lignin, among other conditions.[39]
2) Previous work has demonstrated that oxovanadium catalysts such as **OVS** and **OV1** in the absence of base tend to favour C-O *vs.* benzylic C-H bond cleavage in a variety of phenolic and non-phenolic lignin models. In these cases, however, generation of phenoxy radicals appears to also be deleterious to achieving efficient depolymerization of lignin extracts.
3) While both metal-free acetamido-TEMPO catalyst **MFH** in an acidic medium and oxovanadium catalyst **OV2** with added base show excellent selectivity for benzylic C-H bond cleavage to the ketone, only catalyst **OV2** is then able to cleave the ketone C_α-C_β bond, allowing for significant depolymerization of lignin extracts.
4) Although the detailed mechanism of ketone C_α-C_β bond cleavage is still unclear, preliminary experiments show that this reaction is also promoted by added base.[40] A new generation of base-tethered ligands, such as **AP1** and **AP3**, afford more efficient and selective oxovanadium catalysts for aerobic oxidation of lignin.

Further tuning of the pendant base, however, is needed to achieve improved lignin depolymerization.

As new exciting results on tandem redox[20,25] and biocat-chemcat[14] approaches to lignin valorization are being disclosed, a selective and productive homogeneous oxidation catalyst could be a key component.

5.5 References

(1) Wu, G.; Heitz, M.; Chornet, E. *Ind. Eng. Chem. Res.* **1994**, *33*, 718−723.
(2) Hepditch, M. M.; Thring, R. W. *Can. J. Chem. Eng.* **2000**, *78*, 226–231.
(3) Zakzeski, J.; Bruijnincx, P. C. A.; Jongerius, A. L.; Weckhuysen, B. M. *Chem. Rev.* **2010**, *110*, 3552–3599.
(4) Crestini, C.; Crucianelli, M.; Orlandi, M.; Saladino, R. *Catal. Today* **2010**, *156*, 8–22.
(5) Pandey, M. P.; Kim, C. S. *Chem. Eng. Technol.* **2011**, *34*, 29−41.
(6) Werhan, H.; Mir, J. M.; Voitl, T.; von Rohr, P. R. *Holzforschung* **2011**, *65*, 703–709.
(7) Roberts, V. M.; Stein, V.; Reiner, T.; Lemonidou, A.; Li, X.; Lercher, J. A. *Chem. Eur. J.* **2011**, *17*, 5939–5948.
(8) Beauchet, R.; Monteil-Rivera, F.; Lavoie, J. M. *Bioresource Technol.* **2012**, *121*, 328–334.
(9) Liu, S.; Shi, Z.; Li, L.; Yu, S.; Xie, C.; Song, Z. *RSC Adv.* **2013**, *3*, 5789–5793.
(10) Liguori, L.; Barth, T. *J. Anal. App. Pyrol.* **2013**, *92*, 477–484.
(11) Wang, H.; Tucker, M.; Ji, Y. *J. Appl. Chem.* **2013**, *2013*, 1–9.
(12) Song, Q.; Wang, F.; Cai, J.; Wang, Y.; Zhang, J.; Yu, W.; Xu, J. *Energy Environ. Sci.* **2013**, *6*, 994–1007.
(13) Ragauskas, A. J.; Beckham, G. T.; Biddy, M. J.; Chandra, R.; Chen, F.; Davis, M. F.; Davison, B. H.; Dixon, R. A.; Gilna, P.; Keller, M.; Langan, P.; Naskar, A. K.; Saddler, J. N.; Tschaplinski, T. J.; Tuskan, G. A.; Wyman, C. E. *Science* **2014**, *344*, 1246843–1–10.
(14) Linger, J. G.; Vardon, D. R.; Guarnieri, M. T.; Karp, E. M.; Hunsinger, G. B.; Franden, M. A.; Johnson, C. W.; Chupka, G.; Strathman, T. J.; Pienkos, P. T. Beckham, G. T. *Proc. Nat. Acad. Sci.* **2014**, *111*, 12013–12018.
(15) Ma, R.; Xu, Y.; Zhang, X. *ChemSusChem* **2015**, *8*, 24–51.
(16) a) Hanson, S. K.; Baker, R. T.; Gordon, J. C.; Scott, B. L.; Thorn, D. L. *Inorg. Chem.* **2010**, *49*, 5611–5618; b) Sedai, B.; Díaz-Urrutia, C.; Baker, R. T.; Wu, R.; Silks, L. A. P.; Hanson, S. K. *ACS Catal.* **2011**, *1*, 794–804; c) Sedai, B.; Díaz-Urrutia, C.; Baker, R. T.; Wu, R.; Silks, L. A. P.; Hanson, S. K. *ACS Catal.* **2013**, *3*, 3111–3122; d) Díaz-Urrutia, C.; Sedai, B.; Leckert, K.; Baker, R. T.; Hanson, S. K. *ACS Sustainable Chem. Eng.* ***2016****, submitted;* e) Sedai, B.; Baker, R. T. *Adv. Synth. Catal.* **2014**, *356*, 3563–3574.
(17) a) Son, S.; Toste, F. D. *Angew. Chem. Int. Ed.* **2010**, *49*, 3791–3794; b) Chan, J. M. W.; Bauer, S.; Sorek, H.; Sreekumar, S.; Wang, K.; Toste, F. D. *ACS Catal.* **2013**, *3*, 1369–1377.
(18) Hanson, S. K.; Wu, R.; Silks, L. A. P. *Angew. Chem. Int. Ed.* **2012**, *51*, 3410−3413.
(19) Hanson, S. K.; Silks, L. A. P.; Wu, R. US patent **2012**, 0232279 A1.
(20) Rahimi, A.; Azarpira, A.; Kim, H.; Ralph, J.; Stahl, S. S. *J. Am. Chem. Soc.* **2013**, *135*, 6415–6418.
(21) Hoover, J. M.; Ryland, B. L.; Stahl, S. S. *J. Am. Chem. Soc.* **2013**, *135*, 2357–2367.
(22) a) Mitchell, L. J.; Moody, C. J. *J. Org. Chem.* **2014**, *79*, 11090–11100; b) Mottweiler, J.; Puche, M.; Räuber, C.; Schmidt, T.; Concepción, P.; Corma, A.; Bolm, C. *ChemSusChem* **2015**, *8*, 2106–2113.
(23) a) Sergeev, A. G.; Hartwig, J. F. *Science* **2011**, *332*, 439–443; b) Sergeev, A. G.; Webb, J. D.; Hartwig, J. F. *J. Am. Chem. Soc.* **2012**, *134*, 20226–20229; c) Ren, Y.; Yan, M.; Wang, J.; Zhang, Z. C.; Yao, K. *Angew. Chem. Int. Ed.* **2013**, *52*, 12674 –12678; d) Nichols, J. M.; Bishop, L. M.; Bergman, R. G.; Ellman, J. A. *J. Am. Chem. Soc.* **2010**, *132*,

12554–12555; e) Wu, A.; Patrick, B. O.; Chung, E.; James, B. R. *Dalton Trans.* **2012**, *41*, 11093–11106; f) vom Stein, T.; Weigand, T.; Merkens, C.; Klankenmayer, J.; Leitner, W. *ChemCatChem* **2013**, *5*, 439–441; g) Weickmann, D.; Plietker, B. *ChemCatChem* **2013**, *5*, 2170–2173; h) Nagy, M.; David, K.; Britovsek, G. J. P.; Ragauskas, A. J. *Holzforschung* **2009**, *63*, 513–520.
(24) Rahimi, A.; Ulbrich, A.; Coon, J. J.; Stahl, S. S. *Nature* **2014**, *515*, 249–252.
(25) Lancefield, C. S.; Ojo, O. S.; Tran, F.; Westwood, N. J. *Angew. Chem. Int. Ed.* **2015**, *54*, 258–262.
(26) Wigington, B. N.; Drummond, M. L.; Cundari, T. R.; Thorn, D. L.; Hanson, S. K.; Scott, S. L. *Chem. Eur. J.* **2012**, *18*, 14981–14988
(27) a) Reddy, G. V. B.; Sridhar, M.; Gold, M. H. *Eur. J. Biochem*. **2003**, *270*, 284–292; b) Camarero, S.; Martinez, M. J.; Martinez, A. T. *Biofuels Bioprod. Bioref.* **2014**, *8*, 615–625.
(28) Biannic, B.; Bozell, J. J. *Org. Lett.* **2013**, *15*, 2730–2733.
(29) Canevali, C.; Orlandi, M.; Pardi, L.; Rindone, B.; Scotti, R.; Sipila, J.; Morazzoni, F. *J. Chem. Soc., Dalton Trans.* **2002**, 3007–3014.
(30) Leung, W-H.; Chan, E. Y. Y.; Chow, E. K. F.; Williams, I. D.; Peng, S.-M. *J. Chem. Soc., Dalton Trans.* **1996**, 1229–1236.
(31) Heikkinen, S.; Toikka, M. M.; Karhunen, P. T.; Kilpeläinen, I. A. *J. Am. Chem. Soc.* **2003**, *125*, 4362–4367.
(32) a) Ralph, S. A.; Landucci, L. L.; Ralph, J. NMR database of lignin and cell wall model compounds. http://ars.usda.gov/Services/docs.htm?docid=10491; b) Ralph, J.; Landucci, L. L. in "Lignin and Lignans: Advances in Chemistry," Heitner, C.; Dimmel, D.; Schmidt, J. A. Eds.; CRC: Boca Raton, Fl., 2010; pp 2137–2234.
(33) a) Pu, Y.; Cao, S.; Ragauskas, A. J. *Energy Environ. Sci.* **2011**, *4*, 3154–3166; b) Argyropoulos, D. S. *Res. Chem. Intermed.* **1995**, *21*, 373–395; c) Granata, A.; Argyropoulos, D. S. *J. Agric. Food Chem.* **1995**, *43*, 1538–1544; d) Hallac, B. B.; Pu, Y.; Ragauskas, A. J. *Energy Fuels* **2010**, *24*, 2723–2732; e) Sannigrahi, P.; Ragauskas, A. J.; Miller, S. J. *Energy Fuels* **2010**, *24*, 683–689.
(34) a) Hortling, B.; Turunen, E.; Kokkonen, P.; Handbook of Size Exclusion Chromatography and Related Techniques; Dekker, M. Wayne, NJ., 1995; pp 1355–1383; b) Stewart, J. J.; Kadla, J. F.; Mansfield, S. D. *Holzforschung* **2006**, *60*, 111–122.
(35) Hanson, S. K.; Baker, R. T.; Gordon, J. C.; Scott, B. L.; Silks, L. A. P.; Thorn, D. L. *J. Am. Chem. Soc.* **2010**, *132*, 17804–17816.
(36) a) Mottweiler, J.; Rinesch, T.; Besson, C.; Buendia, J.; Bolm, C. *Green Chem.* **2015**, *17*, 5001–5008; b) Deuss, P. J.; Scott, M.; Tran, F.; Westwood, N. J.; de Vries, J. G.; Barta, K. *J. Am. Chem. Soc.* **2015**, *137*, 7456–7467.
(37) a) Galvin, V. M.; Sawadjoon, S.; Rohde, V.; Dawange, M.; Samec S. M. J. *ChemCatChem* **2014**, *6*, 179–184; b) Kumar, C. R.; Anand, N.; Kloekhorst, A.; Cannila, C.; Bonura, G.; Frusteri, F. Barta, K.; Heeres, H. J. *Green Chem*. **2015**, *17*, 4921**–**4930.
(38) Hanson, S. K.; Wu, R.; Silks, L. A. P. *Org. Lett.* **2011**, *13*, 1908–1911.
(39) a) Pardini, V. L.; Smith, C. Z.; Utley, J. H. P.; Vargas, R. R.; Viertler, H. *J. Org. Chem.* **1991**, *56*, 7305−7313; b) Pardini, V. L.; Vargas, R. R.; Viertler, H. *Tetrahedron* **1992**, *48*, 7221−7228.
(40) Díaz-Urrutia, C.; Baker, R. T. unpublished results.

Chapter 6: Aerobic Oxidative C-C Bond Cleavage of 1,2-Diols by Trialkoxyamine Oxovanadium(V) Catalysts: Evidence for a Two-Electron Pathway

This chapter has been partially published in: a) Díaz-Urrutia, C.; Michel, C.; Fleurat-Lessard, P.; I.; Korobkov, I.; Martinez, A.; Baker, R. T. ***2016****, submitted; b) Díaz-Urrutia, C.; Zhang, D.; Martinez, A.; Baker, R. T.* ***2016****, manuscript in preparation.*

6.1 Introduction

Methods for elaboration of cellulose-derived sugars have been focused either on catalyzed reduction to polyalcohols (*i.e.*, sorbitol, mannitol)[1a,b] or hydrolysis to the platform chemicals 5-hydroxymethylfurfural, levulinic acid and γ-valerolactone.[1c] Selective oxidation of sugars to carbonyl compounds remains a challenge for catalysis; *cf.*, biological oxidation of glucose using phosphate requires ten different enzymes to form two equivalents of pyruvate.[2] While base-catalyzed aldol condensation of biomass-derived aldehydes has been used to increase the carbon number of promising biofuel intermediates,[3a,b] selective C-C bond cleavage of cellulose-derived sugars and polyalcohols using air as an oxidant could provide a complementary technique for biorefinery applications.[3c]

Periodic acid or lead tetraacetate are commonly used for the oxidation and cleavage of polyalchols, but their toxicity and the need for stoichiometric amounts of the reagents make them impractical for their application in biomass conversion.[4] Alternatively, use of

transition metal complexes often requires high catalyst loadings and co-additives.[5] Baker[6] and Hanson[7] have extensively studied complexes **OV1** and **OV2** (Figure 6.1) for the cata-

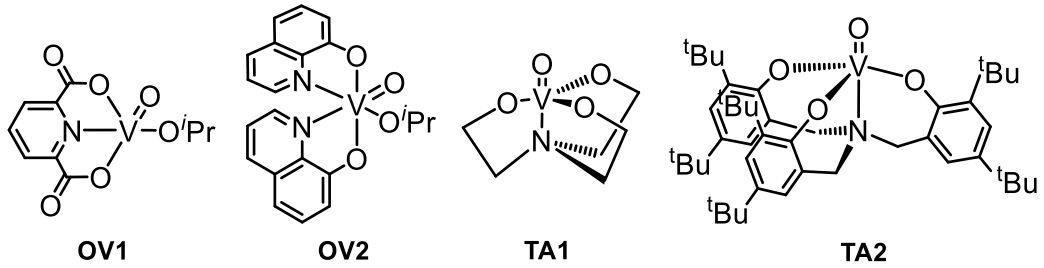

Figure 6.1. Vanadium catalysts **OV1** and **OV2**, and VHPO-like trialkoxyamine oxovanadium(V) catalysts **TA1** and **TA2**.

lytic oxidation of alcohols, diols and lignin models. The C-C bond cleavage of pinacol in the pinacolate oxovanadium complex (**A**) proceeded through a formal one-electron oxidation to produce acetone and a V(IV) complex (**B)** under relative mild conditions (Scheme 6.1a). Under harsher conditions the bis(pyridine) V(IV) product (**B**) can also oxid-

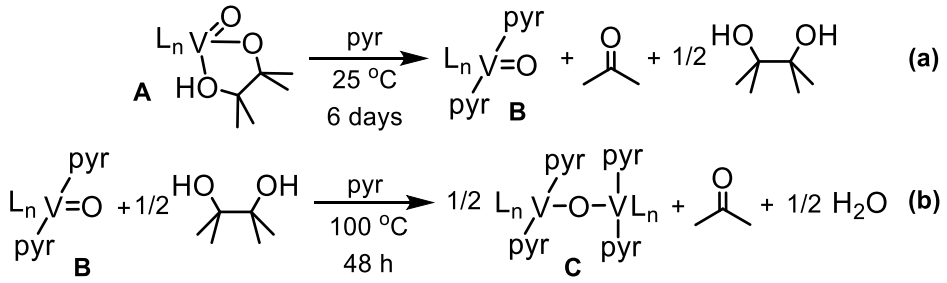

Scheme 6.1. Stepwise one-electron C-C bond cleavage of pinacol using **OV1** or **OV2**.

ize ½ equivalent of pinacol through an additional one-electron oxidation to afford a bimetallic μ-oxo V(III) complex (**C**) and acetone (Scheme 6.1b). While earlier work had demonstrated that oxidation of mono-alcohols to carbonyl compounds using vanadium(V) catalysts commonly proceeds through a one-electron pathway,[8] Hanson and Baker characterized a two-electron, base-assisted dehydrogenation pathway wherein rapid reaction of the V(III) intermediate (**C**) with the V(V) catalyst precursor affords the observed V(IV) product (**B**) facilitated by the sterically undemanding ligand scaffold of **OV1** and **OV2**. Mechanistic details for the pinacol C-C bond cleavage, however, were not elucidated and a radical pathway has not been ruled out (*e.g.*, direct reduction of V(V) to V(IV)).

Vanadium haloperoxidases (VHPOs) have been proposed as models for bio-inorganic catalysts due to their ability to, for example, oxidize halides and more complex substrates such as sulfides in the presence of peroxides.[9] One distinct feature of VHPOs is their five-coordinate V(V) centers in a trigonal-bipyramidal geometry with a nitrogen *trans* to an oxygen and three other oxygens occupying the basal plane of the V center.[9d] Surprisingly, no change in the oxidation state of the metal (*e.g.*, to +4 or +3) has been observed for these enzymes.[9e] Several VHPO model complexes have been prepared and investigated; among them, complexes **TA1**[10] and **TA2**[11-12] [L = triethoxyamine (**TA1**), tris[2-(3,5-di-*tert*-butyl-phenoxy)methyl]amine (**TA2**)] (Figure 6.1) show outstanding performance for the carboxylation of alkanes, oxidation of sulfides, alkanes and bromination of aromatics.[10-12] However, all previously reported reactions require at least stoichiometric amounts of peroxides, reactions of **TA1** or **TA2** using air as an oxidant are unknown.[10-12] Intrigued by the versatile reactivity of the trialkoxyamine oxovanadium complexes, their use as catalysts for the aerobic oxidation of 1,2-diols was investigated.

This *Chapter* reports that the selective oxidative cleavage of the C-C bond in 1,2-diols, using **TA1** and **TA2,** proceeds through a direct two-electron pathway from V(V) to V(III). The steric impedance created by the ^{t}Bu groups of **TA2** enables the observation and characterization of the non-oxo mononuclear V(III) product, whereas under the same conditions the less bulky ligand scaffold around the vanadium centre in **TA1** afforded an insoluble inorganic polymer. Molecular oxygen then acts as an efficient oxidant for the non-oxo V(III) complex, closing the catalytic cycle. Further mechanistic insights are provided by kinetic and computational studies.

6.2 Materials and Methods

6.2.1 General Considerations

Unless specified otherwise all reactions were carried out under dry nitrogen atmosphere using glovebox or Schlenk techniques. Acetonitrile (CH_3CN), toluene, diethyl ether (Et_2O), dimethylsulfoxide (DMSO), dimethoxyethane (DME) and dichloromethane (DCM) were purchased from Sigma Aldrich or Alfa Aesar. Toluene, diethyl ether and dimethoxyethane were dried on columns of activated alumina using a J. C. Meyer solvent purification system. Acetonitrile and dichloromethane were dried by refluxing over CaH_2, distilling and

stirring over activated alumina. Pinacol, *meso*-hydrobenzoin and 2-phenoxyethanol were purchased from Sigma Aldrich and Alfa Aesar, and dried under vacuum prior to use. Deuterated acetonitrile (CD_3CN), chloroform ($CDCl_3$), benzene (C_6D_6), toluene (toluene-d_8) and dimethylsulfoxide (DMSO-d_6) solvents were purchased from Cambridge Isotope Laboratories and dried following the previous procedures. All other reagents were used as received. ^{1}H, ^{2}H, $^{13}C\{^{1}H\}$ and ^{51}V NMR spectra were obtained at room temperature on Bruker AVANCE 300 MHz, 400 MHz or 500 MHz spectrometers, with chemical shifts referenced to the residual solvent signal (^{1}H and ^{13}C), externally to $VOCl_3$ (0 ppm, ^{51}V) or internally adding one drop of $CDCl_3$ (7.26 ppm, ^{2}H). For ^{1}H NMR the residual internal solvent peaks are C_6D_6 (δ 7.16), CD_3CN (δ 1.94) and $CDCl_3$ (δ 7.26). GC-MS measurements were conducted in HPLC-MS grade $CHCl_3$ or CH_3CN solvent using an Agilent GC/MS system (6890N and 5975B) in EI mode equipped with an Agilent HP-5MS column (30m x 250 um x 0.25 um). IR spectra were obtained on a Thermo Nicolet NEXUS 670 FTIR spectrometer. UV-vis spectra were recorded in dry CH_2Cl_2 on Varian Cary 50 Bio UV-Visible or Agilent Cary 7000 spectrophotometers, using sealable quartz cuvettes (1.0 cm path length). The spin-only magnetic moment in solution at room temperature was obtained by the Evans' method.[13] Elemental analysis was performed at the Laboratoire d'Analyse Élémentaire de l'Université de Montréal. Turnover numbers (TON) were calculated as the maximum moles of substrate consumed over the amount (in moles) of the catalysts used. Compounds **OV2**,[7b] **TA1**,[10a] **TA2**[11a] and hydrobenzoin isotopomers (1,2-C-^{2}H and 1,2-O-^{2}H)[14] were prepared following the published procedures. Hemicarcerand **TA3** and **TA4** were received and used without further purification from Prof. Alexandre Martinez (ENS Lyon, France).

6.2.2 X-ray Crystallography

Data collection results for compounds **TA5**, **TA6**, **TA8** and **TA9** represent the best data sets obtained in several trials for each sample (see Table 6.1). The crystals were mounted on thin glass fibers using paraffin oil. Prior to data collection crystals were cooled to 200K.

Data were collected on a Bruker AXS SMART single-crystal diffractometer equipped with a sealed Mo tube source (wavelength 0.71073 Å) APEX II CCD detector. Raw data collection and processing were performed with APEX II software package from BRUKER AXS.[15] Diffraction data for both samples were collected with a sequence of 0.3° ω scans

Table 6.1. Crystallographic data for **TA8**, **TA5** and **TA6**.

	TA5	**TA6**	**TA8**	**TA9**
formula	$C_{50}H_{71}N_2O_4V$	$C_{47}H_{72}NO_5SV$	$C_{47}H_{69}N_2O_3V$	$C_{49}H_{76}NO_5V$
fw	894.12	906.19	760.98	810.04
a (Å)	10.1797(3)	20.2333(6)	13.852(3)	14.3565(8)
b (Å)	30.5777(7)	12.1753(4)	12.082(2)	20.0648(11)
c (Å)	17.2440(4)	22.4518(7)	26.805(5)	16.5163(10)
α (deg)	90	90	90	90
β (deg)	107.1212(15)	97.3613(15)	91.787(8)	93.048(3)
γ (deg)	90	90	90	90
crystal system	monoclinic	monoclinic	monoclinic	Monoclinic
Space group	P 21/n	P 21/n	P 21/n	P 21/n
V ($Å^3$)	5129.6(2)	5485.3(3)	4483.9(15)	4751.0(5)
D_c (g cm^{-1})	1.158	1.097	1.127	1.132
μ (mm^{-1})	0.239	0.261	0.261	0.252
Z	4	4	4	4
F(000)	1928	1960	1648.0	1760
T/K	200(2)	200(2)	200	200(2)
R_1 [I>2σ(I)]	0.0586	0.0681	0.0721	0.0485
wR_1 [I>2σ(I)]	0.1426	0.1782	0.1975	0.1091

at 0, 120, and 240° in φ. Initial unit cell parameters were determined from 60 data frames with 0.3° ω scan each collected at the different sections of the Ewald sphere. Semi-empirical absorption corrections based on equivalent reflections were applied.[16] Systematic absences in the diffraction data set and unit-cell parameters were consistent with monoclinic **P***2₁/n* (№14, alternative settings) for all compounds. Solutions in the centrosymmetric space groups for **TA5** and **TA6** yielded chemically reasonable and computationally stable results of refinement. Structures were solved by direct methods, completed with difference Fourier synthesis, and refined with full-matrix least-squares procedures based on F^2.

The structural model for **TA5** compound revealed one target molecule co-crystallized with one molecule of pyridine. Both molecules are located on the general positions of the unit cell. In the final refinement stage, thermal motion parameters for the ^{t}Bu fragment based at C(38) suggested a rotational disorder not related to the symmetry elements.

Disorder was successfully modeled, however the set of geometrical (SADI) restraints were applied to achieve acceptable fragment geometries. Disordered fragment occupancies were refined initially to obtain reasonable thermal motion parameters values. After initial refinement, occupancy was restrained to 75% : 25% respectively. All non-hydrogen atoms in the structure **TA5** were refined with full set of anisotropic thermal displacement coefficients. However, in order to obtain acceptable parameter values for pyridine solvent molecule a set of thermal motion restraints (SIMU, RIGU) was employed.

Diffraction data for the crystal of **TA6** complex were collected to 0.75Å resolution, however due to small crystal size and weak diffraction it was discovered that both R(int) and R(sigma) exceeded 35% for the data below 0.95Å resolution. Based on R(sigma) value data were truncated to 0.90Å resolution for refinement. The asymmetric unit for the structure of **TA6** contains one molecule of target compound and one molecule of co-crystallized toluene solvent. Both molecules are located on general positions of the unit cell. In the final refinement stage, thermal motion parameters for the ^{t}Bu fragments based at C(23) and C(38) suggested a rotational disorder not related to the symmetry elements. Disorder was successfully modeled, however the set of geometrical (SADI) and thermal motion (SIMU, RIGU) restraints were applied to achieve acceptable fragment geometries and thermal motion values. Disordered fragment occupancies were initially refined but restrained to fixed values in later stages of refinement. Occupancies were constrained to 50%: 50% for C(23)-based ^{t}Bu fragment and to 60% : 40% for C(38) based ^{t}Bu group respectively. After refinement of the main compound molecule was practically completed, location and arrangement of residual density peaks suggested that co-crystallized toluene solvent molecule is disordered over two positions by rotation non-related to the unit cell symmetry elements. To conserve satisfactory data-to-parameters ratio, the disordered toluene fragment was refined anisotropically with a set of geometry constrains (AFIX 66) to ensure proper fragment geometry. Occupancy for two disordered positions of the toluene molecule were initially refined, but were restrained at 60% : 40% in the latest stages of refinement.

For all the compounds all hydrogen atom positions were calculated based on the geometry of the related non-hydrogen atoms. All hydrogen atoms were treated as idealized

contributions during the refinement. All scattering factors are contained in several versions of the SHELXTL program library, with the latest version used being v.6.14.[17]

6.2.3 Computational Details

Density functional theory (DFT) calculations have been performed using the B3LYP[18] exchange-correlation functional and Gaussian 09 package.[19] The structures of all species were optimized in the gas phase using the triple-ζ basis set TZVP.[20] Tight SCF convergence criteria (10^{-8} au) were used for all calculations. Harmonic frequency calculations were used to determine the nature of stationary points and Gibbs free energies at 298 K and 1 atm. The optimization of structures and calculations of free energies were conducted both in vacuum and in solvent (using water as a solvent and the PCM implicit solvation model with the default parameters). The analysis of MO compositions in terms of contributions from atoms and fragment orbitals was performed and the Mayer bond orders[21] between atoms and atomic valence indices were calculated using the AOMix package.[22]

Energy and forces were computed by density functional theory with the M06[23] exchange-correlation functional. A polarizable continuum model[24] (PCM) of toluene was used as implemented in Gaussian09 to describe the solvent effects. Transition states were localized using the string theory as implemented in Opt'n Path.[25] Geometries were optimized and characterized with the LANL08(f) basis set and associated pseudopotentials for Pd[26] and the 6-311++G(2d,p) basis set for other atoms. The LANL08(f) basis set and pseudopotentials were taken from the EMSL Basis Set Exchange Web site.[27] In ESI, we show that this computational level properly describe the vanadium complex geometries. All structures were optimized and frequency calculations were performed to ensure the absence of any imaginary frequencies on local minima, and the presence of only one imaginary frequency on transition states. Using these frequencies in the harmonic approximation, Gibbs free energies were computed at 368 K and 1 bar.

6.2.4 Kinetic Experiments

All experiments were performed in a variable temperature NMR probe using a Bruker AVANCE 300 MHz spectrometer and under oxygen-free conditions. As a general procedure, in 0.6 mL of toluene-d_8 was added complex **TA2** (6.79×10^{-3} mmol), different

concentrations of hydrobenzoin and 6 uL of 1,3,5-trimethylbenzene as internal standard. ^{1}H NMR spectra were recorded at intervals, and the disappearance of the substrate was determined by integration against the internal standard. The rate constants were the average of two independent experiments and the uncertainties are the standard deviation of that average. The Eyring plot was obtained using the rate constants from the previous method at different temperatures. The estimated uncertainty in the temperature for the NMR probe is 0.1 K. The activation enthalpy ($\Delta H^{\neq}$) and entropy ($\Delta S^{\neq}$) were calculated from an unweighted non-linear least-squares regression using Origin 6.0. The uncertainties for the $\Delta H^{\neq}$ and $\Delta S^{\neq}$ were calculated using the propagation formulas derived from the Eyring equation published elsewhere.[28]

6.2.5 Synthesis of TA8

In a 25 mL Schlenk round-bottom flask, **TA2** (100 mg, 0.136 mmol) and hydrobenzoin (87 mg, 0.41 mmol) were dissolved in 2 mL of benzene. The mixture was heated to 80 ^{o}C with constant stirring for 18 h. The dark-purple solution was cooled to room temperature and the solvent was removed under vacuum. Then 2 mL of acetonitrile was added and the flask was cooled at -35 ^{o}C for 24 h. The pale-brown precipitate was collected by filtration, washed with cold acetonitrile and dried to give 75 mg of **TA8** (73% yield). X-ray quality crystals were obtained from a concentrated solution of toluene. Complex **TA8** is highly air sensitive; upon exposure to air an immediate change of color occurs from pale-brown to dark-red. NMR spectra revealed that the dark-red compound corresponds to oxovanadium(V) complex **TA2**. For **TA8**: ^{1}H NMR (300 MHz, C_6D_6): δ 9.87 (br, $\Delta\nu_{1/2}$ = 290 Hz), 1.19 (br s, $\Delta\nu_{1/2}$ = 36 Hz), -1.84 (br, $\Delta\nu_{1/2}$ = 143); IR (NaCl plate): $\nu_{C\equiv N}$ = 2296 cm^{-1}; UV-Vis (CH_2Cl_2): λ_{max}/nm (ε/M^{-1} cm^{-1}): 353 (2700), 478 (470), 821 (196), note: the band at 802 nm is out of the range of the visible lamp; μ_B = 2.37 B.M.; Anal. Calcd. for $C_{47}H_{69}N_2O_3V$: C 74.18 H 9.14 N 3.68; Found: C 73.43 H 9.10 N 3.30. For the aquo complex only observed in solution, **TA7**: ^{1}H NMR (300 MHz, C_6D_6): δ 11.53 (br, $\Delta\nu_{1/2}$ = 85 Hz), 1.19 (br, $\Delta\nu_{1/2}$ = 36 Hz), -1.18 (br, $\Delta\nu_{1/2}$ = 138 Hz), -6.98 (br). The dimethoxyethane adduct (**TA9**) was obtained in a similar manner as **TA8**. The ORTEP representation is depicted in Figure A61.

6.2.6 Synthesis of TA5

In a 20 mL scintillation vial containing **TA2** (64 mg, 0.09 mmol) was added 2 mL of pyridine. An immediately change of color to dark-purple was observed. The reaction mixture was stirred for 30 min at room temperature and then cooled at -30 ^{o}C for 24 h. The resulting precipitate was washed with cold ether and dried to afford 52 mg of **TA5** in 72 % yield. Large purple crystals suitable for X-ray diffraction were obtained after cooling for several days. ^{1}H NMR (300 MHz, pyr-d_5): δ 7.41 (d, 3H, J = 2.5 Hz, Ar-H), 6.97 (d, 3H, J = 2.5 Hz, Ar-H), 3.35 (s br, 6H, CH_2), 1.74 (s, 27H, ^{t}Bu), 1.31 (s, 27H, ^{t}Bu); ^{51}V NMR (78.9 MHz, pyr-d_5): δ -410 (br); IR (NaCl plate): $\nu_{V=O}$ = 945 cm^{-1}; Anal. Calcd. for $C_{50}H_{71}N_2O_4V(C_5H_5N)$: C 73.88 H 8.57 N 4.70; Found: C 73.52 H 8.65 N 4.63. Note that the crystal lattice contains one molecule of pyridine which is reflected in the elemental analysis.

6.2.7 Synthesis of TA6

Similarly to the above procedure, **TA2** (100 mg, 0.136 mmol) was dissolved in 1 mL of DMSO to afford 35 mg of **TA6** in 32% yield. ^{1}H NMR (300 MHz, DMSO-d_6): δ 7.10 (d, 3H, J = 2.5 Hz, Ar), 6.93 (d, 2H, J = 2.5 Hz, Ar), 3.36 (s br, 6H, CH_2), 1.48 (s, 27H, ^{t}Bu), 1.22 (s, 27H, ^{t}Bu); ^{51}V NMR (78.9 MHz, DMSO-d_6): δ -416 (br); IR (NaCl plate): $\nu_{V=O}$ = 938 cm^{-1}; Anal. Calcd for $C_{49}H_{76}NO_5VS(C_{3.5}H_4)$: C 70.52 H 8.91 N 1.63 S 3.73; Found: C 68.18 H 8.95 N 1.65 S 3.98. Note that the crystal lattice contains half molecule of toluene which is reflected in the elemental analysis.

6.2.8 General Procedure for Catalytic Experiments

In a 20 mL scintillation vial 20 mg of substrate was dissolved in 1 mL of solvent together with the corresponding amount of catalyst and 3 mM of dimethylsulfone or 1,3,5-trimethylbenzene as internal standard. An initial ^{1}H NMR spectrum was recorded and then the solution was transferred to a sealed 25 mL Schlenk flask open to air with constant stirring and heating by mineral oil bath. After the reaction was complete a second ^{1}H NMR spectrum was recorded. Integration against the internal standard allows the calculation of conversions and yields. Yields are expressed as a percentage of the theoretical maximum in moles based on the initial amount of substrate.

6.2.9 Attempted Oxidation of 2-Phenoxyethanol

In a 20 mL scintillation vial 2-phenoxyethanol (6.5 mg, 0.047 mmol) and complex **TA1** (10 mg, 0.047 mmol) were dissolved in 0.8 mL of CD_3CN together with dimethylsulfone as an internal standard (3.0 mM). The sample was transferred to a sealed Schlenk tube opened to air with constant stirring. The flask was heated at 80 ^oC for 48 h. Analysis by ^1H NMR of the bulk sample revealed no conversion of 2-phenoxyethanol. A similar experiment was carried out using stoichiometric amounts of **TA1** and 2-phenoxyethanol in pyridine-d_5 heating at 100 ^oC for 48 h. No conversion of the alcohol was observed.

6.3 Results and Discussion

6.3.1 Reactivity of Trialkoxyamine Vanadium Complexes

Initially, **TA1** and **TA2** were tested for the oxidation of unactivated primary and secondary alcohols. The stoichiometric reaction between **TA1** or **TA2** and 2-phenoxyethanol in CD_3CN under either aerobic or anaerobic conditions (80 ^oC, 48 h) did not afford any oxidized product. Similar results were obtained for 1,2-diphenylethanol. Dissolving **TA1** in neat 2-phenoxyethanol displayed a new signal at -582 ppm in the ^{51}V NMR spectrum due presumably to alcohol exchange with one of the alkoxy sidearms as in **TA1a,b** (Figure 6.2). Crans and co-workers observed similar ^{51}V NMR signals when **TA1**

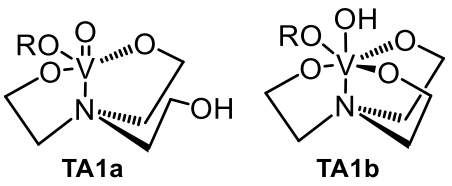

ROH	K(M^{-1})
EtOH	0.27
$(CH_3)_2CHOH$	0.52
^{t}BuOH	0.40

Figure 6.2. Proposed structures for the equilibrium of **TA1** with different alcohols and their experimental equilibrium constants (K).[10a]

was dissolved in ethanol, 2-propanol or *tert*-butyl alcohol, respectively which they used to determine the equilibrium constants.[10a]

The addition of pyridine or DMSO to **TA2** produces an immediate color change corresponding with the formation of solvent adducts. An independent synthesis was carried out by adding an excess of solvent to complex **TA2** at room temperature. After stirring for 30 min, the samples were cooled overnight at -30 ^oC to give a dark purple precipitate which was washed with cold acetonitrile and dried yielding **TA5** (72%) and **TA6** (32%),

respectively (Scheme 6.2). Dissolving complexes **TA5** or **TA6** in non-coordinating solvents (*e.g.*, hexanes) gave an immediate color change from dark purple to dark red, indicating reformation of **TA2**. In contrast, complex **TA1** does not react with pyridine or DMSO, suggesting that the more electron-rich **TA1** vanadium center is less reactive towards coordination with donor solvents.

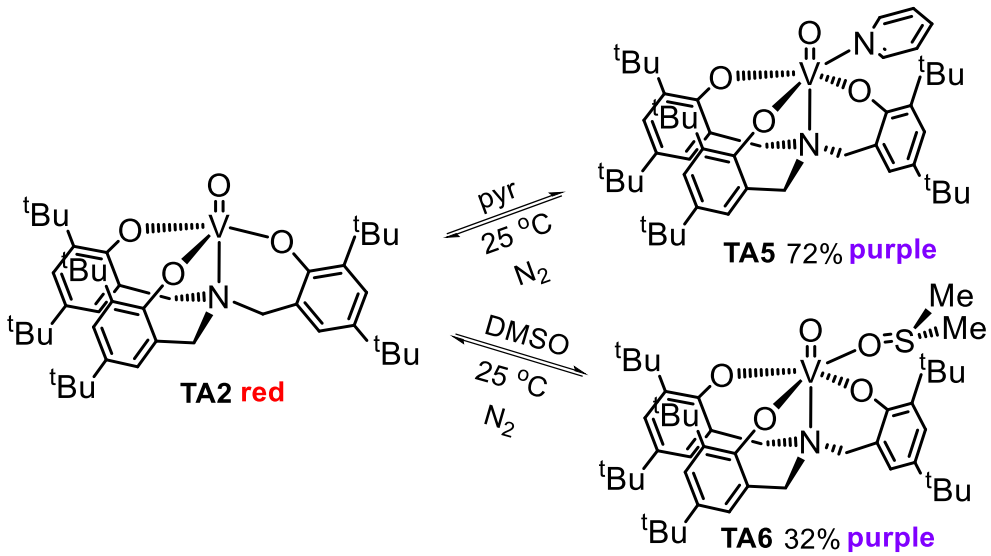

Scheme 6.2. Reaction of **TA2** with pyridine and DMSO to form **TA5** and **TA6**.

In order to understand the structural changes that pyridine and DMSO cause to **TA2**, crystals of **TA5** and **TA6** were grown directly from saturated solutions of pyridine or DMSO, respectively. The molecular structures of **TA5** and **TA6** are displayed in Figure 6.3. The geometry around the vanadium centre is distorted octahedral with the vanadium center out of the plane with respect to the phenolate oxygens. Upon coordination of the solvent to **TA2** the bond length V(1)-N(1) decreased from 2.438(4) Å to 2.3899(19) Å for **TA5** and 2.368(3) Å for **TA6** (Table 6.2). The crystal structures also show a decrease in the bond length of the oxo bond V(1)-O(4) from 1.621(3) Å, in complex **TA2**, to 1.5946(16) Å and 1.602(2) Å for **TA5** and **TA6**, respectively. The bond angle for N(1)-V(1)-O(4) for **TA2** is 179.82(14) deg, while the solvent adducts show a decrease in planarity to 174.68(8) deg for **TA5** and 174.16(12) deg for **TA6**, respectively (Table 6.3). A perfect tetrahedral configuration is observed around the amine in the DMSO adduct as shown by the C-N-C angles. A more distorted configuration is observed, however, for the pyridine adduct. An analogue of complex **TA2** with Cl_2-substituted tris(phenolate) ligand reported by Kol and

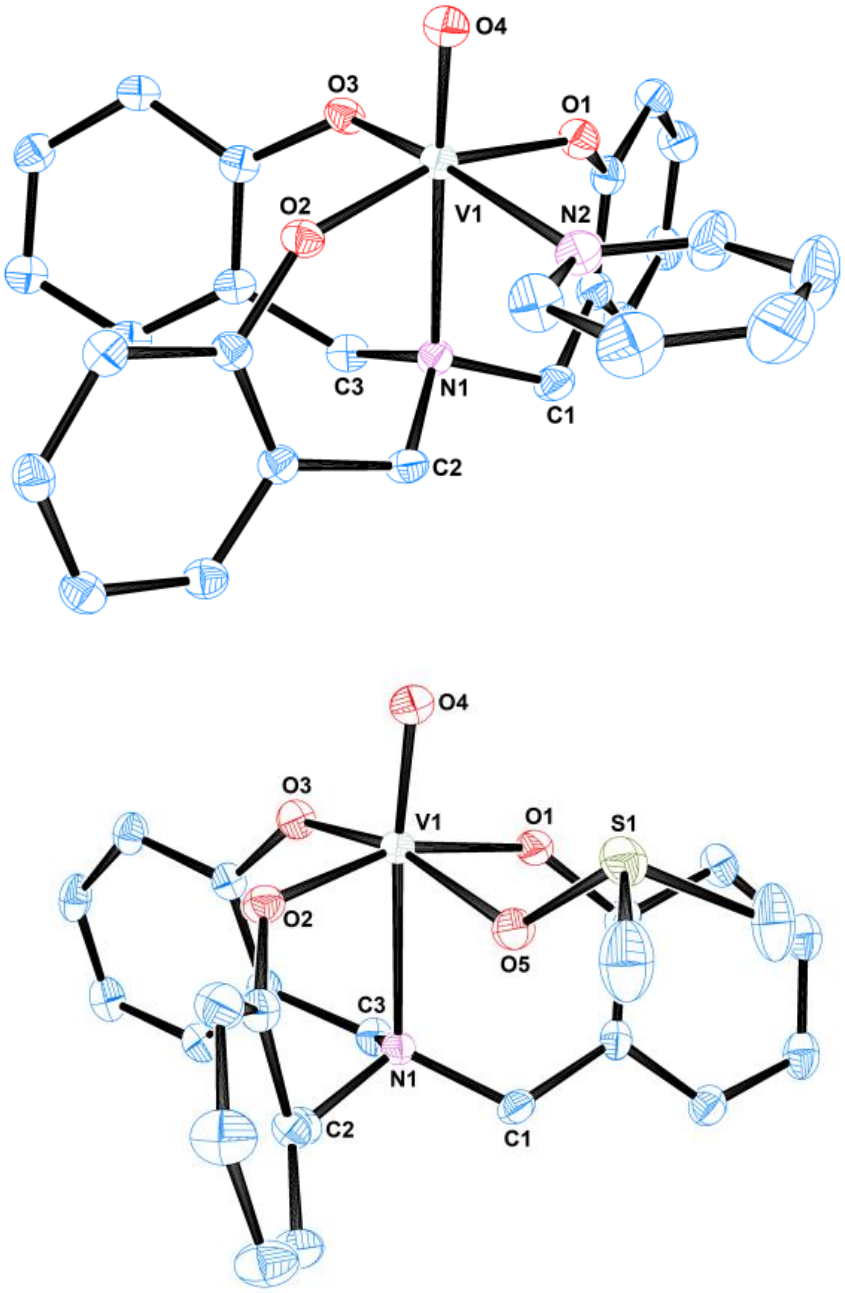

Figure 6.3. ORTEP representation of **TA5** (top) and **TA6** (bottom) with thermal ellipsoids at 35% probability, hydrogen atoms, *tert*-butyl groups and co-solvent molecules are omitted for clarity. See Tables 6.2 and 6.3 for selected bond lengths and bond angles.

co-workers[11a] reacted with propanol producing a octahedral vanadium complex characterized by multinuclear NMR. In contrast, the electron-richer **TA2** complex did not react under the same conditions.

Table 6.2. Selected bond lengths (Å) for compound **TA2**, **TA5** and **TA6**.

Bond Lengths (Å)			
	TA2[12a]	**TA5**	**TA6**
V(1)-O(1)	1.810(4)	1.8652(15)	1.856(2)
V(1)-O(2)	1.748(5)	1.8517(15)	1.879(2)
V(1)-O(3)	1.809(4)	1.8803(16)	1.831(2)
V(1)-O(4)	1.621(3)	1.5946(16)	1.602(2)
V(1)-N(1)	2.438(4)	2.3899(19)	2.368(3)
V(1)-N(2)	N/A	2.249(2)	N/A
V(1)-O(5)	N/A	N/A	2.060(2)
O(5)-S(1)	N/A	N/A	1.523(2)

Table 6.3. Selected bond angles (deg) for compounds **TA2**, **TA5** and **TA6**.

Bond Angles (deg)			
	TA2[12a]	**TA5**	**TA6**
N(1)-V(1)-O(4)	179.82(14)	174.68(8)	174.16(12)
N(2)-V(1)-O(4)	N/A	88.22(8)	N/A
O(4)-V(1)-O(5)	N/A	N/A	95.06(11)
O(1)-V(1)-O(4)	98.34(14)	97.60(8)	96.25(12)
O(2)-V(1)-O(4)	97.87(17)	97.63(8)	99.56(12)
O(3)-V(1)-O(4)	98.22(15)	101.20(8)	98.71(12)
V(1)-N(1)-C(1)	110.7(3)	110.29(14)	111.6(2)
V(1)-N(1)-C(2)	111.2(3)	111.96(14)	111.73(19)
V(1)-N(1)-C(3)	109.4(3)	110.99(13)	107.73(19)
C(1)-N(1)-C(2)	108.7(5)	111.96(14)	109.0(3)
C(1)-N(1)-C(3)	106.0(4)	108.66(18)	108.3(3)
C(2)-N(1)-C(3)	136.1(4)	109.74(18)	108.4(3)

6.3.2 Aerobic Catalytic Oxidation of 1,2-Diols

The oxidation of pinacol under air using equimolar amounts of **TA1** (CD_3CN, 80 ^oC, 18 h) afforded 100% conversion to acetone (Scheme 6.3, see Table 6.4). Decreasing the catalyst loading of **TA1** to 1 mol% afforded moderate conversion (52%) over 18 h. When

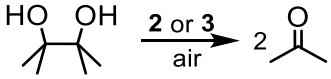

Scheme 6.3. Aerobic oxidation of pinacol using **TA1** and **TA2**.

Table 6.4. Catalytic C-C bond cleavage of pinacol.

Entry	Cat (mol%)	solvent	Time	T (^oC)	Conv. (%)[a]	TON
1	**TA1** (10)	pyr-d_5	18 h	80	100	10
2	**TA1** (1)	pyr-d_5	18 h	80	87	87
3	**TA1** (1)	CD_3CN	18 h	80	52	52
4	**TA1** (1)	DMSO-d_6	18 h	100	40	40
5	**TA2** (2)	C_6D_6	18 h	80	61	31
6	**TA2** (1)	CD_3CN	18 h	80	46	46
7	**TA2** (1)	DMSO-d_6	18 h	80	9	9
8	**TA2** (1)	pyr-d_5	18 h	80	86	86
9	control	pyr-d_5	14 d	100	0	n/a

[a]NMR integration against an internal standard.

pyridine or DMSO were used with **TA1**, the conversions were surprisingly similar to those found in acetonitrile. Control experiments (no catalyst) in pyridine-d_5 showed no reaction upon heating pinacol under air at 100 ^oC for 25 days. Catalyst **TA2** displayed similar activity as **TA1** in acetonitrile. However, the performance of **TA2** decreased to 9% conversion in DMSO-d_6. In contrast, pyridine-d_5 did not have any impact on the performance of **TA2** for the conversion of pinacol, giving similar turnover number to that observed with **TA1** under the same conditions. The stoichiometric reaction of **TA1** and pinacol in air showed no formation of any paramagnetic or new V(V) species upon reaction completion.

The aerobic oxidation of more electron-poor 1,2-diol hydrobenzoin was also studied using **TA1** and **TA2**. With 10 mol% of **TA1**, total conversion of hydrobenzoin was achieved in CD_3CN at 80 ^oC with excellent selectivity for benzaldehyde (Scheme 6.4;

Table 6.5, entry 1). In DMSO, high conversions and selectivities were also reached with 1 mol% **TA1** (table 6.5, entry 4). Decreasing the loading to 0.1 mol% still provided both excellent conversion and selectivity (99% and 98% respectively, Table 6.5, entry 5). Alde-

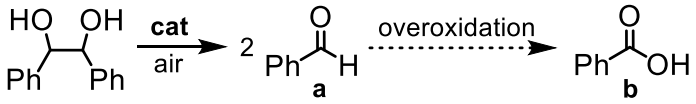

Scheme 6.4. Aerobic oxidation of hydrobenzoin to benzaldehyde (**a**) and overoxidation product benzoic acid (**b**).

Table 6.5. Catalytic C-C bond cleavage of hydrobenzoin.[a]

Entry	Cat (mol%)	solvent	Time	Conv. (%)[b]	**a**[c] (%)	**b**[c] (%)	TON	Select. (%)[d]
1	**TA1** (10)	CD_3CN	18 h	100	98	3	10	94
2	**TA1** (1)	CD_3CN	18 h	100	56	34	100	24
3	**TA1** (0.1)	CD_3CN	18 h	45	12	1	450	85
4	**TA1** (1)	DMSO-d_6	18 h	100	83	1	100	98
5	**TA1** (0.1)	DMSO-d_6	18 h	99	91	<1	990	98
6	**TA2** (1)	DMSO-d_6	18 h	100	91	<1	100	98
7	**TA2** (0.1)	DMSO-d_6	18 h	83	62	<1	830	97
8	**TA2** (1)	CD_3CN	18 h	100	92	10	100	80
9	**TA2** (1)	CD_3CN	7 h	70	56	3	70	90
10	**TA2** (0.1)	CD_3CN	18 h	16	5	0	160	100
11	**TA2** (1)	pyr-d_5	18 h	100	84	10	100	79
12	**TA2** (0.1)	pyr-d_5	18 h	55	74	5	550	87
13	**OV2** (0.1)	CD_3CN	18 h	100	44	40	1000	5
14	control	CD_3CN	18 h	<1	n.d.[e]	<1	n/a	n/a

[a]Temperature: 80 °C; [b]NMR integration against an internal standard; [c]Yields are based on the maximum theoretical amount of moles produced respect to the substrate. [d]Selectivity for aldehyde = (%**a** - %**b**) / (%**a** + %**b**) x 100; [e]not detected.

hydes are important target functional groups in biomass conversion as they are easier (*vs.* carboxylic acids) to functionalize to more complex molecules.[29] In the case of catalyst **TA2**, the pinacol solvent dependence (DMSO *vs.* acetonitrile) was not observed for the oxidation of hydrobenzoin (Table 6.5, entries 6, 8 and 11). Under these conditions,

overoxidation to benzoic acid was not observed and high selectivity for aldehydes was obtained even with catalyst loadings as low as 0.1 mol% (Table 6.5, entries 7 and 12).

Catalyst **TA1** does not show any solvent dependence for the catalytic oxidation of pinacol or hydrobenzoin. This can account for (i) the lack of deactivation observed with complex **TA1** and (ii) the deactivation observed when coordinating solvents are used with catalyst **TA2**. The bond distance of the solvent molecule to the vanadium center is longer for **TA5** compared with **TA6**. The bond lengths of vanadium center to the coordinating solvent suggest a higher solvent-metal interaction when DMSO is bound to **TA2**, deactivating the metal and subsequently the C-C bond cleavage. In the oxidation of hydrobenzoin, both solvents achieve similar conversions, indicating that more activated substrates (more electron-poor) are less affected by the solvent-substrate competition.

Previously reported catalysts **OV1** and **OV2** cleave the C-H bond of 1,2-diols through the dehydrogenation of the vicinal hydrogen, followed by cleavage of the C-C bond of the reduced ketone or hydroxyketone (intermediate). In the case of hydrobenzoin, deprotonation affords mono- and di-ketone before the C-C bond scission occurs, producing a mixture of aldehyde and carboxylic acid (Scheme 6.5). The ^{1}H NMR spectrum of the rea-

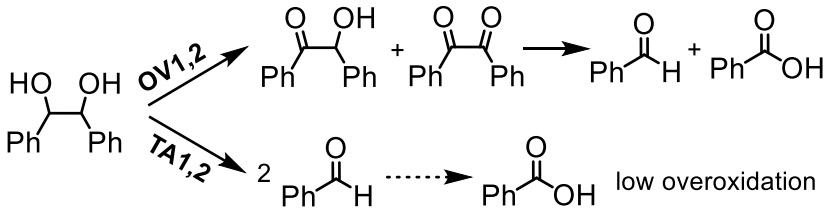

Scheme 6.5. Comparison for the oxidation of hydrobenzoin using catalysts **OV1,2** and **TA1,2**.

ction mixture from the catalytic oxidation of hydrobenzoin using **TA1** or **TA2** revealed no formation of mono- or di-ketone intermediates (Scheme 6.5). Although similar catalytic activity can be achieved with **OV2** in the absence of base (Table 6.5, entry 13), much lower selectivity to aldehyde (5% with **OV1** *vs.* 98% with **TA1**) is observed when compared to catalysts **TA1** and **TA2**.

6.3.3 Hemicarcerand Oxovanadium(V) Complexes

Molecular behaviour in small spaces (*e.g.*, enzymes) provides rate enhancement, reaction specificity, activity at moderate temperatures and pressures and capacity for regulation.[30] Several systems have been proposed to mimic the cage-like nature of

enzymes. Endohedral hemicarcerands, for example, allow guests to enter and exit the cavity at high temperatures but will form stable complexes at ambient temperatures, with first row transition metals exhibiting remarkable binding properties toward neutral or charged guest molecules.[30,31] These structures could offer higher catalyst stability (prevent self-degradation of the ligand) and shape selectivity (inside the cavity).

Oxovanadium(V) hemicarcerand **TA4** and its model compound **TA3** (Figure 6.4) have been reported as efficient catalysts for the oxidation of sulfides in high yields and conver-

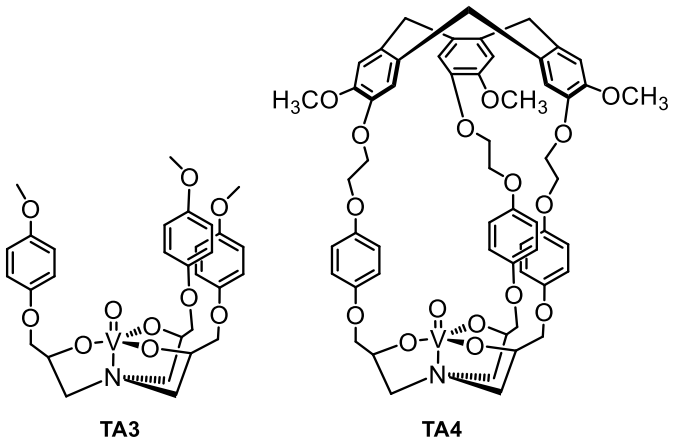

Figure 6.4. Hemicarcerand trialkoxyamine oxovanadium complexes.

sions (*e.g.* >95%).[31b,c] Complexes **TA3** and **TA4** share a similar atrane moiety as catalyst **TA1** with an extended cyclotriveratrylene substituent that provides a lipophilic cavity in complex **TA4**.

Initially, complexes **TA3** and **TA4** were used as catalysts for the aerobic oxidation of hydrobenzoin. Model complex **TA3** (open cavity) showed moderate conversion (64%) affording benzaldehyde (44%) and benzoic acid (4%) using 1 mol% catalyst (CH_3CN, 80 ^oC, 18 h). Under similar conditions hemicarcerand **TA4** showed lower conversion (57% and 32% yield benzaldehyde and 1% benzoic acid) due to slow diffusion of the substrate into the hydrophobic cage that contains the metal center.

In complementary reactions, complexes **TA3** and **TA4** were also effective for the disassembly of lignin models such as **LM2**. Using 1 mol% **TA3** (DMSO-d_6, 120 ^oC, 18 h) 91% conversion was obtained affording 38% benzaldehyde, 22% methyl benzoate, 8% benzoic acid, 20% benzoin methyl ether and 5% methanol. However, hemicarcerand **TA4**

afforded lower conversion (87%) with similar product distributions indicating lack of shape selectivity for this complex.

6.3.4 DFT Mechanistic Study

The first step of the C-C bond cleavage of 1,2-diols presumably involves protonation of the V(O)L complex and formation of a covalent bond between the complex and deprotonated 1,2-diol. Previous reports speculated that protonation of one of the atrane arms or of the oxo ligand would maintain the five-coordinate structure, leaving an open coordination site for the incoming OR ligand.[10a] A third alternative is protonation of the amine either *endo* or *exo*. These proposed intermediates were studied using DFT calculations.

The structure of **TA1** was optimized at the spin-restricted B3LYP/TZVP level of theory using the X-ray structure as the initial point.[10a] The optimization resulted in the lowest-energy minimum structure with C_3 symmetry and with a close resemblance to the X-ray structure. The optimized V=O, V-O_L and V-N_L lengths were 1.584 Å, 1.810 Å and 2.527 Å, respectively. Due to a rather long V-N_L length and a weak covalent interaction between the corresponding two atoms (the Mayer bond order of only 0.17), the V coordination environment can be described as distorted tetrahedral. The bond orders for V-O bonds are 2.15 and 0.98 for each of three V-O_L bonds. The calculated valence index for V is 5.45. Thus, we can see that vanadium is coordinatively saturated and the new metal-ligand bond can only be formed at the expense of one of the existing V-O interactions. Considering that the V-N_L interaction is weak, the potential energy surface of V-N_L was calculated to explore the possibility of an alternative structure in which the N lone pair position is inverted (points in the opposite direction, away from V atom). It was found that, as the V-N_L length is elongated, the electronic energy rises and does not show an additional energy minimum at a longer V-N length. If the N atom of the amine group is protonated (a cationic $[VO(LH)]^+$ species), the structure with the N-H bond pointing away from the V atom (Figure 6.5, B) is 31.0 kJ mol^{-1} lower in energy than the structure with the N-H bond pointing towards the V atom (Figure 6.5, C). However, protonation at the oxygen site is preferred over the N site and gives the lowest energy (Figure 6.5, A).

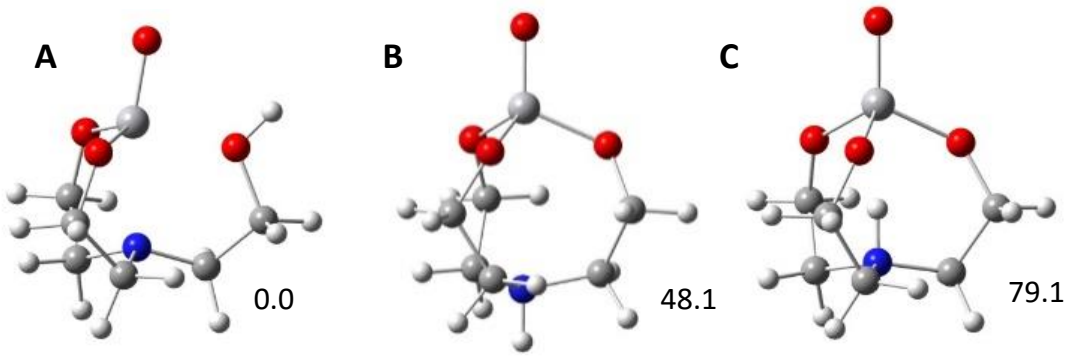

Figure 6.5. Optimized structures of the protonated, cationic $[V(O)LH)]^+$ complex with the relative Gibbs free energies (kJ mol^{-1}) at 298 K.

We then explored the different interactions when ethanediol protonates the V(O)L complex. The lowest energy structure (Figure 6.6, A) was obtained in the case where the

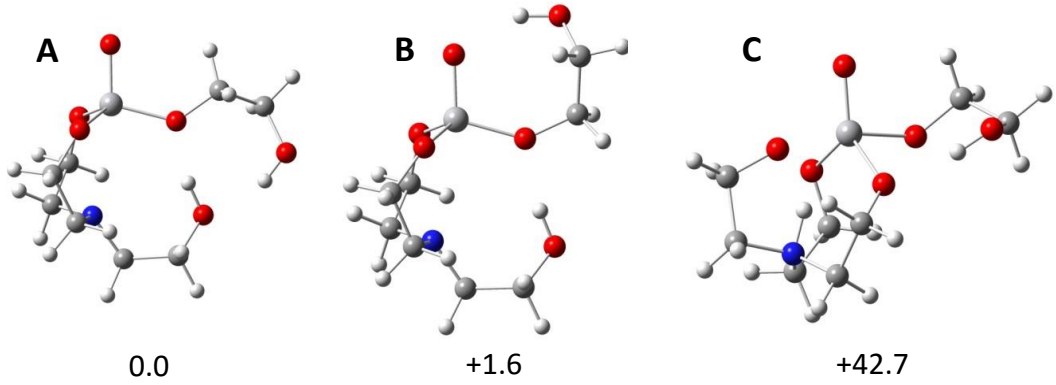

Figure 6.6. Optimized structures of the energy minima in a first step of the reaction of [V(O)L] with CH_2OH-CH_2OH. Relative Gibbs free energies (kcal mol^{-1}) at 298 K are shown below the structures.

substrate enters the coordination sphere of the V atom, displacing one of the V-O_L bond and the proton is transferred from the first OH group of the substrate to the O atom of the ligand. That proton is still involved in the H-bond interaction between these two oxygen sites. The second OH group of the substrate is also involved in the H-bond interaction with the protonated arm of the atrane ligand L. An alternative structure where the OH group of the substrate is involved in the H-bond interaction with the vanadyl oxygen (Figure 6.6, B) instead of the O arm of the ligand is slightly higher in energy (by 1.6 kcal mol^{-1}). A similar

structure has been proposed by Crans and co-workers where the alcohol is coordinated to the vanadium (V-OR) while the vanadyl oxo is protonated (Figure 6.2, **TA1b**).[10a] This interaction was also evaluated, however, no energy minimum was found. The structure in which the proton is transferred from the substrate to the N atom of the ligand (Figure 6.6, C) is significantly higher in energy (42.7 kcal mol^{-1}) and, thus, can be ruled out as a reactive intermediate in the catalytic cycle.

6.3.5 Direct Two-Electron Oxidation of 1,2-Diols

The stoichiometric reaction of **TA2** with hydrobenzoin under nitrogen (C_6D_6, 80 ºC, 15 h) afforded 60% yield of benzaldehyde and a drastic change in color of the reaction mixture from dark-red to purple. The ^{1}H NMR spectrum of the reaction between **TA2** and three equivalents of hydrobenzoin revealed characteristic paramagnetic broad signals at 11.53 ppm ($\Delta\nu_{1/2}$ = 85 Hz), 1.19 ppm ($\Delta\nu_{1/2}$ = 36 Hz) and -1.18 ppm (br, $\Delta\nu_{1/2}$ = 138 Hz). Similar results were found using pinacol. Figure 6.7 shows the ^{1}H NMR spectrum of the

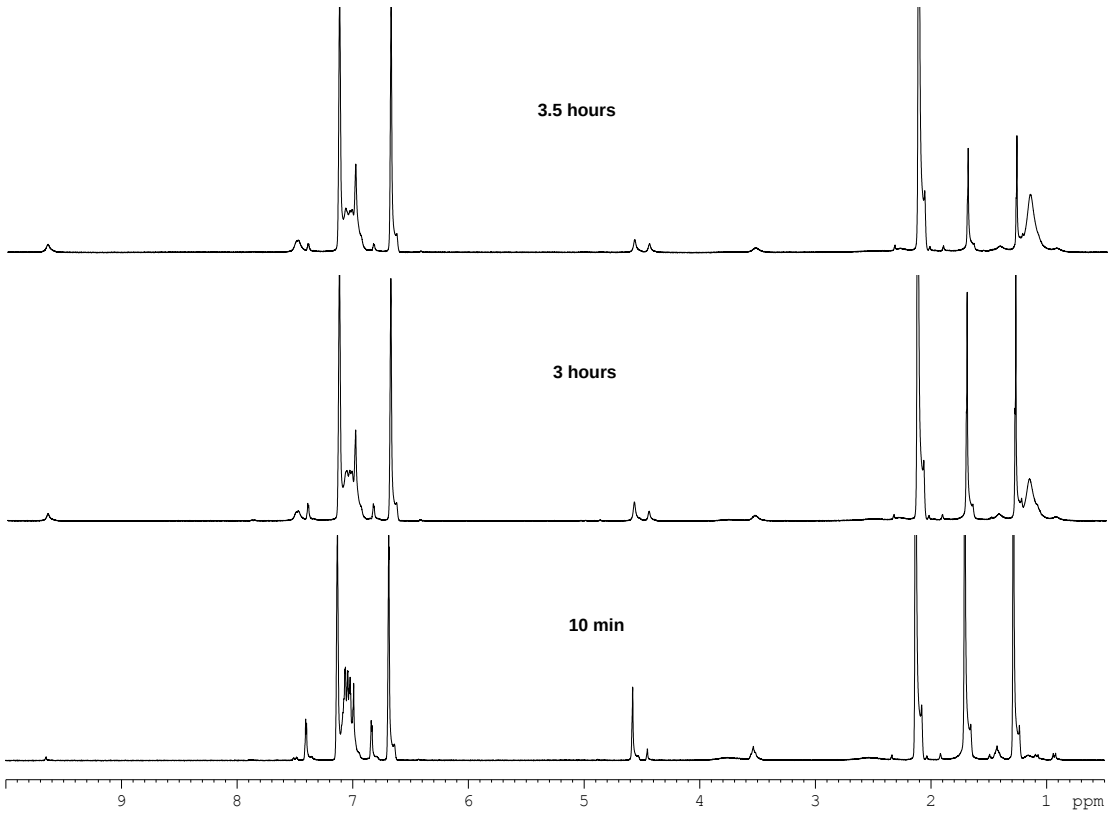

Figure 6.7. ^{1}H NMR (300 MHz, C_6D_6, 333.15 K) at different times of the reaction of **TA2** and hydrobenzoin.

reaction mixture of **TA2** and hydrobenzoin (C_6D_6, 60 °C) at different times. As the reaction progresses, the paramagnetic broad signals start to grow (see above) and the amount of **TA2** (seen as a doublet at 7.43 ppm) decreases. Varying the moles of substrate, the stoichiometry is deduced to be equimolar in complex **TA2** and substrate as depicted in Scheme 6.6. The stoichiometric reaction under nitrogen between complex **TA1** and hydro-

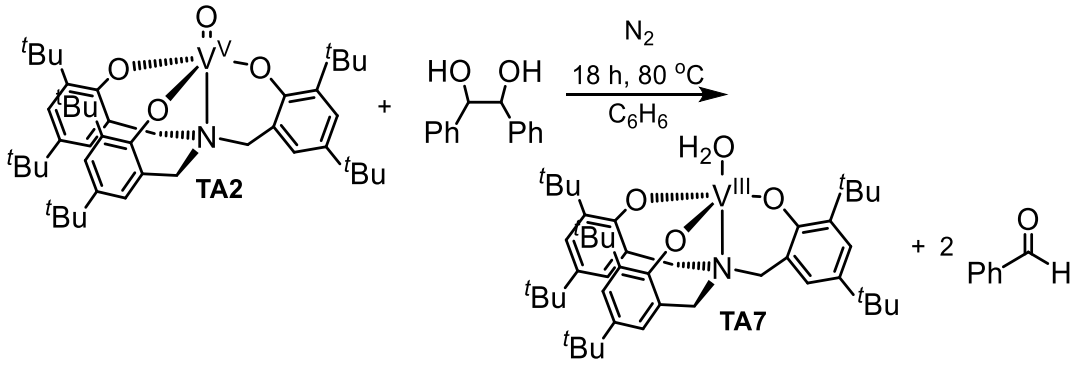

Scheme 6.6. Direct two-electron oxidative C-C bond cleavage of hydrobenzoin using catalyst **TA2**.

benzoin gave 31% yield of benzaldehyde and an insoluble dark precipitate (C_6D_6, 80 °C, 18 h). The less bulky triethanolamine ligand in **TA1** might facilitate the oligomerization of the V(III) complex.

From the reaction of **TA2** and hydrobenzoin was isolated a pale yellow precipitate complex **TA8** in 73% yield after recrystallization in acetonitrile at -35 °C. The effective magnetic moment of **TA8** was determined using the Evans method[13] to be μ_B = 2.37 B.M. characteristic of a d^2 V(III) complex.[32] Recrystallizing in hot toluene gave large beige crystals suitable for X-ray diffraction. The structure (Figure 6.8) shows a trigonal bipyramidal geometry about the V(III) center with one molecule of acetonitrile *trans* to the triethanolamine nitrogen and C_3 symmetry along the V1-N1 axis. We speculate that the V(III) product has a molecule of water as an L donor in the apical position preceding replacement with one acetonitrile molecule (better donor). A similar V(III) structure was obtained with a molecule of dimethoxyethane in the apical position (Figure A61). As expected for a d^2 *versus* d^0 metal, the bond distance V1-N1 of the V(III) complex **TA8** is shorter than the oxovanadium(V) complex **TA2** (2.438(4) Å). Two related non-oxo V(III) complexes were independently synthesized using VCl_3 and the corresponding triaryloxy amino ligand bearing a THF[11a] or CH_3OH[33] in the apical position. The **TA8** complex was

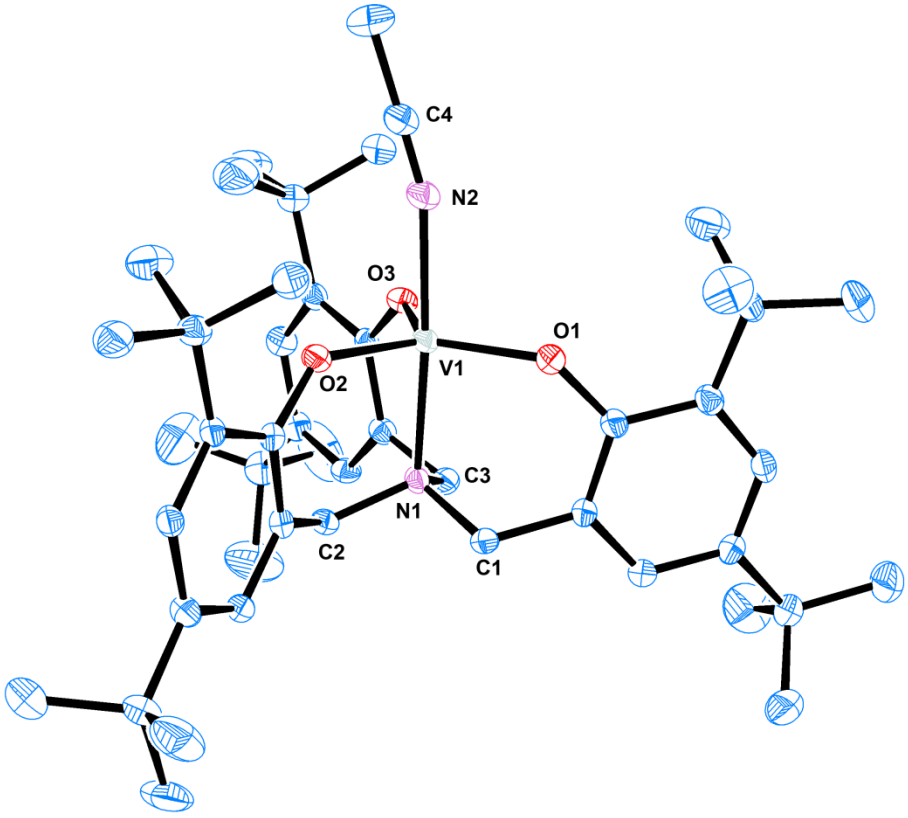

Figure 6.8. ORTEP representation of **TA8** with thermal ellipsoids at 35% probability, hydrogen atoms and second asymmetric unit are omitted for clarity. Selected bond lengths (Å) and bond angles (deg): V1-O1= 1.814(3), V1-O2= 1.914(3), V1-O3= 1.890(3), V1-N1= 2.130(3), V1-N2= 2.141(3), N1-V1-N2= 176.01(11), N1-V1-O1=91.69(12), V1-N2-C4= 164.1(3).

further characterized by elemental analysis, IR and UV-Vis spectroscopy. Interestingly, upon exposure to oxygen, **TA8** rapidly changed color from pale yellow to dark red regenerating the oxovanadium(V) complex **TA2** and one equivalent of acetonitrile. Even in the solid state, the V(III) complex is extremely air sensitive. This process is important for enabling a facile closing of the catalytic cycle, in contrast to catalysts **OV1** or **OV2** for which reoxidation from V(IV) to V(V) is slow. Using a similar triaryloxyamine oxovanadium(V) catalyst, Hirao and co-workers[12a] observed a reduced vanadium complex (either III or IV) through the disappearance of the ^{51}V NMR signals in the bromination of 1,3,5-trimethoxybenzene with $AlBr_3$.

A pseudo-first-order rate law was obtained for the reaction of **TA2** and an excess of hydrobenzoin. An Eyring plot (Figure 6.9 and Table 6.6) in toluene-d_8 using kinetic data at

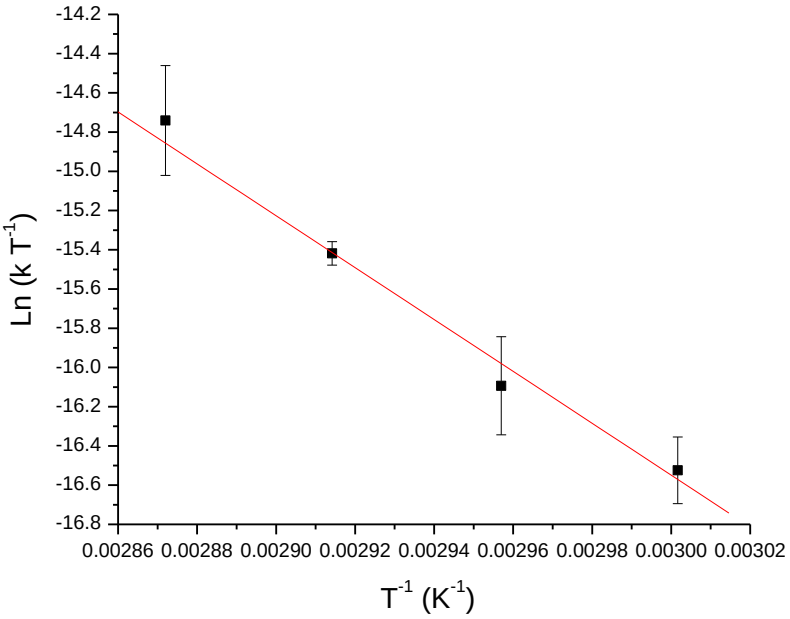

Figure 6.9. Eyring plot for the reaction of **TA2** with hydrobenzoin (5.66 x 10^{-2} M) in toluene-d_8. Activation parameters were calculated using kinetic data at several temperatures (333.15 - 348.15 K).

Table 6.6. Values of k_{obs} for the reaction of **TA2** with hydrobenzoin (5.66 x 10^{-2} M) in toluene-d_8.

Temperature (K)	10^5 k_{obs} (s^{-1})[a]
333.15	2.22 ± 0.380
338.15	3.47 ± 0.878
343.15	6.91 ± 0.402
348.15	13.8 ± 3.99

[a]The uncertainty is the standard deviation of the average of two independent experiments.

several temperatures (333.15 K - 348.15 K) provided the activation parameters; $\Delta H^{\neq}$ = 110 ± 5 kJ mol^{-1} and $\Delta S^{\neq}$ = -5.24 ± 13 J K^{-1} mol^{-1}.[34] The low value of the activation entropy is consistent with that expected based on the calculated transition state (see Figure 6.11). The kinetic isotope effect (KIE) was evaluated using the O-D labeled hydrobenzoin(1,2-^{2}HO). The observed KIE, k_H/k_D at 348.15 K, in toluene-d_8 of 2.41 ± 0.72 corresponds with the primary isotope effect of a hydrogen atom transfer to the V=O moiety (Scheme 6.7). On the other hand, the catalytic oxidation of the C-D labeled hydrobenzoin (1,2-^{2}H) with 1 mol% of **TA2** (CD_3CN, 80 ºC, 7 h) afforded 100% of deuterium incorporation in the benz-

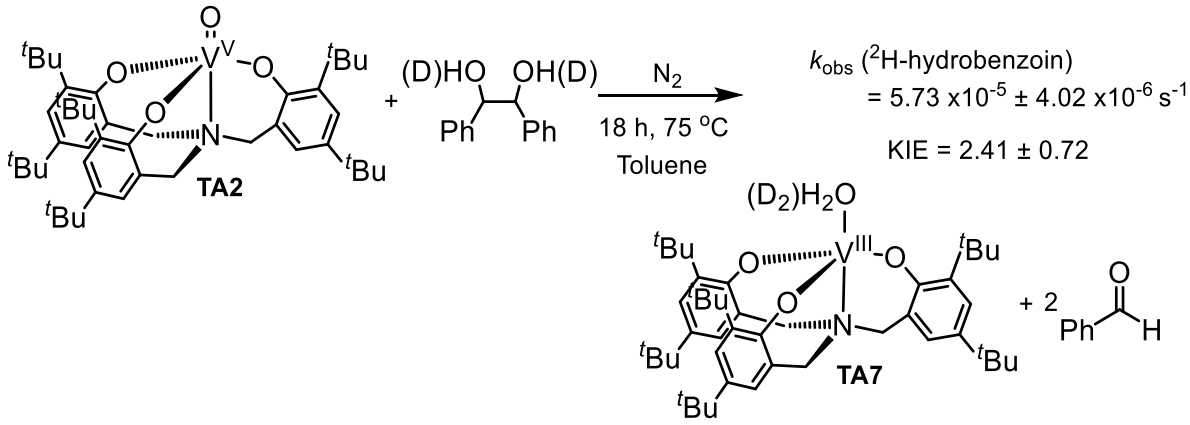

Scheme 6.7. Kinetic isotope effect (KIE) for the C-C bond cleavage of hydrobenzoin using **TA2**.

aldehyde product which is consistent with a direct C-C bond cleavage and no formation of dehydrogenation intermediates.

To provide a better understanding of the underlying processes governing the C-C bond cleavage of pinacol by the catalysts **TA1** and **TA2** in toluene, the reaction network was determined based on DFT calculations. In these calculations, the large ^{t}Bu groups of **TA2** were replaced by methyl groups. The corresponding Gibbs energy profiles are shown in Figure 6.10. The overall reaction is exothermic (-247 kJ mol^{-1}) as depicted in Scheme 6.8.

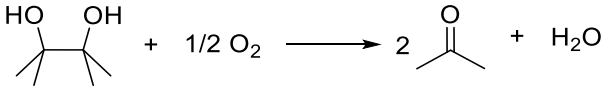

Scheme 6.8. Balanced equation for the C-C bond cleavage of pinacol.

The first step is the coordination of the pinacol to the catalyst denoted by **I**, yielding intermediate **II** in which a proton was transferred from pinacol to one arm of the catalyst or **III** in which the proton is transferred to the oxo moiety to give an alkoxy hydroxy vanadium complex. This process is endothermic due to the entropic penalty and can yield a range of conformational isomers, especially with the flexible catalyst **TA1**. In the reactive isomer of **III**, one proton of the pinacol was transferred to the V(V)=O moiety and the resulting alkoxy group coordinated the vanadium in the equatorial plane. The remaining alcohol group then H-bonds to the newly formed hydroxyl, stabilizing this active species. Note that the oxidation state of vanadium is still +5 in this intermediate. Then, the C-C bond breaks, with a barrier of roughly 100-110 kJ/mol and a C-C bond distance of 2.80 Å with **TA2** and 2.79 Å with **TA1** (see Figure 6.11). This process is accompanied by proton

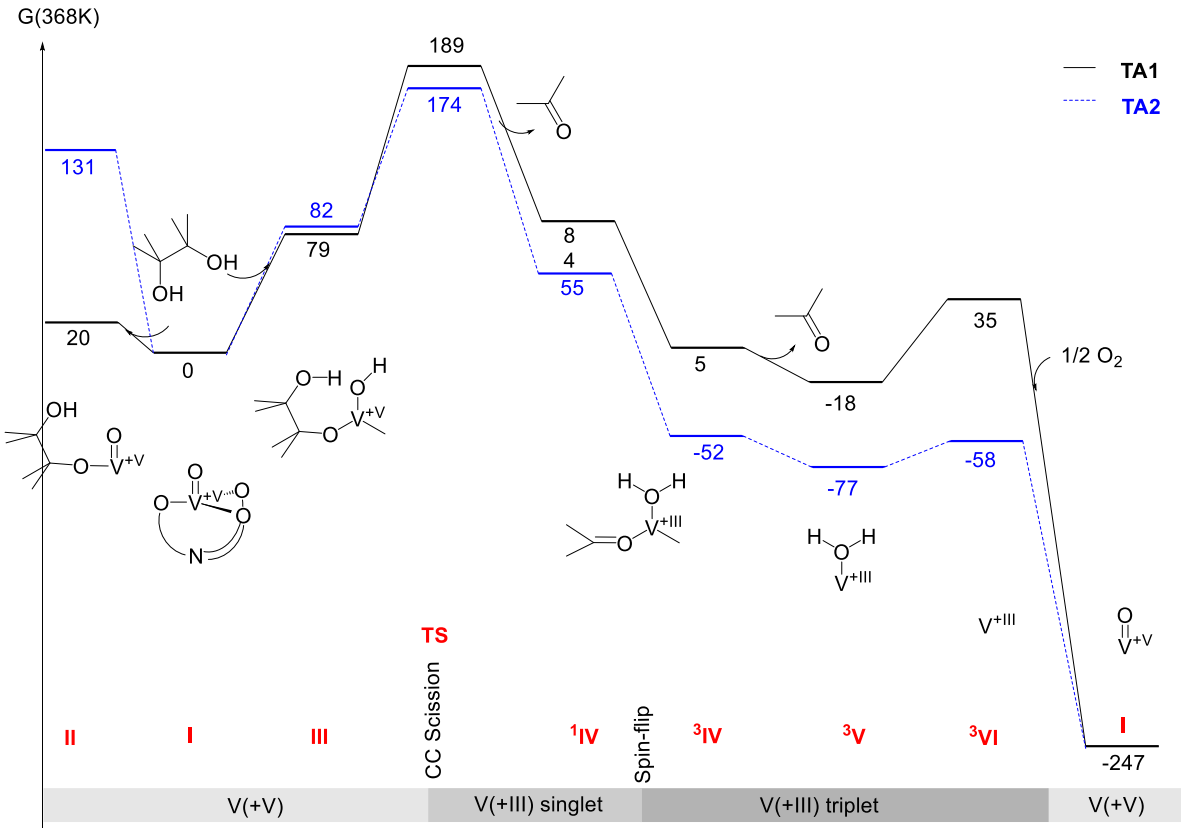

Figure 6.10. Free energy profile in kJ/mol, at 368 K and 1 bar, for the catalytic oxidation of pinacol with catalyst **TA1** (plain black curve) and **TA2** (dashed blue curve).

transfer from the pinacol hydroxyl to the V-OH, yielding one coordinated water, a coordinated acetone and a free acetone in compound ^{1}**III** (singlet state).

The rate determining process is the C-C bond scission/proton transfer from the pinacol-catalyst complex **III**. As the formation of **III** is faster than the C-C bond scission, it is possible to assume that **III** is in equilibrium with **I** and pinacol, so that the kinetic law is expected to be first order in both pinacol and the catalyst, in agreement with the kinetic data (Figure A54).[35] The activation barrier for this rate determining step can be decomposed into its enthalpic and entropic contribution. For **TA2**, one finds $\Delta H^{\neq}$= 98.7 kJ mol^{-1} and $\Delta S^{\neq}$= -18.7 J K^{-1}mol^{-1} in good agreement with the experimental values.

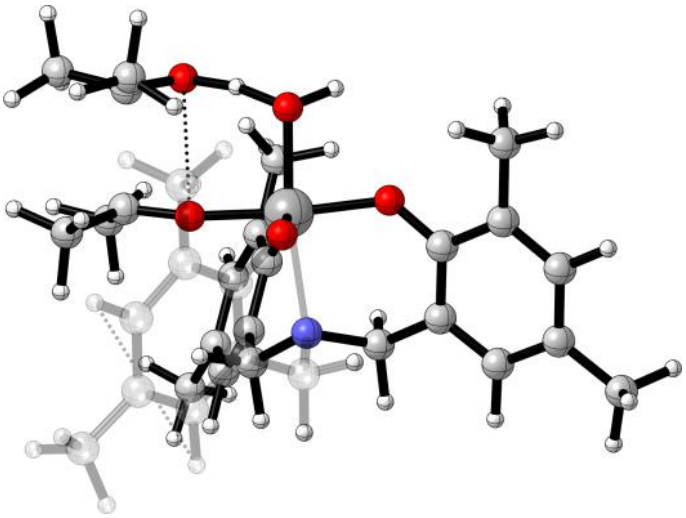

Figure 6.11. Transition state (**TS**) for the C-C bond breaking of pinacol with catalyst **TA2**.

6.4 Conclusions

Catalysts **TA1** and **TA2** cleaved the C-C bond of 1,2-diols using low catalyst loadings, mild conditions and no need for co-additives, with a remarkable selectivity not involving ketone intermediates, and using air as the only oxidant. Catalyst **TA2** showed an unprecedented direct two-electron oxidation for the cleavage of 1,2-diols with formation of a non-oxo V(III) intermediate. The activation parameters $\Delta H^{\neq}$ = 110 ± 4.55 kJ mol^{-1} and $\Delta S^{\neq}$ = -5.24 ± 13.4 J K^{-1} mol^{-1} are in good agreement with the theoretical calculations for the rate determining step. In contrast, under similar conditions catalyst **TA1** produced an insoluble precipitate, decreasing conversion and yields. The precipitate is likely an oxo-bridged inorganic polymer promoted by the small ligand scaffold of **TA1** compared to **TA2**. DFT calculations showed that the first step of the reaction between the trialkoxyamine vanadium catalyst and the 1,2-diol occurs through protonation of one of the alkoxide or phenolate arms. Hemicarcerand complexes were also shown to be effective for the aerobic C-C bond cleavage of 1,2-diols and lignin models. However, lower conversions were observed due to slow diffusion of the substrate into the hemicarcerand hydrophobic cavity.

The two-electron oxidation process may likely also occur in the VHPOs but the reaction with oxygen is so fast that the V(III) product is never observed.[9e] The bulky triaryloxyamine ligand in catalyst **TA2** prevents subsequent intermolecular steps that allowed for observation of the V(III) product under anaerobic conditions for the first time.

The mechanistic information for the C-C bond cleavage of 1,2-diols using trialkoxyamine oxovanadium(V) catalysts will allow the design of new ligand scaffolds for broader substrate scope and more efficient reactions.

6.5 References

(1) a) Kusserow, B.; Schimpf, S.; Claus, P. *Adv. Synth. Catal.* **2003**, *345*, 289−299; b) Castoldi, M. C. M.; Camara, L. D. T.; Aranda, D. A. G. *React. Kinet. Catal. Lett.* **2009**, *98*, 83−89; c) Román-Leshkov, Y.; Barrett, C. J.; Liu, Z. Y.; Dumesic, J. A. *Nature* **2007**, *447*, 982−985.
(2) Lodish, H.; Berk, A.; Zipursky, S. L.; Matsudaira, P.; Baltimore, D.; Darnell, J. *Molecular Cell Biology*, 4th Ed., W. H. Freeman: New York, 2000.
(3) a) Huber, G. W.; Chheda, J. N.; Barrett, C. J.; Dumesic, J. A. *Science* **2005**, *308*, 1446−1450; b) Sutton, A. D.; Waldie, F. D.; Wu, R.; Schlaf, M.; Silks, L. A.; Gordon, J. C. *Nature Chem.* **2013**, *5*, 428−432; c) Kamm, B.; Gruber, P. R.; Kamm, M. Eds. *Biorefineries - Industrial Processes and Products*, 2006, Vol. 2, p. 136.
(4) a) Fieser, L. F.; Fieser, M. In *Reagents for Organic Synthesis*; Wiley-VCH: New York, 1967; p 815; (b) Shing, T. K. M. In *Comprehensive Organic Synthesis*; Trost, B. M., Eds.; Pergamon Press: Oxford, 1991; p 703; c) Knochel, P.; Molander, G. A. In *Comprehensive Organic Synthesis*; 2nd Ed.; Wong, A. W. H.; Shing, T. K. M., Eds.; Elsevier B.V: Amsterdam, 2014; p. 801.
(5) a) Amadio, E.; Di Lorenzo, R.; Zonta, C.; Licini, G. *Coord. Chem. Rev.* **2015**, *301−302*, 147−162; b) Okamoto, T.; Sasaki, K.; Oka, S. *J. Am. Chem. Soc.* **1988**, *110*, 1187–1196; c) Takezawa, E.; Sakaguchi, S.; Ishii, Y. *Org. Lett.* **1999**, *1*, 713–715; d) Ishii, Y.; Yamawaki, K.; Ura, T.; Yamada, H.; Yoshida, T.; Ogawa, M. *J. Org. Chem.* **1988**, *53*, 3581–3593; e) Du, G.; Woo, L. K. *Organometallics* **2003**, *22*, 450–455.
(6) a) Sedai, B.; Díaz-Urrutia, C.; Baker, R. T.; Wu, R.; Silks, L. A. P.; Hanson, S. K. *ACS Catal.* **2013**, *3*, 3111−3122; b) Sedai, B.; Díaz-Urrutia, C.; Baker, R. T.; Wu, R.; Silks, L. A. P.; Hanson, S. K. *ACS Catal.* **2011**, *1*, 794−804; c) Díaz-Urrutia, C.; Sedai, B.; Leckert, K.; Baker, R. T.; Hanson, S. K. *ACS Sustainable Chem. Eng.* **2016**, *submitted*; d) Díaz-Urrutia, C.; Chen, W-C.; Crites, C.-O.; Daccache, J.; Korobkov, I.; Baker, R. T. *RSC Adv.* **2015**, *5*, 70502–70511; e) Hanson, S. K.; Baker, R. T.; Gordon, J. C.; Scott, B. L.; Sutton, A. D.; Thorn, D. L. *J. Am. Chem. Soc.* **2009**, *131*, 428−429; f) Hanson, S. K.; Baker, R. T.; Gordon, J. C.; Scott, B. L.; Thorn, D. L. *Inorg. Chem.* **2010**, *49*, 5611−5618; g) Hanson, S. K; Baker, R. T.; Gordon, J. C.; Scott, B. L.; Silks, L. A. P.; Thorn, D. L. *J. Am. Chem. Soc.* **2010**, *132*, 17804−17816.
(7) a) Hanson, S. K.; Wu, R.; Silks, L. A. P. *Angew. Chem. Int. Ed.* **2012**, *51*, 3410−3413; b) Hanson, S. K.; Wu, R.; Silks, L. A. P. *Org. Lett.* **2011**, *13*, 1908–1911; c) Wigington, B. N.; Drummond, M. L.; Cundari, T. R.; Thorn, D. L.; Hanson, S. K.; Scott, S. L. *Chem. Eur. J.* **2012**, *18*, 14981–14988.
(8) a) Son, S.; Toste, F. D. *Angew. Chem. Int. Ed.* **2010**, *49*, 3791–3794; b) Weng, S. S.; Shen, M. W.; Kao, J. Q.; Munot, Y. S.; Chen, C. T. *Proc. Natl. Acad. Sci. U.S.A.* **2006**, *103*, 3522–3527; c) Maeda, Y.; Kakiuchi, N.; Matsumura, S.; Nishimura, T.; Kawamura, T.; Uemura, S. *J. Org. Chem.* **2002**, *67*, 6718–6724.
(9) a) Pessoa, J. C; Garribba, E.; Santos, M. F. A.; Santos-Silva, T. *Coord. Chem. Rev.* **2015**, *301*, 49−86; b) Colpas, G. J.; Hamstra, B. J.; Kampf, J. W.; Pecoraro, V. L. *J. Am. Chem. Soc.* **1994**, *116*, 3627−3628; c) Andersson, M.; Willetts, A.; Allenmark, S. *J. Org. Chem.* **1997**, *62*, 8455−8458; d) Messerschmidt, A.; Wever, R. *Proc. Natl. Acad. Sci. U.*S.A. **1996**, *93*, 392−396; e) Gupta, R.; Hou, G.; Renirie, R.; Wever, R.; Polenova, T. *J. Am. Chem. Soc.* **2015**, *137*, 5618−5628.

(10) a) Crans, D. C.; Chen, H.; Anderson, O. P.; Miller, M. M. *J. Am. Chem. Soc.* **1993**, *115*, 6769−6779; b) Reis, P. M.; Armando, J.; Silva, L.; da Silva, J. J. R. F.; Pombeiro, A. J. L. *Chem. Comm.* **2000**, 1845−1846; c) Reis, P. M.; Silva, J. A. L. da Silva, J. J. R. F.; Pombeiro, A. J. L.; *J. Mol. Catal. A-Chem.* **2004**, *224*, 189–195; d) Reis, P. M.; Silva, J. A. L.; Palavra, A. F.; Fraústo da Silva, J. J. R.; Kitamura, T.; Fujiwara, Y.; Pombeiro, A. J. L. *Angew. Chem. Int. Ed.* **2003**, *42*, 821–823; e) Kirillova, M. V.; Kuznetsov, M. L.; da Silva, J. A. L.; Silva, M. F. C. G.; da Silva, J. J. R. F; Pombeiro, A. J. L. *Chem. Eur. J.* **2008**, *14*, 1828–1842; f) Kirillova, M. V.; Kuznetsov, M. L.; Reis, P. M.; da Silva, J. A. L.; da Silva, J. J. R. F.; Pombeiro, A. J. L. *J. Am. Chem. Soc.* **2007**, *129*, 10531–10545.
(11) a) Groysman, S.; Goldberg, I.; Goldschmidt, Z.; Kol, M. *Inorg. Chem.* **2005**, *44*, 5073−5080; b) Mba, M.; Pontini, M.; Lovat, S.; Zonta, C.; Bernardinelli, G.; Kündig, P. E.; Licini, G. *Inorg. Chem.* **2008**, *47*, 8616−8618.
(12) For related structures of **TA2**, see: a) Kikushima, K.; Moriuchi, T.; Hirao, T. *Tetrahedron* **2010**, *66*, 6906−6911; b) Redshaw, C.; Rowan, M. A.; Homden, D. M.; Dale, S. H.; Elsegood, M. R. J.; Matsuic, S.; Matsuura, S. *Chem. Comm.* **2006**, 3329–3331; c) Soshnikov, I, E.; Semikolenova, N. V.; Bryliakov, K. P.; Zakharov, V. A.; Redshaw, C.; Talsi, E. P. *J. Mol. Catal. A-Chem.* **2009**, *303*, 23–29.
(13) Evans, D. F. *J. Chem. Soc.* **1959**, 2003–2005.
(14) Wiberg, K. B. *J. Am. Chem. Soc.* **1954**, *76*, 5371–5375.
(15) APEX Software Suite v.2010; Bruker AXS: Madison, W. **2005**.
(16) Blessing, R. *Acta Cryst.* **1995**, *A51*, 33−38.
(17) Sheldrick, G. M. *Acta Cryst.* **2008**, A64, 112−122.
(18) a) Becke, A. D. *J. Chem. Phys.* **1993**, *98*, 5648−5652; b) Lee, C.; Yang, W.; Parr, R. G. *Phys. Rev. B* **1988**, *37*, 785−789.
(19) Frisch, M. J.; Trucks, G. W.; Schlegel, H. B.; Scuseria, G. E.; Robb, M. A.; Cheeseman, J. R.; Scalmani, G.; Barone, V.; Mennucci, B.; Petersson, G. A.; Nakatsuji, H.; Caricato, M.; Li, X.; Hratchian, H. P.; Izmaylov, A. F.; Bloino, J.; Zheng, G.; Sonnenberg, J. L.; Hada, M.; Ehara, M.; Toyota, K.; Fukuda, R.; Hasegawa, J.; Ishida, M.; Nakajima, T.; Honda, Y.; Kitao, O.; Nakai, H.; Vreven, T.; Montgomery, J., J. A.; Peralta, J. E.; Ogliaro, F.; Bearpark, M.; Heyd, J. J.; Brothers, E.; Kudin, K. N.; Staroverov, V. N.; Kobayashi, R.; Normand, J.; Raghavachari, K.; Rendell, A.; Burant, J. C.; Iyengar, S. S.; Tomasi, J.; Cossi, M.; Rega, N.; Millam, J. M.; Klene, M.; Knox, J. E.; Cross, J. B.; Bakken, V.; Adamo, C.; Jaramillo, J.; Gomperts, R.; Stratmann, R. E.; Yazyev, O.; Austin, A. J.; Cammi, R.; Pomelli, C.; Ochterski, J. W.; Martin, R. L.; Morokuma, K.; Zakrzewski, V. G.; Voth, G. A.; Salvador, P.; Dannenberg, J. J.; Dapprich, S.; Daniels, A. D.; Farkas, Ö.; Foresman, J. B.; Ortiz, J. V.; Cioslowski, J.; Fox, D. J. Gaussian 09, Revision D.01; Gaussian Inc., Wallingford, CT, 2013.
(20) Schafer, A.; Huber, C.; Ahlrichs, R. *J. Chem. Phys.* **1994**, *100*, 5829−5835.
(21) Mayer, I. *Chem. Phys. Lett.* **1983**, *97*, 270−274.
(22) Gorelsky, S. I. AOMix: Program for Molecular Orbital Analysis, version 6.87; University of Ottawa, Ottawa, Canada, 2015.
(23) a) Zhao, Y.; Truhlar, D.G.; *Theor. Chem. Acc.* **2008**, *120*, 215−241; b) Zhao, Y.; Truhlar, D.G. *Acc. Chem. Res.* **2008**, *41*, 157−167.

(24) a) Mierts, S.; Scrocco, E.; Tomasi, J. *Chem. Phys.* **1981**, *55*, 117−129; b) Cossi, M.; Mennucci, B.; Tomasi, J. *Chem. Phys. Letters* **1994**, *228*, 165–170; c) Mennucci, B.; Cancès, E.; Tomasi, J. *J. Phys. Chem. B* **1997**, *101*, 10506−10517.
(25) a) Ren, E. W.; Vanden-Eijnden, E. *Phys. Rev. B* **2002**, *66*, 052301−4; b) Opt'n Path v1.50; Fleurat-Lessard, P.; Dayal, P. Freely available at: http://perso.ens-lyon.fr/paul.fleurat-lessard/ReactionPath.html.
(26) a) Hay, P.; Wadt, W. *J. Chem. Phys.* **1985**, *82*, 299−310; b) Ehlers, A.; Böhme, M.; Dapprich, S.; Gobbi, A.; Höllwarth, A.; Jonas, V.; Köhler, K.; Stegmann, R.; Veldkamp, A.; Frenking, G. *Chem. Phys. Lett.* **1993**, *208*, 111−114; c) Roy, L.; Hay, P.; Martin, R.; *J. Chem. Theory Comput.* **2008**, *4*, 1029−1031.
(27) a) Feller, D. *J Comp Chem.* **1996**, *17*, 1571−1586; b) Schuchardt, K. L.; Didier, B. T.; Elsethagen, T.; Sun, L.; Gurumoorthi, V.; Chase, J.; Li, J.; Windus, T. L. *J. Chem. Inf. Model* **2007**, *47*, 1045−1052.
(28) Morse, P. M. S.; Wilson, M. D.; Girolami, S. R. *Organometallics* **1994**, *13*, 1646–1655.
(29) Bjørsvik, H-R.; Liguori, L. *Org. Process Res. Dev.* **2002**, *6*, 279–290.
(30) a) Voet, D. *Biochemistry*, 3rd ed., Wiley, New York, 2004; b) Meeuwissen, J.; Reek, J. N. H. *Nature Chem.* **2010**, *2*, 615–621; c) Hoppe, E.; Limberg, C. *Chem. Eur. J.* **2007**, *13*, 7006−7016; d) Homden, D. M.; Redshaw, C. *Chem. Rev.* **2008**, *108*, 5086−5130.
(31) a) Makita, Y.; Sugimoto, K.; Furuyoshi, K.; Ikeda, K.; Fujiwara, S-i.; Shin-ike, T.; Ogawa, A. *Inorg. Chem.* **2010**, *49*, 7220−7222; b) Perraud, O.; Sorokin, A. B.; Dutasta, J-P.; Martinez, A. *Chem. Commun.* **2013**, *49*, 1288−1290; c) Martinez, A.; Dutasta, J-P. *J. Catal.* **2009**, *267*, 188−192.
(32) Cotton, A. F.; Wilkinson, G. *Advanced Inorganic Chemistry*; Wiley and Sons: New York, 1972; pp 538.
(33) Kajiwara, T.; Wagner, R.; Bill, E.; Weyhermüller, T.; Chaudhuri, P. *Dalton Trans.* **2011**, *40*, 12719−12726.
(34) The uncertainties were calculated based on error propagation formulas. See: ref 28.
(35) a) Chéron, N.; Ramozzi, R.; El Kaim, L.; Grimaud, L.; Fleurat-Lessard, P. *J. Org. Chem.* **2012**, *77*, 1351−1366; b) Kozuch, S.; Shaik, S. *Acc. Chem. Res.* **2011**, *44*, 101–110.

Chapter 7: Summary, Conclusions and Future Directions

7.1 Summary

Oxovanadium(V) complexes are promising catalysts for the disassembly of lignin models and polyalcohols. *Chapters 2* and *3* presented the expanded substrate scope for the aerobic cleavage of phenoxyethanol (**LM1** and **LM3**), β-O-4 (**LM4**) and β-1 (**LM6-9**) lignin models using 5- and 6-coodinate oxovanadium(V) catalysts [(dipic)V^{V}(O)(O^{i}Pr) **OV1** and $(HQ)_2V^{V}$(O)(O^{i}Pr) **OV2**].[1] In substrates containing secondary alcohols, the C-H bond cleavage occurs through a base-assisted, two-electron oxidation process, affording a ketone intermediate which subsequently leads to C-O or C-C bond cleavage depending on the type of catalyst. The ketone C-C bond cleavage occurs more rapidly in the presence of exogenous base but the detailed reaction pathway still remains unknown. It was established, however, that selectivity using catalysts **OV1** and **OV2** is solvent-dependent. For example, in the aerobic oxidation of lignin model **LM2**, C-H bond cleavage is favoured under basic conditions. In contrast, a mixture of C-H and C-O bond cleavage products is obtained in less basic solutions. Similar to the observations of Hanson and co-workers for phenolic β-O-4 lignin models,[2] *Chapter 2* demonstrated different product selectivity for phenolic and non-phenolic β-1 lignin models.

In order to improve the selectivity and increase the rate of the reaction, *Chapter 4* reported the synthesis, characterization and reactivity of several new amine bis(phenolate) oxovanadium(V) complexes with pendant bases attached to their ligands (*e.g.*, **AP1** and **AP3**).[3] The new catalysts were synthesized from inexpensive and commercially available precursors in two steps. Catalysts **AP1** and **AP3** displayed higher performance for the oxidation of lignin models **LM2**, **LM3** and **LM4** compared with previously reported **OV1** and **OV2** catalysts. Higher conversion and yields are achieved with catalyst loadings as low as 0.01 mol%, without the need for co-additives (*e.g.*, exogenous base). Interestingly, catalysts **AP1** and **AP3** also catalyze the Cannizzaro[4] and Tishchenko[5] reactions to produce

benzyl alcohol from benzaldehyde and methyl benzoate. While the detailed role of the pendant base is still unknown, the performance of catalyst **AP3** (dimethylamino backbone) *versus* **AP6** (propyl backbone) is higher for all lignin models analyzed in *Chapter 4*. Full characterization of the V(V) complexes derived from thermolysis of **AP7** (and related metal complex **AP8**) and its role in the lignin model oxidation mechanism is currently under investigation.

The work in *Chapter 5* compared several known catalysts for the depolymerization of real lignin extracts using comparable conditions and analytical techniques.[6] A systematic analysis of the different catalysts for the aerobic oxidation and depolymerization of organosolv lignin was determined using GPC, ^{1}H-^{13}C NMR and ^{31}P NMR spectroscopy (after derivatization to phosphite esters). Studied catalysts included first-generation oxovanadium(V) catalysts (**OV1**, **OV2** and **OVS**), second-generation amine bis(phenolate) oxovanadium(V) catalysts (**AP1** and **AP3**) and several other base-metal catalysts such as CuCl/TEMPO/lutidine **(Cu*)**, Cobalt-salen complex (**CoL)** and metal free system **MFH**. Oxidation catalysts **Cu*** and **MFH** were only able to oxidize the organosolv lignin, as observed by 2D NMR, with a negligible reduction of the molecular weight. The **CoL** catalyst was not able to reduce the molecular weight since the organosolv lignin did not contain high concentrations of phenolic lignin for which **CoL** is more active. In contrast, oxovanadium catalysts **OV1**, **OV1**, **AP1** and **AP3** showed the best performance for the oxidation and depolymerization of organosolv lignin. As observed previously in *Chapters 2* and *3*, oxovanadium catalysts **OV1** and **OV2** performed poorly in terms of turnover numbers and reaction rates. Catalyst **OV1** is deactivated by the water content in the organsolv lignin, forming a less active dioxo vanadium(V) anion (similar to **OV9**). On the other hand, catalyst **OV2** displayed the highest degree of depolymerization, decreasing the molecular weight and the concentration of lignin-derived phosphite esters as determined by GPC and quantitative $^{31}P\{^{1}H\}$ NMR spectroscopy. Moreover, amine bis(phenolate) oxovanadium(V) catalysts **AP3** showed the best degree of depolymerization as observed by GPC compared with all other catalysts studied. The molecular weight decreased by half (*e.g.,* 1211 Da for control experiment and 663 Da for catalyzed reaction) representing the best catalytic system reported to date in the literature.[7]

Intrigued by the reactivity of oxovanadium(V) catalysts (*e.g.*, **OV1** and **OV2**) to promote the selective C-C bond cleavage of pinacol, *Chapter 6* explored the expansion of the substrate scope to polyalcohols (simple models of cellulose biomass and its partial hydrogenolysis products). Trialkoxyamine oxovanadium(V) catalysts bearing triethoxyamine and tris(2-3,5-di-*tert*-butylphenoxy-methyl)amine ligands were optimized for the aerobic selective oxidative C-C bond cleavage of 1,2-diols.[8] Catalysts **TA1** and **TA2** oxidize 1,2-diols with very good rates (< 7 h), under mild conditions (< 80 ^{o}C), using low catalyst loadings (0.1 mol%) and with excellent selectivity for aldehydes (> 99%). In comparison, under similar conditions oxovanadium catalyst **OV2** only produces 5% selectivity for aldehydes. Notably, the anaerobic oxidation of 1,2-diols (*e.g.*, pinacol and 1,2-hydrobenzoin) using catalyst **TA2** afforded a non-oxo vanadium(III) intermediate which represents a direct two-electron oxidation of the substrate. The vanadium (III) complex was isolated as an acetonitrile (**TA8**) or dimethoxyethane (**TA9**) adduct with the ligand occupying the apical position *trans* to the amine nitrogen. These complexes are highly air-sensitive, allowing for facile regeneration of the oxovanadium(V) complex **TA2,** thus closing the catalytic cycle. The kinetic activation parameters for the anaerobic two-electron oxidation of 1,2-hydrobenzoin were $\Delta H^{\neq}$ = 110 ± 4.55 kJ mol^{-1} and $\Delta S^{\neq}$ = -5.24 ± 13.4 J K^{-1} mol^{-1}, in good agreement with the theoretical calculations. The kinetic isotope effect (KIE), k_H/k_D at 348.15 K, in toluene-d_8 of 2.41 ± 0.72 corresponds to a primary isotope effect of proton transfer from the pinacol hydroxyl groups to the V-OH moiety in concert with the C-C bond cleavage step. These observations clearly indicate that the C-C bond cleavage of 1,2-diols does not undergo an α-hydrogen abstraction mechanism as was previously reported.[9]

The versatility of the oxovanadium(V) catalysts is shown in Figure 7.1 as a summary of the most important complexes reported in this *Thesis* for the valorization of lignocellulose biomass.

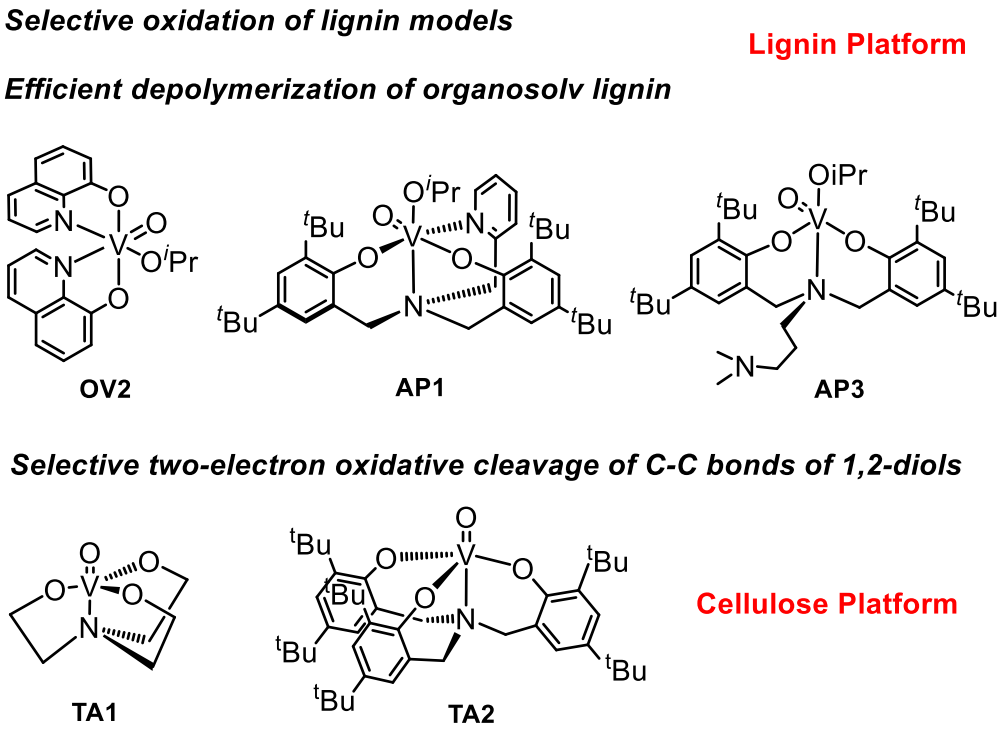

Figure 7.1. Most important oxovanadium catalysts presented in this *Thesis* for the valorization of lignin and cellulose.

7.2 Conclusions

As discussed in the previous section, oxovanadium(V) catalysts have a great potential for the valorization of lignocellulose biomass. While the first generation of oxovanadium catalysts (**OV1** and **OV2**) provide interesting selectivity and unique mechanisms towards the disassembly of lignin models, the slow rate of reaction and the need for exogenous base are significant drawbacks for application to the depolymerization of lignin extracts. As seen in recent reports, the combination of vanadium and copper catalysts offers an increasing efficiency through synergies of the two different metals for the depolymerization of kraft lignin.[10] New approaches using **OV1** and **OV2** should be focused on developing tandem catalytic systems with other transition metals or co-additives. Additionally, more information about the nature of the C-C bond cleavage of the ketone intermediate (*e.g.*, **OP1**, **OP2** and **OP9**) is required to fully optimize this catalytic system.

New bis(phenolate) oxovanadium(V) catalysts **AP1** and **AP2** represent a considerable advance for the aerobic disassembly of lignin models and the depolymerization of organosolv lignin. The facile manipulation of the bis(phenol) framework provides an

incredible opportunity for new ligand designs containing different pendant bases or other functional groups. On the other hand, the kinetic and mechanistic observations for the trialkoxyamine oxovanadium(V) catalysts (**TA1** and **TA2**) facilitate the development of new ligand frameworks for more efficient and broad substrate scope. For example, more electron-poor phenolate moieties could contribute to increase the electrophilicity of the vanadium centre, facilitating the C-C bond cleavage of the coordinated substrate. Hemicarcerand oxovanadium(V) complexes also offer several advantages in terms of shape selectivity and improved reaction rates. However, the studies indicate that complexes **TA3** and **TA4** do not achieve significant differences compared with the simple atrane complex **TA1**. New hemicarcerand oxovanadium complexes bearing large cavities and with different degrees of hydrophobicity are currently under investigation.

Several homogenous and heterogeneous techniques were discussed in *Chapter 1*, however, an efficient and economically viable valorization of lignin is still required. Although this *Thesis* has focused on the aerobic oxidation mediated by homogeneous transition metal catalysts as the main approach, many others techniques, such as biochemical and heterogeneous catalysis are certainly promising.

7.3 Future Directions

Future work based on this *Thesis* will be focused on the full understanding of the chemical transformations discussed here. Despite the good activity of **AP1** and **AP3** for the aerobic oxidation of lignin models and the outstanding performance for the depolymerization of organosolv lignin, the details of the mechanism of these reactions remain unknown. Future work should concentrate on clarifying all variables that control these transformations in order to design the next generation of oxovanadium complex catalysts.

On the other hand, bio-catalysis has been proposed as a powerful alternative for the valorization of lignin. In Nature, several fungi and bacteria depolymerize lignin by using a pool of different enzymes.[11] The most attractive approach is the *biological funneling*, in which aromatic catabolism converts heterogeneous substrates to a central intermediate.[12] In Scheme 7.1, the central intermediate is acetyl coenzyme A (Acetyl-CoA), which is transformed to polyhydroxyalkanoates (PHA) through another enzymatic pathway. PHAs

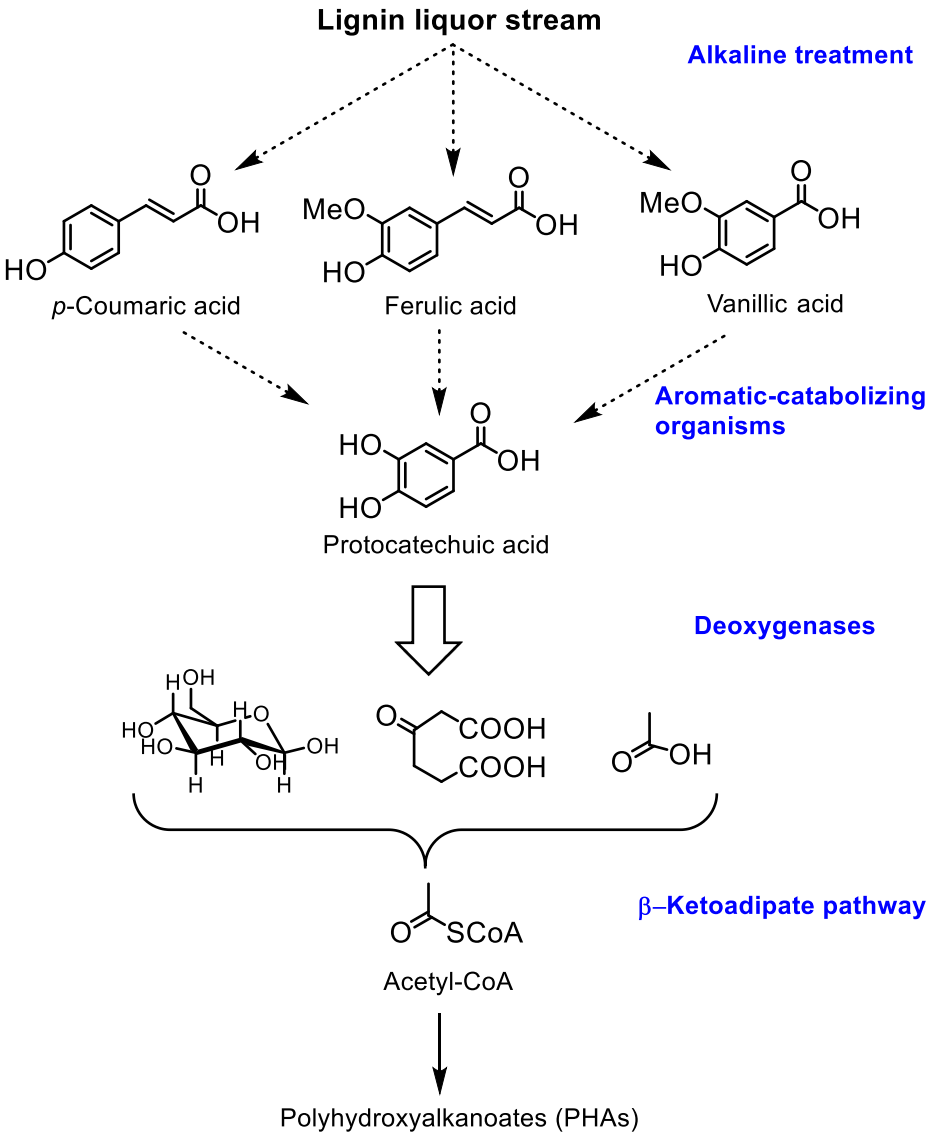

Scheme 7.1. Biological funneling of lignocellulose biomass.[12]

are versatile substrates for the production of bio-polymers and plastics. The most important stage of this process is the formation of the depolymerization products, *p*-coumaric acid, ferulic acid and vanillic acid, respectively. However, the alkaline treatment requires stoichiometric amounts of base, affording low yields of monomers. Transition metal catalysts could indeed take advantage of their versatile and greater activity to produce large amounts of monomers or dimers for subsequent application to the *biological funnel* strategy.

Furthermore, separation of the lignin degradation products is also a difficult task. Many research groups have considered utilizing partially degraded lignin as a starting material for

other chemical transformations, preserving the rich aromatic structure of lignin. The primary goal is to use chemically modified lignin or lignin fragments as an alternative of petrochemical polymers. However, unmodified lignin tends to aggregate in polymer composites due to π-π stacking of the aromatic rings and hydrogen bonding between different functional groups (*e.g.*, ethers and alcohols).[13] Previous attempts to produce polymers based on lignin have had serious drawbacks such as low lignin incorporation (< 10 wt. %), high heterogeneity of functional groups and polydispersity, and poor physical properties (*e.g.*, impact strength, brittleness). In the last year, an exponential increase in the interest for this field has arisen as revealed by the high numbers of new review articles in this area.[14] The role of catalysis, specifically transition metal catalysis, lies in the manufacturing of the lignin building blocks for the production of the complex polymers. Scheme 7.2 depicts an example for the production of complex molecules from lignin fragments using monomers such as syringyl, guaiacyl and hydroquinone.[15] The application of these new materials range from packing to energy storage materials. However, the production of such monomers must be catalyzed using inexpensive and practical methods.

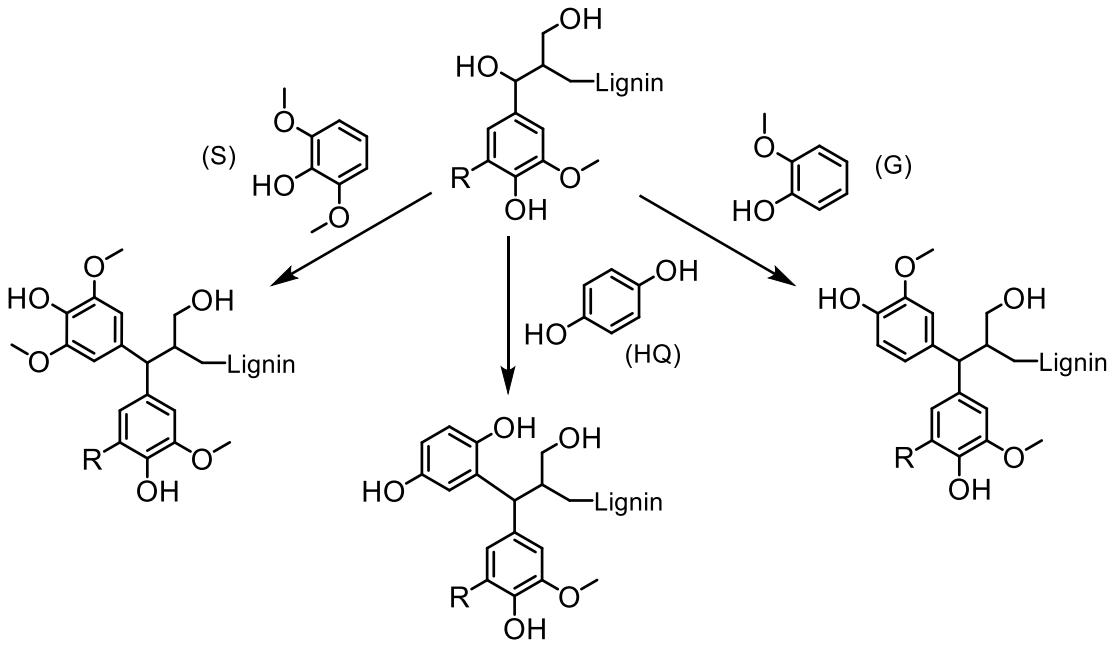

Scheme 7.2. Partially degraded lignin as a chemical precursor for synthetic molecules. The molecules are represented by syringyl (S), guaiacyl (G) and hydroquinone (HQ), respectively.[15c]

On the industrial side, Dupont, Renmatix, Genomatica, Gevo, Rennovia, Segetis and BioAmber, among others, are focusing on the production of high-value sugar-based

chemicals such as levulinic acid, 5-hydroxymethylfurfural, γ-valerolactone and other C6 molecules to mention a few examples. However, only Spero Energy and Borregaard have successfully obtained high yields of chemicals from lignin.

Recently, Abu-Omar's group used inexpensive base-metal supported nickel catalysts under a pressure of hydrogen for the production up to 68% yield of four phenolic products based on the amount of lignin present.[16] Furthermore, the carbohydrate content was recovery as a solid residue after the lignin content was converted into the desire phenolic products. The carbohydrate residue were treated with iron chloride for the production of furfural and levulinic acid in excellent yields. Later this technology was used for the spin-off company Spero Energy.

There is still a long way to go in order to achieve an effective method for the valorization of lignocellulose biomass. The challenge remains unsolved despite the recent advances in homogeneous and heterogeneous catalysis.[17] This *Thesis* contributes to the field of homogeneous vanadium catalysis for the aerobic oxidation of lignin and cellulose models. The transition to a carbon-neutral global economy, with the total eradication of petroleum, is going to be difficult but undoubtedly necessary to avoid the most catastrophic consequences of climate change.

7.4 References

(1) Sedai, B.; Díaz-Urrutia, C.; Baker, R. T.; Wu, R.; Silks, L. A.; Hanson, S. K. *ACS Catal.* **2011**, *1*, 794–804; b) Sedai, B.; Díaz-Urrutia, C.; Baker, R. T.; Wu, R.; Silks, L. A.; Hanson, S. K. *ACS Catal.* **2013**, 3, 3111–3122; c) Díaz-Urrutia, C.; Sedai, B.; Leckert, K.; Baker, R. T.; Hanson, S. K. *ACS Sustainable Chem. Eng.* **2016**, *submitted*.
(2) Hanson, S. K.; Wu, R.; Silks, L. A. P. *Angew. Chem. Int. Ed.* **2012**, *51*, 3410−3413
(3) Díaz-Urrutia, C.; Daccache, J.; Michel, C.; Fleurat-Lessard, P.; Korobkov, I.; Baker, R. T. **2016**, *submitted*.
(4) (a) Cannizzaro, S. *Justus Liebigs Ann. Chem*. **1853**, *88*, 129−130; (b) For a recent example of Cannizzaro reaction see: Basavaiah, D.; Sharada, D. S.; Veerendhar, A. *Tetrahedron Lett*. **2006**, *47*, 5771−5774.
(5) (a) Tischtschenko, W. J. *Russ. Phys. Chem.* **1906**, *38*, 355, 482; (b) Ogata, Y.; Kawasaki, A.; Kishi, I. *Tetrahedron* **1967**, *23*, 825−830.
(6) Díaz-Urrutia, C.; Chen, W-C.; Crites, C-O.; Daccache, J.; Korobkov, I.; Baker, R. T. *RSC Adv.* **2015**, 5, 70502–70511.
(7) a) Mottweiler, J.; Rinesch, T.; Besson, C.; Buendia, J.; Bolm, C. *Green Chem.* **2015**, *17*, 5001–5008; b) Deuss, P. J.; Scott, M.; Tran, F.; Westwood, N. J.; de Vries, J. G.; Barta, K. *J. Am. Chem. Soc.* **2015**, *137*, 7456–7467; c) Galvin, V. M.; Sawadjoon, S.; Rohde, V.; Dawange, M.; Samec S. M. J. *ChemCatChem* **2014**, *6*, 179–184; d) Kumar, C. R.; Anand, N.; Kloekhorst, A.; Cannila, C.; Bonura, G.; Frusteri, F. Barta, K.; Heeres, H. J. *Green Chem*. **2015**, *17***,** 4921–4930
(8) Díaz-Urrutia, C.; Michel, C.; Fleurat-Lessard, P.; Gorelsky, S. I.; Korobkov, I.; Martinez, A.; Baker, R. T. **2016**, *submitted*; b) Díaz-Urrutia, C.; Zhang, D.; Martinez, A.; Baker, R. T. **2016**, *manuscript in preparation*.
(9) a) Hanson, S. K.; Baker, R. T.; Gordon, J. C.; Scott, B. L.; Thorn, D. L. *Inorg. Chem.* **2010**, *49*, 5611−5618; b) Hanson, S. K.; Baker, R. T.; Gordon, J. C.; Scott, B. L.; Sutton, A. D.; Thorn, D. L. *J. Am. Chem. Soc.* **2009**, *131*, 428−429.
(10) Mottweiler, J.; Puche, M.; Räuber, C.; Schmidt, T.; Concepción, P.; Corma, A.; Bolm, C. *ChemSusChem* **2015**, *8*, 2106–2113.
(11) a) Guerriero, G.; Hausman, J-F.; Strauss, J.; Ertan, H.; Siddiqui, K. S. *Eng. Life Sci.* **2016**, *16*, 1–16; b) Dashtban, M.; Schraft, H.; Syed, T. A.; Qin, W. *Int. J. Biochem. Mol. Biol.* **2010**, *1*, 36–50; c) Kirk, T. K.; Farell, R. L. *Annu. Rev. Microbiol.* **1987**, *41*, 465–505.
(12) Linger, J. G.; Vardon, D. R.; Guarnieri, M. T.; Karp, E. M.; Hunsinger, G. B.; Franden, M. A.; Johnson, C. W.; Chupka, G.; Strathman, T. J.; Pienkos, P. T. Beckham, G. T. *Proc. Nat. Acad. Sci.* **2014**, *111*, 12013–12018.
(13) Deng, Y.; Feng, X.; Yang, D.; Yi, C.; Qiu, X. *BioResources* **2012**, *7*, 1145–1156.
(14) a) Upton, B. M.; Kasko, A. M. *Chem. Rev.* **2016**, *116*, 2275–2306; b) Ma, S.; Li, T.; Liu, X.; Zhu, J. *Polym. Int.* **2016**, *65*, 164–173; c) Delidovich, I.; Hausoul, P. J. C.; Deng, L.; Pfützenreuter, R.; Rose, M.; Palkovits, R. *Chem. Rev.* **2016**, *116*, 1540−1599; d) Llevot, A.; Grau, E.; Carlotti, S.; Grelier, S.; Cramail, H. *Macromol. Rapid Commun.* **2016**, *37*, 9−28; e) Chatterjee, S.; Saito, T. *ChemSusChem* **2015**, *8*, 3941–3958; f) Matsushita, Y. *J. Wood Sci.* **2015**, *61*, 230–250; g) Thakur, V. K.; Thakur, M. K.; Raghavan, P.; Kessler, M. R. *ACS Sustainable Chem. Eng.* **2014**, *2*, 1072–1092.
(15) a) Saito, T.; Brown, R. H.; Hunt, M. A.; Pickel, D. L.; Pickel, J. M.; Messman, J. M.; Baker, F. S.; Keller, M.; Naskar, M. K. *Green Chem.* **2012**, *14*, 3295–3303; b) Sun, Y.;

Yang, L.; Lu, X.; He, C. *J. Mater. Chem. A* **2015**, *3*, 3699–3709; c) Nilsson, T. Y.; Wagner, M.; Inganäs, O. *ChemSusChem* **2015**, *8*, 4081–4085.
(16) Luo, H.; Klein, I. M.; Jiang, Y.; Zhu, H.; Liu, B.; Kenttamaa, H. K.; Abu-Omar, M. M. *ACS Sustainable Chem. Eng.* **2016**, *4*, 2316–2322; b) Klein, I.; Saha, B.; Abu-Omar, M. M. *Catal. Sci. Technol.* **2015**, *5*, 3242–3245.
(17) a) Kärkäs, M. D.; Matsuura, B. S.; Monos, T. M.; Magallanes, G.; Stephenson, C. R. J. *Org. Biomol. Chem.* **2016**, *14*, 1853–1914; b) Li, S-H.; Liu, S.; Colmenares, J. C.; Xu, Y-J. *Green Chem.* **2016**, *18*, 594–607; c) Behling, R.; Valange, S.; Chatel, G. *Green Chem.* **2016**, *18*, 1839–1854; d) Deuss, P. J.; Barta, K. *Coord. Chem. Rev.* **2016**, *306*, 510–532; e) Li, C.; Zhao, X.; Wang, A.; Huber, G. W.; Zhang, T. *Chem. Rev.* **2015**, *115*, 11559–11624.

Appendices

The NMR data for *Chapter 2* can be found in Sedai, B.; Díaz-Urrutia, C.; Baker, R. T.; Wu, R.; Silks, L. A.; Hanson, S. K. ACS Catal. **2011**, *1*, 794–804 and Sedai, B.; Díaz-Urrutia, C.; Baker, R. T.; Wu, R.; Silks, L. A.; Hanson, S. K. ACS Catal. **2013**, *3*, 3111–3122.

The crystallographic (atomic coordinates, bond lengths and bond angles) and NMR data for **AP1** (**AP1a** and **AP1b**) is reported in Díaz-Urrutia, C.; Chen, W-C.; Crites, C-O.; Daccache, J.; Korobkov, I.; Baker, R. T. *RSC Adv.* **2015**, *5*, 70502–70511.

NMR spectra

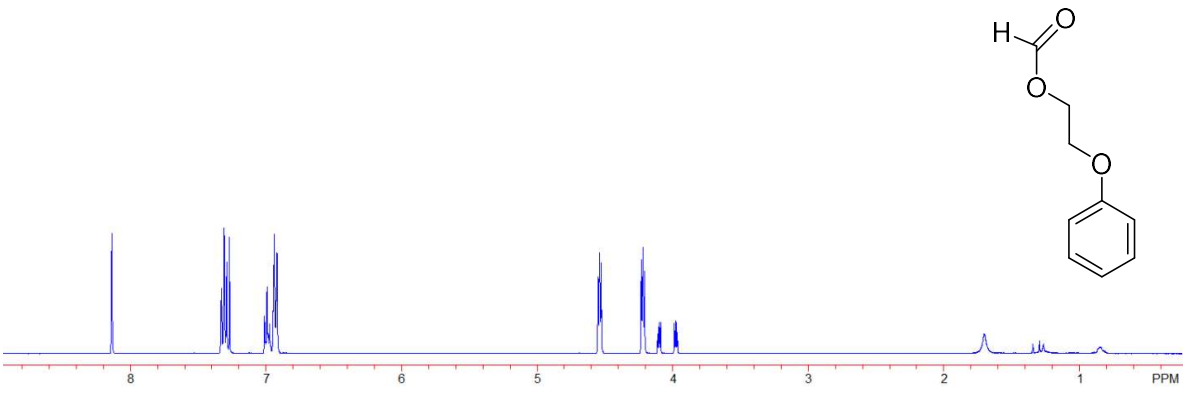

Figure A1. ^{1}H NMR (400 MHz, $CDCl_3$) spectrum of 2-phenoxyethyl formate **OP18**.

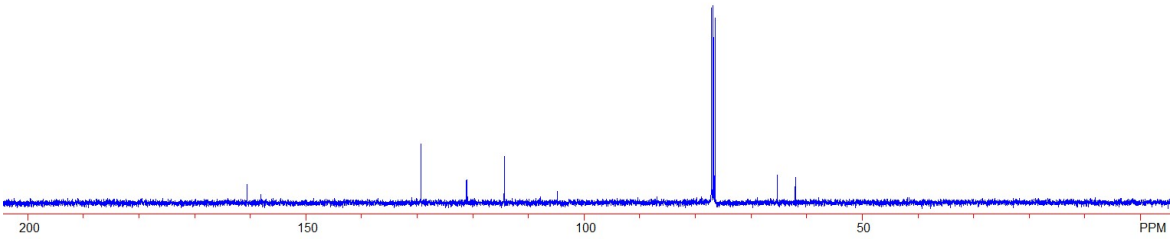

Figure A2. $^{13}C\{^{1}H\}$ NMR (100 MHz, $CDCl_3$) spectrum of 2-phenoxyethyl formate **OP8**.

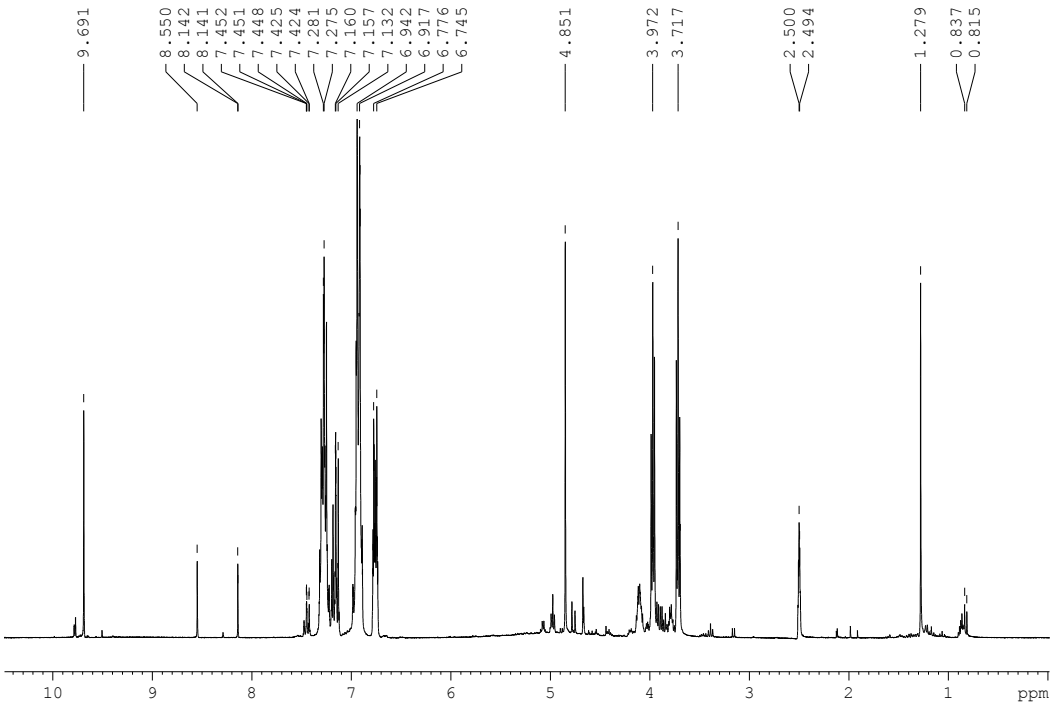

Figure A3. ^{1}H NMR (400 MHz, DMSO-d_6) spectrum of the reaction mixture (DMSO-d_6 solution) from the thermolysis of 2-phenoxyacetaldehyde **OP20** under air after 48 h at 100 °C.

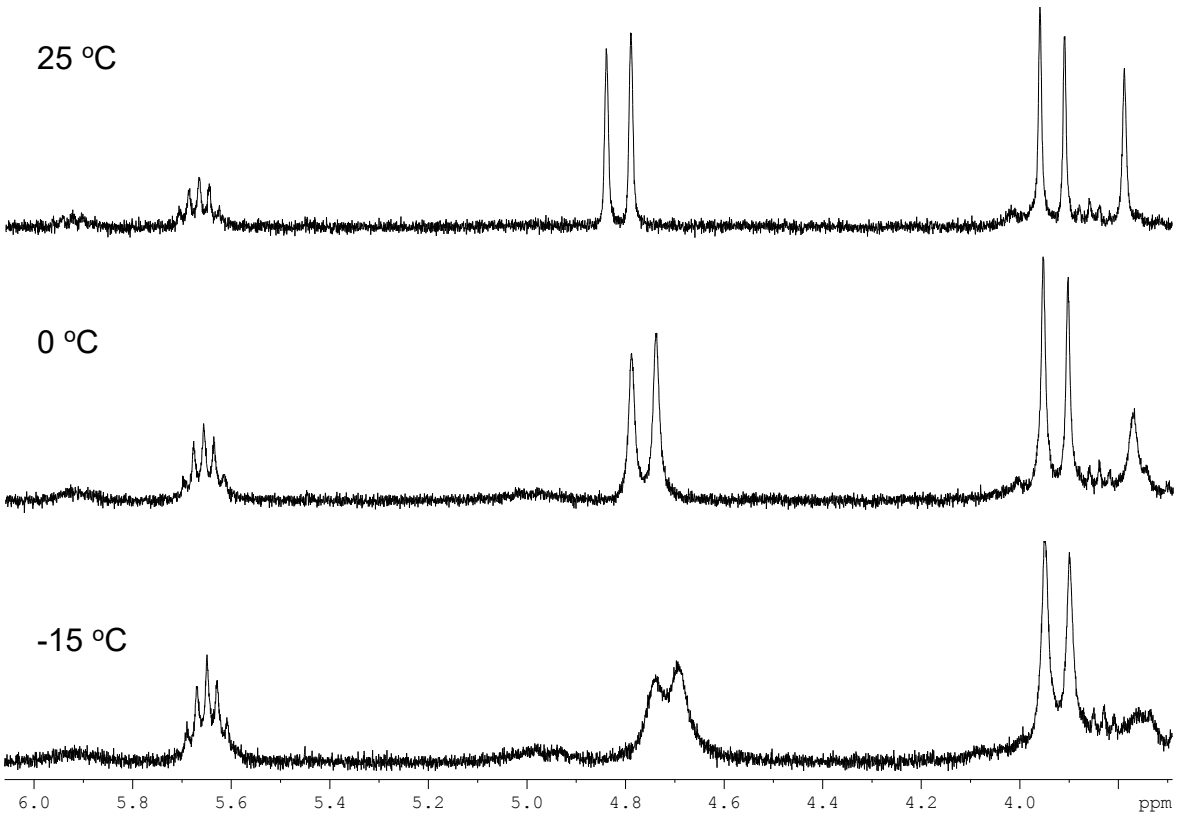

Figure A4. Variable temperature ^{1}H NMR spectra (CD_3CN, 300 MHz) for complex **AP3**.

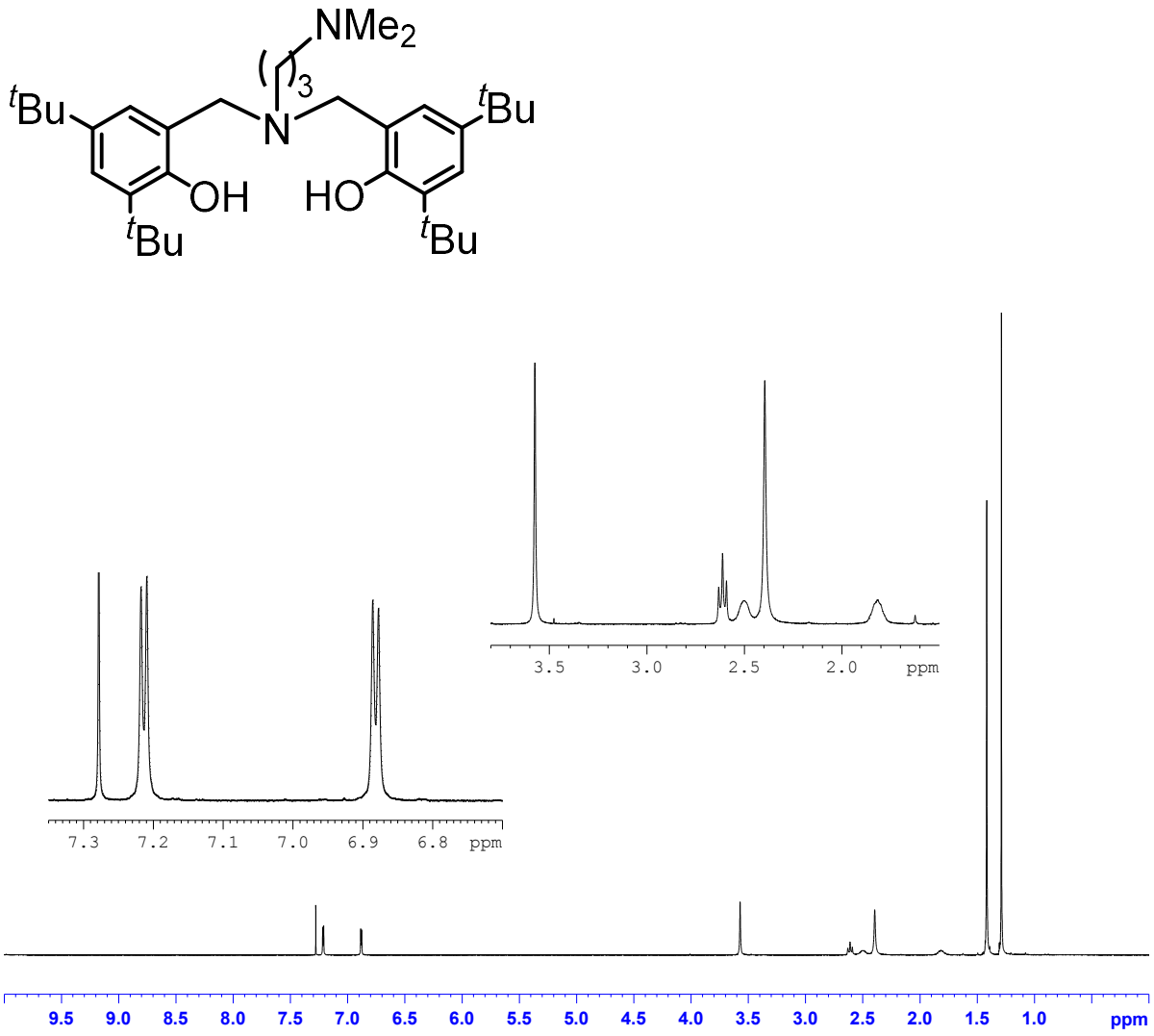

Figure A5. ^{1}H NMR (300 MHz, $CDCl_3$) spectrum for **PL2**.

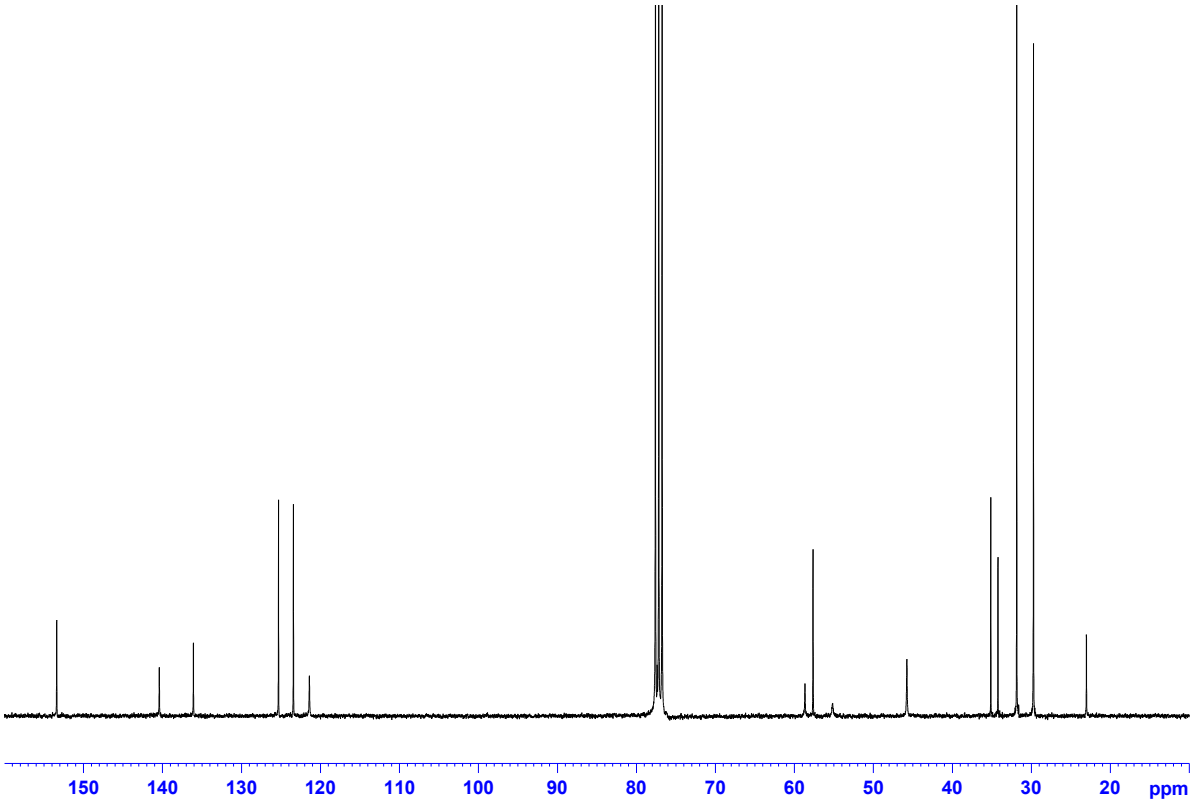

Figure A6. $^{13}C\{^{1}H\}$ NMR (75.5 MHz, $CDCl_3$) spectrum for **PL2**.

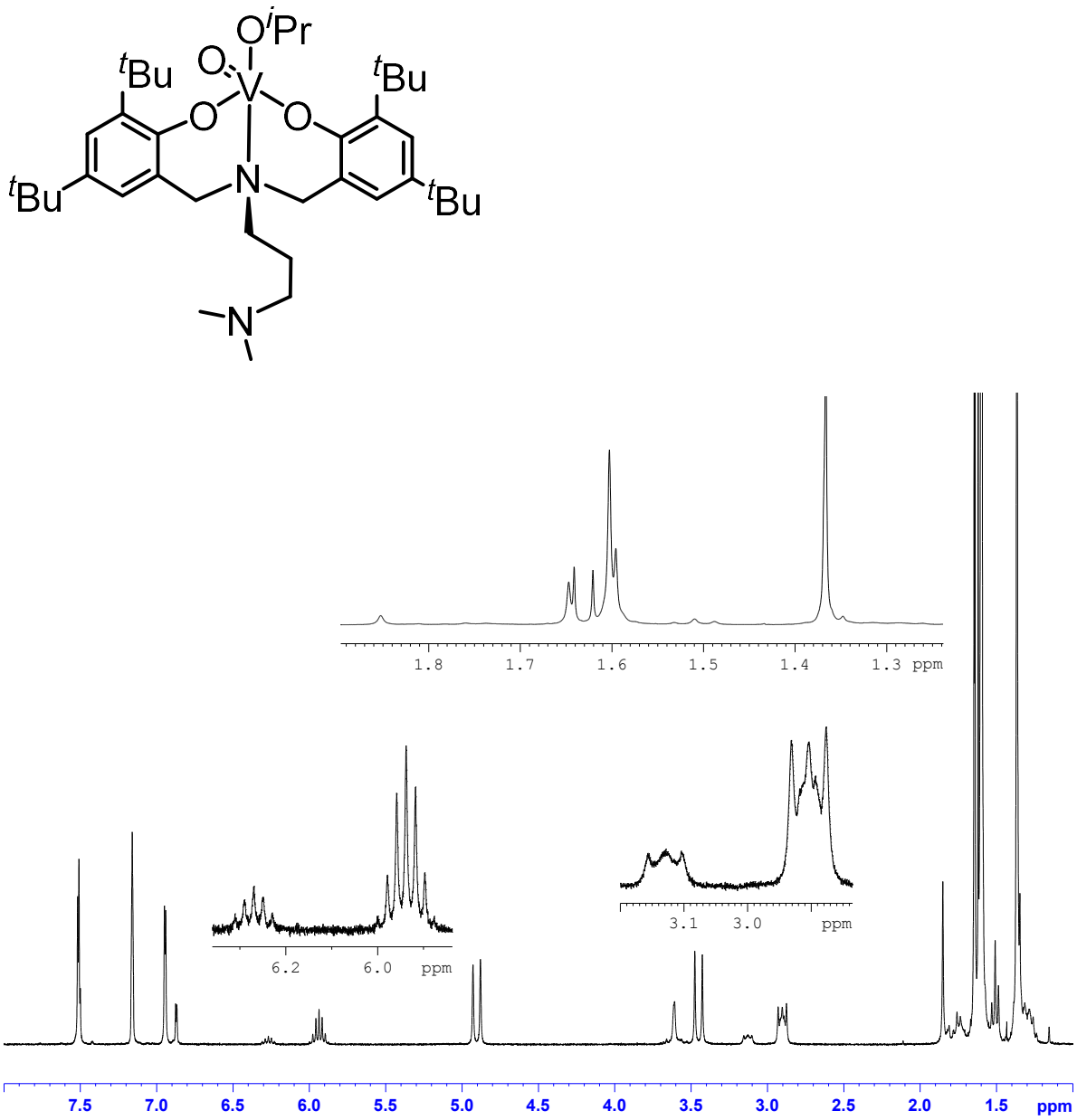

Figure A7. ^{1}H NMR (300 MHz, C_6D_6) spectrum for **AP3**.

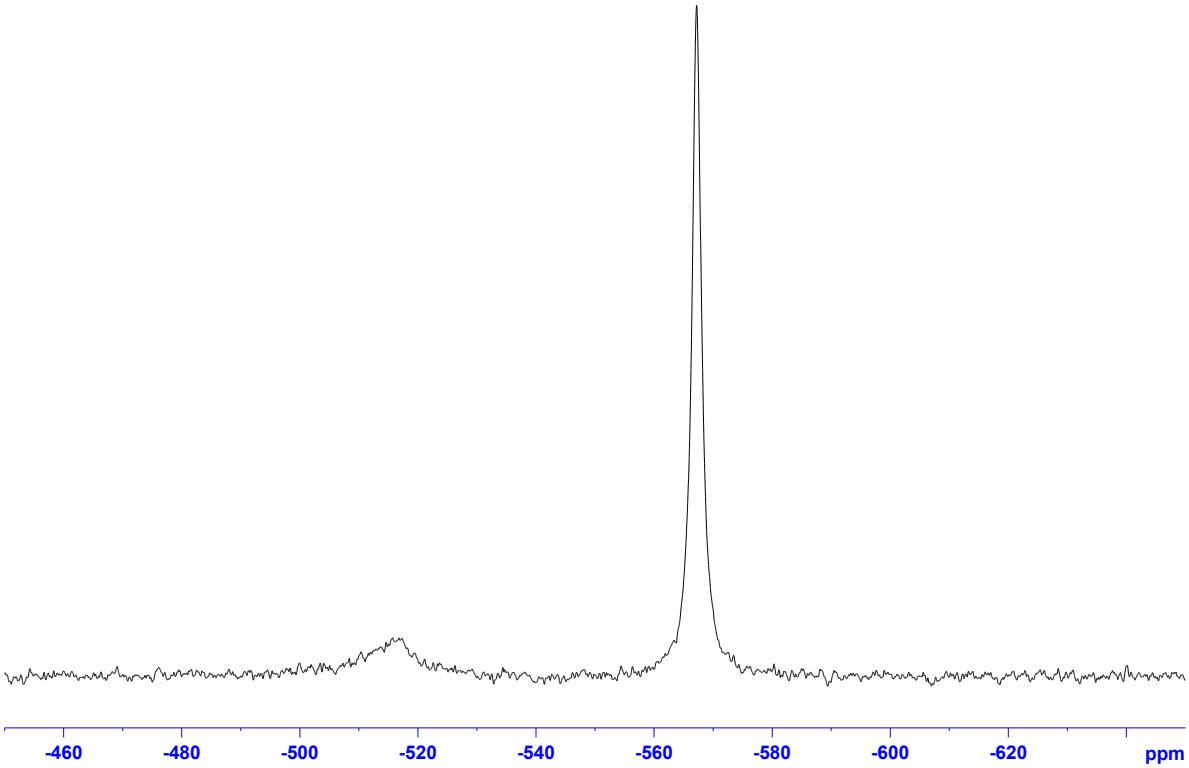

Figure A8. ^{51}V NMR (78.9 MHz, C_6D_6) spectrum for **AP3**.

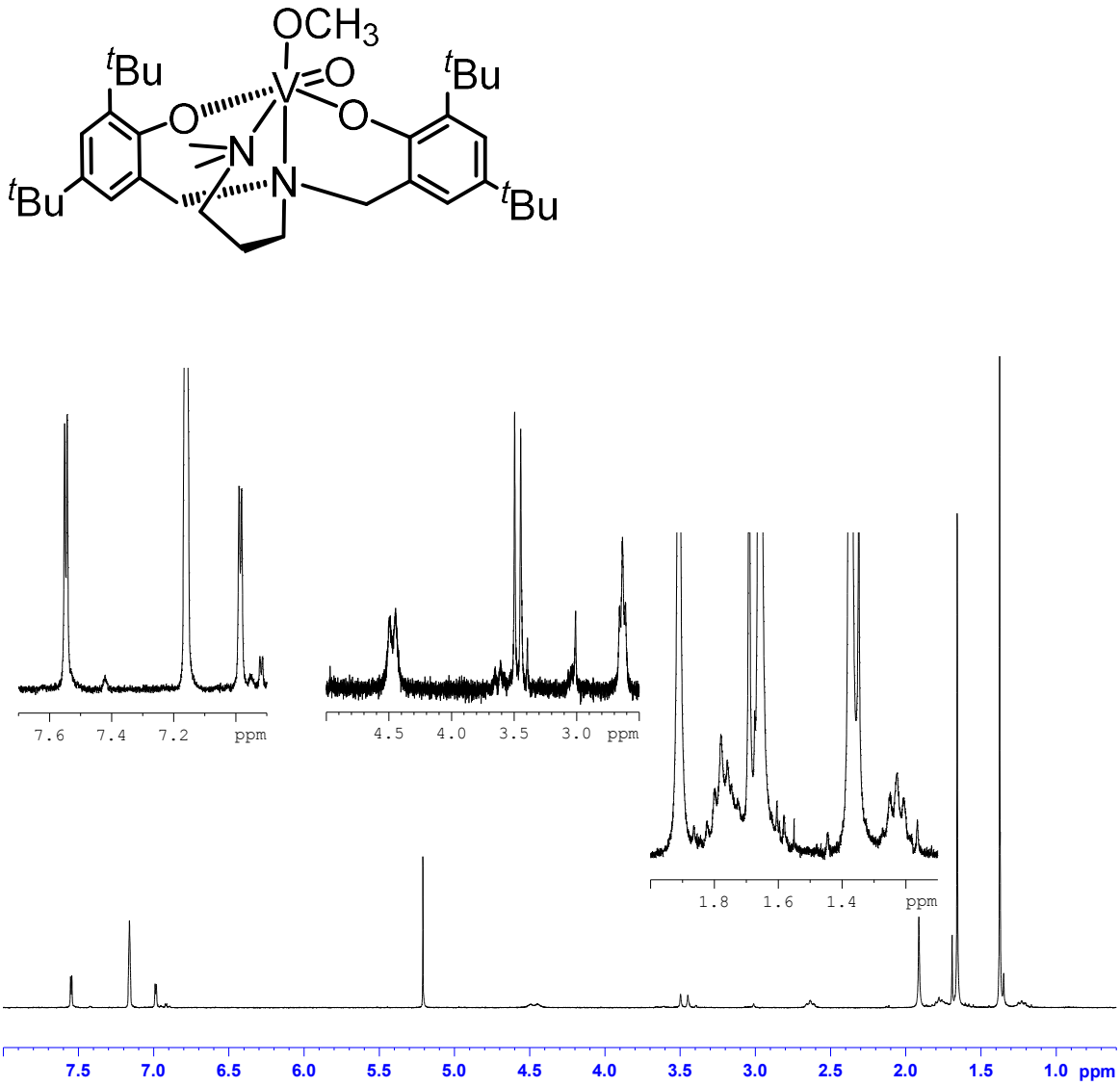

Figure A9. ^{1}H NMR (300 MHz, C_6D_6) spectrum for **AP2**.

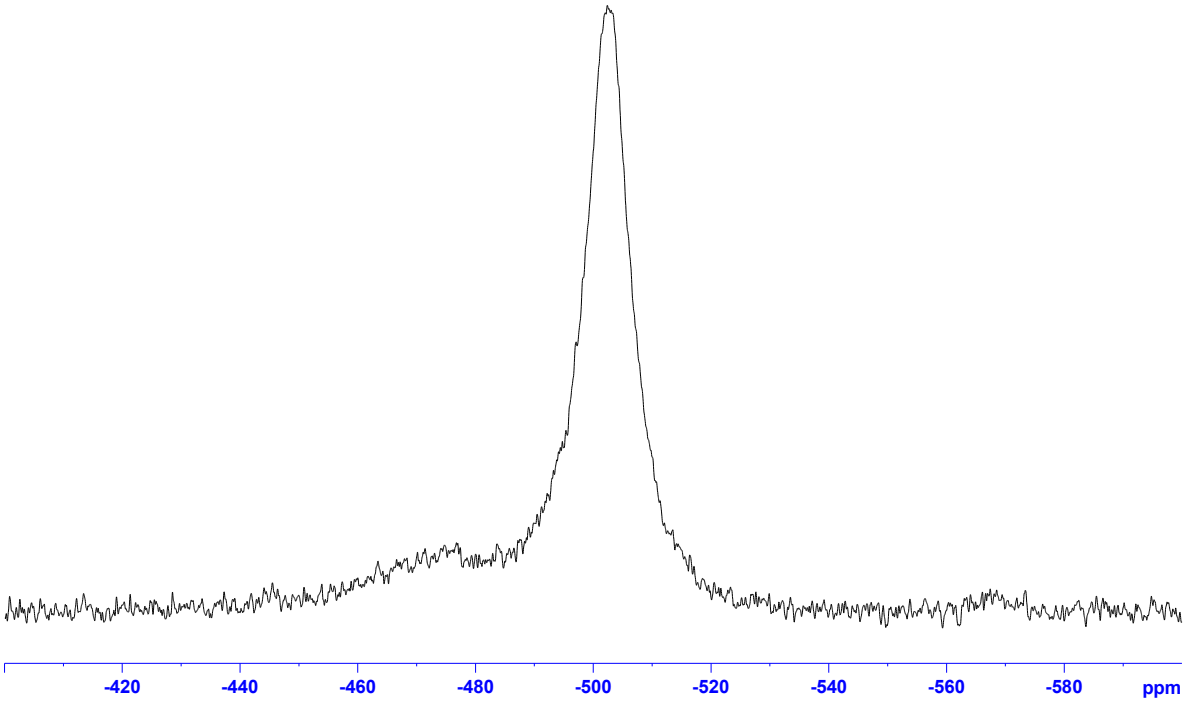

Figure A10. ^{51}V NMR (78.9 MHz, C_6D_6) spectrum for **AP2**.

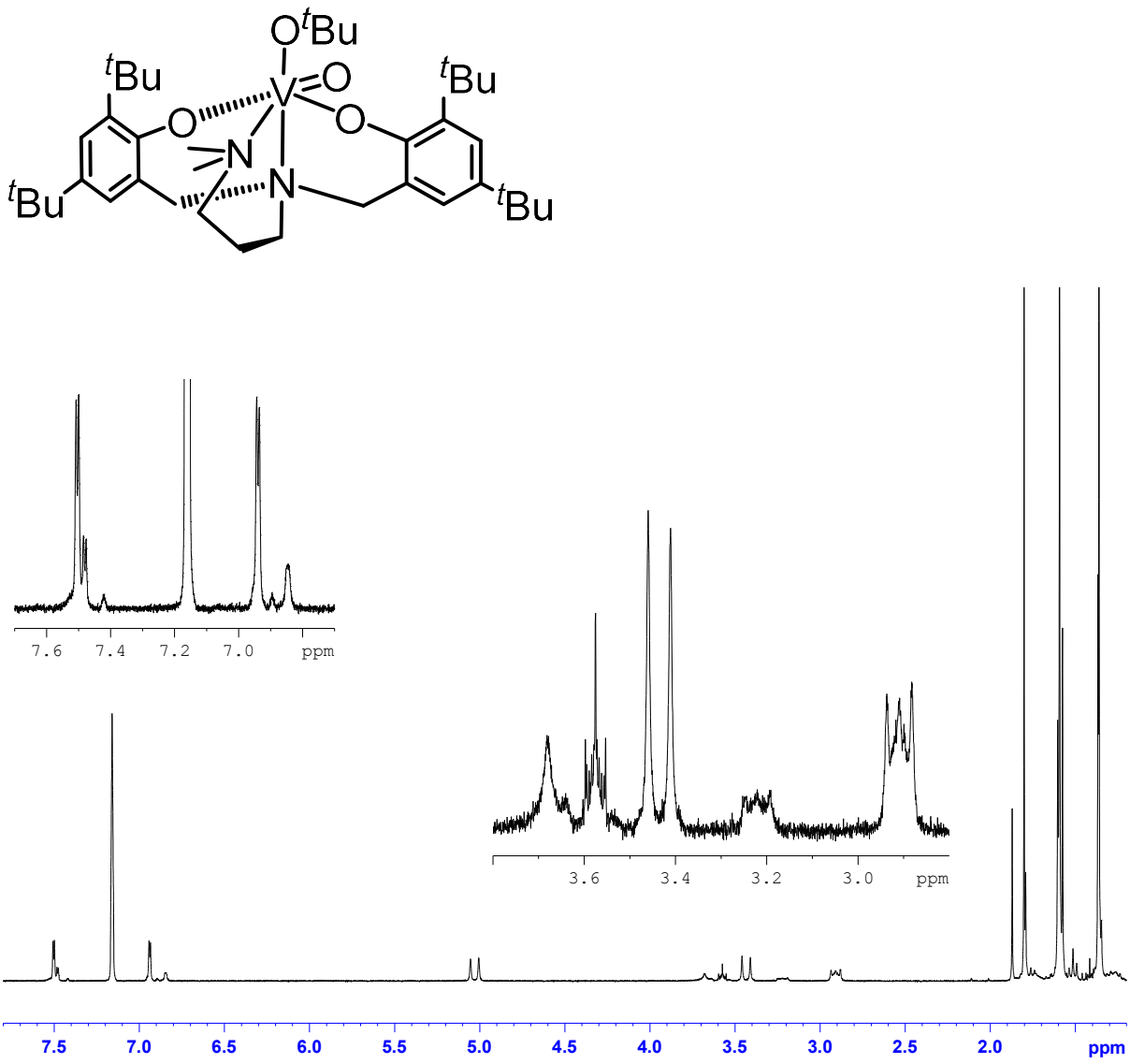

Figure A11. ^{1}H NMR (300 MHz, C_6D_6) spectrum for **AP4**.

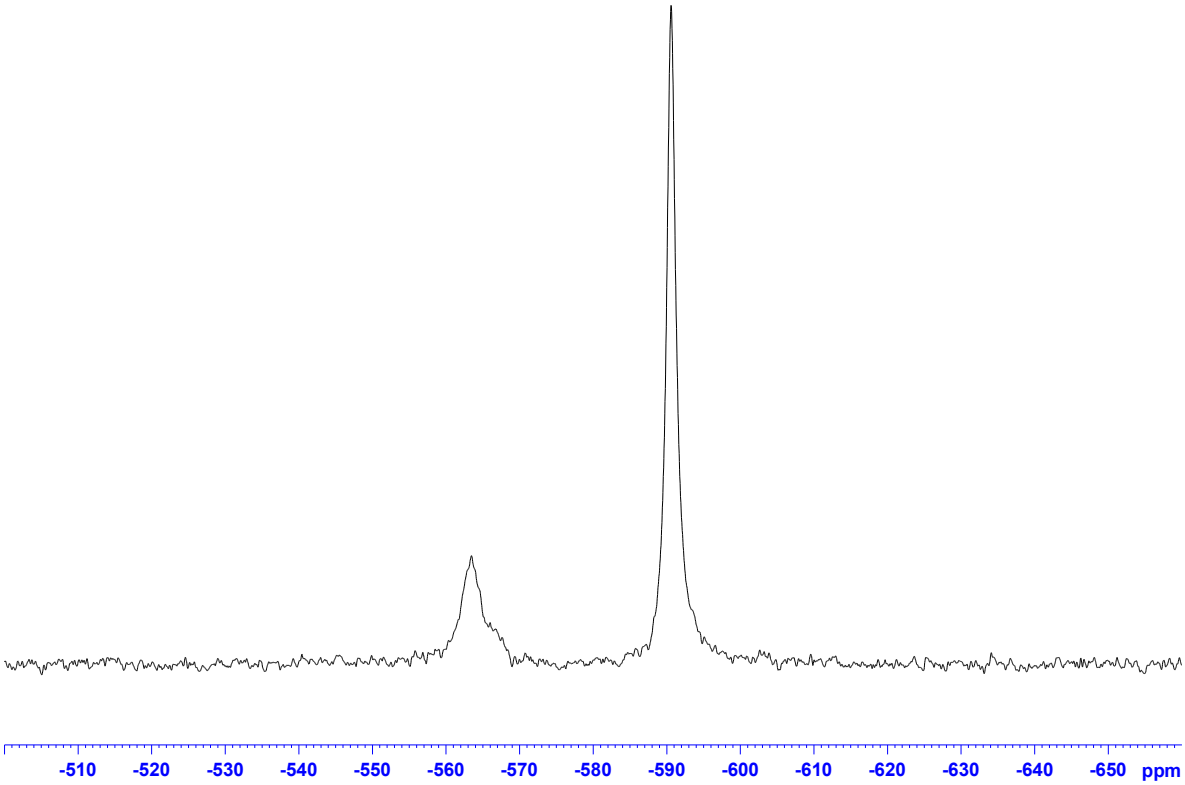

Figure A12. ^{51}V NMR (78.9 MHz, C_6D_6) spectrum for **AP4**.

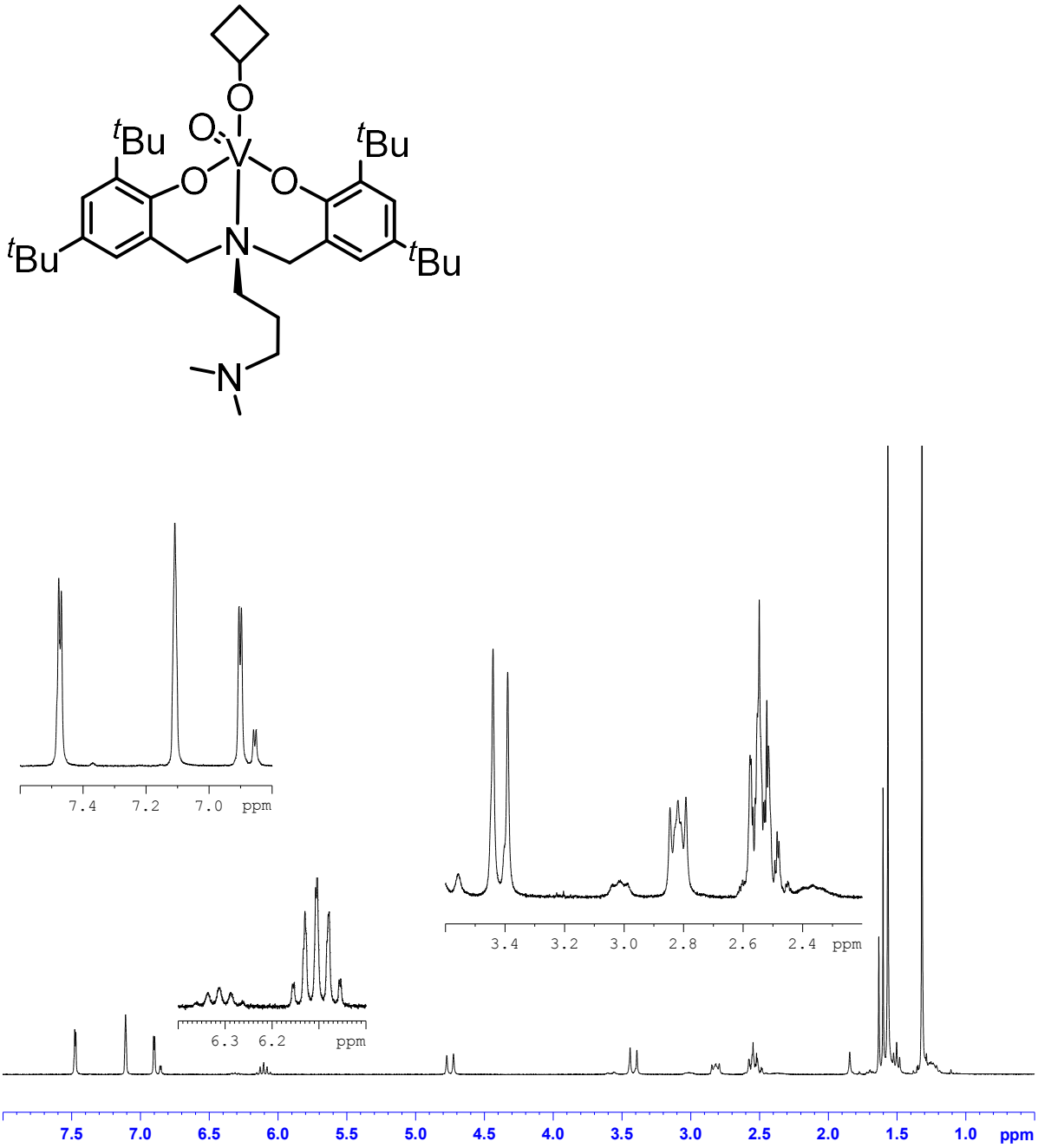

Figure A13. ^{1}H NMR (300 MHz, C_6D_6) spectrum for **AP5**.

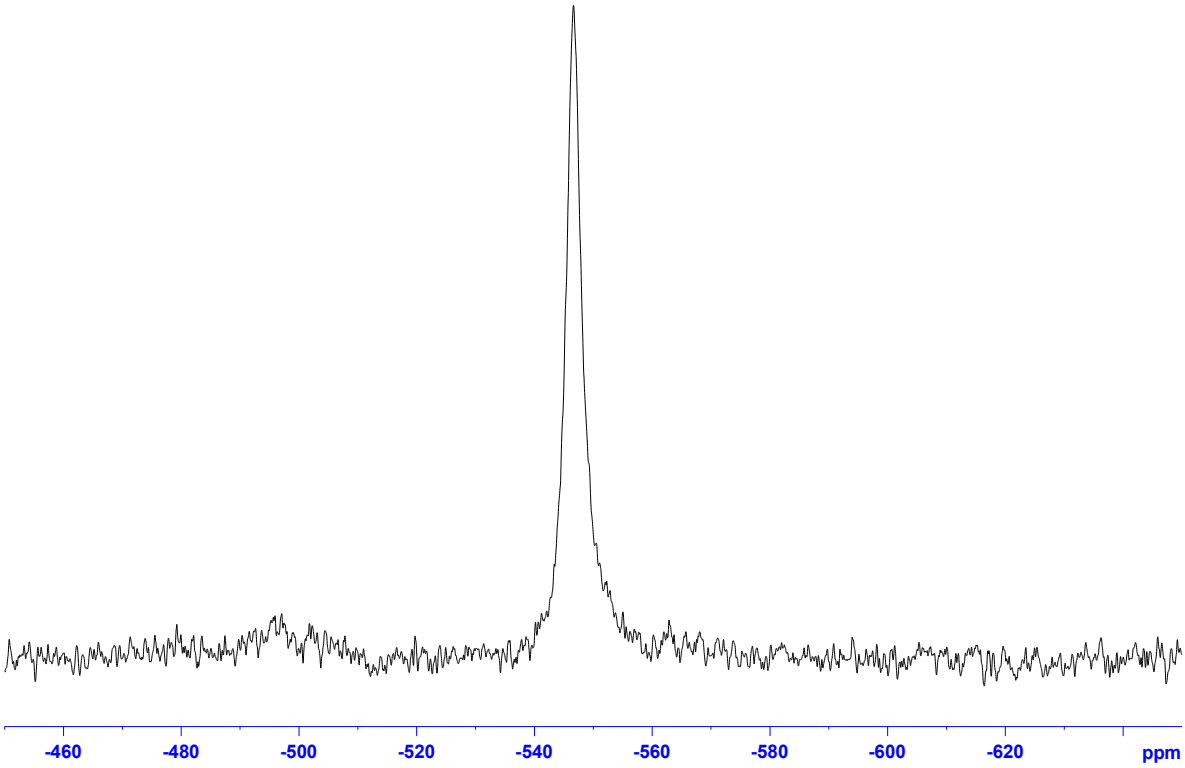

Figure A14. ^{51}V NMR (78.9 MHz, C_6D_6) spectrum for **AP5**.

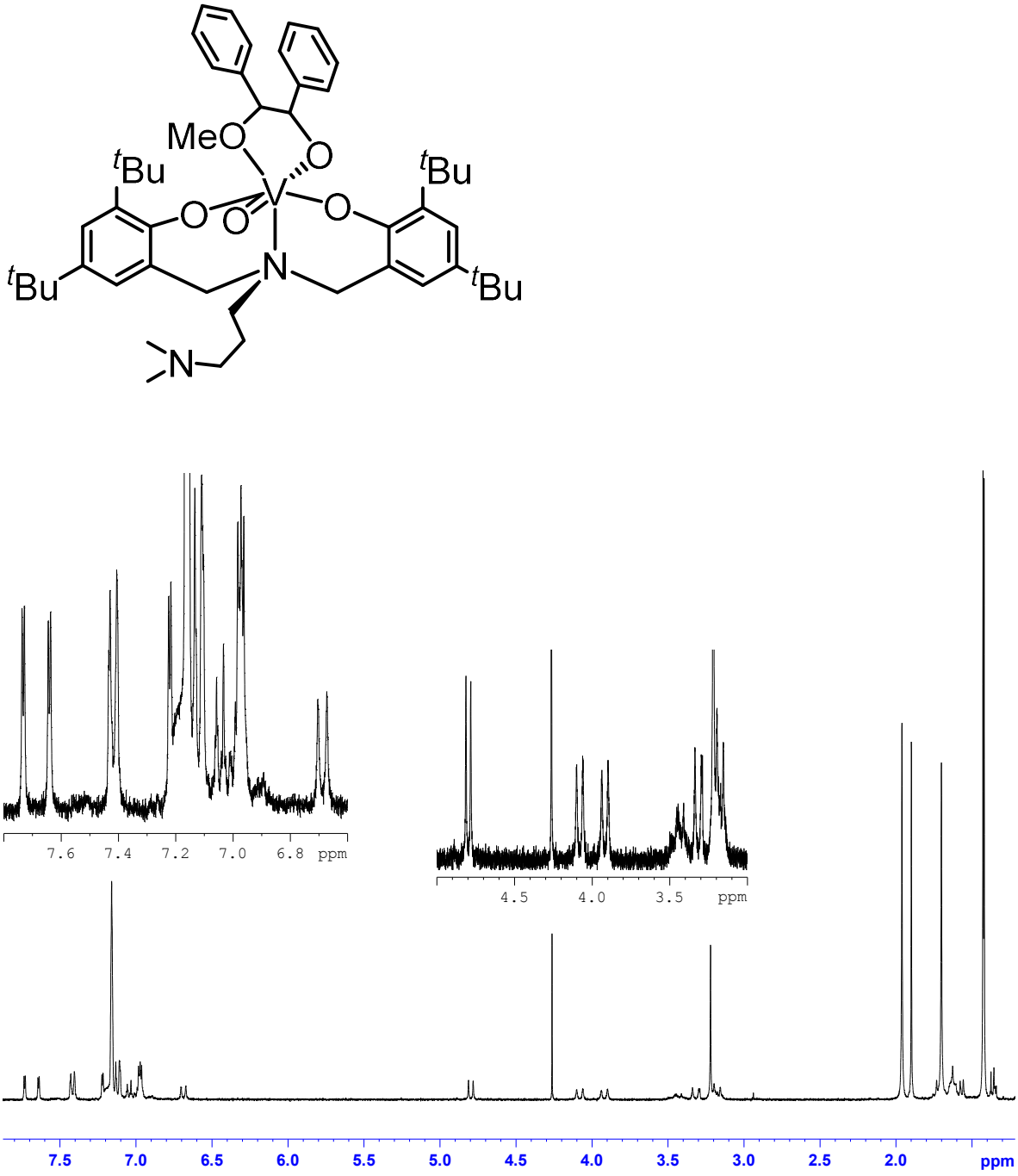

Figure A15. ^{1}H NMR (300 MHz, C_6D_6) spectrum for **AP7**.

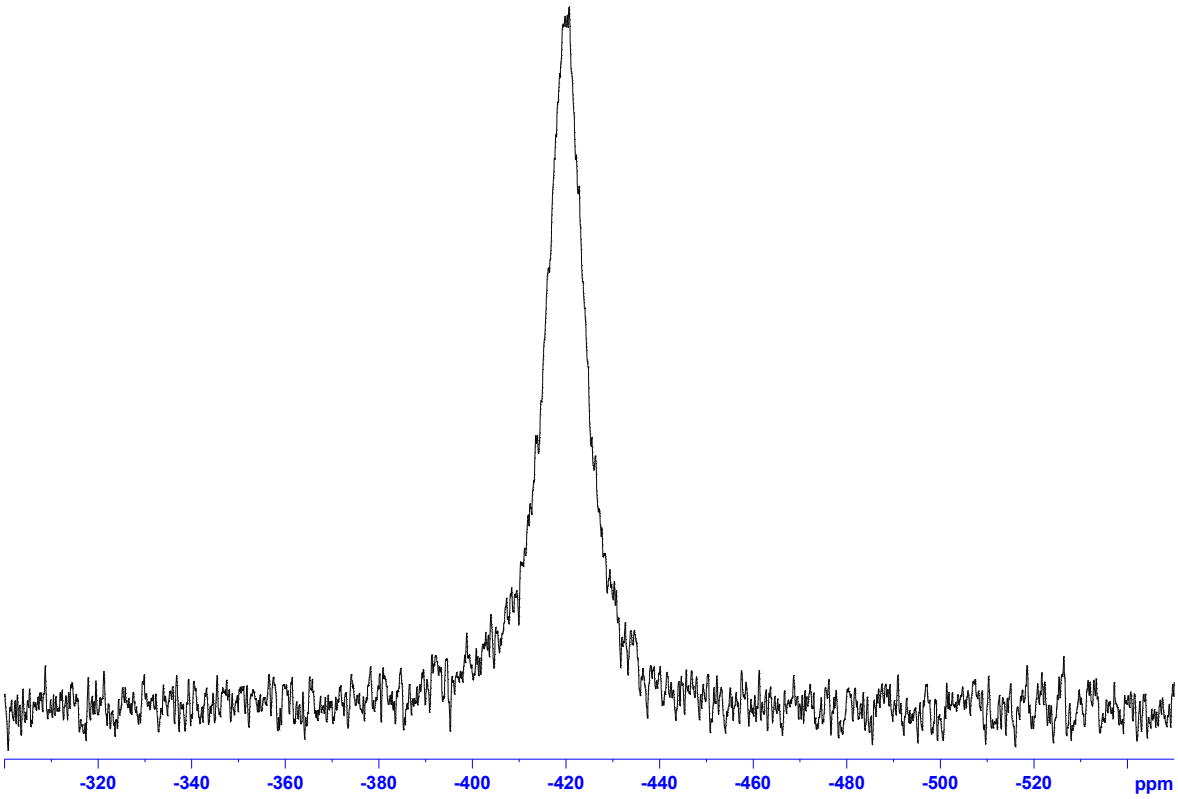

Figure A16. ^{51}V NMR (75.5 MHz, C_6D_6) spectrum for **AP7**.

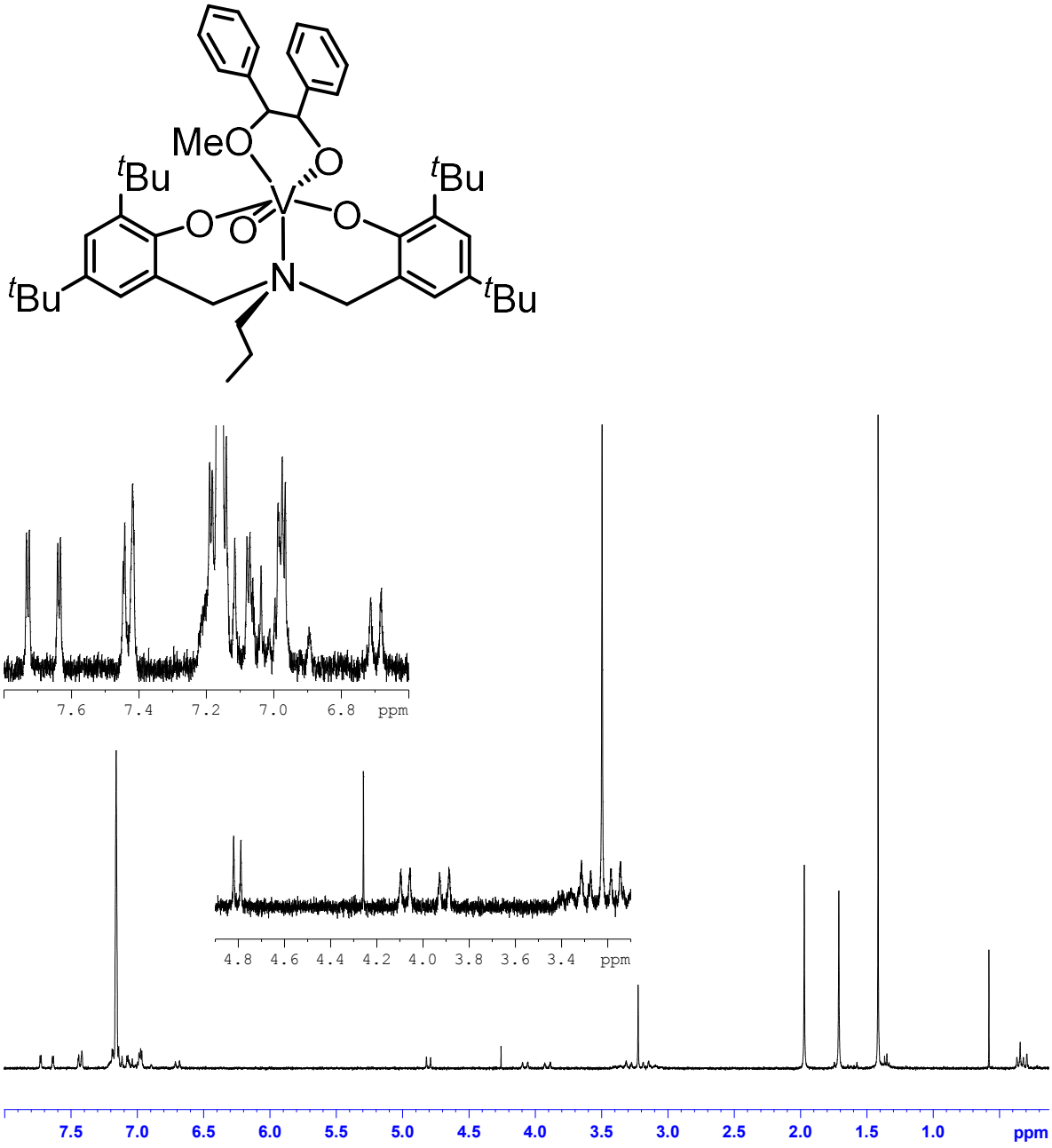

Figure A17. ^{1}H NMR (300 MHz, C_6D_6) spectrum for **AP8**.

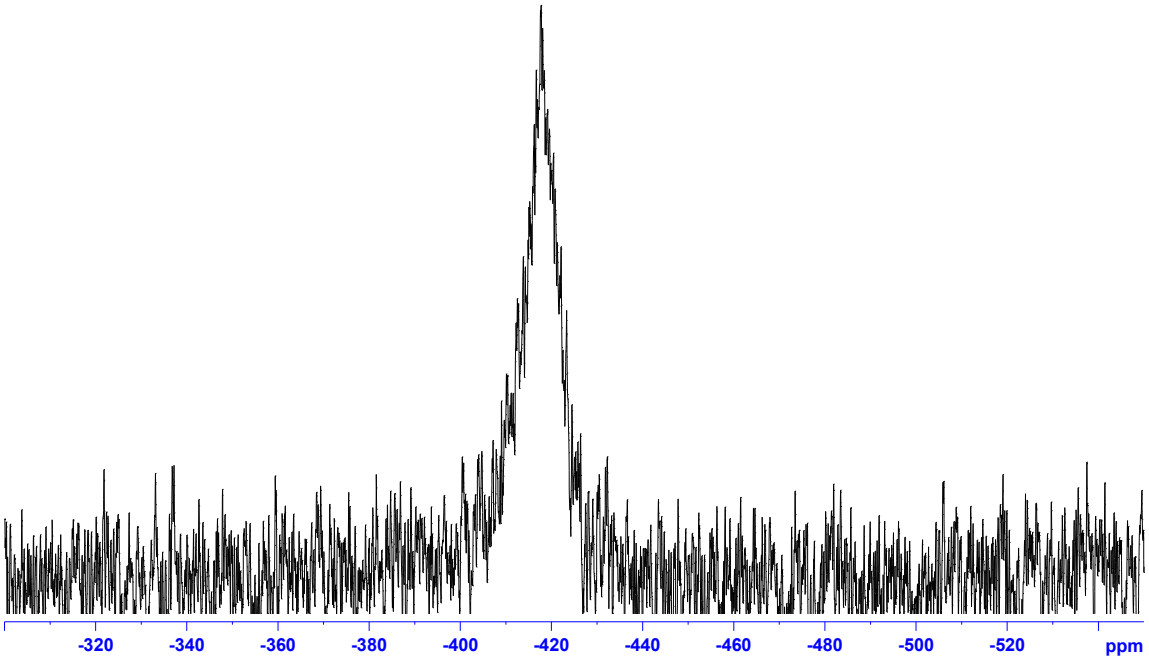

Figure A18. ^{51}V NMR (75.5 MHz, C_6D_6) spectrum for **AP8**.

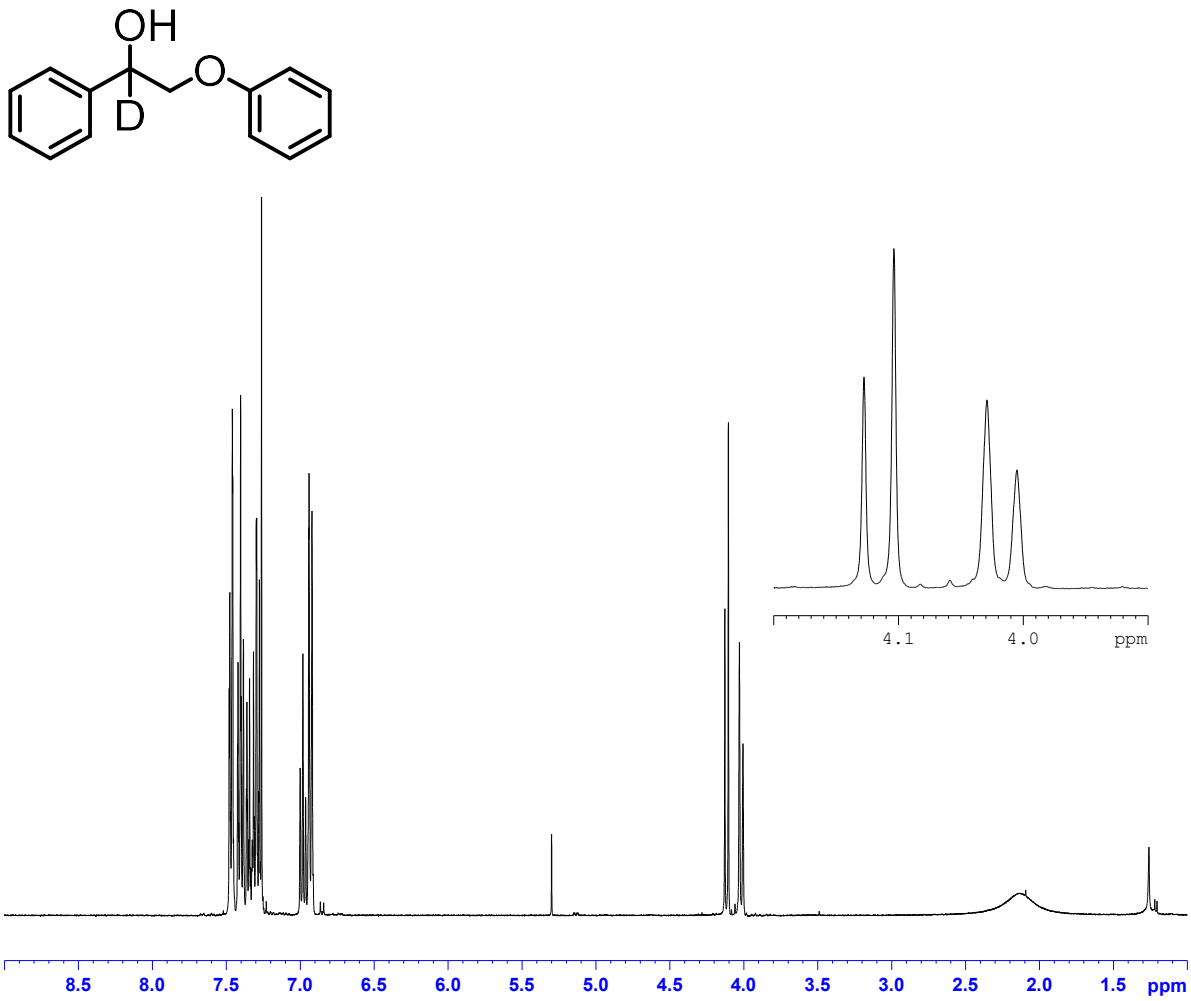

Figure A19. ^{1}H NMR (300 MHz, $CDCl_3$) spectrum for **LM3-$^{2}H_1$**.

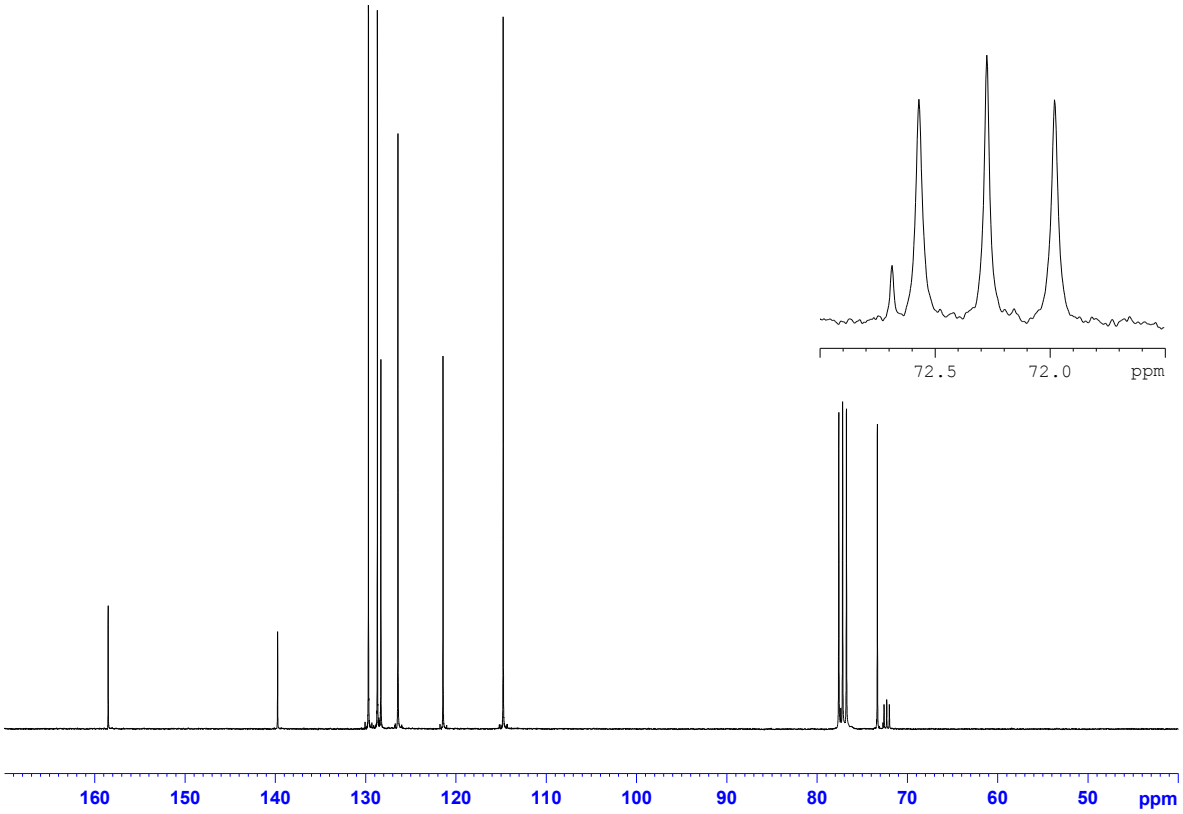

Figure A20. $^{13}C\{^{1}H\}$ NMR (75.5 MHz, $CDCl_3$) spectrum for **LM3-$^{2}H_1$**.

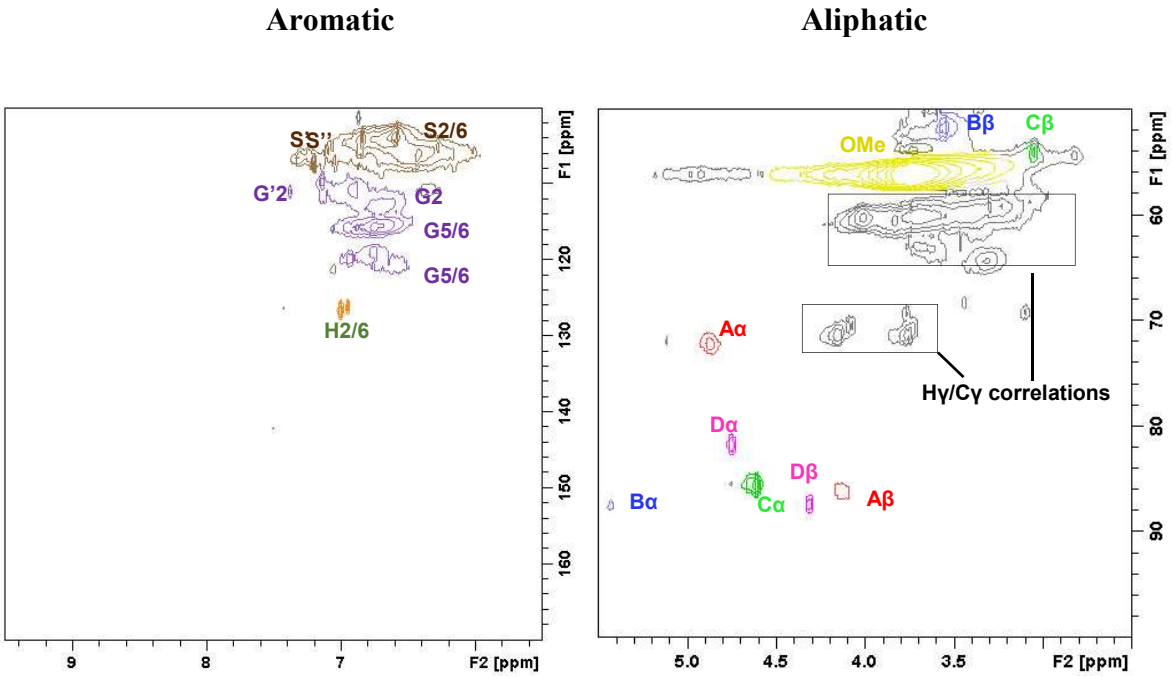

Figure A21. q-HSQC NMR spectrum (500 MHz; DMSO-d_6) of pure organosolv lignin.

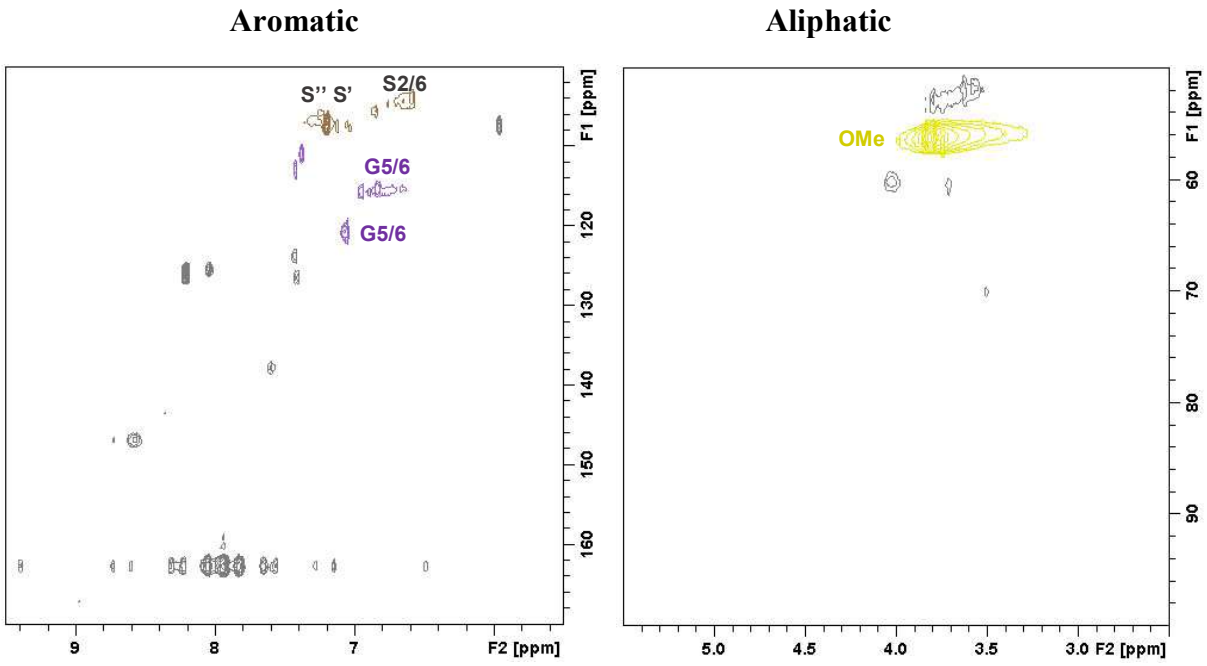

Figure A22. q-HSQC NMR spectrum (500 MHz, DMSO-d_6) for the catalytic oxidation of organosolv lignin using 10 wt. % **OV1** and 10 wt. % Et_3N. For all runs: solvent = EtOAc; temperature = 100 ºC; pressure of synthetic air = 8.2 atm; reaction time = 18 h.

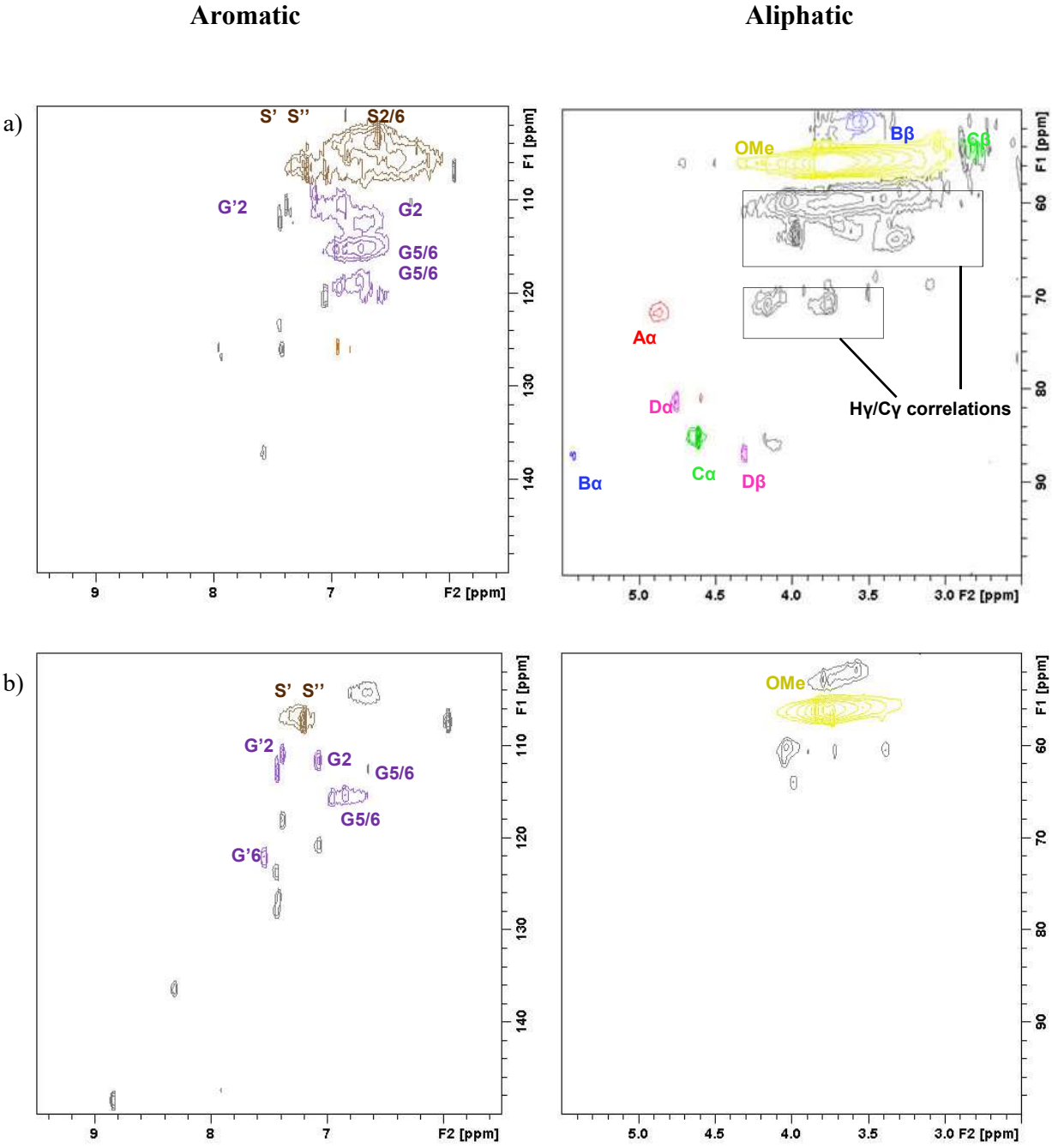

Figure A23. q-HSQC NMR spectra (500 MHz, DMSO-d_6) of organosolv lignin for a) control experiment (no catalyst **OV2**) and b) catalytic oxidation using 10 wt. % **OV2** and 10 wt. % Et_3N. For all runs: solvent: *n*-butyl acetate; temperature = 100 °C; pressure of synthetic air = 8.2 atm; reaction time = 18 h.

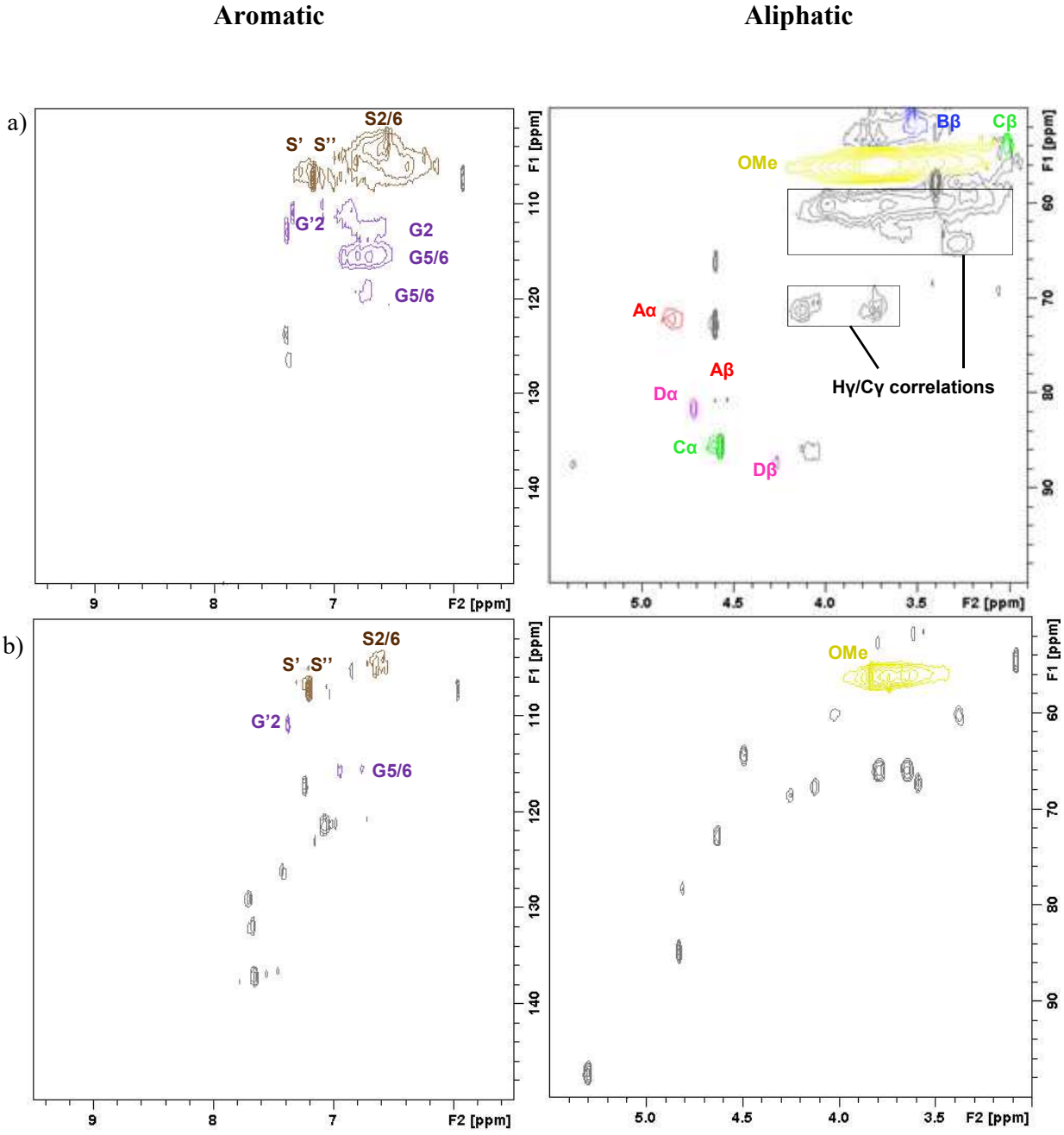

Figure A24. q-HSQC NMR spectra (500 MHz, DMSO-d_6) of organosolv lignin for a) control experiment (no catalyst, TEMPO or base) and b) catalytic oxidation with 10 wt. % CuOTf, 10 wt. % TEMPO and 100 wt. % 2,6-lutidine. For all runs: solvent = DMF; temperature = 100 ºC; pressure of synthetic air = 8.2 atm; reaction time = 18 h. Some of the correlations may be affected by paramagnetism of copper(II) traces.

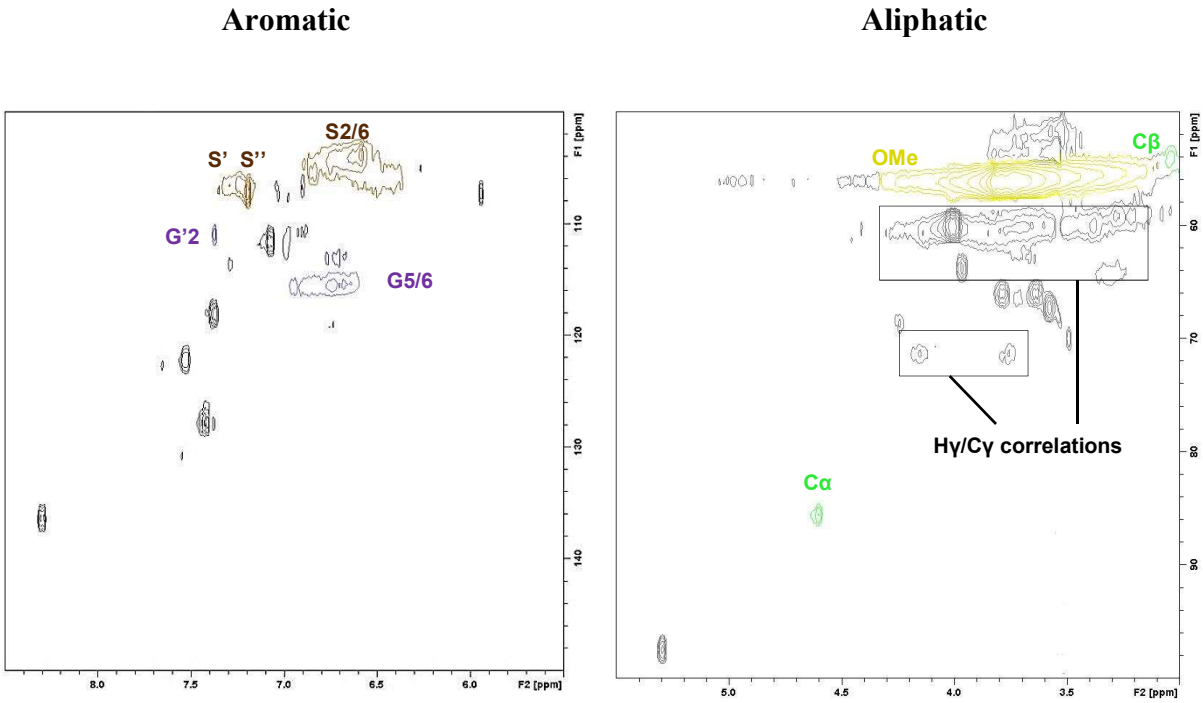

Figure A25. q-HSQC NMR spectrum (500 MHz, DMSO-d_6) for the reaction of organosolv lignin using 10 wt. % **OV2** in the absence of base. For all runs: solvent = 8:1 (v/v) EtOAc/THF; temperature = 80 ºC; atmospheric pressure of air; reaction time = 24 h.

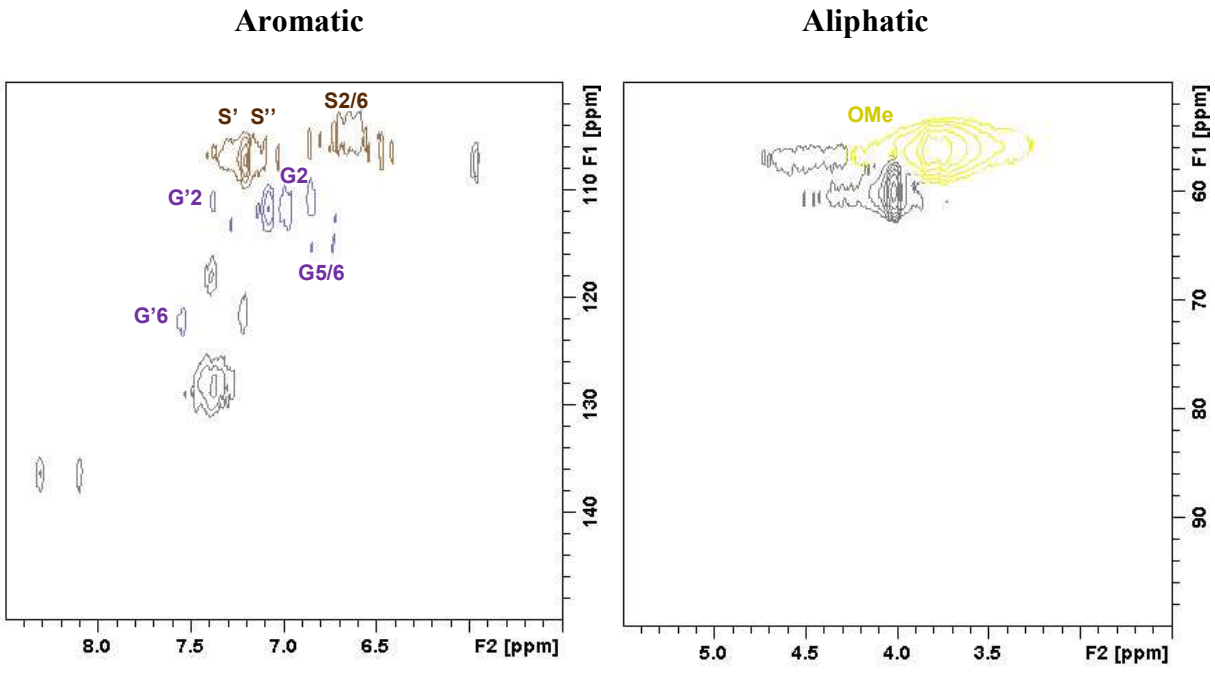

Figure A26. q-HSQC NMR spectrum (500 MHz, DMSO-d_6) for the catalytic oxidation of organosolv lignin using 10 wt. % **OV2**, 10 wt. % Et_3N. For all runs: solvent = EtOAc; temperature = 100 °C; pressure of synthetic air = 8.2 atm; reaction time = 4 h.

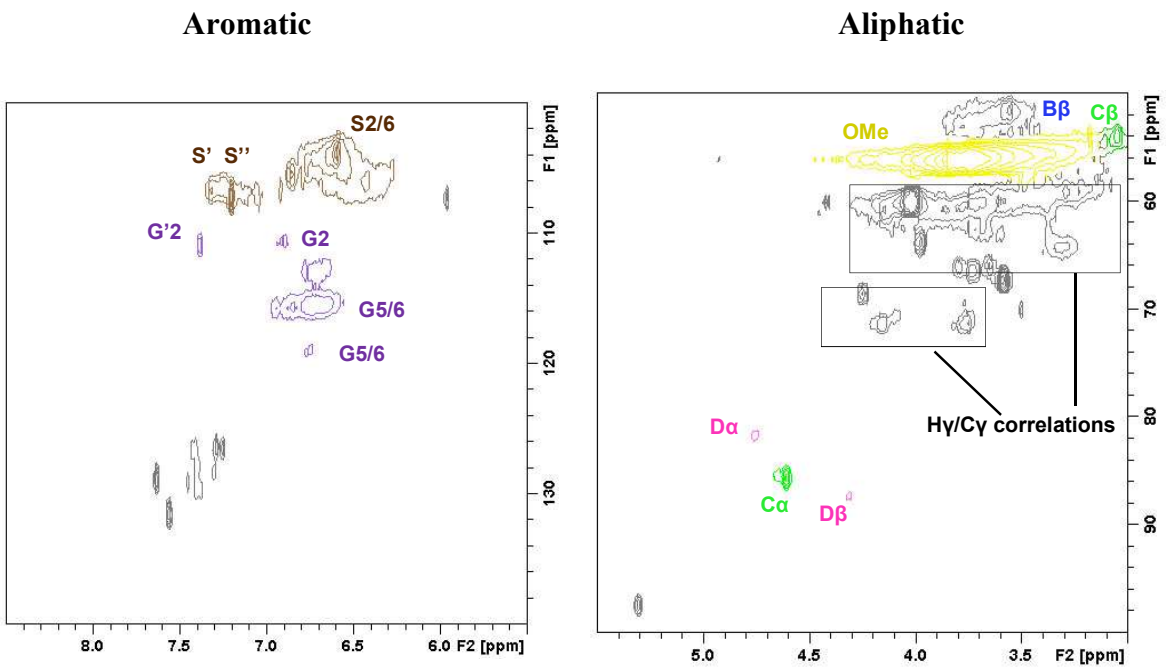

Figure A27. q-HSQC NMR spectrum (500 MHz, DMSO-d_6) of the reaction of organosolv lignin using catalyst **OVS**; 10 wt. % **OVS**. For all runs: solvent = 8:1 (v/v) EtOAc/THF; temperature = 80 ^{o}C; sealed vial under atmospheric pressure of air; reaction time = 24 h.

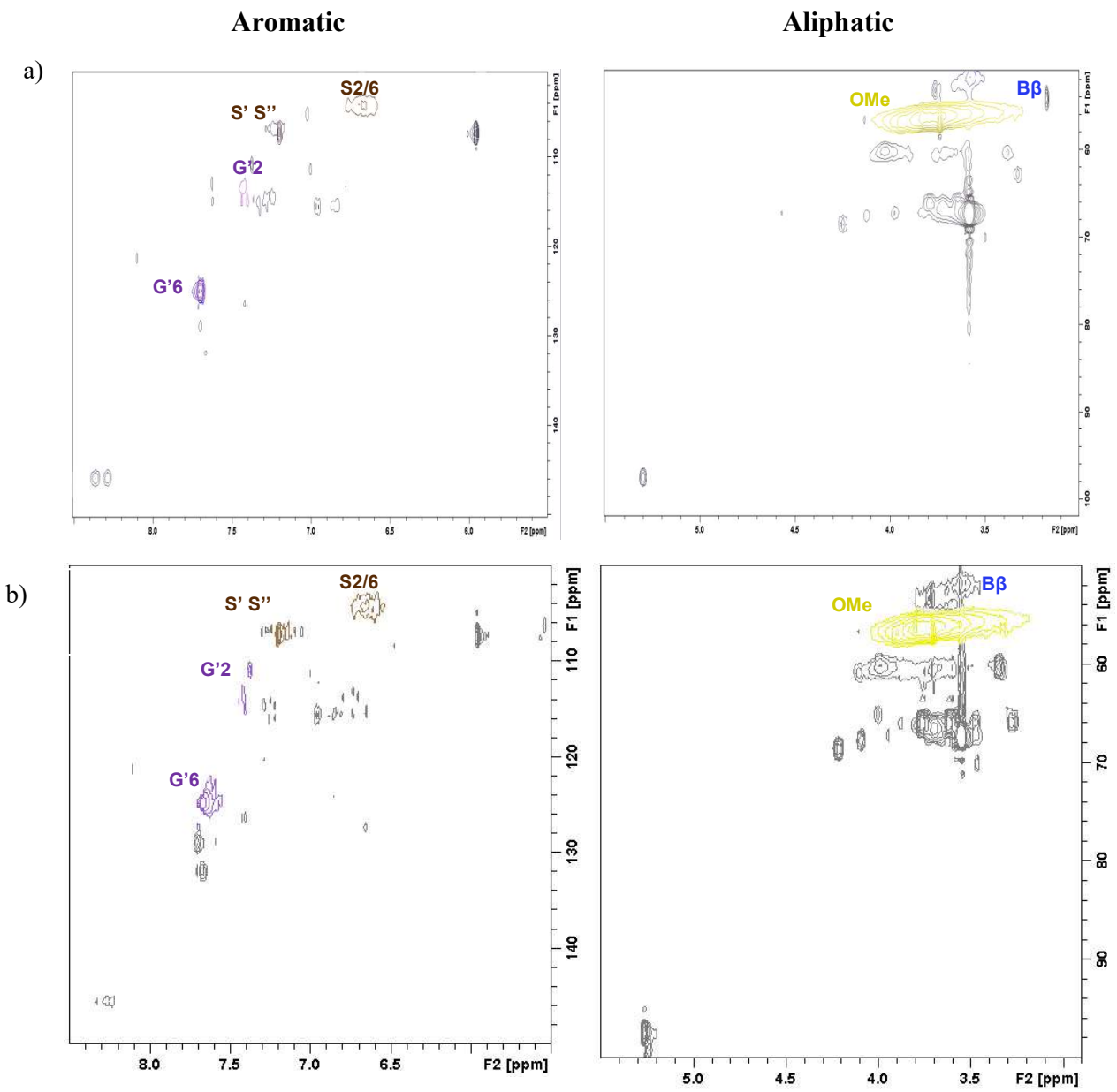

Figure A28. q-HSQC NMR spectrum (500 MHz, DMSO-d_6) of the reaction of organosolv lignin for a) control experiment (no 4-acetamido-TEMPO) and b) 5 wt. % 4-acetamido-TEMPO, 10 wt. % HNO_3 (70%), 10 wt. % HCl (37%). For all runs: solvent = 19:1 (v/v) CH_3CN/H_2O; temperature = 65 ºC; pressure of synthetic air = 8.2 atm; reaction time = 24 h.

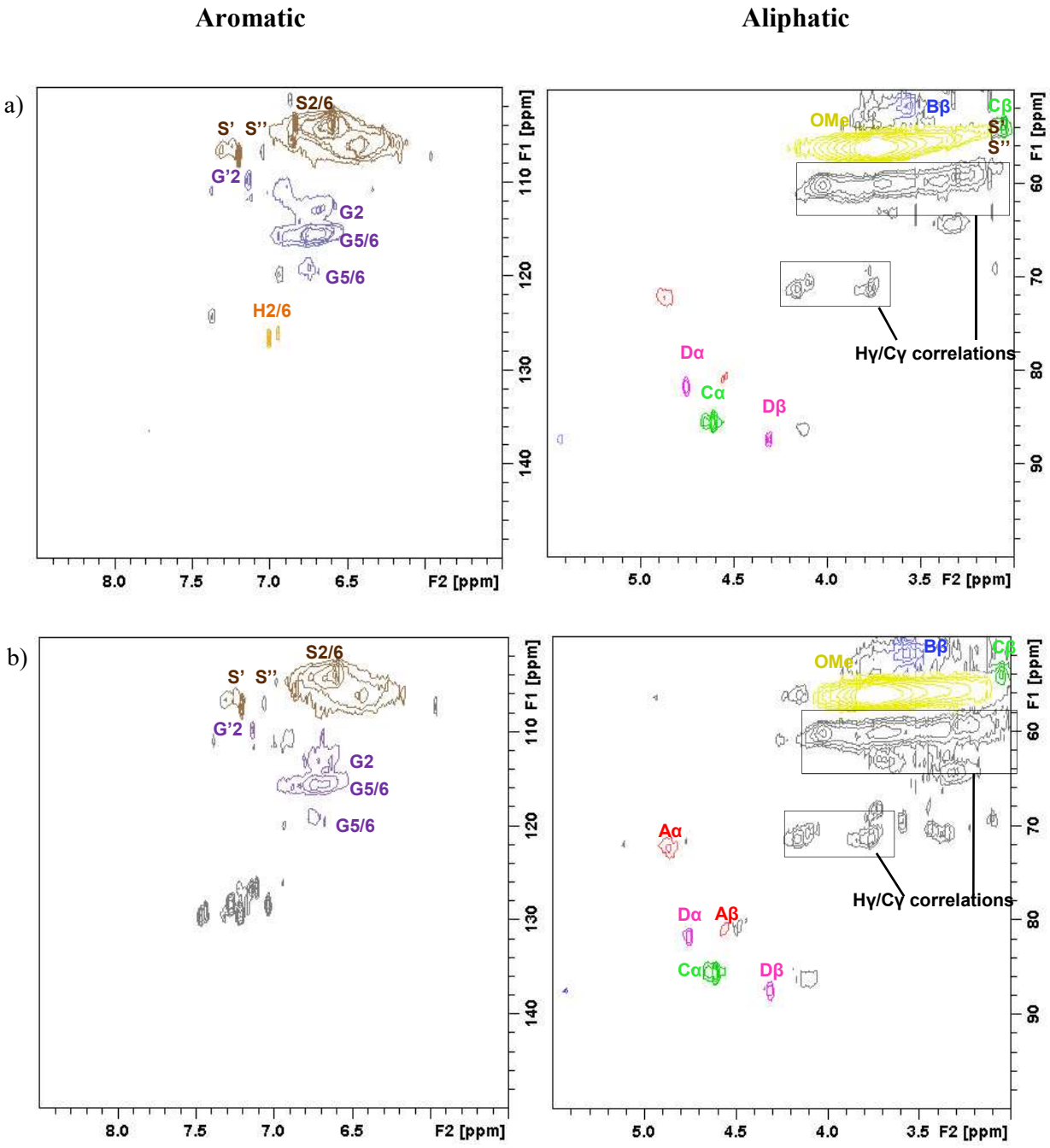

Figure A29. q-HSQC NMR spectrum (500 MHz, DMSO-d_6) of the reaction of organosolv lignin for a) control experiment (no catalyst **CoL**) and b) using 10 wt. % **CoL** and 100 wt. % pyridine. For all runs: solvent = 1:1 (v/v) MeOH/DMSO; temperature = 100 ºC; pressure of synthetic air = 8.2 atm; reaction time = 18 h.

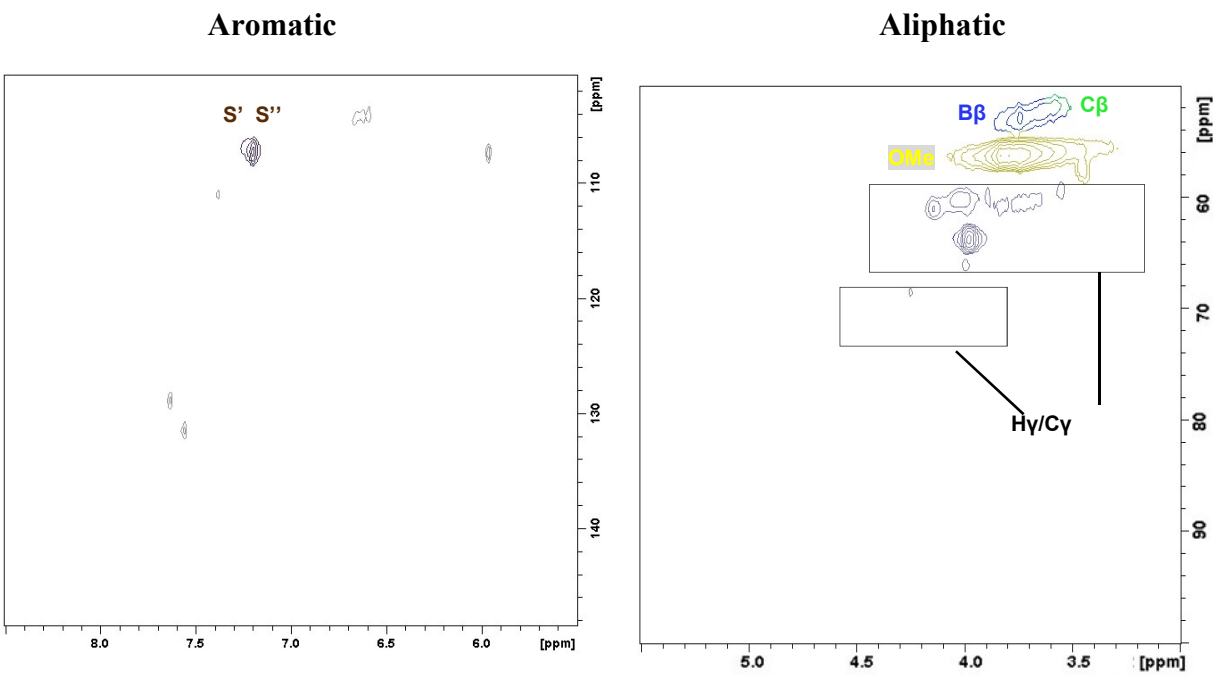

Figure A30. q-HSQC NMR spectrum (500 MHz, DMSO-d_6) of the reaction of organosolv lignin for 10 wt. % **AP1**. For all runs: solvent = EtOAc; temperature = 100 °C; pressure of synthetic air = 8.2 atm; reaction time = 18 h.

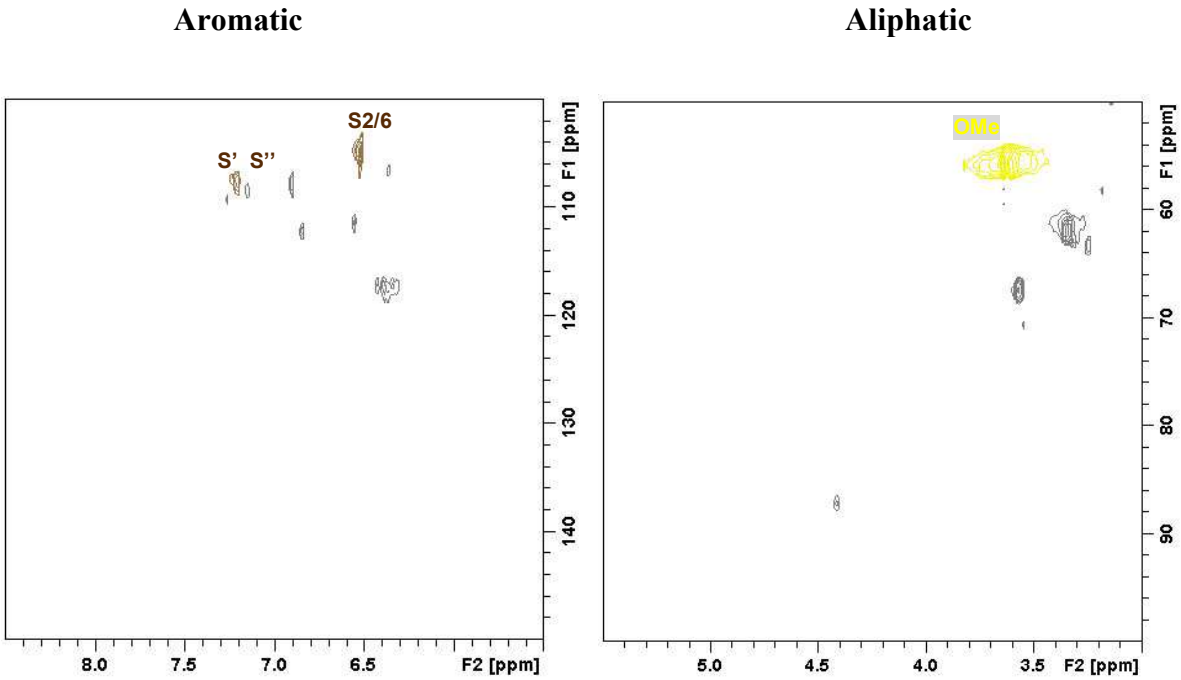

Figure A31. q-HSQC NMR spectrum (500 MHz, DMSO-d_6) of the reaction of organosolv lignin using the Chornet method (135 wt. % NaOH, 5 wt. % $CuSO_4$ and 0.5 wt. % $FeCl_3$). For all runs: solvent = THF; temperature = 100 °C; pressure of synthetic air = 8.2 atm; reaction time = 18 h.

Aromatic **Aliphatic**

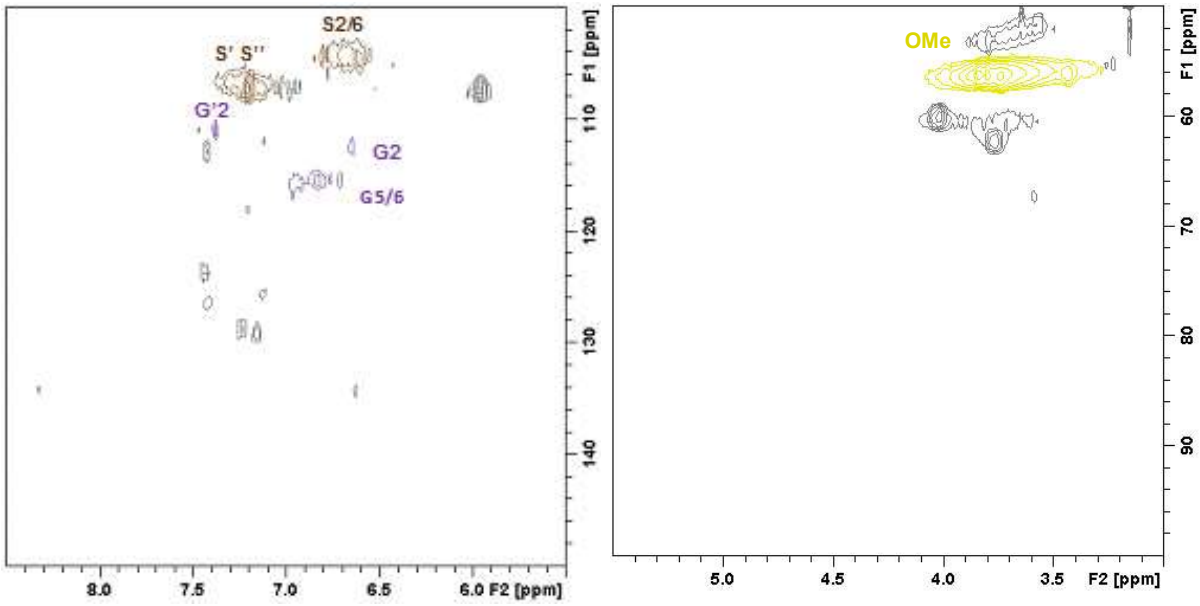

Figure A32. q-HSQC NMR spectrum (500 MHz, DMSO-d_6) of the catalytic oxidation of organosolv lignin using 10 wt. % **OV2**, 10 wt. % Et_3N. For all runs: solvent = DMSO; temperature = 100 ºC; pressure of synthetic air = 8.2 atm; reaction time = 18 h.

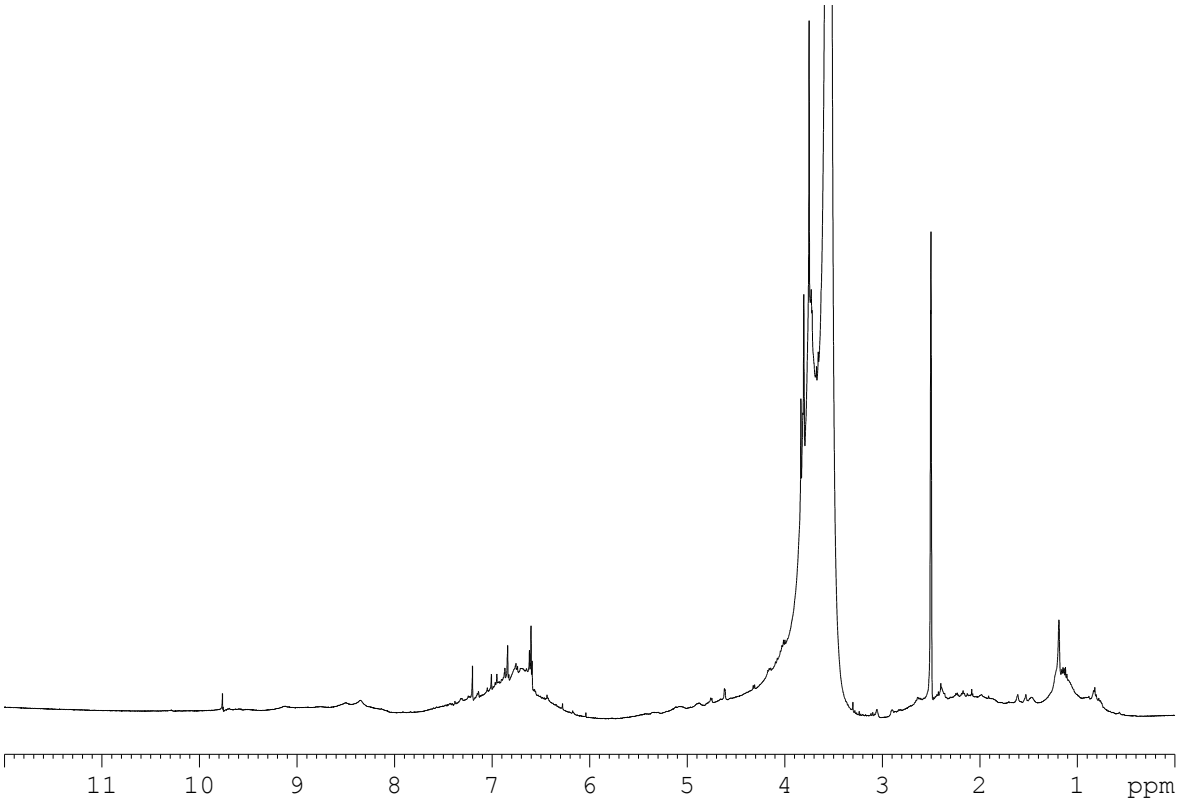

Figure A33. ^{1}H NMR spectrum (500 MHz, DMSO-d_6) of organosolv lignin

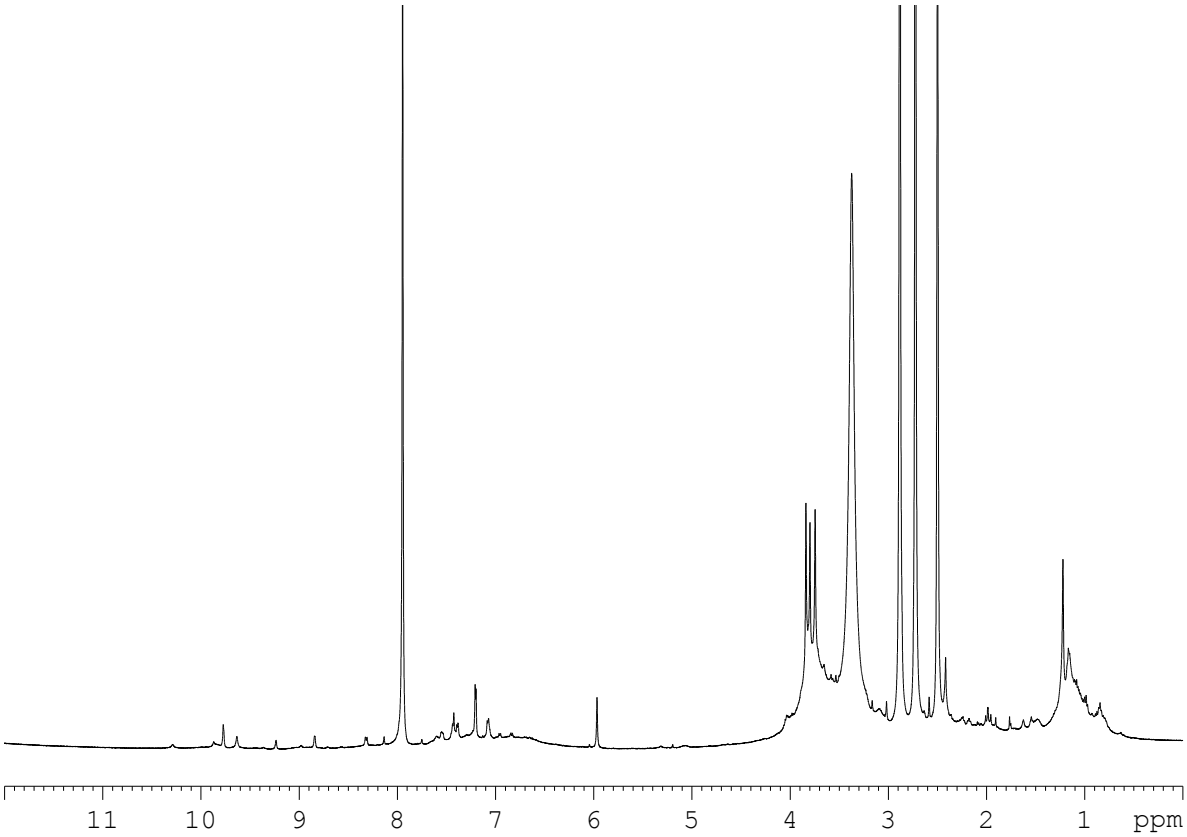

Figure A34. ^{1}H NMR spectrum (500 MHz, DMSO-d_6) of the catalytic oxidation of organosolv lignin using 10 wt. % **OV2** and 10 wt. % Et_3N. For all runs: solvent = EtOAc; temperature = 100 ^{o}C; pressure of synthetic air = 8.2 atm; reaction time = 18 h.

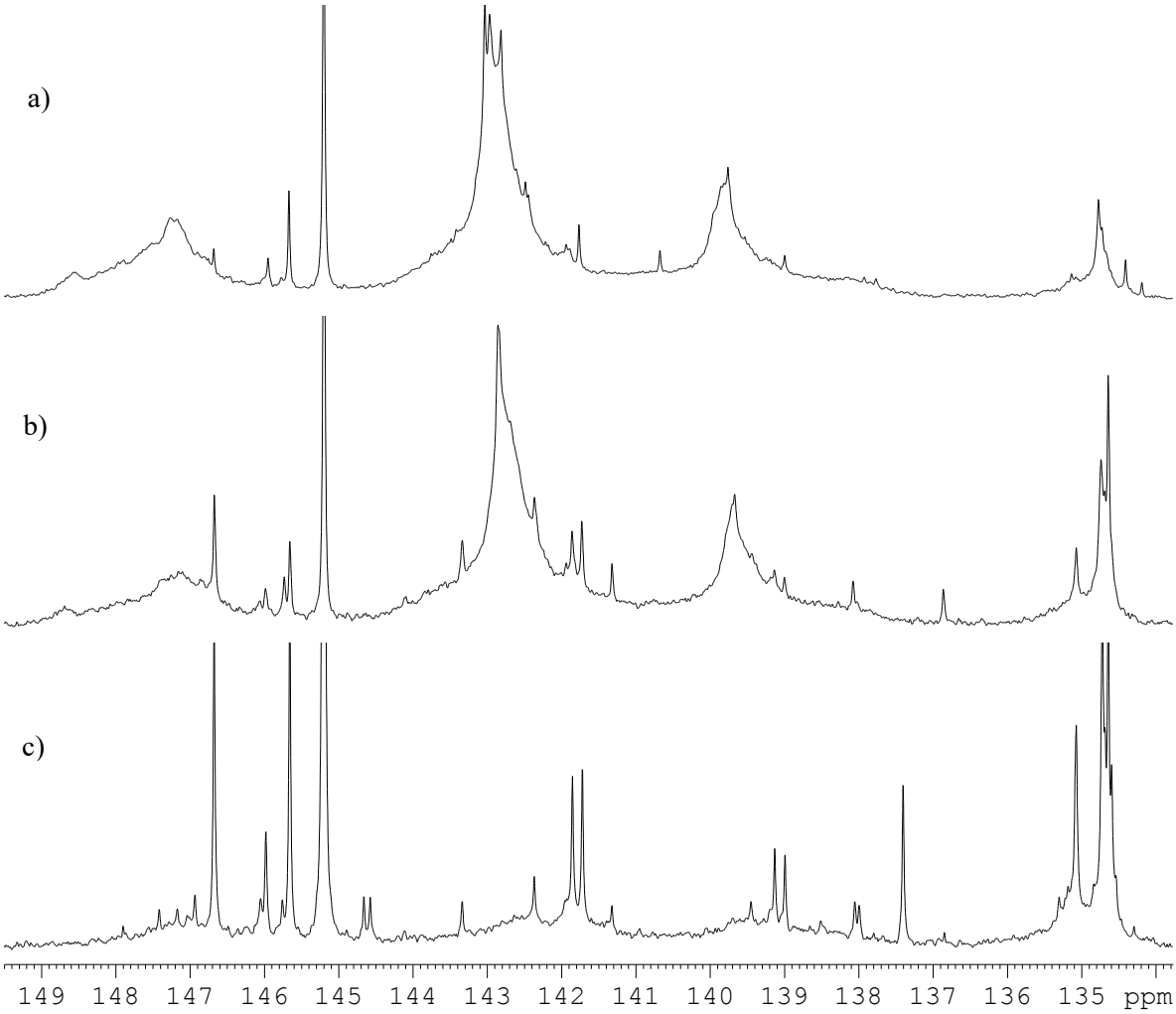

Figure A35. Quantitative $^{31}P\{^{1}H\}$ NMR spectra (121 MHz, line broadening 2.5 Hz) of derived phosphite esters from a) organosolv lignin, b) control experiment (base with no catalyst) and c) residue after the catalytic lignin oxidation using 10 wt. % **OV2** and 10 wt. % Et_3N. For all runs: solvent = EtOAc; temperature = 100 ºC; pressure of synthetic air = 8.2 atm; reaction time = 18 h.

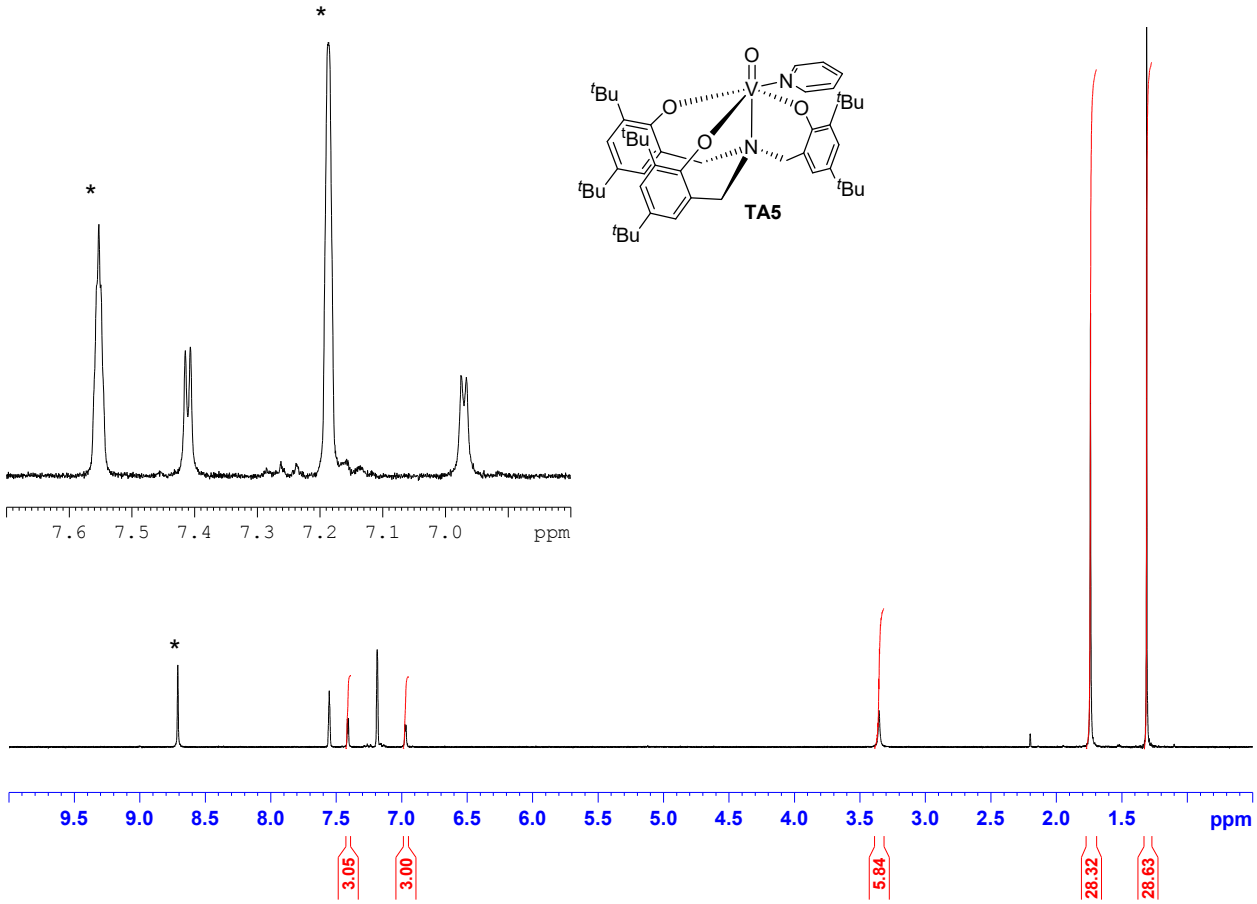

Figure A36. ^{1}H NMR spectrum (300 MHz, pyr-d_5) for **TA5**. Solvent peaks denote by (*).

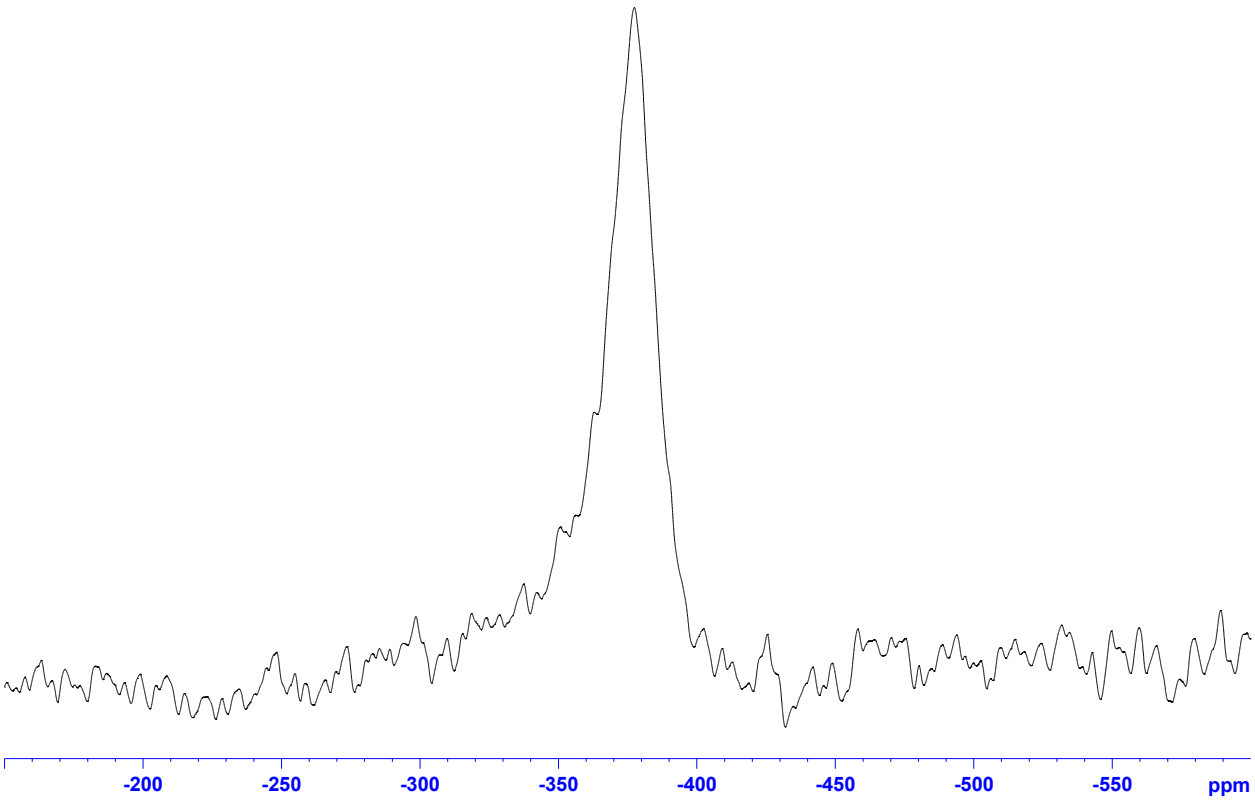

Figure A37. ^{51}V NMR spectrum (78.9 MHz, pyr-d_5) for **TA5**.

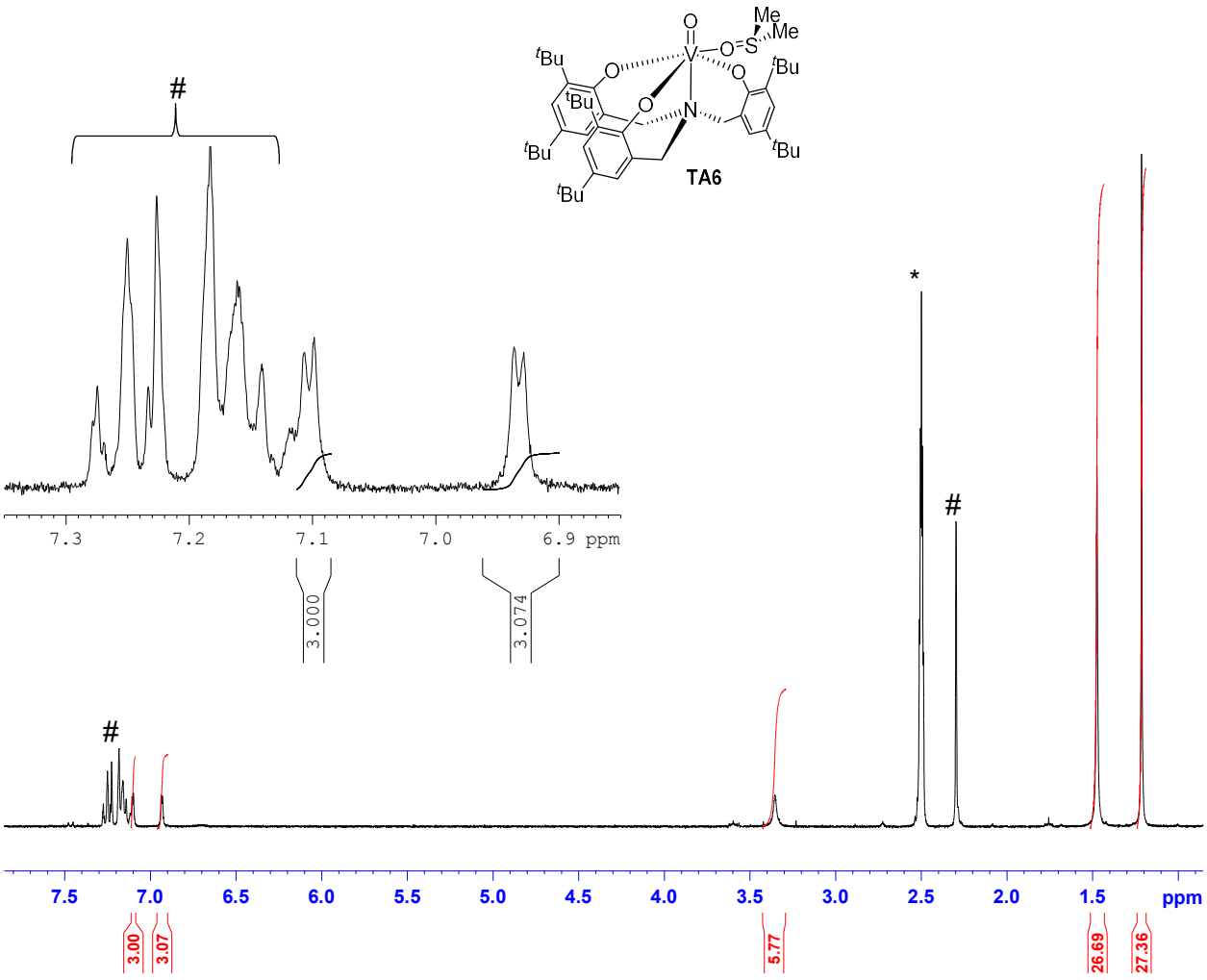

Figure A38. ^{1}H NMR spectrum (300 MHz, DMSO-d_6) for **TA6**. Solvent peaks denote by (*) and co-crystallization solvent, toluene, by (#)

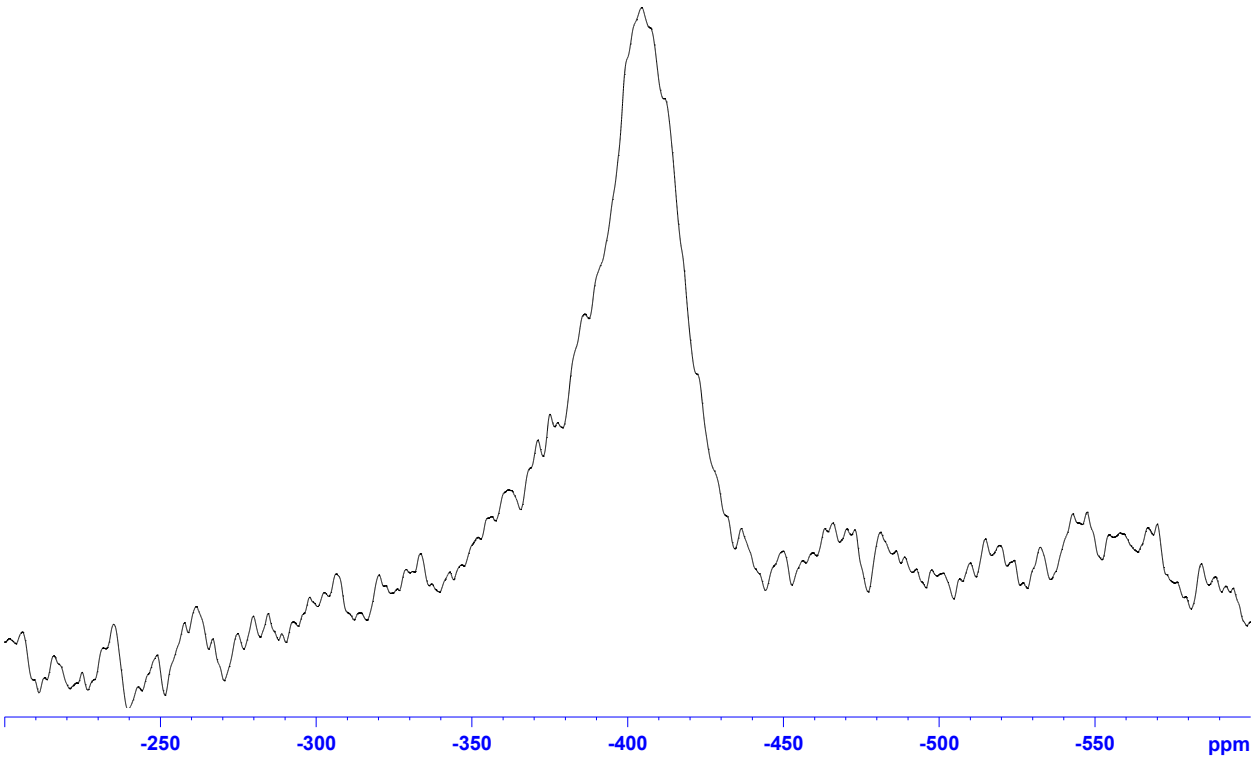

Figure A39. ^{51}V NMR spectrum (78.9 MHz, DMSO-d_6) for **TA6**.

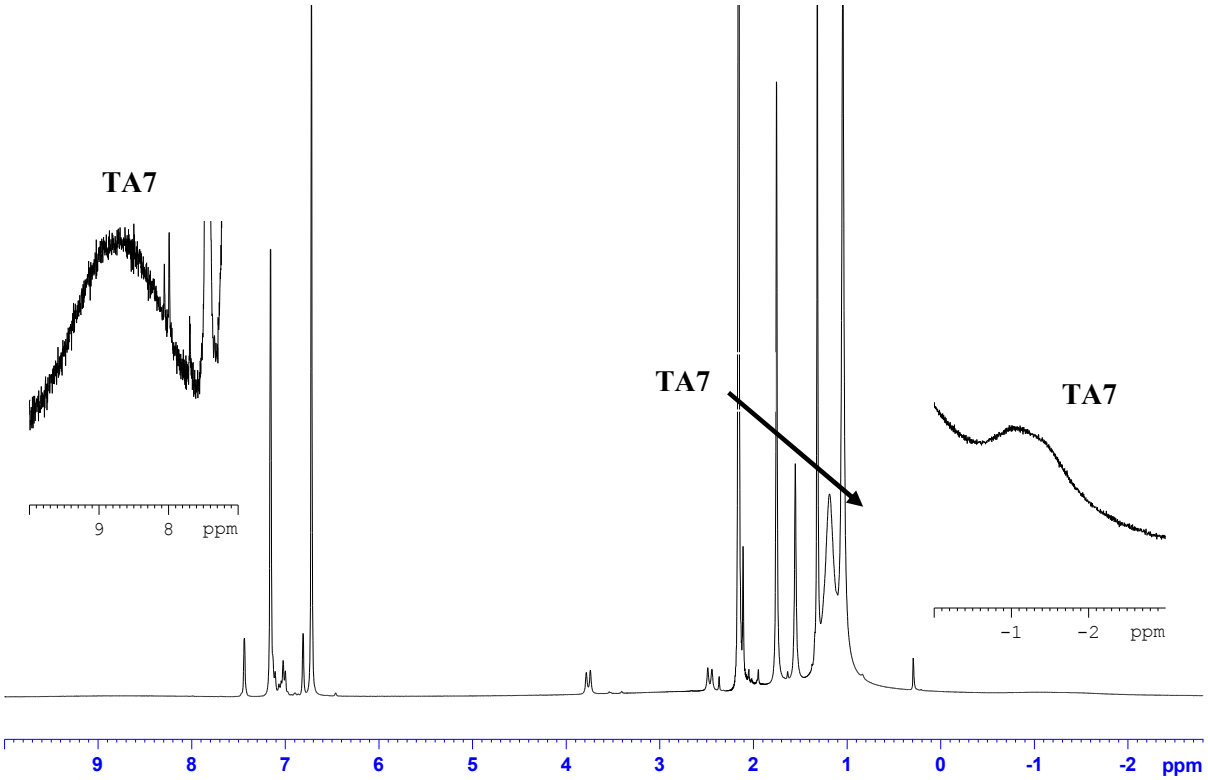

Figure A40. ^{1}H NMR (300 MHz, C_6D_6) spectrum for the reaction mixture of pinacol and **TA2** under nitrogen (80 ºC, 20 h) showing the formation of the paramagnetic specie **TA7**.

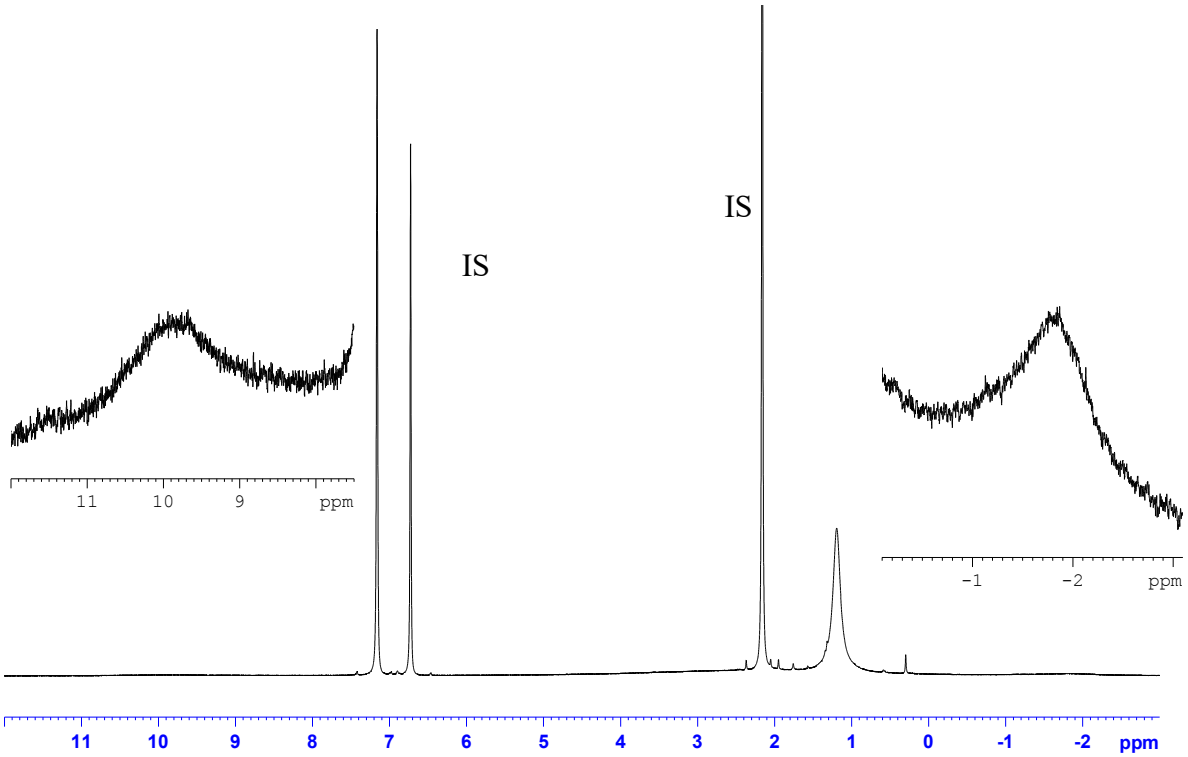

Figure A41. ^{1}H NMR (300 MHz, C_6D_6) spectrum for the paramagnetic complex **TA7** (IS = internal standard).

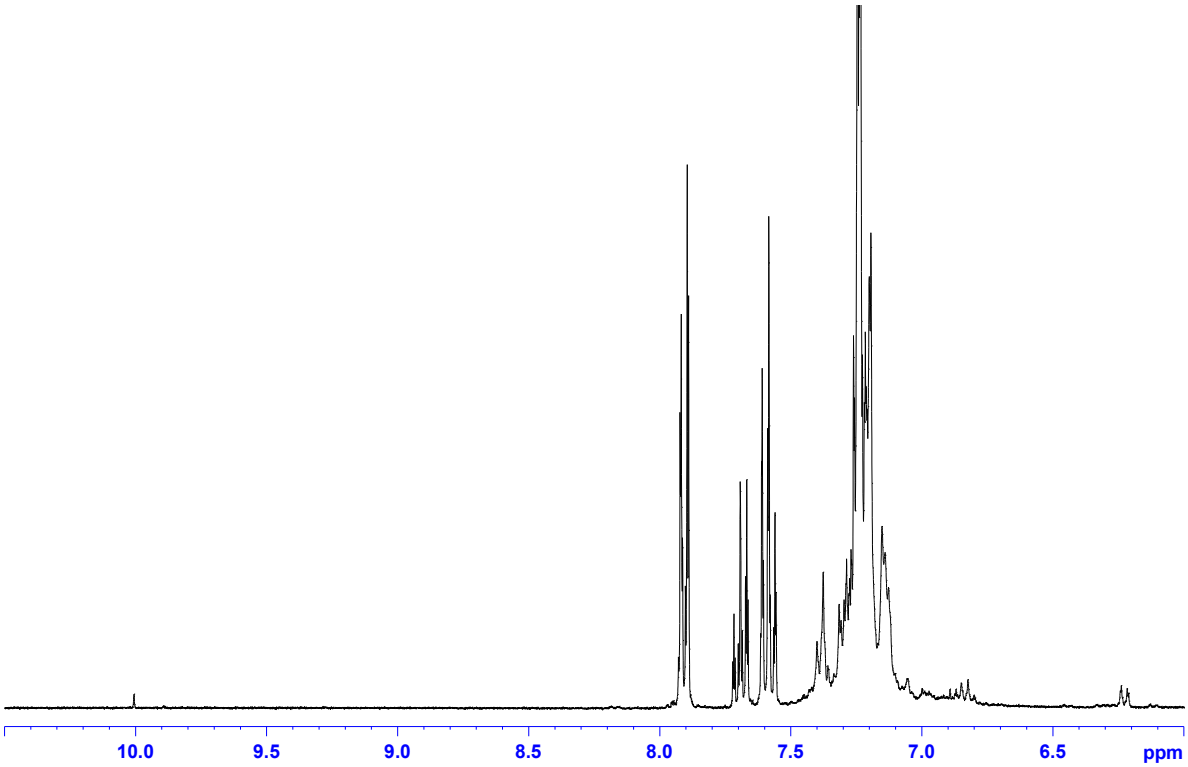

Figure A42. ^{1}H NMR (300 MHz, CD_3CN) spectrum for the reaction mixture of the aerobic oxidation of hydrobenzoin(1,2-^{2}H) with 1 mol % **TA2** (CD_3CN, 80 ^{o}C, 7 h).

GPC Data

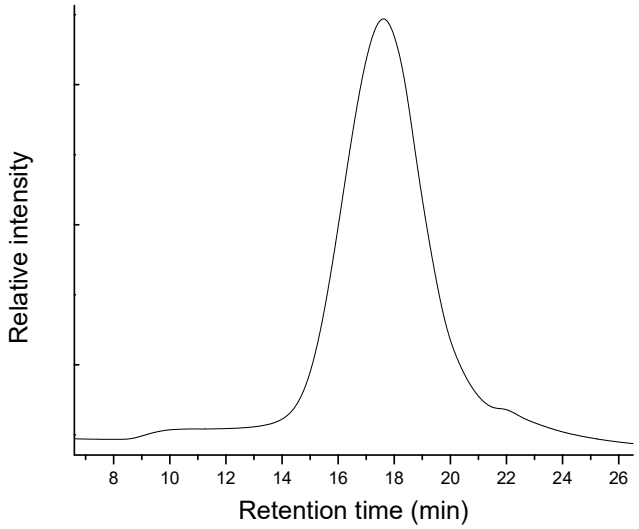

Figure A43. GPC chromatogram (THF solvent, elution rate: 1 mL/min, 254.4 nm detection) for organosolv lignin.

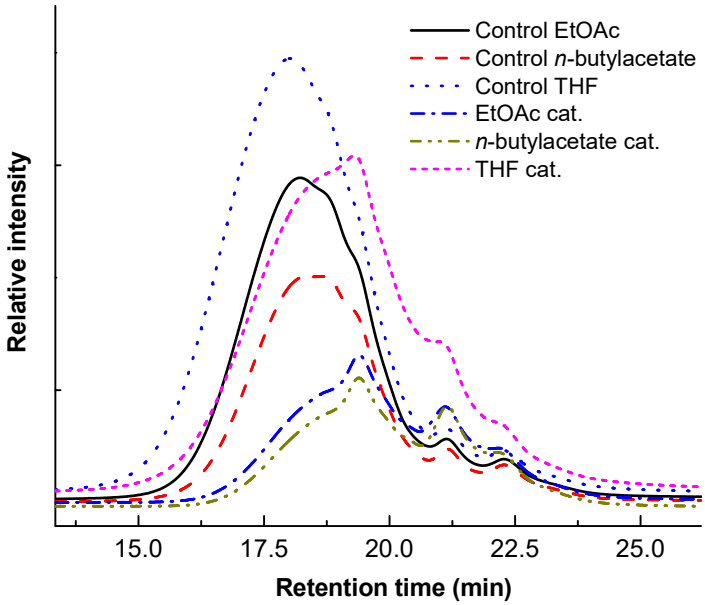

Figure 44. GPC chromatograms (THF solvent, elution rate: 1 mL/min, 254.4 nm detection) for the catalytic oxidation of organosolv lignin; solvent screening using 10 wt. % catalyst **OV2** and 10 wt. % Et_3N compared with the control experiment (no catalyst). For all runs: temperature = 100 ºC; pressure of synthetic air = 8.2 atm; reaction time = 18 h.

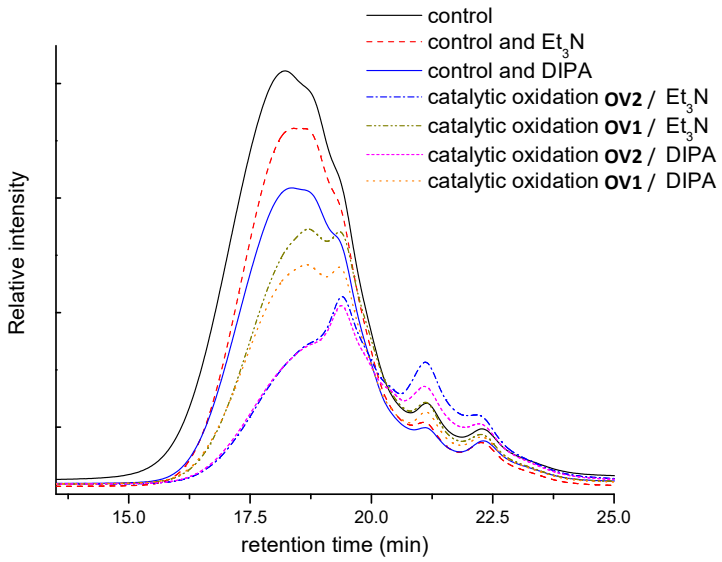

Figure A45. GPC chromatograms (THF solvent, elution rate: 1 mL/min, 254.4 nm detection) for the catalytic oxidation of organosolv lignin using different bases; 10 wt. % catalyst **OV1** or **OV2** and 10 wt. % base compared with the control experiment (no catalyst). For all runs: solvent = EtOAc; temperature = 100 ºC; pressure of synthetic air = 8.2 atm; reaction time = 18 h.

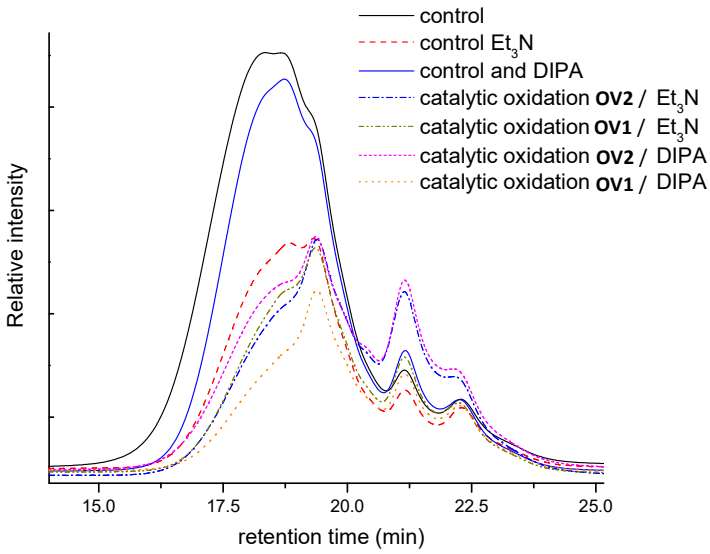

Figure A46. GPC chromatograms (THF solvent, elution rate: 1 mL/min, 254.4 nm) for the catalytic oxidation of organosolv lignin using different bases; 10 wt. % catalyst **OV1** or **OV2** and 10 wt. % base compared with the control experiment (no catalyst). For all runs: solvent = *n*-butyl acetate; temperature = 100 ºC; pressure of synthetic air = 8.2 atm; reaction time = 18 h.

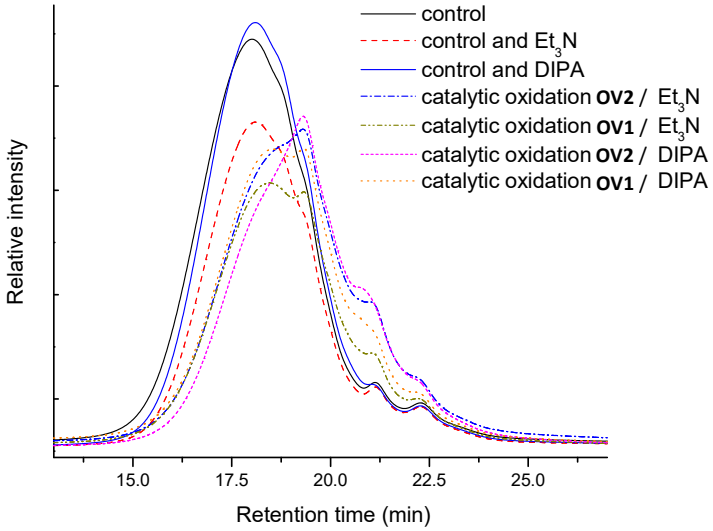

Figure A47. GPC chromatograms (THF solvent, elution rate: 1 mL/min, 254.4 nm detection) for the catalytic oxidation of organosolv lignin using different bases; 10 wt. % catalyst **OV1** or **OV2** and 10 wt. % base compared with the control experiment (no catalyst). For all runs: solvent = THF; temperature = 100 ºC; pressure of synthetic air = 8.2 atm; reaction time = 18 h.

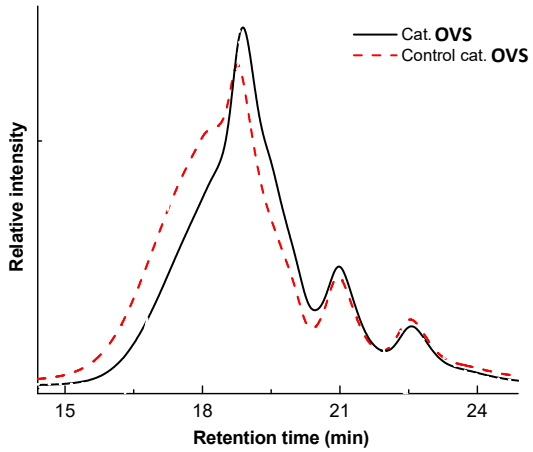

Figure A48. GPC chromatograms (THF solvent, elution rate: 1 mL/min, 254.4 nm detection) for the reaction of organosolv lignin using catalyst **OVS**; 10 wt. % **OVS**. For all runs: solvent = 8:1 (v/v) EtOAc/THF; temperature = 80 ºC; sealed vial under atmospheric pressure of air; reaction time = 24 h.

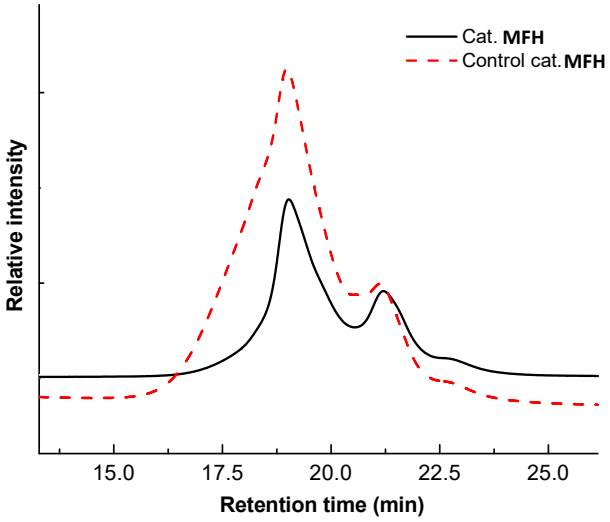

Figure A49. GPC chromatograms (THF solvent, elution rate: 1 mL/min, 254.4 nm detection) for the reaction of organosolv lignin using the metal-free system **MFH**, 5 wt. % 4-acetamido-TEMPO, 10 wt. % nitric acid (70%), 10 wt. % HCl (37%). For all runs: solvent = 19:1 (v/v) CH_3CN/H_2O; temperature = 65 ºC; pressure of synthetic air = 8.2 atm; reaction time = 24 h.

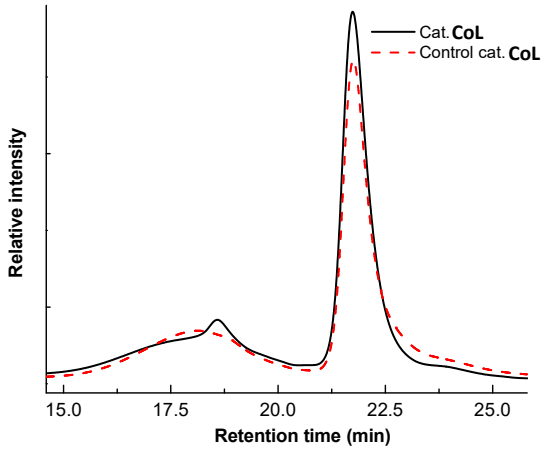

Figure A50. GPC chromatograms (THF solvent, elution rate: 1 mL/min, 254.4 nm detection) for reaction of organosolv lignin using catalyst **CoL**; 10 wt % **CoL** and 100 wt. % pyridine. For all runs: solvent = 1:1 (v/v) MeOH/DMSO; temperature = 100 ºC; pressure of synthetic air = 8.2 atm; reaction time = 18 h.

Calibration Curves

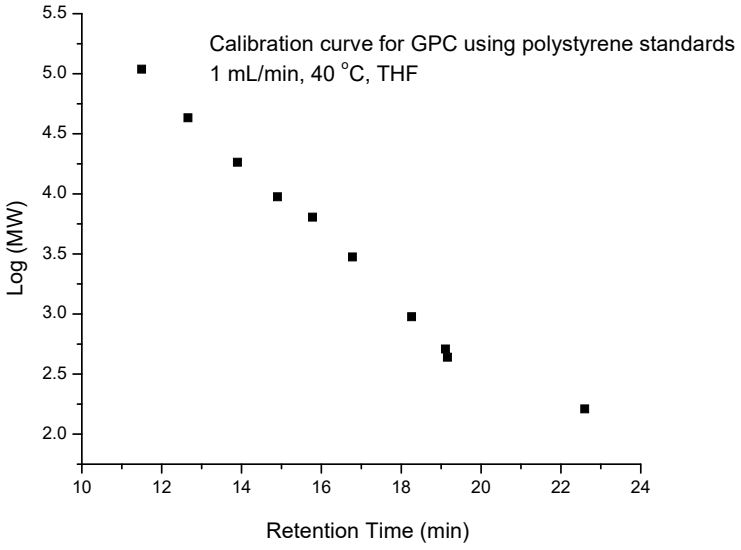

Figure A51. GPC calibration curve using polystyrene standards (Mw = 109,000-162 Da).

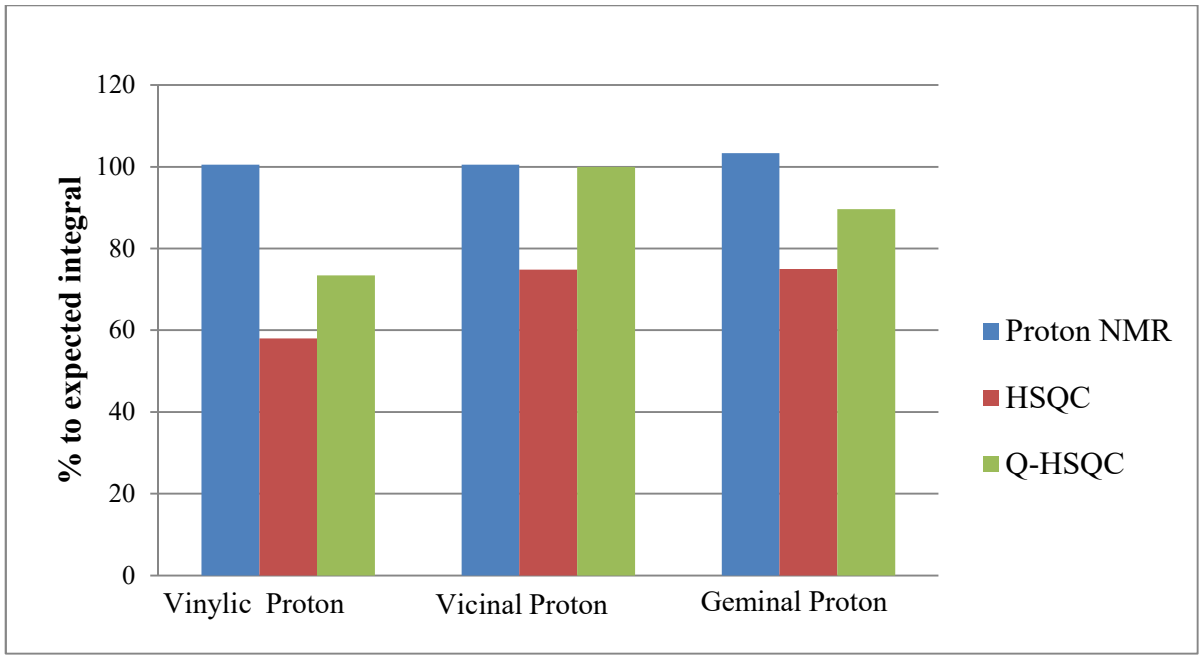

Figure A52. Comparison of relative integrals of ^{1}H, HSQC, and q-HSQC NMR spectra of cyclohexene in $CDCl_3$. Precision of the q-HSQC method was determined by measuring the integrals of cross-peaks of cyclohexene four times with the relative standard error being less than 1.4%. The accuracy of q-HSQC was evaluated by comparing the percentage of protons integrated for cyclohexene to ^{1}H-NMR.

Kinetic Data

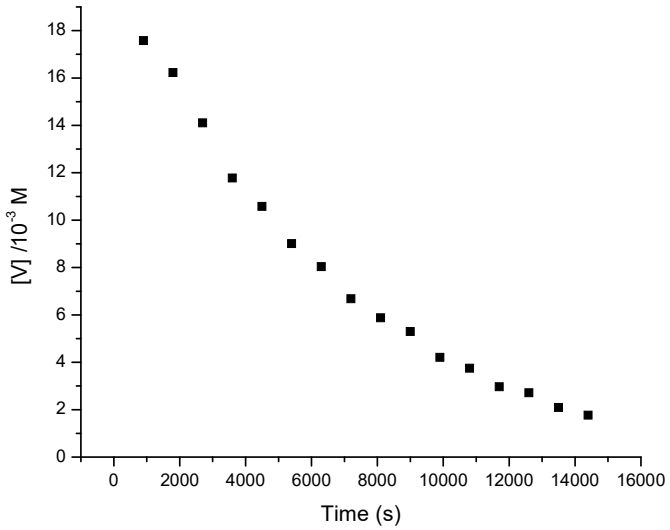

Figure A53. Kinetic data for the pseudo-zero-order rate law approximation for the reaction of **TA2** with hydrobenzoin at 353.15 K in C_6D_6.

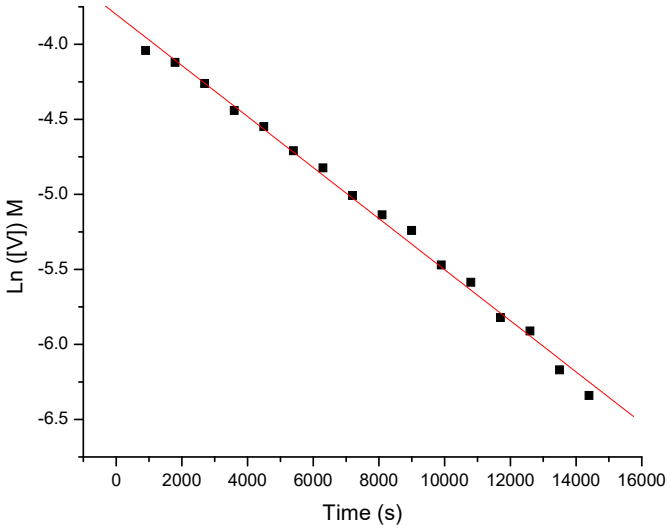

Figure A54. Kinetic data for the pseudo-first-order rate law approximation for the reaction of **TA2** with hydrobenzoin at 353.15 K in C_6D_6.

IR and UV-vis Spectra

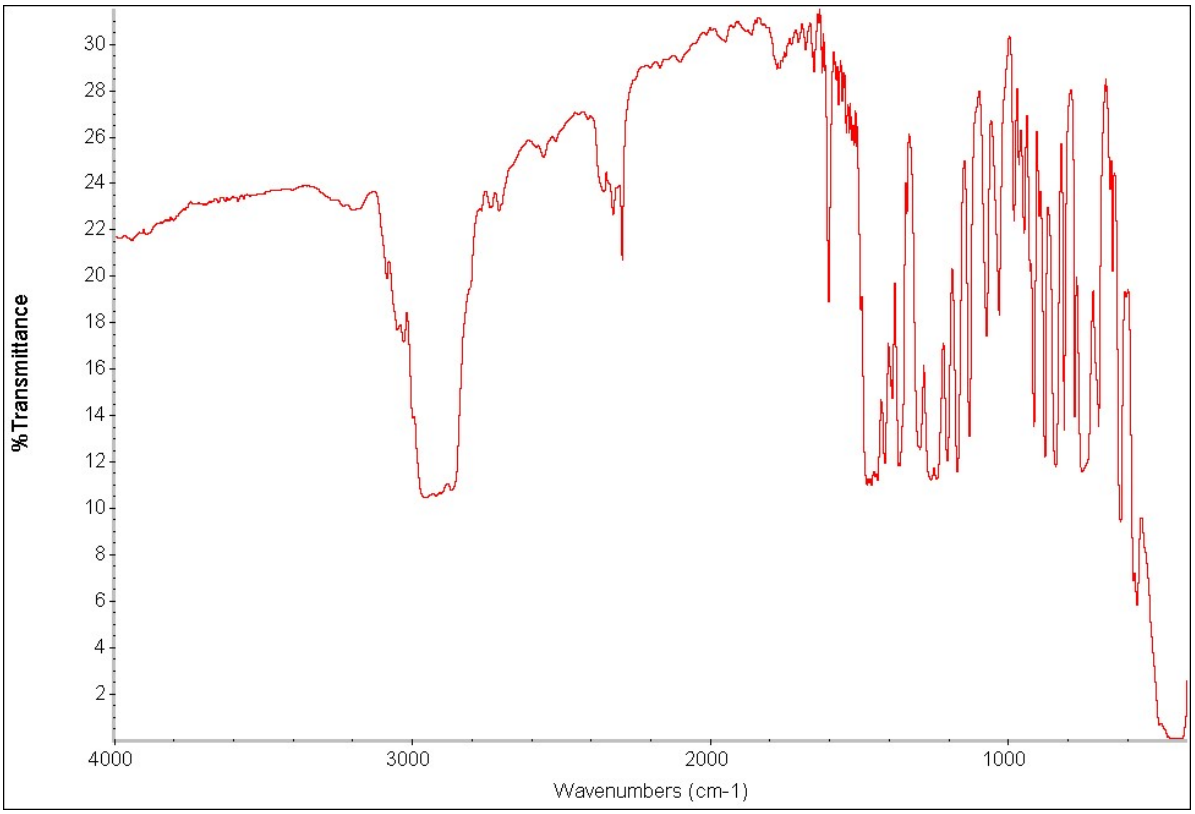

Figure A55. IR spectrum for **TA8**.

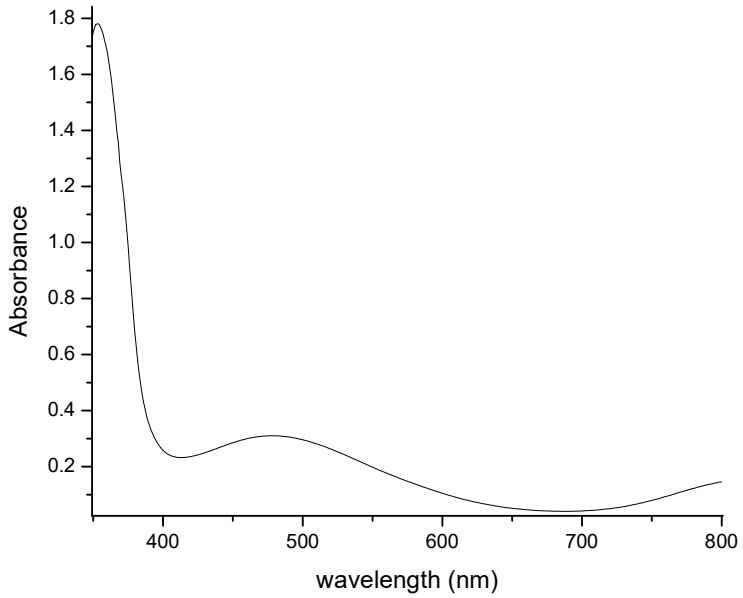

Figure A56. UV-Vis spectrum for **TA8**.

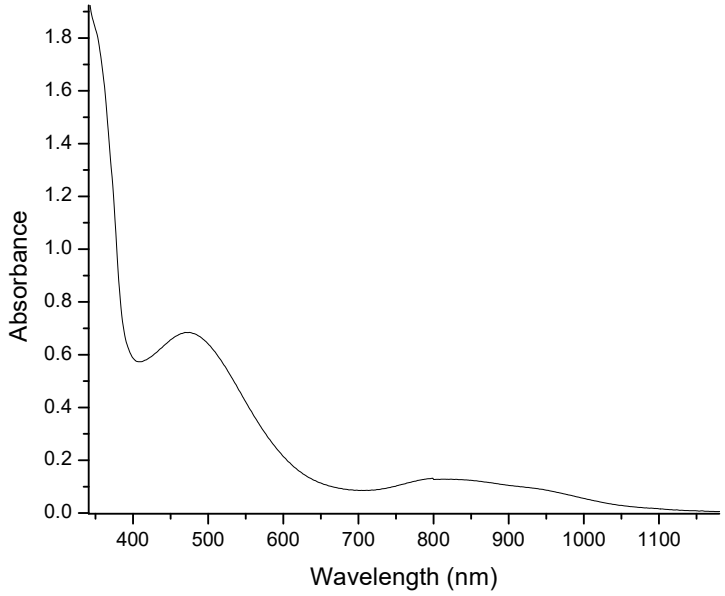

Figure A57. UV-Vis spectrum for **TA8** extended range to 1200 nm.

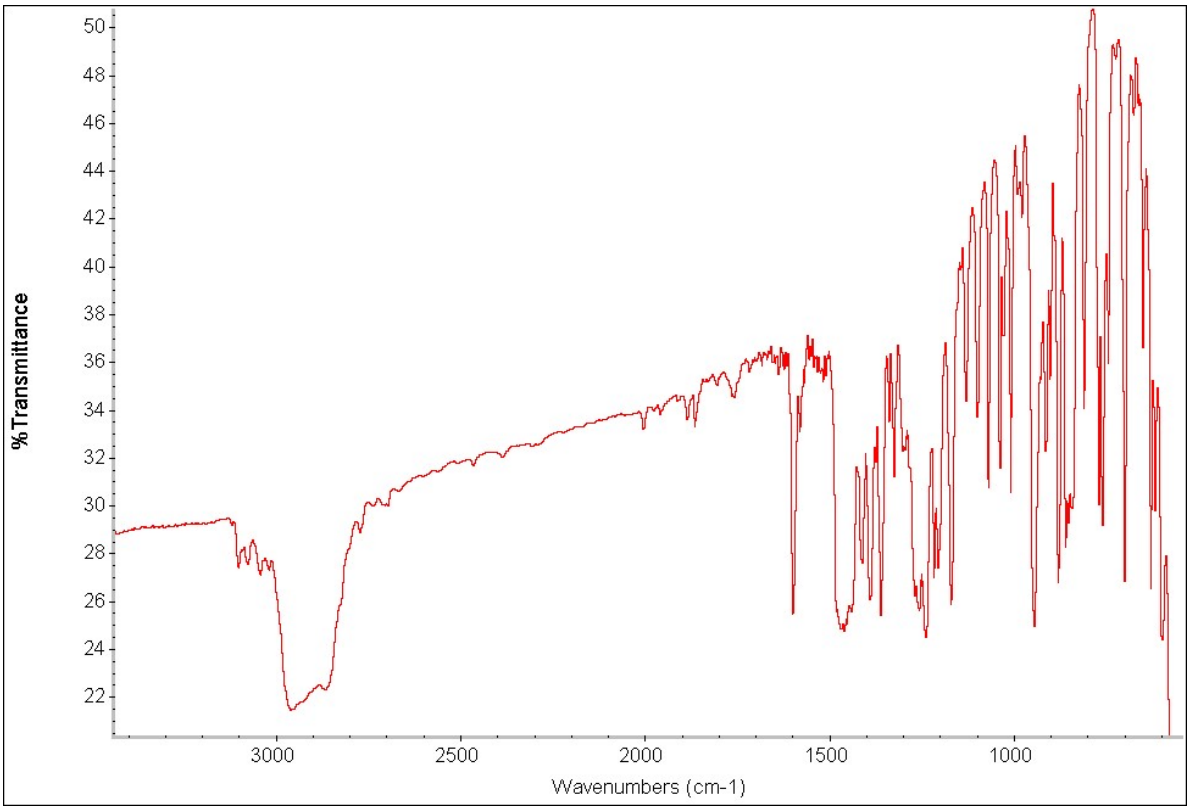

Figure A58. IR spectrum for **TA5**.

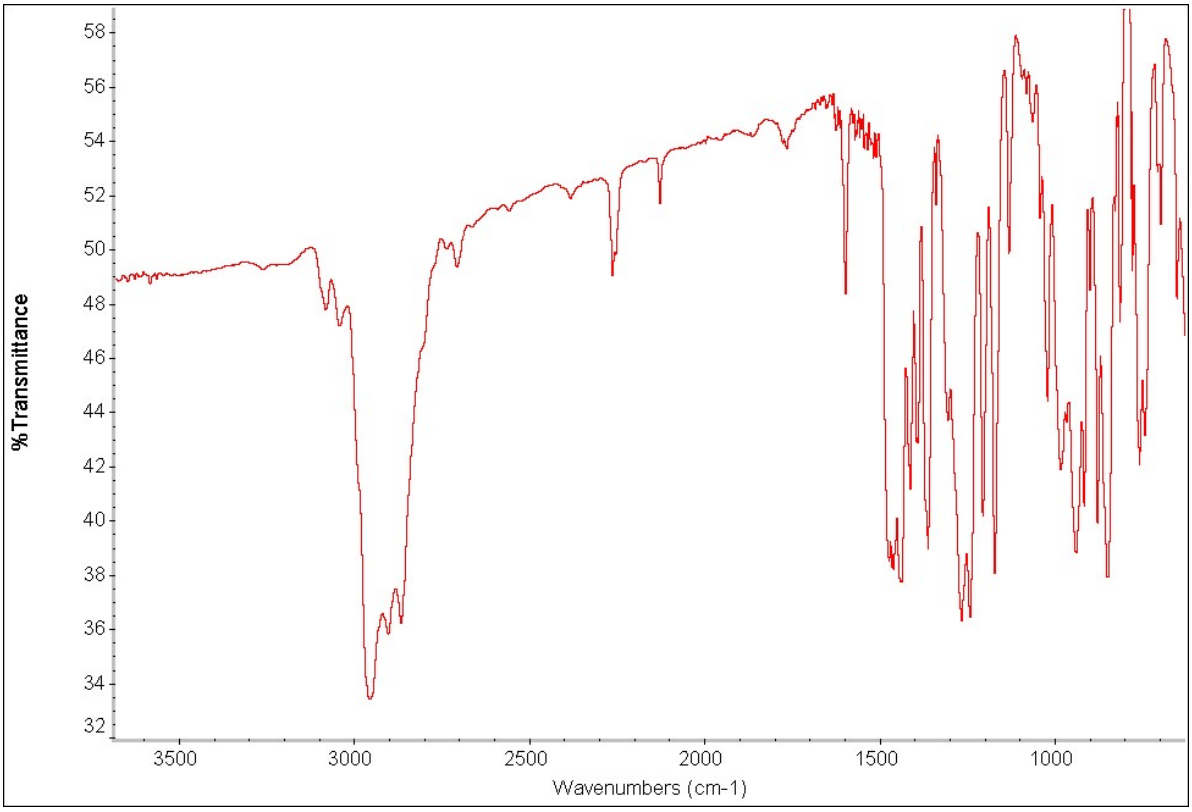

Figure A59. IR spectrum for **TA6**.

X-Ray Crystallography Data

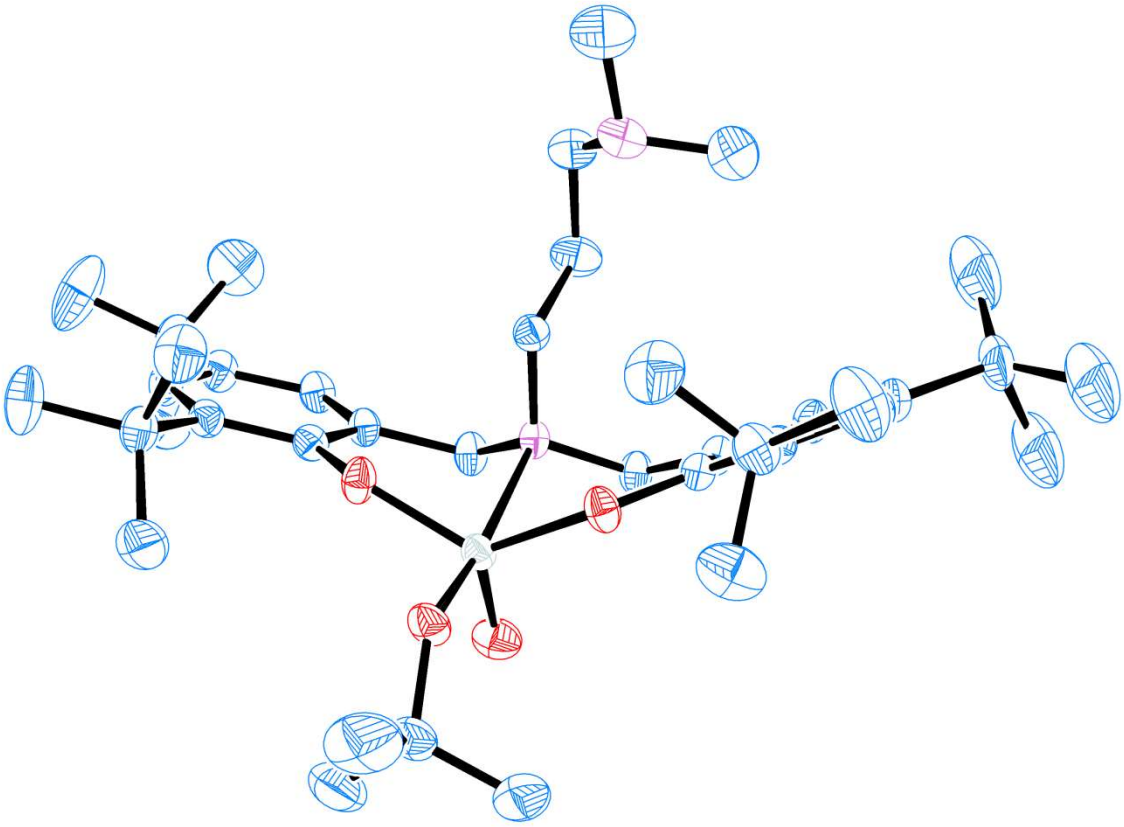

Figure A60. ORTEP representation for **AP4** Thermal ellipsoids set at 50% probability, hydrogen atoms and solvent molecules are omitted for clarity.

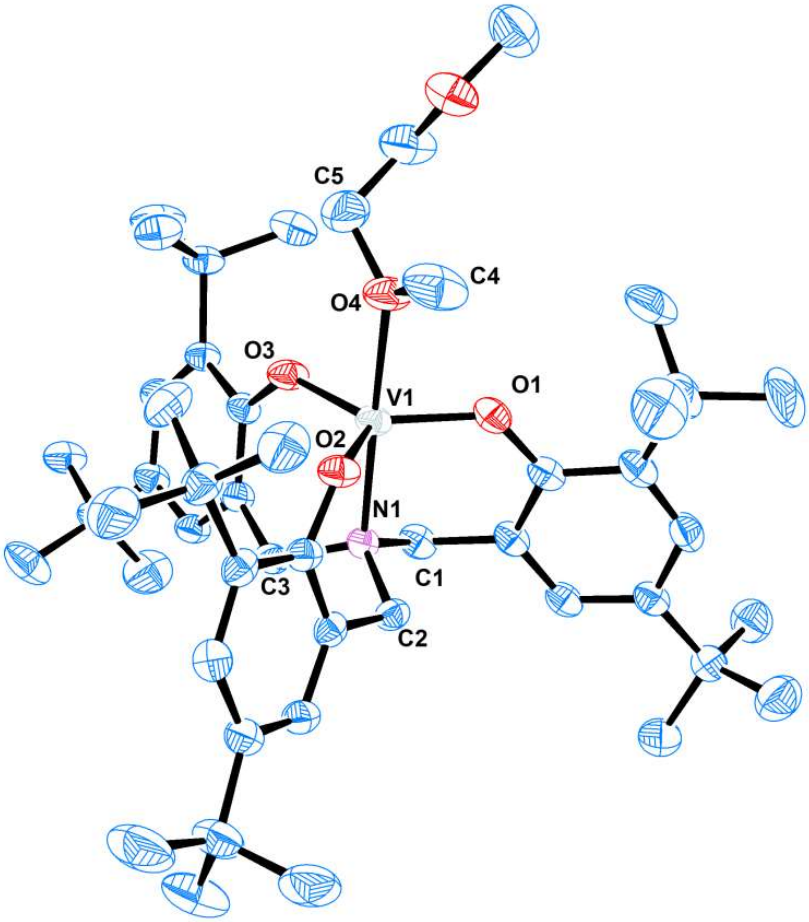

Figure A61. ORTEP representation for **TA9**. Thermal ellipsoids set at 50% probability, hydrogen atoms and second asymmetric unit are omitted for clarity.

Table A1. Atomic coordinates (x 10^4) **AP2**.

	x	y	z
V(1)	8229(1)	7796(1)	3783(1)
O(1)	7726(2)	7660(3)	4760(3)
O(2)	7629(2)	8582(2)	3033(3)
O(3)	8782(2)	6742(2)	3985(3)
O(4)	8809(2)	8615(3)	4338(3)
N(1)	7629(2)	6678(3)	2880(3)
N(2)	8993(2)	7962(3)	2245(4)
C(1)	7014(3)	7043(4)	2296(4)
C(2)	6924(3)	8562(4)	3137(4)
C(3)	6592(3)	7747(4)	2869(4)
C(4)	5877(3)	7645(4)	2990(4)
C(5)	5465(3)	8374(4)	3332(4)
C(6)	5810(3)	9194(4)	3550(4)
C(7)	6528(3)	9322(4)	3467(4)
C(8)	4665(3)	8308(4)	3401(5)
C(9)	4386(3)	8820(5)	4333(6)
C(10)	4365(4)	8734(6)	2387(7)
C(11)	4415(3)	7315(4)	3451(6)
C(12)	6868(3)	10248(4)	3700(6)
C(13)	6332(3)	10970(4)	4012(7)
C(14)	7238(4)	10589(5)	2708(5)
C(15)	7399(3)	10159(4)	4566(6)
C(16)	7354(2)	6066(3)	3703(5)
C(17)	8578(3)	5979(4)	4505(4)
C(18)	7896(3)	5634(4)	4404(4)
C(19)	7704(3)	4844(4)	4937(4)
C(20)	8157(3)	4381(4)	5588(4)
C(21)	8838(3)	4727(4)	5650(4)
C(22)	9069(3)	5495(4)	5125(4)
C(23)	7938(3)	3512(4)	6170(5)
C(24)	7406(7)	3706(8)	6989(10)
C(25)	7615(7)	2849(7)	5385(9)
C(26)	8567(6)	3019(8)	6639(12)
C(24')	7135(8)	3300(13)	6060(17)
C(25')	8313(10)	2721(11)	5735(16)
C(26')	8061(11)	3606(13)	7334(11)
C(27)	9847(3)	5770(4)	5146(5)
C(28)	10254(3)	5212(5)	5947(6)
C(29)	10167(3)	5579(5)	4065(5)
C(30)	9950(3)	6779(4)	5411(5)
C(31)	8043(3)	6118(4)	2134(5)
C(32)	8443(3)	6623(4)	1300(5)

C(33)	9100(3)	7098(4)	1668(4)
C(34)	8725(3)	8679(5)	1527(5)
C(35)	9693(3)	8259(4)	2607(5)
C(36)	8877(3)	8879(5)	5399(5)

Table A2. Bond lengths (Å) for **AP2**.

V(1)-O(1)	1.591(3)	C(8)-C(11)	1.531(9)
V(1)-O(4)	1.782(4)	C(8)-C(10)	1.552(10)
V(1)-O(2)	1.887(3)	C(12)-C(15)	1.511(9)
V(1)-O(3)	1.888(3)	C(12)-C(13)	1.526(8)
V(1)-N(1)	2.310(4)	C(12)-C(14)	1.539(9)
V(1)-N(2)	2.466(5)	C(16)-C(18)	1.511(7)
O(2)-C(2)	1.355(6)	C(17)-C(18)	1.405(7)
O(3)-C(17)	1.358(6)	C(17)-C(22)	1.419(7)
O(4)-C(36)	1.420(7)	C(18)-C(19)	1.392(7)
N(1)-C(16)	1.480(6)	C(19)-C(20)	1.380(7)
N(1)-C(31)	1.487(7)	C(20)-C(21)	1.399(7)
N(1)-C(1)	1.494(6)	C(20)-C(23)	1.532(8)
N(2)-C(35)	1.481(7)	C(21)-C(22)	1.383(8)
N(2)-C(33)	1.480(7)	C(22)-C(27)	1.542(7)
N(2)-C(34)	1.489(7)	C(23)-C(25')	1.472(14)
C(1)-C(3)	1.501(7)	C(23)-C(24)	1.490(11)
C(2)-C(3)	1.395(8)	C(23)-C(26')	1.518(14)
C(2)-C(7)	1.412(8)	C(23)-C(25)	1.528(10)
C(3)-C(4)	1.385(7)	C(23)-C(26)	1.527(11)
C(4)-C(5)	1.397(8)	C(23)-C(24')	1.573(13)
C(5)-C(6)	1.397(8)	C(27)-C(30)	1.528(8)
C(5)-C(8)	1.536(7)	C(27)-C(28)	1.526(8)
C(6)-C(7)	1.390(7)	C(27)-C(29)	1.541(8)
C(7)-C(12)	1.533(8)	C(31)-C(32)	1.508(8)
C(8)-C(9)	1.509(8)	C(32)-C(33)	1.512(8)

Table A3. Bond angles (deg) for **AP2**.

O(1)-V(1)-O(4)	98.39(18)	O(3)-V(1)-N(1)	76.56(15)
O(1)-V(1)-O(2)	96.36(17)	O(1)-V(1)-N(2)	178.20(18)
O(4)-V(1)-O(2)	99.89(16)	O(4)-V(1)-N(2)	83.32(16)
O(1)-V(1)-O(3)	97.33(18)	O(2)-V(1)-N(2)	83.87(15)
O(4)-V(1)-O(3)	98.38(17)	O(3)-V(1)-N(2)	81.83(15)
O(2)-V(1)-O(3)	155.26(17)	N(1)-V(1)-N(2)	87.93(15)
O(1)-V(1)-N(1)	90.32(17)	C(2)-O(2)-V(1)	122.7(3)
O(4)-V(1)-N(1)	170.47(17)	C(17)-O(3)-V(1)	125.4(3)
O(2)-V(1)-N(1)	82.86(15)	C(36)-O(4)-V(1)	128.5(4)

C(16)-N(1)-C(31)	108.3(4)	C(7)-C(12)-C(14)	108.7(5)
C(16)-N(1)-C(1)	107.1(4)	N(1)-C(16)-C(18)	115.7(4)
C(31)-N(1)-C(1)	107.0(4)	O(3)-C(17)-C(18)	121.1(5)
C(16)-N(1)-V(1)	104.4(3)	O(3)-C(17)-C(22)	119.8(5)
C(31)-N(1)-V(1)	116.7(3)	C(18)-C(17)-C(22)	119.0(5)
C(1)-N(1)-V(1)	112.9(3)	C(19)-C(18)-C(17)	119.9(5)
C(35)-N(2)-C(33)	106.5(4)	C(19)-C(18)-C(16)	117.3(5)
C(35)-N(2)-C(34)	107.3(5)	C(17)-C(18)-C(16)	122.8(5)
C(33)-N(2)-C(34)	109.9(5)	C(20)-C(19)-C(18)	122.7(5)
C(35)-N(2)-V(1)	108.3(3)	C(19)-C(20)-C(21)	116.1(5)
C(33)-N(2)-V(1)	113.4(3)	C(19)-C(20)-C(23)	122.0(5)
C(34)-N(2)-V(1)	111.0(3)	C(21)-C(20)-C(23)	121.8(5)
N(1)-C(1)-C(3)	115.0(4)	C(22)-C(21)-C(20)	124.3(5)
O(2)-C(2)-C(3)	116.6(5)	C(21)-C(22)-C(17)	117.9(5)
O(2)-C(2)-C(7)	123.1(5)	C(21)-C(22)-C(27)	120.8(5)
C(3)-C(2)-C(7)	120.2(5)	C(17)-C(22)-C(27)	121.1(5)
C(4)-C(3)-C(2)	120.9(5)	C(25')-C(23)-C(26')	111.5(10)
C(4)-C(3)-C(1)	120.8(5)	C(24)-C(23)-C(25)	108.1(8)
C(2)-C(3)-C(1)	117.6(5)	C(24)-C(23)-C(26)	110.5(8)
C(3)-C(4)-C(5)	120.7(6)	C(25)-C(23)-C(26)	106.1(8)
C(6)-C(5)-C(4)	116.9(5)	C(25')-C(23)-C(20)	109.6(9)
C(6)-C(5)-C(8)	120.9(5)	C(24)-C(23)-C(20)	111.9(6)
C(4)-C(5)-C(8)	122.1(5)	C(26')-C(23)-C(20)	111.2(8)
C(7)-C(6)-C(5)	124.6(5)	C(25)-C(23)-C(20)	108.5(6)
C(6)-C(7)-C(2)	116.5(5)	C(26)-C(23)-C(20)	111.6(6)
C(6)-C(7)-C(12)	121.6(5)	C(25')-C(23)-C(24')	106.6(10)
C(2)-C(7)-C(12)	121.8(5)	C(26')-C(23)-C(24')	104.9(10)
C(9)-C(8)-C(11)	109.1(6)	C(20)-C(23)-C(24')	112.8(8)
C(9)-C(8)-C(5)	111.5(5)	C(30)-C(27)-C(28)	107.5(5)
C(11)-C(8)-C(5)	112.0(5)	C(30)-C(27)-C(22)	112.3(5)
C(9)-C(8)-C(10)	109.4(6)	C(28)-C(27)-C(22)	111.4(5)
C(11)-C(8)-C(10)	107.6(6)	C(30)-C(27)-C(29)	108.9(5)
C(5)-C(8)-C(10)	107.2(5)	C(28)-C(27)-C(29)	107.8(5)
C(15)-C(12)-C(13)	108.6(6)	C(22)-C(27)-C(29)	108.7(5)
C(15)-C(12)-C(7)	110.6(5)	N(1)-C(31)-C(32)	117.1(5)
C(13)-C(12)-C(7)	112.2(4)	C(31)-C(32)-C(33)	115.2(5)
C(15)-C(12)-C(14)	109.0(5)	N(2)-C(33)-C(32)	115.7(4)
C(13)-C(12)-C(14)	107.5(6)		

Table A4. Atomic coordinates (x 10^4) for **AP3**.

	x	y	z
V(1)	5320(1)	4858(1)	1599(1)
O(1)	7011(1)	6047(1)	1484(1)
O(2)	5092(2)	4110(1)	2322(1)
O(3)	3849(2)	5001(2)	1194(1)
O(4)	5379(2)	3381(1)	1118(1)
N(1)	5516(2)	6752(2)	2318(1)
N(2)	9816(3)	8644(2)	3659(1)
C(1)	7631(2)	7404(2)	1493(1)
C(2)	8973(2)	7876(2)	1304(1)
C(3)	9538(2)	9273(2)	1312(1)
C(4)	8877(2)	10213(2)	1503(1)
C(5)	7582(2)	9701(2)	1708(1)
C(6)	6960(2)	8326(2)	1707(1)
C(7)	9793(2)	6902(2)	1119(1)
C(8)	11220(3)	7638(3)	932(2)
C(9)	8818(3)	5771(2)	536(1)
C(10)	10214(3)	6270(2)	1710(1)
C(11)	9535(2)	11744(2)	1511(1)
C(12)	8374(3)	12227(3)	1125(2)
C(13)	10885(3)	12094(3)	1214(2)
C(14)	10034(3)	12526(3)	2224(1)
C(12')	9520(17)	11957(14)	807(5)
C(13')	11122(12)	12235(15)	1908(7)
C(14')	8682(15)	12580(12)	1805(8)
C(15)	5553(2)	7841(2)	1931(1)
C(16)	4120(2)	6423(2)	2543(1)
C(17)	4435(2)	4229(2)	2825(1)
C(18)	3938(2)	5332(2)	2949(1)
C(19)	3239(2)	5423(2)	3456(1)
C(20)	3021(2)	4447(2)	3847(1)
C(21)	3579(2)	3393(2)	3726(1)
C(22)	4303(2)	3251(2)	3231(1)
C(23)	2173(3)	4547(3)	4381(1)
C(24)	2887(5)	6000(4)	4812(2)
C(25)	2257(8)	3557(5)	4828(3)
C(26)	610(4)	4422(7)	4051(2)
C(24')	1769(17)	5779(11)	4487(7)
C(25')	2997(14)	4351(15)	5037(5)
C(26')	718(10)	3260(11)	4189(6)
C(27)	4938(2)	2093(2)	3127(1)
C(28)	6603(3)	2671(3)	3180(1)
C(29)	4735(3)	1190(3)	3643(1)

C(30)	4153(3)	1177(2)	2454(1)
C(31)	6843(2)	7140(2)	2874(1)
C(32)	7191(3)	8505(2)	3328(1)
C(33)	8551(3)	8789(3)	3877(1)
C(34)	10326(4)	9561(4)	3228(2)
C(35)	11029(4)	8806(4)	4215(2)
C(36)	4412(2)	2553(2)	509(1)
C(37)	5196(3)	2814(3)	-30(1)
C(38)	3969(3)	1069(3)	571(2)

Table A5. Bond lengths (Å) for **AP3**.

V(1)-O(3)	1.5883(15)	C(11)-C(12)	1.519(3)
V(1)-O(4)	1.7671(13)	C(11)-C(12')	1.535(10)
V(1)-O(2)	1.8250(14)	C(11)-C(14')	1.536(10)
V(1)-O(1)	1.8276(12)	C(11)-C(13)	1.538(3)
V(1)-N(1)	2.2813(16)	C(11)-C(14)	1.538(3)
O(1)-C(1)	1.361(2)	C(16)-C(18)	1.501(3)
O(2)-C(17)	1.360(2)	C(17)-C(18)	1.396(3)
O(4)-C(36)	1.441(2)	C(17)-C(22)	1.408(3)
N(1)-C(15)	1.480(2)	C(18)-C(19)	1.389(3)
N(1)-C(31)	1.490(3)	C(19)-C(20)	1.386(3)
N(1)-C(16)	1.491(2)	C(20)-C(21)	1.388(3)
N(2)-C(33)	1.445(4)	C(20)-C(23)	1.538(3)
N(2)-C(34)	1.452(4)	C(21)-C(22)	1.394(3)
N(2)-C(35)	1.457(4)	C(22)-C(27)	1.530(3)
C(1)-C(6)	1.399(3)	C(23)-C(24')	1.462(9)
C(1)-C(2)	1.412(2)	C(23)-C(25)	1.496(5)
C(2)-C(3)	1.395(3)	C(23)-C(26)	1.517(5)
C(2)-C(7)	1.533(3)	C(23)-C(25')	1.539(10)
C(3)-C(4)	1.390(3)	C(23)-C(24)	1.552(4)
C(4)-C(5)	1.395(3)	C(23)-C(26')	1.580(8)
C(4)-C(11)	1.533(3)	C(27)-C(30)	1.532(3)
C(5)-C(6)	1.382(3)	C(27)-C(29)	1.535(3)
C(6)-C(15)	1.508(2)	C(27)-C(28)	1.536(3)
C(7)-C(8)	1.531(3)	C(31)-C(32)	1.524(3)
C(7)-C(10)	1.532(3)	C(32)-C(33)	1.518(4)
C(7)-C(9)	1.532(3)	C(36)-C(37)	1.503(4)
C(11)-C(13')	1.518(10)	C(36)-C(38)	1.510(4)

Table A6. Bond angles (deg) for **AP3**.

O(3)-V(1)-O(4)	100.82(7)	C(13')-C(11)-C(12')	108.8(7)
O(3)-V(1)-O(2)	113.74(7)	C(4)-C(11)-C(12')	108.9(6)
O(4)-V(1)-O(2)	95.79(6)	C(13')-C(11)-C(14')	109.7(7)
O(3)-V(1)-O(1)	114.10(7)	C(4)-C(11)-C(14')	112.7(5)
O(4)-V(1)-O(1)	96.95(6)	C(12')-C(11)-C(14')	108.8(7)
O(2)-V(1)-O(1)	126.77(7)	C(12)-C(11)-C(13)	108.3(2)
O(3)-V(1)-N(1)	86.96(7)	C(4)-C(11)-C(13)	112.86(18)
O(4)-V(1)-N(1)	172.19(6)	C(12)-C(11)-C(14)	109.5(2)
O(2)-V(1)-N(1)	80.26(6)	C(4)-C(11)-C(14)	109.04(18)
O(1)-V(1)-N(1)	80.32(5)	C(13)-C(11)-C(14)	107.6(2)
C(1)-O(1)-V(1)	139.53(12)	N(1)-C(15)-C(6)	113.17(15)
C(17)-O(2)-V(1)	138.29(13)	N(1)-C(16)-C(18)	113.79(16)
C(36)-O(4)-V(1)	130.40(13)	O(2)-C(17)-C(18)	120.22(17)
C(15)-N(1)-C(31)	112.31(14)	O(2)-C(17)-C(22)	119.19(17)
C(15)-N(1)-C(16)	107.94(15)	C(18)-C(17)-C(22)	120.57(17)
C(31)-N(1)-C(16)	112.16(15)	C(19)-C(18)-C(17)	119.55(19)
C(15)-N(1)-V(1)	105.96(12)	C(19)-C(18)-C(16)	118.60(18)
C(31)-N(1)-V(1)	111.88(11)	C(17)-C(18)-C(16)	121.85(17)
C(16)-N(1)-V(1)	106.19(11)	C(20)-C(19)-C(18)	121.81(19)
C(33)-N(2)-C(34)	114.2(3)	C(19)-C(20)-C(21)	117.08(18)
C(33)-N(2)-C(35)	110.8(3)	C(19)-C(20)-C(23)	120.2(2)
C(34)-N(2)-C(35)	109.8(2)	C(21)-C(20)-C(23)	122.7(2)
O(1)-C(1)-C(6)	119.99(15)	C(20)-C(21)-C(22)	123.93(19)
O(1)-C(1)-C(2)	119.63(16)	C(21)-C(22)-C(17)	116.94(18)
C(6)-C(1)-C(2)	120.35(16)	C(21)-C(22)-C(27)	122.12(18)
C(3)-C(2)-C(1)	116.87(17)	C(17)-C(22)-C(27)	120.94(17)
C(3)-C(2)-C(7)	121.71(16)	C(25)-C(23)-C(26)	113.7(4)
C(1)-C(2)-C(7)	121.39(16)	C(24')-C(23)-C(20)	116.1(5)
C(4)-C(3)-C(2)	124.25(17)	C(25)-C(23)-C(20)	113.0(3)
C(3)-C(4)-C(5)	116.59(17)	C(26)-C(23)-C(20)	108.2(2)
C(3)-C(4)-C(11)	122.87(17)	C(24')-C(23)-C(25')	109.6(7)
C(5)-C(4)-C(11)	120.52(17)	C(20)-C(23)-C(25')	111.4(5)
C(6)-C(5)-C(4)	121.97(18)	C(25)-C(23)-C(24)	106.8(3)
C(5)-C(6)-C(1)	119.89(16)	C(26)-C(23)-C(24)	106.6(3)
C(5)-C(6)-C(15)	119.21(17)	C(20)-C(23)-C(24)	108.1(2)
C(1)-C(6)-C(15)	120.90(16)	C(24')-C(23)-C(26')	108.6(7)
C(8)-C(7)-C(10)	107.39(19)	C(20)-C(23)-C(26')	107.4(4)
C(8)-C(7)-C(9)	107.79(18)	C(25')-C(23)-C(26')	102.8(7)
C(10)-C(7)-C(9)	109.80(18)	C(22)-C(27)-C(30)	109.78(18)
C(8)-C(7)-C(2)	112.29(17)	C(22)-C(27)-C(29)	112.11(18)
C(10)-C(7)-C(2)	109.00(17)	C(30)-C(27)-C(29)	107.58(19)
C(9)-C(7)-C(2)	110.51(17)	C(22)-C(27)-C(28)	110.62(18)
C(13')-C(11)-C(4)	107.9(6)	C(30)-C(27)-C(28)	109.9(2)
C(12)-C(11)-C(4)	109.49(17)	C(29)-C(27)-C(28)	106.74(19)

N(1)-C(31)-C(32)	115.71(18)	O(4)-C(36)-C(37)	108.67(18)
C(33)-C(32)-C(31)	111.2(2)	O(4)-C(36)-C(38)	109.2(2)
N(2)-C(33)-C(32)	114.1(2)	C(37)-C(36)-C(38)	111.9(2)

Table A7. Atomic coordinates (x 10^4) for **AP4**.

	x	y	z
V(1)	820(1)	2935(1)	810(1)
V(2)	3337(1)	246(1)	1701(1)
O(1)	894(1)	1320(1)	874(1)
O(2)	1115(1)	4042(1)	599(1)
O(3)	574(1)	3528(2)	1085(1)
O(4)	495(1)	2756(1)	485(1)
O(5)	3388(1)	1840(1)	1599(1)
O(6)	3645(1)	-832(2)	1914(1)
O(7)	3063(1)	-410(2)	1451(1)
O(8)	3063(1)	530(2)	2045(1)
N(1)	1320(1)	3007(1)	1158(1)
N(2)	2393(1)	2579(2)	687(1)
N(3)	3810(1)	97(2)	1341(1)
N(4)	4894(1)	488(3)	1791(1)
C(1)	1210(1)	2348(2)	1453(1)
C(2)	974(1)	564(2)	1122(1)
C(3)	1137(1)	1017(2)	1408(1)
C(4)	1219(1)	241(2)	1660(1)
C(5)	1142(1)	-988(2)	1642(1)
C(6)	987(1)	-1412(2)	1355(1)
C(7)	902(1)	-683(2)	1088(1)
C(8)	1220(1)	-1806(2)	1936(1)
C(9)	1608(1)	-1524(3)	2087(1)
C(10)	1228(1)	-3140(3)	1842(1)
C(11)	920(1)	-1587(3)	2189(1)
C(12)	741(1)	-1217(2)	773(1)
C(13)	1023(1)	-1010(3)	501(1)
C(14)	365(1)	-615(3)	683(1)
C(15)	677(1)	-2583(2)	799(1)
C(16)	1368(1)	4296(2)	1250(1)
C(17)	1382(1)	4887(2)	663(1)
C(18)	1509(1)	5072(2)	980(1)
C(19)	1777(1)	5962(2)	1045(1)
C(20)	1922(1)	6682(2)	804(1)
C(21)	1804(1)	6436(2)	491(1)

C(22)	1541(1)	5546(2)	408(1)
C(23)	2217(1)	7659(2)	884(1)
C(24)	2542(2)	7105(6)	1086(2)
C(25)	2023(2)	8614(8)	1106(2)
C(26)	2379(2)	8288(8)	599(2)
C(24')	2608(2)	7088(6)	861(2)
C(25')	2150(2)	8296(8)	1188(2)
C(26')	2224(2)	8628(7)	609(2)
C(27)	1442(1)	5257(2)	54(1)
C(28)	1675(1)	6021(3)	-179(1)
C(29)	1023(1)	5498(3)	-15(1)
C(30)	1534(1)	3929(3)	-13(1)
C(31)	1661(1)	2482(2)	1005(1)
C(32)	2030(1)	2599(2)	1198(1)
C(33)	2357(1)	2067(2)	1007(1)
C(34)	2669(1)	1914(3)	503(1)
C(35)	2503(1)	3831(3)	699(1)
C(36)	109(1)	3092(2)	413(1)
C(37)	72(1)	4447(3)	433(1)
C(38)	28(1)	2632(3)	76(1)
C(39)	-149(1)	2520(3)	662(1)
C(40)	3681(1)	708(2)	1038(1)
C(41)	3483(1)	2565(2)	1350(1)
C(42)	3637(1)	2059(2)	1071(1)
C(43)	3741(1)	2801(2)	820(1)
C(44)	3691(1)	4048(2)	831(1)
C(45)	3541(1)	4519(2)	1112(1)
C(46)	3439(1)	3823(2)	1377(1)
C(47)	3791(1)	4827(2)	538(1)
C(48)	4174(1)	4468(4)	408(1)
C(49)	3808(1)	6168(3)	624(1)
C(50)	3485(1)	4654(3)	277(1)
C(51)	3280(1)	4396(2)	1685(1)
C(52)	3533(1)	4077(3)	1978(1)
C(53)	3269(1)	5778(2)	1663(1)
C(54)	2878(1)	3955(3)	1736(1)
C(55)	3854(1)	-1211(2)	1266(1)
C(56)	3909(1)	-1684(2)	1858(1)
C(57)	4020(1)	-1928(2)	1542(1)
C(58)	4282(1)	-2833(2)	1485(1)
C(59)	4436(1)	-3521(2)	1734(1)
C(60)	4334(1)	-3218(2)	2046(1)
C(61)	4079(1)	-2299(2)	2119(1)
C(62)	4724(1)	-4527(2)	1667(1)
C(63)	4813(1)	-5278(3)	1964(1)
C(64)	4572(1)	-5359(3)	1401(1)

C(65)	5095(1)	-3964(3)	1556(1)
C(66)	3992(1)	-1976(3)	2469(1)
C(67)	4247(1)	-2668(3)	2708(1)
C(68)	3584(1)	-2291(4)	2541(1)
C(69)	4072(1)	-629(3)	2526(1)
C(70)	4160(1)	642(2)	1476(1)
C(71)	4518(1)	494(4)	1284(1)
C(72)	4864(3)	1119(8)	1531(2)
C(72')	4845(3)	926(8)	1435(2)
C(73)	5037(1)	-682(3)	1783(1)
C(74)	5046(2)	1110(7)	2088(2)
C(74')	5212(2)	1329(6)	1860(3)
C(75)	2695(1)	291(3)	2168(1)
C(76)	2653(2)	1102(6)	2466(2)
C(77)	2617(2)	-987(6)	2244(2)
C(78)	2417(2)	759(8)	1895(2)
C(76')	2724(2)	546(6)	2527(2)
C(77')	2645(2)	-1105(6)	2112(2)
C(78')	2389(2)	973(8)	1998(2)

Table A8. Bond lengths (Å) for **AP4**.

V(1)-O(3)	1.5854(16)	C(12)-C(13)	1.534(3)
V(1)-O(4)	1.7693(14)	C(16)-C(18)	1.505(3)
V(1)-O(1)	1.8251(15)	C(17)-C(18)	1.398(3)
V(1)-O(2)	1.8390(14)	C(17)-C(22)	1.406(3)
V(1)-N(1)	2.2694(16)	C(18)-C(19)	1.390(3)
V(2)-O(7)	1.5862(18)	C(19)-C(20)	1.382(3)
V(2)-O(8)	1.7654(16)	C(20)-C(21)	1.385(3)
V(2)-O(5)	1.8224(16)	C(20)-C(23)	1.535(3)
V(2)-O(6)	1.8345(15)	C(21)-C(22)	1.395(3)
V(2)-N(3)	2.264(2)	C(22)-C(27)	1.538(3)
O(1)-C(2)	1.354(2)	C(23)-C(25')	1.465(8)
O(2)-C(17)	1.352(2)	C(23)-C(26)	1.490(7)
O(4)-C(36)	1.442(3)	C(23)-C(24')	1.527(7)
O(5)-C(41)	1.354(3)	C(23)-C(24)	1.542(7)
O(6)-C(56)	1.350(3)	C(23)-C(26')	1.562(8)
O(8)-C(75)	1.430(3)	C(23)-C(25)	1.567(8)
N(1)-C(1)	1.480(2)	C(27)-C(29)	1.530(3)
N(1)-C(16)	1.487(2)	C(27)-C(30)	1.531(4)
N(1)-C(31)	1.489(3)	C(27)-C(28)	1.533(3)
N(2)-C(35)	1.441(4)	C(31)-C(32)	1.526(3)
N(2)-C(34)	1.449(4)	C(32)-C(33)	1.529(4)
N(2)-C(33)	1.450(4)	C(36)-C(38)	1.509(4)
N(3)-C(70)	1.483(3)	C(36)-C(37)	1.509(4)
N(3)-C(55)	1.488(3)	C(36)-C(39)	1.525(4)
N(3)-C(40)	1.491(3)	C(40)-C(42)	1.510(3)
N(4)-C(72)	1.287(10)	C(41)-C(42)	1.400(3)
N(4)-C(73)	1.392(5)	C(41)-C(46)	1.406(3)
N(4)-C(74')	1.486(6)	C(42)-C(43)	1.379(3)
N(4)-C(74)	1.501(8)	C(43)-C(44)	1.393(3)
N(4)-C(72')	1.560(10)	C(44)-C(45)	1.388(3)
C(1)-C(3)	1.507(3)	C(44)-C(47)	1.536(3)
C(2)-C(3)	1.400(3)	C(45)-C(46)	1.394(3)
C(2)-C(7)	1.411(3)	C(46)-C(51)	1.537(3)
C(3)-C(4)	1.382(3)	C(47)-C(48)	1.516(4)
C(4)-C(5)	1.389(3)	C(47)-C(49)	1.528(4)
C(5)-C(6)	1.386(3)	C(47)-C(50)	1.533(4)
C(5)-C(8)	1.538(3)	C(51)-C(54)	1.521(4)
C(6)-C(7)	1.397(3)	C(51)-C(53)	1.533(3)
C(7)-C(12)	1.536(3)	C(51)-C(52)	1.539(4)
C(8)-C(11)	1.522(4)	C(55)-C(57)	1.507(3)
C(8)-C(10)	1.526(4)	C(56)-C(57)	1.398(3)
C(8)-C(9)	1.532(4)	C(56)-C(61)	1.404(3)
C(12)-C(14)	1.530(3)	C(57)-C(58)	1.388(3)
C(12)-C(15)	1.532(3)	C(58)-C(59)	1.390(3)

C(59)-C(60)	1.386(3)	C(70)-C(71)	1.515(4)
C(59)-C(62)	1.537(3)	C(71)-C(72')	1.394(8)
C(60)-C(61)	1.396(3)	C(71)-C(72)	1.731(8)
C(61)-C(66)	1.531(3)	C(75)-C(77)	1.475(7)
C(62)-C(63)	1.516(4)	C(75)-C(78')	1.490(7)
C(62)-C(64)	1.527(4)	C(75)-C(76')	1.515(7)
C(62)-C(65)	1.530(4)	C(75)-C(76)	1.538(7)
C(66)-C(68)	1.519(4)	C(75)-C(77')	1.572(7)
C(66)-C(69)	1.534(4)	C(75)-C(78)	1.576(7)
C(66)-C(67)	1.535(3)		

Table A9. Bond angles (deg) for **AP4**.

O(3)-V(1)-O(4)	103.67(8)	C(35)-N(2)-C(34)	108.9(2)
O(3)-V(1)-O(1)	112.38(8)	C(35)-N(2)-C(33)	111.9(2)
O(4)-V(1)-O(1)	95.27(7)	C(34)-N(2)-C(33)	110.7(2)
O(3)-V(1)-O(2)	112.72(8)	C(70)-N(3)-C(55)	112.74(19)
O(4)-V(1)-O(2)	94.65(7)	C(70)-N(3)-C(40)	112.27(19)
O(1)-V(1)-O(2)	129.75(7)	C(55)-N(3)-C(40)	107.28(17)
O(3)-V(1)-N(1)	87.66(7)	C(70)-N(3)-V(2)	110.04(13)
O(4)-V(1)-N(1)	168.66(7)	C(55)-N(3)-V(2)	106.77(14)
O(1)-V(1)-N(1)	80.36(6)	C(40)-N(3)-V(2)	107.45(15)
O(2)-V(1)-N(1)	80.47(6)	C(72)-N(4)-C(73)	120.7(6)
O(7)-V(2)-O(8)	105.64(10)	C(73)-N(4)-C(74')	108.1(4)
O(7)-V(2)-O(5)	110.73(9)	C(72)-N(4)-C(74)	117.3(5)
O(8)-V(2)-O(5)	94.09(7)	C(73)-N(4)-C(74)	108.6(4)
O(7)-V(2)-O(6)	111.77(9)	C(73)-N(4)-C(72')	107.6(5)
O(8)-V(2)-O(6)	93.25(7)	C(74')-N(4)-C(72')	93.4(5)
O(5)-V(2)-O(6)	132.91(8)	N(1)-C(1)-C(3)	115.21(16)
O(7)-V(2)-N(3)	89.32(9)	O(1)-C(2)-C(3)	120.05(18)
O(8)-V(2)-N(3)	165.02(7)	O(1)-C(2)-C(7)	119.53(17)
O(5)-V(2)-N(3)	80.97(7)	C(3)-C(2)-C(7)	120.40(18)
O(6)-V(2)-N(3)	80.20(7)	C(4)-C(3)-C(2)	119.81(19)
C(2)-O(1)-V(1)	138.03(13)	C(4)-C(3)-C(1)	118.63(18)
C(17)-O(2)-V(1)	140.13(13)	C(2)-C(3)-C(1)	121.51(17)
C(36)-O(4)-V(1)	136.97(15)	C(3)-C(4)-C(5)	121.90(19)
C(41)-O(5)-V(2)	140.85(14)	C(6)-C(5)-C(4)	116.94(19)
C(56)-O(6)-V(2)	141.26(14)	C(6)-C(5)-C(8)	123.0(2)
C(75)-O(8)-V(2)	140.30(17)	C(4)-C(5)-C(8)	120.07(19)
C(1)-N(1)-C(16)	106.81(15)	C(5)-C(6)-C(7)	124.1(2)
C(1)-N(1)-C(31)	112.49(16)	C(6)-C(7)-C(2)	116.75(18)
C(16)-N(1)-C(31)	113.26(16)	C(6)-C(7)-C(12)	121.49(19)
C(1)-N(1)-V(1)	107.23(12)	C(2)-C(7)-C(12)	121.75(18)
C(16)-N(1)-V(1)	106.40(12)	C(11)-C(8)-C(10)	110.1(2)
C(31)-N(1)-V(1)	110.28(11)	C(11)-C(8)-C(9)	108.4(2)

C(10)-C(8)-C(9)	106.4(3)	O(4)-C(36)-C(38)	105.6(2)
C(11)-C(8)-C(5)	109.3(2)	O(4)-C(36)-C(37)	109.21(19)
C(10)-C(8)-C(5)	111.8(2)	C(38)-C(36)-C(37)	111.7(2)
C(9)-C(8)-C(5)	110.7(2)	O(4)-C(36)-C(39)	109.24(19)
C(14)-C(12)-C(15)	108.7(2)	C(38)-C(36)-C(39)	112.2(3)
C(14)-C(12)-C(13)	109.2(2)	C(37)-C(36)-C(39)	108.8(2)
C(15)-C(12)-C(13)	107.2(2)	N(3)-C(40)-C(42)	113.82(18)
C(14)-C(12)-C(7)	110.53(19)	O(5)-C(41)-C(42)	119.7(2)
C(15)-C(12)-C(7)	111.97(18)	O(5)-C(41)-C(46)	119.75(19)
C(13)-C(12)-C(7)	109.25(18)	C(42)-C(41)-C(46)	120.5(2)
N(1)-C(16)-C(18)	113.10(16)	C(43)-C(42)-C(41)	119.7(2)
O(2)-C(17)-C(18)	120.09(18)	C(43)-C(42)-C(40)	119.4(2)
O(2)-C(17)-C(22)	119.85(18)	C(41)-C(42)-C(40)	120.8(2)
C(18)-C(17)-C(22)	120.02(18)	C(42)-C(43)-C(44)	122.0(2)
C(19)-C(18)-C(17)	119.76(19)	C(45)-C(44)-C(43)	116.7(2)
C(19)-C(18)-C(16)	119.57(18)	C(45)-C(44)-C(47)	123.3(2)
C(17)-C(18)-C(16)	120.65(17)	C(43)-C(44)-C(47)	120.0(2)
C(20)-C(19)-C(18)	121.9(2)	C(44)-C(45)-C(46)	124.1(2)
C(19)-C(20)-C(21)	116.8(2)	C(45)-C(46)-C(41)	117.0(2)
C(19)-C(20)-C(23)	120.7(2)	C(45)-C(46)-C(51)	121.8(2)
C(21)-C(20)-C(23)	122.4(2)	C(41)-C(46)-C(51)	121.21(19)
C(20)-C(21)-C(22)	124.1(2)	C(48)-C(47)-C(49)	107.8(3)
C(21)-C(22)-C(17)	117.16(19)	C(48)-C(47)-C(50)	110.1(3)
C(21)-C(22)-C(27)	121.45(19)	C(49)-C(47)-C(50)	108.2(2)
C(17)-C(22)-C(27)	121.33(18)	C(48)-C(47)-C(44)	110.5(2)
C(25')-C(23)-C(24')	114.1(5)	C(49)-C(47)-C(44)	111.6(2)
C(25')-C(23)-C(20)	114.0(4)	C(50)-C(47)-C(44)	108.6(2)
C(26)-C(23)-C(20)	115.3(4)	C(54)-C(51)-C(53)	107.8(2)
C(24')-C(23)-C(20)	108.0(3)	C(54)-C(51)-C(46)	109.6(2)
C(26)-C(23)-C(24)	108.9(5)	C(53)-C(51)-C(46)	111.8(2)
C(20)-C(23)-C(24)	109.6(3)	C(54)-C(51)-C(52)	110.6(3)
C(25')-C(23)-C(26')	107.4(5)	C(53)-C(51)-C(52)	106.9(2)
C(24')-C(23)-C(26')	102.5(5)	C(46)-C(51)-C(52)	110.1(2)
C(20)-C(23)-C(26')	110.2(4)	N(3)-C(55)-C(57)	113.20(19)
C(26)-C(23)-C(25)	109.1(5)	O(6)-C(56)-C(57)	119.92(19)
C(20)-C(23)-C(25)	107.4(3)	O(6)-C(56)-C(61)	119.76(19)
C(24)-C(23)-C(25)	106.2(4)	C(57)-C(56)-C(61)	120.3(2)
C(29)-C(27)-C(30)	110.0(2)	C(58)-C(57)-C(56)	119.7(2)
C(29)-C(27)-C(28)	108.2(2)	C(58)-C(57)-C(55)	120.3(2)
C(30)-C(27)-C(28)	107.3(2)	C(56)-C(57)-C(55)	119.9(2)
C(29)-C(27)-C(22)	110.39(19)	C(57)-C(58)-C(59)	121.7(2)
C(30)-C(27)-C(22)	109.03(19)	C(60)-C(59)-C(58)	117.0(2)
C(28)-C(27)-C(22)	111.8(2)	C(60)-C(59)-C(62)	121.9(2)
N(1)-C(31)-C(32)	115.88(17)	C(58)-C(59)-C(62)	121.0(2)
C(31)-C(32)-C(33)	110.2(2)	C(59)-C(60)-C(61)	123.9(2)
N(2)-C(33)-C(32)	113.5(2)	C(60)-C(61)-C(56)	117.2(2)

C(60)-C(61)-C(66)	121.0(2)	C(70)-C(71)-C(72)	103.7(4)
C(56)-C(61)-C(66)	121.8(2)	N(4)-C(72)-C(71)	109.0(6)
C(63)-C(62)-C(64)	108.8(3)	C(71)-C(72')-N(4)	113.4(6)
C(63)-C(62)-C(65)	107.4(3)	O(8)-C(75)-C(77)	115.3(3)
C(64)-C(62)-C(65)	108.9(2)	O(8)-C(75)-C(78')	113.4(4)
C(63)-C(62)-C(59)	112.2(2)	O(8)-C(75)-C(76')	105.3(3)
C(64)-C(62)-C(59)	110.0(2)	C(78')-C(75)-C(76')	114.1(4)
C(65)-C(62)-C(59)	109.4(2)	O(8)-C(75)-C(76)	106.1(3)
C(68)-C(66)-C(61)	109.6(2)	C(77)-C(75)-C(76)	111.6(4)
C(68)-C(66)-C(69)	111.5(3)	O(8)-C(75)-C(77')	103.3(3)
C(61)-C(66)-C(69)	109.5(2)	C(78')-C(75)-C(77')	110.4(5)
C(68)-C(66)-C(67)	108.2(2)	C(76')-C(75)-C(77')	109.6(4)
C(61)-C(66)-C(67)	111.8(2)	O(8)-C(75)-C(78)	104.2(3)
C(69)-C(66)-C(67)	106.3(2)	C(77)-C(75)-C(78)	110.5(5)
N(3)-C(70)-C(71)	117.2(2)	C(76)-C(75)-C(78)	108.6(4)
C(72')-C(71)-C(70)	115.0(5)		

Table A10. Atomic coordinates (x 10^4) for **AP7**.

	x	y	z
V(1)	4918(2)	3176(1)	8737(1)
C(51)	7050(20)	3320(10)	7459(8)
C(52)	3460(19)	1924(9)	6255(7)
Cl(1)	7744(6)	4028(3)	7204(2)
Cl(2)	6896(6)	2615(3)	7065(2)
Cl(3)	4124(7)	2638(3)	6016(2)
Cl(4)	2472(7)	1478(4)	5827(2)
O(1)	5687(9)	2626(4)	8427(4)
O(2)	6027(8)	3329(4)	9294(3)
O(3)	3227(8)	3151(4)	8472(3)
O(4)	5307(8)	3968(4)	8400(3)
O(5)	3913(9)	4186(4)	9177(3)
N(1)	4224(11)	2266(5)	9227(4)
N(2)	5510(14)	122(6)	8840(5)
C(1)	4782(13)	2289(6)	9747(5)
C(2)	6794(14)	2887(6)	9551(5)
C(3)	6236(14)	2324(6)	9765(5)
C(4)	6984(13)	1834(6)	10037(5)
C(5)	8317(13)	1911(6)	10092(5)
C(6)	8828(14)	2489(6)	9870(5)
C(7)	8166(14)	3000(6)	9604(5)
C(8)	9092(15)	1382(7)	10416(6)

C(9)	8784(16)	625(7)	10222(6)
C(10)	8744(15)	1414(7)	10948(5)
C(11)	10555(16)	1485(9)	10389(7)
C(12)	8777(14)	3634(6)	9376(6)
C(13)	10220(14)	3692(7)	9561(6)
C(14)	8123(14)	4301(6)	9565(6)
C(15)	8730(14)	3608(7)	8817(5)
C(16)	2769(12)	2362(7)	9278(5)
C(17)	2312(13)	2673(6)	8394(5)
C(18)	2007(13)	2250(6)	8802(5)
C(19)	1034(13)	1751(7)	8761(5)
C(20)	346(13)	1680(7)	8315(6)
C(21)	594(12)	2102(6)	7916(5)
C(22)	1571(13)	2624(6)	7944(5)
C(23)	-690(15)	1113(7)	8270(6)
C(24)	-251(16)	444(7)	8503(7)
C(25)	-1115(16)	954(8)	7743(7)
C(26)	-1849(16)	1359(8)	8533(7)
C(27)	1790(15)	3109(7)	7502(5)
C(28)	3251(13)	3110(7)	7372(5)
C(29)	1368(15)	3853(7)	7634(6)
C(30)	1012(15)	2881(7)	7013(5)
C(31)	4471(13)	1571(5)	8986(5)
C(32)	3965(15)	920(6)	9233(5)
C(33)	4171(16)	255(6)	8906(6)
C(34)	6118(19)	-111(9)	9299(7)
C(35)	5673(19)	-401(8)	8459(7)
C(36)	4536(14)	4585(6)	8401(5)
C(37)	4295(14)	4805(6)	8924(5)
C(38)	5228(15)	5138(7)	8096(5)
C(39)	4532(15)	5623(7)	7814(6)
C(40)	5187(18)	6103(8)	7521(6)
C(41)	6472(16)	6118(7)	7523(6)
C(42)	7192(17)	5660(8)	7819(7)
C(43)	6551(16)	5192(7)	8120(6)
C(44)	3266(15)	5374(6)	8942(5)
C(45)	3564(15)	6028(6)	9109(6)
C(46)	2611(15)	6547(7)	9109(6)
C(47)	1386(16)	6392(7)	8946(6)
C(48)	1067(16)	5726(7)	8779(6)
C(49)	1974(16)	5207(8)	8792(6)
C(50)	3894(14)	4285(7)	9708(5)

Table A11. Bond lengths (Å) for **AP7**.

V(1)-O(1)	1.582(9)	C(12)-C(13)	1.566(17)
V(1)-O(4)	1.820(8)	C(16)-C(18)	1.482(17)
V(1)-O(2)	1.866(9)	C(17)-C(22)	1.401(17)
V(1)-O(3)	1.868(9)	C(17)-C(18)	1.410(17)
V(1)-N(1)	2.319(10)	C(18)-C(19)	1.395(17)
C(51)-Cl(1)	1.70(2)	C(19)-C(20)	1.369(18)
C(51)-Cl(2)	1.72(2)	C(20)-C(21)	1.374(17)
C(52)-Cl(3)	1.674(18)	C(20)-C(23)	1.532(18)
C(52)-Cl(4)	1.729(19)	C(21)-C(22)	1.428(16)
O(2)-C(2)	1.333(14)	C(22)-C(27)	1.530(18)
O(3)-C(17)	1.333(14)	C(23)-C(25)	1.49(2)
O(4)-C(36)	1.429(14)	C(23)-C(24)	1.490(18)
O(5)-C(37)	1.431(14)	C(23)-C(26)	1.51(2)
O(5)-C(50)	1.434(14)	C(27)-C(29)	1.539(18)
N(1)-C(1)	1.484(15)	C(27)-C(30)	1.569(19)
N(1)-C(31)	1.508(14)	C(27)-C(28)	1.580(18)
N(1)-C(16)	1.541(15)	C(31)-C(32)	1.518(16)
N(2)-C(34)	1.43(2)	C(32)-C(33)	1.565(17)
N(2)-C(33)	1.439(17)	C(36)-C(37)	1.494(17)
N(2)-C(35)	1.446(18)	C(36)-C(38)	1.538(18)
C(1)-C(3)	1.517(16)	C(37)-C(44)	1.532(17)
C(2)-C(3)	1.364(17)	C(38)-C(39)	1.381(18)
C(2)-C(7)	1.447(17)	C(38)-C(43)	1.382(18)
C(3)-C(4)	1.401(17)	C(39)-C(40)	1.407(19)
C(4)-C(5)	1.399(16)	C(40)-C(41)	1.340(19)
C(5)-C(6)	1.375(17)	C(41)-C(42)	1.38(2)
C(5)-C(8)	1.538(18)	C(42)-C(43)	1.395(19)
C(6)-C(7)	1.378(17)	C(44)-C(45)	1.360(17)
C(7)-C(12)	1.512(17)	C(44)-C(49)	1.423(19)
C(8)-C(10)	1.486(19)	C(45)-C(46)	1.406(17)
C(8)-C(11)	1.543(19)	C(46)-C(47)	1.363(19)
C(8)-C(9)	1.569(19)	C(47)-C(48)	1.389(19)
C(12)-C(15)	1.494(18)	C(48)-C(49)	1.371(19)
C(12)-C(14)	1.546(17)		

Table A12. Bond angles (deg) for **AP7**.

O(1)-V(1)-O(4)	99.5(4)	C(5)-C(8)-C(9)	109.1(13)
O(1)-V(1)-O(2)	102.3(5)	C(11)-C(8)-C(9)	106.8(13)
O(4)-V(1)-O(2)	97.0(4)	C(15)-C(12)-C(7)	112.5(12)
O(1)-V(1)-O(3)	106.1(5)	C(15)-C(12)-C(14)	111.2(11)
O(4)-V(1)-O(3)	93.6(4)	C(7)-C(12)-C(14)	109.3(11)
O(2)-V(1)-O(3)	147.6(4)	C(15)-C(12)-C(13)	107.7(11)
O(1)-V(1)-N(1)	88.6(4)	C(7)-C(12)-C(13)	110.3(12)
O(4)-V(1)-N(1)	171.8(4)	C(14)-C(12)-C(13)	105.7(12)
O(2)-V(1)-N(1)	82.1(4)	C(18)-C(16)-N(1)	113.4(11)
O(3)-V(1)-N(1)	83.2(4)	O(3)-C(17)-C(22)	122.9(12)
Cl(1)-C(51)-Cl(2)	114.2(12)	O(3)-C(17)-C(18)	117.4(12)
Cl(3)-C(52)-Cl(4)	113.2(11)	C(22)-C(17)-C(18)	119.4(13)
C(2)-O(2)-V(1)	130.2(8)	C(19)-C(18)-C(17)	121.6(13)
C(17)-O(3)-V(1)	137.1(8)	C(19)-C(18)-C(16)	121.6(12)
C(36)-O(4)-V(1)	123.3(8)	C(17)-C(18)-C(16)	116.8(12)
C(37)-O(5)-C(50)	112.2(10)	C(20)-C(19)-C(18)	119.0(13)
C(1)-N(1)-C(31)	111.1(10)	C(19)-C(20)-C(21)	120.6(13)
C(1)-N(1)-C(16)	104.9(10)	C(19)-C(20)-C(23)	118.5(13)
C(31)-N(1)-C(16)	109.4(10)	C(21)-C(20)-C(23)	120.8(13)
C(1)-N(1)-V(1)	113.0(7)	C(20)-C(21)-C(22)	122.1(13)
C(31)-N(1)-V(1)	110.9(7)	C(17)-C(22)-C(21)	117.1(12)
C(16)-N(1)-V(1)	107.2(7)	C(17)-C(22)-C(27)	121.8(13)
C(34)-N(2)-C(33)	110.2(15)	C(21)-C(22)-C(27)	121.1(12)
C(34)-N(2)-C(35)	109.1(14)	C(25)-C(23)-C(24)	107.0(13)
C(33)-N(2)-C(35)	111.0(14)	C(25)-C(23)-C(26)	107.4(14)
N(1)-C(1)-C(3)	112.1(12)	C(24)-C(23)-C(26)	108.1(15)
O(2)-C(2)-C(3)	117.4(13)	C(25)-C(23)-C(20)	113.4(13)
O(2)-C(2)-C(7)	121.4(12)	C(24)-C(23)-C(20)	112.1(12)
C(3)-C(2)-C(7)	121.2(13)	C(26)-C(23)-C(20)	108.7(13)
C(2)-C(3)-C(4)	120.6(14)	C(22)-C(27)-C(29)	109.3(12)
C(2)-C(3)-C(1)	118.0(13)	C(22)-C(27)-C(30)	112.7(12)
C(4)-C(3)-C(1)	121.1(13)	C(29)-C(27)-C(30)	107.9(12)
C(5)-C(4)-C(3)	120.6(13)	C(22)-C(27)-C(28)	110.7(11)
C(6)-C(5)-C(4)	116.3(13)	C(29)-C(27)-C(28)	109.8(12)
C(6)-C(5)-C(8)	124.7(13)	C(30)-C(27)-C(28)	106.3(12)
C(4)-C(5)-C(8)	118.8(13)	N(1)-C(31)-C(32)	118.0(11)
C(5)-C(6)-C(7)	126.9(14)	C(31)-C(32)-C(33)	111.5(11)
C(6)-C(7)-C(2)	114.3(12)	N(2)-C(33)-C(32)	111.9(13)
C(6)-C(7)-C(12)	124.7(14)	O(4)-C(36)-C(37)	110.8(11)
C(2)-C(7)-C(12)	121.0(12)	O(4)-C(36)-C(38)	106.9(11)
C(10)-C(8)-C(5)	111.6(13)	C(37)-C(36)-C(38)	113.9(11)
C(10)-C(8)-C(11)	109.1(14)	O(5)-C(37)-C(36)	105.8(10)
C(5)-C(8)-C(11)	112.5(13)	O(5)-C(37)-C(44)	111.2(11)
C(10)-C(8)-C(9)	107.4(12)	C(36)-C(37)-C(44)	112.5(12)

C(39)-C(38)-C(43)	118.1(14)	C(45)-C(44)-C(49)	119.8(13)
C(39)-C(38)-C(36)	120.4(14)	C(45)-C(44)-C(37)	121.1(14)
C(43)-C(38)-C(36)	121.4(13)	C(49)-C(44)-C(37)	119.1(12)
C(38)-C(39)-C(40)	119.3(15)	C(44)-C(45)-C(46)	120.1(15)
C(41)-C(40)-C(39)	121.6(16)	C(47)-C(46)-C(45)	119.9(14)
C(40)-C(41)-C(42)	120.3(17)	C(46)-C(47)-C(48)	120.6(14)
C(41)-C(42)-C(43)	118.5(17)	C(49)-C(48)-C(47)	120.3(16)
C(38)-C(43)-C(42)	121.8(16)	C(48)-C(49)-C(44)	119.2(14)

Table A13. Atomic coordinates (x 10^4) for **TA5**.

	x	y	z
V(1)	6350(1)	7986(1)	5978(1)
O(1)	6761(2)	8581(1)	6109(1)
O(2)	6052(2)	7406(1)	6184(1)
O(3)	8041(2)	7893(1)	5770(1)
O(4)	5326(2)	8010(1)	5079(1)
N(1)	7701(2)	7940(1)	7368(1)
N(2)	4556(2)	8142(1)	6442(1)
N(3)	9016(6)	4242(2)	6836(4)
C(1)	7816(3)	8378(1)	7758(2)
C(2)	7845(2)	8818(1)	6540(2)
C(3)	8437(3)	8725(1)	7360(2)
C(4)	9540(3)	8968(1)	7819(2)
C(5)	10083(3)	9315(1)	7485(2)
C(6)	9461(3)	9404(1)	6671(2)
C(7)	8351(3)	9171(1)	6181(2)
C(8)	11255(3)	9597(1)	8021(2)
C(9)	12310(3)	9312(1)	8617(2)
C(10)	12007(3)	9853(1)	7516(2)
C(11)	10642(4)	9922(1)	8486(2)
C(12)	7676(3)	9296(1)	5291(2)
C(13)	8430(4)	9678(1)	5025(2)
C(14)	6196(3)	9441(1)	5184(2)
C(15)	7701(4)	8913(1)	4728(2)
C(16)	7051(3)	7656(1)	7847(1)
C(17)	6269(2)	7087(1)	6752(1)
C(18)	6829(2)	7190(1)	7572(1)
C(19)	7076(2)	6862(1)	8152(2)
C(20)	6735(2)	6431(1)	7948(2)
C(21)	6142(2)	6339(1)	7125(2)
C(22)	5893(2)	6650(1)	6513(1)

C(23)	6934(3)	6066(1)	8584(2)
C(24)	7707(4)	6223(1)	9435(2)
C(25)	5525(3)	5903(1)	8600(2)
C(26)	7724(4)	5681(1)	8374(2)
C(27)	5221(3)	6529(1)	5617(2)
C(28)	6246(3)	6616(1)	5139(2)
C(29)	3904(3)	6795(1)	5260(2)
C(30)	4834(3)	6040(1)	5514(2)
C(31)	9117(2)	7775(1)	7439(2)
C(32)	8824(2)	7534(1)	6009(1)
C(33)	9250(2)	7433(1)	6838(1)
C(34)	9939(2)	7045(1)	7101(2)
C(35)	10255(2)	6755(1)	6562(2)
C(36)	9929(2)	6884(1)	5754(2)
C(37)	9225(2)	7270(1)	5446(1)
C(38)	10931(3)	6316(1)	6852(2)
C(39)	10141(5)	6089(1)	7353(3)
C(40)	11043(5)	6026(1)	6166(2)
C(41)	12416(4)	6409(1)	7409(3)
C(39')	9784(12)	5955(4)	6417(8)
C(40')	12131(12)	6213(4)	6540(8)
C(41')	11222(15)	6223(4)	7740(6)
C(42)	9002(3)	7409(1)	4561(2)
C(43)	7494(3)	7505(1)	4110(2)
C(44)	9845(3)	7822(1)	4556(2)
C(45)	9478(4)	7056(1)	4071(2)
C(46)	3659(3)	7829(1)	6496(2)
C(47)	2421(3)	7914(1)	6622(2)
C(48)	2041(3)	8340(1)	6681(2)
C(49)	2932(3)	8662(1)	6625(2)
C(50)	4173(3)	8552(1)	6510(2)
C(51)	8632(8)	4619(3)	7115(5)
C(52)	8235(7)	4969(2)	6630(4)
C(53)	8249(6)	4954(2)	5870(4)
C(54)	8618(6)	4594(2)	5578(3)
C(55)	8942(5)	4248(2)	6045(5)

Table A14. Bond lengths (Å) for **TA5**.

V(1)-O(4)	1.5946(16)	C(20)-C(21)	1.397(3)
V(1)-O(2)	1.8517(15)	C(20)-C(23)	1.535(3)
V(1)-O(1)	1.8652(15)	C(21)-C(22)	1.389(3)
V(1)-O(3)	1.8803(16)	C(22)-C(27)	1.540(3)
V(1)-N(2)	2.249(2)	C(23)-C(24)	1.525(4)
V(1)-N(1)	2.3899(19)	C(23)-C(26)	1.527(4)
O(1)-C(2)	1.347(3)	C(23)-C(25)	1.527(4)
O(2)-C(17)	1.352(2)	C(27)-C(28)	1.531(4)
O(3)-C(32)	1.349(3)	C(27)-C(29)	1.534(4)
N(1)-C(16)	1.482(3)	C(27)-C(30)	1.542(3)
N(1)-C(1)	1.487(3)	C(31)-C(33)	1.508(3)
N(1)-C(31)	1.497(3)	C(32)-C(33)	1.401(3)
N(2)-C(50)	1.329(3)	C(32)-C(37)	1.411(3)
N(2)-C(46)	1.345(3)	C(33)-C(34)	1.384(3)
N(3)-C(55)	1.343(7)	C(34)-C(35)	1.390(3)
N(3)-C(51)	1.351(7)	C(35)-C(36)	1.391(3)
C(1)-C(3)	1.501(3)	C(35)-C(38)	1.524(3)
C(2)-C(3)	1.394(3)	C(36)-C(37)	1.401(3)
C(2)-C(7)	1.415(3)	C(37)-C(42)	1.536(3)
C(3)-C(4)	1.385(3)	C(38)-C(41')	1.498(9)
C(4)-C(5)	1.396(3)	C(38)-C(40')	1.506(9)
C(5)-C(6)	1.387(4)	C(38)-C(40)	1.508(4)
C(5)-C(8)	1.540(4)	C(38)-C(39)	1.511(4)
C(6)-C(7)	1.392(3)	C(38)-C(41)	1.560(5)
C(7)-C(12)	1.534(4)	C(38)-C(39')	1.622(9)
C(8)-C(11)	1.521(4)	C(42)-C(44)	1.529(4)
C(8)-C(9)	1.523(4)	C(42)-C(43)	1.531(4)
C(8)-C(10)	1.533(4)	C(42)-C(45)	1.533(4)
C(12)-C(15)	1.526(4)	C(46)-C(47)	1.365(4)
C(12)-C(14)	1.529(4)	C(47)-C(48)	1.372(4)
C(12)-C(13)	1.541(3)	C(48)-C(49)	1.361(4)
C(16)-C(18)	1.498(3)	C(49)-C(50)	1.377(4)
C(17)-C(18)	1.397(3)	C(51)-C(52)	1.345(8)
C(17)-C(22)	1.417(3)	C(52)-C(53)	1.317(7)
C(18)-C(19)	1.386(3)	C(53)-C(54)	1.308(6)
C(19)-C(20)	1.383(3)	C(54)-C(55)	1.312(7)

Table A15. Bond angles (deg) for **TA5**.

O(4)-V(1)-O(2)	97.63(8)	C(9)-C(8)-C(10)	107.8(3)
O(4)-V(1)-O(1)	97.60(8)	C(11)-C(8)-C(5)	108.4(2)
O(2)-V(1)-O(1)	162.69(7)	C(9)-C(8)-C(5)	110.6(2)
O(4)-V(1)-O(3)	101.20(8)	C(10)-C(8)-C(5)	112.0(2)
O(2)-V(1)-O(3)	95.93(7)	C(15)-C(12)-C(14)	110.3(3)
O(1)-V(1)-O(3)	89.13(7)	C(15)-C(12)-C(7)	111.1(2)
O(4)-V(1)-N(2)	88.22(8)	C(14)-C(12)-C(7)	109.2(2)
O(2)-V(1)-N(2)	86.49(7)	C(15)-C(12)-C(13)	106.9(2)
O(1)-V(1)-N(2)	85.82(7)	C(14)-C(12)-C(13)	107.6(2)
O(3)-V(1)-N(2)	169.84(7)	C(7)-C(12)-C(13)	111.8(2)
O(4)-V(1)-N(1)	174.68(8)	N(1)-C(16)-C(18)	115.60(18)
O(2)-V(1)-N(1)	80.23(6)	O(2)-C(17)-C(18)	120.12(19)
O(1)-V(1)-N(1)	83.88(7)	O(2)-C(17)-C(22)	119.8(2)
O(3)-V(1)-N(1)	83.90(7)	C(18)-C(17)-C(22)	120.1(2)
N(2)-V(1)-N(1)	86.79(7)	C(19)-C(18)-C(17)	120.1(2)
C(2)-O(1)-V(1)	135.26(15)	C(19)-C(18)-C(16)	118.8(2)
C(17)-O(2)-V(1)	145.89(15)	C(17)-C(18)-C(16)	120.9(2)
C(32)-O(3)-V(1)	123.81(14)	C(20)-C(19)-C(18)	121.8(2)
C(16)-N(1)-C(1)	105.27(17)	C(19)-C(20)-C(21)	116.9(2)
C(16)-N(1)-C(31)	109.47(18)	C(19)-C(20)-C(23)	122.7(2)
C(1)-N(1)-C(31)	108.66(18)	C(21)-C(20)-C(23)	120.4(2)
C(16)-N(1)-V(1)	111.96(14)	C(22)-C(21)-C(20)	124.2(2)
C(1)-N(1)-V(1)	110.29(14)	C(21)-C(22)-C(17)	116.9(2)
C(31)-N(1)-V(1)	110.99(13)	C(21)-C(22)-C(27)	121.7(2)
C(50)-N(2)-C(46)	116.2(2)	C(17)-C(22)-C(27)	121.4(2)
C(50)-N(2)-V(1)	121.45(17)	C(24)-C(23)-C(26)	108.2(3)
C(46)-N(2)-V(1)	120.87(17)	C(24)-C(23)-C(25)	107.8(2)
C(55)-N(3)-C(51)	114.4(6)	C(26)-C(23)-C(25)	108.4(2)
N(1)-C(1)-C(3)	114.61(19)	C(24)-C(23)-C(20)	112.4(2)
O(1)-C(2)-C(3)	119.3(2)	C(26)-C(23)-C(20)	111.1(2)
O(1)-C(2)-C(7)	120.9(2)	C(25)-C(23)-C(20)	108.9(2)
C(3)-C(2)-C(7)	119.7(2)	C(28)-C(27)-C(29)	110.3(2)
C(4)-C(3)-C(2)	120.4(2)	C(28)-C(27)-C(22)	109.0(2)
C(4)-C(3)-C(1)	119.9(2)	C(29)-C(27)-C(22)	110.6(2)
C(2)-C(3)-C(1)	119.6(2)	C(28)-C(27)-C(30)	107.3(2)
C(3)-C(4)-C(5)	121.7(2)	C(29)-C(27)-C(30)	107.8(2)
C(6)-C(5)-C(4)	116.7(2)	C(22)-C(27)-C(30)	111.8(2)
C(6)-C(5)-C(8)	122.6(2)	N(1)-C(31)-C(33)	117.17(19)
C(4)-C(5)-C(8)	120.6(2)	O(3)-C(32)-C(33)	117.9(2)
C(5)-C(6)-C(7)	124.1(2)	O(3)-C(32)-C(37)	121.4(2)
C(6)-C(7)-C(2)	117.4(2)	C(33)-C(32)-C(37)	120.7(2)
C(6)-C(7)-C(12)	121.6(2)	C(34)-C(33)-C(32)	119.9(2)
C(2)-C(7)-C(12)	121.0(2)	C(34)-C(33)-C(31)	120.6(2)
C(11)-C(8)-C(9)	109.5(3)	C(32)-C(33)-C(31)	119.1(2)
C(11)-C(8)-C(10)	108.5(3)	C(33)-C(34)-C(35)	121.5(2)

C(34)-C(35)-C(36)	117.1(2)	C(35)-C(38)-C(39')	104.7(5)
C(34)-C(35)-C(38)	120.9(2)	C(44)-C(42)-C(43)	108.6(2)
C(36)-C(35)-C(38)	122.0(2)	C(44)-C(42)-C(45)	108.0(2)
C(35)-C(36)-C(37)	124.2(2)	C(43)-C(42)-C(45)	106.7(2)
C(36)-C(37)-C(32)	116.2(2)	C(44)-C(42)-C(37)	108.4(2)
C(36)-C(37)-C(42)	121.2(2)	C(43)-C(42)-C(37)	112.9(2)
C(32)-C(37)-C(42)	122.5(2)	C(45)-C(42)-C(37)	112.0(2)
C(41')-C(38)-C(40')	112.8(7)	N(2)-C(46)-C(47)	123.5(3)
C(40)-C(38)-C(39)	110.8(3)	C(46)-C(47)-C(48)	119.1(3)
C(41')-C(38)-C(35)	116.0(5)	C(49)-C(48)-C(47)	118.3(3)
C(40')-C(38)-C(35)	113.8(5)	C(48)-C(49)-C(50)	119.4(3)
C(40)-C(38)-C(35)	113.0(2)	N(2)-C(50)-C(49)	123.4(3)
C(39)-C(38)-C(35)	109.1(2)	C(52)-C(51)-N(3)	121.6(7)
C(40)-C(38)-C(41)	107.8(3)	C(53)-C(52)-C(51)	120.1(6)
C(39)-C(38)-C(41)	108.2(3)	C(54)-C(53)-C(52)	120.1(6)
C(35)-C(38)-C(41)	107.7(2)	C(53)-C(54)-C(55)	119.4(6)
C(41')-C(38)-C(39')	104.0(6)	C(54)-C(55)-N(3)	124.3(6)
C(40')-C(38)-C(39')	104.0(7)		

Table A16. Atomic coordinates (x 10^4) for **TA6**.

	x	y	z
V(1)	3639(1)	7611(1)	1973(1)
S(1)	2796(1)	5422(1)	2173(1)
O(1)	4142(1)	7060(2)	2658(1)
O(2)	4082(1)	8920(2)	1962(1)
O(3)	3263(1)	7761(2)	1168(1)
O(4)	3022(1)	8014(2)	2299(1)
O(5)	3301(1)	6022(2)	1843(1)
N(1)	4544(1)	6843(2)	1544(1)
C(1)	4680(2)	5699(3)	1748(2)
C(2)	4527(2)	6189(3)	2834(2)
C(3)	4809(2)	5548(3)	2415(2)
C(4)	5215(2)	4661(3)	2624(2)
C(5)	5337(2)	4393(3)	3227(2)
C(6)	5037(2)	5052(3)	3624(2)
C(7)	4635(2)	5952(3)	3454(2)
C(8)	5780(2)	3429(4)	3462(2)
C(9)	6051(3)	2809(5)	2945(2)
C(10)	6363(2)	3871(4)	3903(3)
C(11)	5376(2)	2612(4)	3791(2)
C(12)	4318(2)	6636(3)	3917(2)
C(13)	4564(2)	7834(4)	3906(2)
C(14)	4499(2)	6215(4)	4556(2)
C(15)	3552(2)	6615(4)	3780(2)
C(16)	5144(2)	7519(3)	1743(2)
C(17)	4564(2)	9355(3)	1672(2)
C(18)	5095(2)	8688(3)	1545(2)
C(19)	5592(2)	9138(3)	1254(2)
C(20)	5597(2)	10240(3)	1100(2)
C(21)	5067(2)	10873(3)	1242(2)
C(22)	4543(2)	10478(3)	1524(2)
C(23)	6146(2)	10717(3)	763(2)
C(24)	6773(5)	9950(10)	841(6)
C(25)	6358(7)	11825(9)	1021(7)
C(26)	5895(8)	10795(12)	105(5)
C(24')	6829(5)	10423(10)	1072(6)
C(25')	6109(7)	12004(7)	727(5)
C(26')	6034(7)	10305(10)	121(4)
C(27)	3971(2)	11213(3)	1667(2)
C(28)	3956(2)	11256(4)	2345(2)
C(29)	4052(2)	12399(4)	1444(3)
C(30)	3300(2)	10790(4)	1348(2)
C(31)	4425(2)	6859(3)	879(2)

C(32)	3192(2)	6996(3)	741(2)
C(33)	3758(2)	6432(3)	608(2)
C(34)	3702(2)	5590(3)	196(2)
C(35)	3088(2)	5293(3)	-116(2)
C(36)	2539(2)	5902(4)	-3(2)
C(37)	2560(2)	6745(3)	413(2)
C(38)	3048(2)	4401(4)	-600(3)
C(39)	3303(6)	3358(11)	-338(7)
C(40)	3501(5)	4724(12)	-1087(6)
C(41)	2365(4)	4300(9)	-950(5)
C(39')	3581(7)	3553(13)	-487(9)
C(40')	3173(10)	5012(17)	-1188(8)
C(41')	2376(6)	3894(18)	-733(12)
C(42)	1937(2)	7436(4)	484(2)
C(43)	1317(2)	7026(5)	85(2)
C(44)	2069(2)	8623(4)	311(3)
C(45)	1766(2)	7413(4)	1128(2)
C(46)	3258(2)	4412(4)	2613(2)
C(47)	2395(2)	4555(4)	1608(2)
C(48)	8763(3)	3727(5)	2053(3)
C(49)	8755(3)	2658(6)	1835(3)
C(50)	8284(4)	1914(5)	1991(4)
C(51)	7823(4)	2239(7)	2364(5)
C(52)	7831(4)	3309(8)	2581(4)
C(53)	8301(4)	4053(5)	2426(4)
C(54)	9247(5)	4498(8)	1897(5)
C(55)	8462(6)	3803(7)	2206(6)
C(56)	8779(5)	3111(10)	1839(5)
C(57)	8633(5)	1995(9)	1819(5)
C(58)	8171(5)	1571(7)	2164(6)
C(59)	7854(6)	2262(8)	2531(6)
C(60)	7999(7)	3378(8)	2551(6)
C(61)	8663(9)	4940(12)	2276(8)

Table A17. Bond lengths (Å) for **TA6**.

V(1)-O(4)	1.602(2)	C(23)-C(25)	1.509(9)
V(1)-O(2)	1.831(2)	C(23)-C(24')	1.509(9)
V(1)-O(1)	1.856(2)	C(23)-C(26')	1.516(9)
V(1)-O(3)	1.879(2)	C(23)-C(24)	1.568(9)
V(1)-O(5)	2.060(2)	C(23)-C(25')	1.570(9)
V(1)-N(1)	2.368(3)	C(27)-C(28)	1.525(6)
S(1)-O(5)	1.523(2)	C(27)-C(30)	1.539(6)
S(1)-C(47)	1.766(4)	C(27)-C(29)	1.544(6)
S(1)-C(46)	1.768(4)	C(31)-C(33)	1.501(4)
O(1)-C(2)	1.346(4)	C(32)-C(33)	1.400(5)
O(2)-C(17)	1.348(4)	C(32)-C(37)	1.425(5)
O(3)-C(32)	1.332(4)	C(33)-C(34)	1.374(5)
N(1)-C(31)	1.481(4)	C(34)-C(35)	1.394(5)
N(1)-C(1)	1.481(4)	C(35)-C(36)	1.385(5)
N(1)-C(16)	1.488(4)	C(35)-C(38)	1.531(6)
C(1)-C(3)	1.496(5)	C(36)-C(37)	1.383(5)
C(2)-C(3)	1.399(5)	C(37)-C(42)	1.541(5)
C(2)-C(7)	1.411(5)	C(38)-C(39)	1.466(10)
C(3)-C(4)	1.401(5)	C(38)-C(41')	1.487(12)
C(4)-C(5)	1.382(5)	C(38)-C(39')	1.491(11)
C(5)-C(6)	1.396(6)	C(38)-C(41)	1.503(8)
C(5)-C(8)	1.529(5)	C(38)-C(40')	1.565(12)
C(6)-C(7)	1.388(5)	C(38)-C(40)	1.566(9)
C(7)-C(12)	1.534(5)	C(42)-C(43)	1.527(5)
C(8)-C(11)	1.536(6)	C(42)-C(45)	1.528(6)
C(8)-C(10)	1.537(7)	C(42)-C(44)	1.530(6)
C(8)-C(9)	1.543(7)	C(48)-C(49)	1.3900
C(12)-C(14)	1.523(6)	C(48)-C(53)	1.3900
C(12)-C(13)	1.541(6)	C(48)-C(54)	1.432(10)
C(12)-C(15)	1.543(5)	C(49)-C(50)	1.3900
C(16)-C(18)	1.490(5)	C(50)-C(51)	1.3900
C(17)-C(18)	1.404(5)	C(51)-C(52)	1.3900
C(17)-C(22)	1.406(5)	C(52)-C(53)	1.3900
C(18)-C(19)	1.381(5)	C(55)-C(56)	1.3900
C(19)-C(20)	1.385(5)	C(55)-C(60)	1.3900
C(20)-C(21)	1.390(5)	C(55)-C(61)	1.446(14)
C(20)-C(23)	1.536(5)	C(56)-C(57)	1.3900
C(21)-C(22)	1.391(5)	C(57)-C(58)	1.3900
C(22)-C(27)	1.530(5)	C(58)-C(59)	1.3900
C(23)-C(26)	1.501(9)	C(59)-C(60)	1.3900

Table A18. Bond angles (deg) for **TA6**.

O(4)-V(1)-O(2)	98.71(12)	C(11)-C(8)-C(10)	109.1(4)
O(4)-V(1)-O(1)	96.25(12)	C(5)-C(8)-C(9)	111.4(4)
O(2)-V(1)-O(1)	96.26(11)	C(11)-C(8)-C(9)	107.9(4)
O(4)-V(1)-O(3)	99.56(12)	C(10)-C(8)-C(9)	109.8(4)
O(2)-V(1)-O(3)	92.29(11)	C(14)-C(12)-C(7)	112.6(3)
O(1)-V(1)-O(3)	160.67(11)	C(14)-C(12)-C(13)	107.1(4)
O(4)-V(1)-O(5)	95.06(11)	C(7)-C(12)-C(13)	109.9(3)
O(2)-V(1)-O(5)	165.91(10)	C(14)-C(12)-C(15)	107.2(3)
O(1)-V(1)-O(5)	85.15(11)	C(7)-C(12)-C(15)	110.7(3)
O(3)-V(1)-O(5)	82.45(10)	C(13)-C(12)-C(15)	109.4(4)
O(4)-V(1)-N(1)	174.16(12)	N(1)-C(16)-C(18)	114.7(3)
O(2)-V(1)-N(1)	86.12(10)	O(2)-C(17)-C(18)	119.3(3)
O(1)-V(1)-N(1)	79.89(10)	O(2)-C(17)-C(22)	119.6(3)
O(3)-V(1)-N(1)	83.44(10)	C(18)-C(17)-C(22)	121.0(3)
O(5)-V(1)-N(1)	80.31(9)	C(19)-C(18)-C(17)	119.3(3)
O(5)-S(1)-C(47)	102.27(19)	C(19)-C(18)-C(16)	119.6(3)
O(5)-S(1)-C(46)	105.35(17)	C(17)-C(18)-C(16)	121.0(3)
C(47)-S(1)-C(46)	98.4(2)	C(18)-C(19)-C(20)	122.0(4)
C(2)-O(1)-V(1)	139.8(2)	C(19)-C(20)-C(21)	116.7(3)
C(17)-O(2)-V(1)	137.3(2)	C(19)-C(20)-C(23)	121.2(4)
C(32)-O(3)-V(1)	128.2(2)	C(21)-C(20)-C(23)	122.0(4)
S(1)-O(5)-V(1)	127.79(15)	C(20)-C(21)-C(22)	124.6(4)
C(31)-N(1)-C(1)	109.0(3)	C(21)-C(22)-C(17)	116.2(3)
C(31)-N(1)-C(16)	108.4(3)	C(21)-C(22)-C(27)	122.4(3)
C(1)-N(1)-C(16)	108.3(3)	C(17)-C(22)-C(27)	121.4(3)
C(31)-N(1)-V(1)	111.73(19)	C(26)-C(23)-C(25)	111.4(8)
C(1)-N(1)-V(1)	111.6(2)	C(24')-C(23)-C(26')	112.1(8)
C(16)-N(1)-V(1)	107.7(2)	C(26)-C(23)-C(20)	109.5(8)
N(1)-C(1)-C(3)	115.3(3)	C(25)-C(23)-C(20)	109.7(7)
O(1)-C(2)-C(3)	120.8(3)	C(24')-C(23)-C(20)	111.2(7)
O(1)-C(2)-C(7)	117.5(3)	C(26')-C(23)-C(20)	108.3(7)
C(3)-C(2)-C(7)	121.7(3)	C(26)-C(23)-C(24)	108.3(7)
C(2)-C(3)-C(4)	118.4(4)	C(25)-C(23)-C(24)	107.7(7)
C(2)-C(3)-C(1)	124.8(3)	C(20)-C(23)-C(24)	110.2(6)
C(4)-C(3)-C(1)	116.7(3)	C(24')-C(23)-C(25')	107.1(6)
C(5)-C(4)-C(3)	122.3(4)	C(26')-C(23)-C(25')	106.4(6)
C(4)-C(5)-C(6)	116.8(4)	C(20)-C(23)-C(25')	111.7(6)
C(4)-C(5)-C(8)	122.9(4)	C(28)-C(27)-C(22)	110.0(3)
C(6)-C(5)-C(8)	120.3(4)	C(28)-C(27)-C(30)	110.3(4)
C(7)-C(6)-C(5)	124.4(4)	C(22)-C(27)-C(30)	110.6(3)
C(6)-C(7)-C(2)	116.3(4)	C(28)-C(27)-C(29)	108.0(4)
C(6)-C(7)-C(12)	121.5(4)	C(22)-C(27)-C(29)	111.3(3)
C(2)-C(7)-C(12)	122.1(3)	C(30)-C(27)-C(29)	106.6(4)
C(5)-C(8)-C(11)	109.8(3)	N(1)-C(31)-C(33)	115.3(3)
C(5)-C(8)-C(10)	108.8(4)	O(3)-C(32)-C(33)	118.8(3)

O(3)-C(32)-C(37)	122.0(3)	C(35)-C(38)-C(40)	109.6(7)
C(33)-C(32)-C(37)	119.3(3)	C(43)-C(42)-C(45)	106.3(4)
C(34)-C(33)-C(32)	120.6(3)	C(43)-C(42)-C(44)	108.5(4)
C(34)-C(33)-C(31)	121.6(3)	C(45)-C(42)-C(44)	109.0(4)
C(32)-C(33)-C(31)	117.4(3)	C(43)-C(42)-C(37)	112.4(3)
C(33)-C(34)-C(35)	121.6(3)	C(45)-C(42)-C(37)	112.1(3)
C(36)-C(35)-C(34)	116.8(4)	C(44)-C(42)-C(37)	108.4(3)
C(36)-C(35)-C(38)	122.7(4)	C(49)-C(48)-C(53)	120.0
C(34)-C(35)-C(38)	120.3(4)	C(49)-C(48)-C(54)	120.4(5)
C(37)-C(36)-C(35)	124.4(3)	C(53)-C(48)-C(54)	119.6(5)
C(36)-C(37)-C(32)	117.1(3)	C(50)-C(49)-C(48)	120.0
C(36)-C(37)-C(42)	121.4(3)	C(51)-C(50)-C(49)	120.0
C(32)-C(37)-C(42)	121.4(3)	C(50)-C(51)-C(52)	120.0
C(41')-C(38)-C(39')	111.7(10)	C(51)-C(52)-C(53)	120.0
C(39)-C(38)-C(41)	113.1(7)	C(52)-C(53)-C(48)	120.0
C(39)-C(38)-C(35)	110.3(8)	C(56)-C(55)-C(60)	120.0
C(41')-C(38)-C(35)	113.7(12)	C(56)-C(55)-C(61)	120.0(7)
C(39')-C(38)-C(35)	113.5(9)	C(60)-C(55)-C(61)	119.7(7)
C(41)-C(38)-C(35)	112.9(5)	C(55)-C(56)-C(57)	120.0
C(41')-C(38)-C(40')	105.7(10)	C(58)-C(57)-C(56)	120.0
C(39')-C(38)-C(40')	106.3(9)	C(57)-C(58)-C(59)	120.0
C(35)-C(38)-C(40')	105.2(10)	C(60)-C(59)-C(58)	120.0
C(39)-C(38)-C(40)	106.8(7)	C(59)-C(60)-C(55)	120.0
C(41)-C(38)-C(40)	103.7(7)		

Table A19. Atomic coordinates (x 10^4) for **TA8**.

	x	y	z
V(1)	3931(1)	3604(1)	3332(1)
N(1)	4827(2)	2574(2)	3795(1)
N(2)	2990(2)	4537(2)	2842(1)
C(46)	2455(3)	4793(3)	2543(2)
C(47)	1751(4)	5113(5)	2156(2)
O(1)	4620(2)	3274(3)	2787(1)
C(1)	5803(4)	2548(5)	3593(2)
C(2)	5810(3)	1999(4)	3088(2)
C(3)	6416(3)	1114(4)	3004(2)
C(4)	6486(7)	637(7)	2532(3)
C(5)	5889(13)	1079(16)	2152(3)
C(6)	5264(8)	1963(8)	2218(2)
C(7)	5226(3)	2431(4)	2696(2)
C(8)	7203(3)	-337(3)	2431(2)
C(9)	8099(4)	179(5)	2244(3)
C(10)	7479(5)	-994(5)	2903(2)
C(11)	6822(5)	-1188(5)	2054(3)
C(12)	4659(3)	2377(3)	1757(1)
C(13)	4824(3)	3625(3)	1709(2)
C(14)	3582(3)	2183(5)	1830(2)
C(15)	4927(5)	1850(4)	1266(2)
O(1')	4209(6)	2682(8)	2733(3)
C(1')	4867(8)	1395(9)	3558(4)
C(2')	5288(7)	1293(8)	3048(4)
C(3')	6012(8)	528(9)	2972(4)
C(4')	6375(19)	365(19)	2501(6)
C(5')	5960(30)	980(40)	2110(8)
C(6')	5210(20)	1720(20)	2166(6)
C(7')	4910(8)	1933(10)	2653(4)
O(2)	4205(3)	4860(3)	3748(1)
C(16)	4895(4)	3077(4)	4321(2)
C(17)	5391(3)	4187(4)	4327(2)
C(18)	6266(4)	4313(4)	4588(2)
C(19)	6754(5)	5317(5)	4595(3)
C(20)	6274(7)	6198(7)	4368(5)
C(21)	5410(6)	6115(5)	4091(4)
C(22)	4992(4)	5054(4)	4051(2)
C(23)	7812(3)	5404(3)	4830(2)
C(24)	8155(3)	6603(4)	4879(2)
C(25)	7782(4)	4887(4)	5345(2)
C(26)	8528(4)	4760(5)	4519(2)
C(27)	4944(3)	7112(3)	3840(1)

C(28)	4919(4)	7066(4)	3273(2)
C(29)	3904(3)	7164(5)	4017(2)
C(30)	5426(4)	8197(3)	4005(2)
O(2')	4678(6)	4830(6)	3485(3)
C(16')	5849(9)	2983(9)	3752(5)
C(17')	5980(7)	4110(8)	3978(4)
C(18')	6764(8)	4278(9)	4306(4)
C(19')	7004(13)	5328(13)	4484(8)
C(20')	6455(18)	6191(16)	4292(13)
C(21')	5615(14)	6081(12)	4002(9)
C(22')	5418(8)	4999(8)	3814(5)
O(3)	2867(2)	2666(3)	3443(1)
C(31)	4441(3)	1440(4)	3856(2)
C(32)	3433(3)	1354(4)	4045(2)
C(33)	3247(4)	625(4)	4432(2)
C(34)	2304(5)	430(7)	4575(4)
C(35)	1571(7)	941(14)	4298(6)
C(36)	1709(5)	1685(7)	3913(3)
C(37)	2678(3)	1913(4)	3797(2)
C(38)	2112(3)	-323(3)	5011(1)
C(39)	1551(4)	285(4)	5409(2)
C(40)	1496(4)	-1284(4)	4805(2)
C(41)	3009(3)	-808(4)	5258(2)
C(42)	884(2)	2228(3)	3618(1)
C(43)	-90(3)	1768(3)	3779(2)
C(44)	985(3)	1926(4)	3067(2)
C(45)	835(3)	3490(3)	3674(2)
O(3')	2873(6)	3196(8)	3626(3)
C(31')	4440(7)	2549(10)	4265(4)
C(32')	3461(7)	2007(8)	4278(4)
C(33')	3297(8)	1145(10)	4602(4)
C(34')	2399(13)	642(18)	4636(9)
C(35')	1659(17)	1080(30)	4334(15)
C(36')	1782(11)	1907(19)	3985(9)
C(37')	2713(8)	2369(10)	3955(4)

Table A20. Bond lengths (Å) for **TA8**.

V(1)-O(3')	1.756(8)	C(11)-H(11A)	0.9800
V(1)-O(1)	1.814(3)	C(11)-H(11B)	0.9800
V(1)-O(2')	1.845(7)	C(11)-H(11C)	0.9800
V(1)-O(3)	1.890(3)	C(12)-C(15)	1.518(6)
V(1)-O(2)	1.914(3)	C(12)-C(14)	1.529(6)
V(1)-O(1')	2.001(8)	C(12)-C(13)	1.531(5)
V(1)-N(1)	2.130(3)	C(12)-C(6')	1.536(19)
V(1)-N(2)	2.141(3)	C(13)-H(13A)	0.9800
N(1)-C(31')	1.385(11)	C(13)-H(13B)	0.9800
N(1)-C(1)	1.473(6)	C(13)-H(13C)	0.9800
N(1)-C(31)	1.481(5)	C(14)-H(14A)	0.9800
N(1)-C(16')	1.508(13)	C(14)-H(14B)	0.9800
N(1)-C(16)	1.535(5)	C(14)-H(14C)	0.9800
N(1)-C(1')	1.563(11)	C(15)-H(15A)	0.9800
N(2)-C(46)	1.119(5)	C(15)-H(15B)	0.9800
C(46)-C(47)	1.453(6)	C(15)-H(15C)	0.9800
C(47)-H(47A)	0.9800	O(1')-C(7')	1.349(11)
C(47)-H(47B)	0.9800	C(1')-C(2')	1.508(12)
C(47)-H(47C)	0.9800	C(1')-H(1'1)	0.9900
O(1)-C(7)	1.346(5)	C(1')-H(1'2)	0.9900
C(1)-C(2)	1.507(7)	C(2')-C(3')	1.384(12)
C(1)-H(1A)	0.9900	C(2')-C(7')	1.399(12)
C(1)-H(1B)	0.9900	C(3')-C(4')	1.387(15)
C(2)-C(3)	1.383(6)	C(3')-H(3')	0.9500
C(2)-C(7)	1.406(6)	C(4')-C(5')	1.396(15)
C(3)-C(4)	1.395(8)	C(5')-C(6')	1.386(16)
C(3)-H(3)	0.9500	C(5')-H(5')	0.9500
C(4)-C(5)	1.398(9)	C(6')-C(7')	1.403(14)
C(4)-C(8)	1.570(8)	O(2)-C(22)	1.360(5)
C(5)-C(6)	1.390(8)	C(16)-C(17)	1.507(6)
C(5)-H(5)	0.9500	C(16)-H(16A)	0.9900
C(6)-C(7)	1.403(8)	C(16)-H(16B)	0.9900
C(6)-C(12)	1.556(8)	C(17)-C(22)	1.388(6)
C(8)-C(4')	1.44(2)	C(17)-C(18)	1.390(6)
C(8)-C(9)	1.490(6)	C(18)-C(19)	1.388(7)
C(8)-C(11)	1.524(7)	C(18)-H(18)	0.9500
C(8)-C(10)	1.533(7)	C(19)-C(20)	1.385(8)
C(9)-H(9A)	0.9800	C(19)-C(23)	1.582(7)
C(9)-H(9B)	0.9800	C(20)-C(21)	1.393(7)
C(9)-H(9C)	0.9800	C(20)-H(20)	0.9500
C(10)-H(10A)	0.9800	C(21)-C(22)	1.408(7)
C(10)-H(10B)	0.9800	C(21)-C(27)	1.515(8)
C(10)-H(10C)	0.9800	C(23)-C(19')	1.434(18)

C(23)-C(25)	1.517(6)	C(34)-C(35)	1.385(7)
C(23)-C(24)	1.529(6)	C(34)-C(38)	1.509(8)
C(23)-C(26)	1.528(7)	C(35)-C(36)	1.386(7)
C(24)-H(24A)	0.9800	C(35)-H(35)	0.9500
C(24)-H(24B)	0.9800	C(36)-C(37)	1.413(7)
C(24)-H(24C)	0.9800	C(36)-C(42)	1.520(8)
C(25)-H(25A)	0.9800	C(38)-C(41)	1.507(6)
C(25)-H(25B)	0.9800	C(38)-C(39)	1.528(6)
C(25)-H(25C)	0.9800	C(38)-C(40)	1.532(6)
C(26)-H(26A)	0.9800	C(38)-C(34')	1.597(19)
C(26)-H(26B)	0.9800	C(39)-H(39A)	0.9800
C(26)-H(26C)	0.9800	C(39)-H(39B)	0.9800
C(27)-C(28)	1.521(6)	C(39)-H(39C)	0.9800
C(27)-C(30)	1.530(5)	C(40)-H(40A)	0.9800
C(27)-C(29)	1.532(6)	C(40)-H(40B)	0.9800
C(27)-C(21')	1.606(18)	C(40)-H(40C)	0.9800
C(28)-H(28A)	0.9800	C(41)-H(41A)	0.9800
C(28)-H(28B)	0.9800	C(41)-H(41B)	0.9800
C(28)-H(28C)	0.9800	C(41)-H(41C)	0.9800
C(29)-H(29A)	0.9800	C(42)-C(44)	1.532(5)
C(29)-H(29B)	0.9800	C(42)-C(45)	1.534(5)
C(29)-H(29C)	0.9800	C(42)-C(43)	1.534(5)
C(30)-H(30A)	0.9800	C(42)-C(36')	1.610(18)
C(30)-H(30B)	0.9800	C(43)-H(43A)	0.9800
C(30)-H(30C)	0.9800	C(43)-H(43B)	0.9800
O(2')-C(22')	1.347(11)	C(43)-H(43C)	0.9800
C(16')-C(17')	1.499(13)	C(44)-H(44A)	0.9800
C(16')-H(16C)	0.9900	C(44)-H(44B)	0.9800
C(16')-H(16D)	0.9900	C(44)-H(44C)	0.9800
C(17')-C(22')	1.390(12)	C(45)-H(45A)	0.9800
C(17')-C(18')	1.390(12)	C(45)-H(45B)	0.9800
C(18')-C(19')	1.391(14)	C(45)-H(45C)	0.9800
C(18')-H(18')	0.9500	O(3')-C(37')	1.356(11)
C(19')-C(20')	1.381(15)	C(31')-C(32')	1.508(12)
C(20')-C(21')	1.385(14)	C(31')-H(31C)	0.9900
C(20')-H(20')	0.9500	C(31')-H(31D)	0.9900
C(21')-C(22')	1.424(14)	C(32')-C(33')	1.380(12)
O(3)-C(37)	1.345(5)	C(32')-C(37')	1.400(12)
C(31)-C(32)	1.504(6)	C(33')-C(34')	1.390(15)
C(31)-H(31A)	0.9900	C(33')-H(33')	0.9500
C(31)-H(31B)	0.9900	C(34')-C(35')	1.391(15)
C(32)-C(33)	1.391(6)	C(35')-C(36')	1.383(14)
C(32)-C(37)	1.397(6)	C(35')-H(35')	0.9500
C(33)-C(34)	1.393(8)	C(36')-C(37')	1.409(14)
C(33)-H(33)	0.9500		

Table A21. Bond angles (deg) for **TA8**.

O(3')-V(1)-O(2')	126.5(5)	N(1)-C(1)-H(1B)	109.3
O(1)-V(1)-O(3)	115.36(17)	C(2)-C(1)-H(1B)	109.3
O(1)-V(1)-O(2)	122.93(17)	H(1A)-C(1)-H(1B)	107.9
O(3)-V(1)-O(2)	121.62(17)	C(3)-C(2)-C(7)	120.2(4)
O(3')-V(1)-O(1')	112.8(4)	C(3)-C(2)-C(1)	120.5(4)
O(2')-V(1)-O(1')	120.3(4)	C(7)-C(2)-C(1)	119.2(4)
O(3')-V(1)-N(1)	93.1(3)	C(2)-C(3)-C(4)	121.8(5)
O(1)-V(1)-N(1)	91.69(12)	C(2)-C(3)-H(3)	119.1
O(2')-V(1)-N(1)	91.5(2)	C(4)-C(3)-H(3)	119.1
O(3)-V(1)-N(1)	89.99(13)	C(3)-C(4)-C(5)	116.5(6)
O(2)-V(1)-N(1)	91.24(12)	C(3)-C(4)-C(8)	122.0(6)
O(1')-V(1)-N(1)	91.1(2)	C(5)-C(4)-C(8)	121.5(6)
O(3')-V(1)-N(2)	85.6(3)	C(6)-C(5)-C(4)	123.8(9)
O(1)-V(1)-N(2)	87.01(13)	C(6)-C(5)-H(5)	118.1
O(2')-V(1)-N(2)	92.3(2)	C(4)-C(5)-H(5)	118.1
O(3)-V(1)-N(2)	87.16(13)	C(5)-C(6)-C(7)	117.9(7)
O(2)-V(1)-N(2)	92.63(13)	C(5)-C(6)-C(12)	117.9(6)
O(1')-V(1)-N(2)	86.0(2)	C(7)-C(6)-C(12)	124.2(5)
N(1)-V(1)-N(2)	176.01(11)	O(1)-C(7)-C(6)	120.7(5)
C(1)-N(1)-C(31)	111.0(3)	O(1)-C(7)-C(2)	119.5(4)
C(31')-N(1)-C(16')	117.9(7)	C(6)-C(7)-C(2)	119.7(5)
C(1)-N(1)-C(16)	108.4(3)	C(4')-C(8)-C(9)	118.2(11)
C(31)-N(1)-C(16)	106.0(3)	C(4')-C(8)-C(11)	102.8(11)
C(31')-N(1)-C(1')	111.7(7)	C(9)-C(8)-C(11)	109.6(5)
C(16')-N(1)-C(1')	102.8(6)	C(4')-C(8)-C(10)	112.1(8)
C(31')-N(1)-V(1)	108.0(5)	C(9)-C(8)-C(10)	107.8(5)
C(1)-N(1)-V(1)	108.8(2)	C(11)-C(8)-C(10)	105.7(5)
C(31)-N(1)-V(1)	113.6(2)	C(9)-C(8)-C(4)	106.4(5)
C(16')-N(1)-V(1)	107.2(5)	C(11)-C(8)-C(4)	114.4(5)
C(16)-N(1)-V(1)	108.8(2)	C(10)-C(8)-C(4)	112.8(4)
C(1')-N(1)-V(1)	108.8(4)	C(8)-C(9)-H(9A)	109.5
C(46)-N(2)-V(1)	164.1(3)	C(8)-C(9)-H(9B)	109.5
N(2)-C(46)-C(47)	179.2(5)	H(9A)-C(9)-H(9B)	109.5
C(46)-C(47)-H(47A)	109.5	C(8)-C(9)-H(9C)	109.5
C(46)-C(47)-H(47B)	109.5	H(9A)-C(9)-H(9C)	109.5
H(47A)-C(47)-H(47B)	109.5	H(9B)-C(9)-H(9C)	109.5
C(46)-C(47)-H(47C)	109.5	C(8)-C(10)-H(10A)	109.5
H(47A)-C(47)-H(47C)	109.5	C(8)-C(10)-H(10B)	109.5
H(47B)-C(47)-H(47C)	109.5	H(10A)-C(10)-H(10B)	109.5
C(7)-O(1)-V(1)	131.1(3)	C(8)-C(10)-H(10C)	109.5
N(1)-C(1)-C(2)	111.8(4)	H(10A)-C(10)-H(10C)	109.5
N(1)-C(1)-H(1A)	109.3	H(10B)-C(10)-H(10C)	109.5
C(2)-C(1)-H(1A)	109.3	C(8)-C(11)-H(11A)	109.5

C(8)-C(11)-H(11B)	109.5	C(3')-C(4')-C(8)	120.9(14)
H(11A)-C(11)-H(11B)	109.5	C(5')-C(4')-C(8)	121.7(15)
C(8)-C(11)-H(11C)	109.5	C(6')-C(5')-C(4')	123.7(19)
H(11A)-C(11)-H(11C)	109.5	C(6')-C(5')-H(5')	118.2
H(11B)-C(11)-H(11C)	109.5	C(4')-C(5')-H(5')	118.2
C(15)-C(12)-C(14)	108.3(4)	C(5')-C(6')-C(7')	117.6(15)
C(15)-C(12)-C(13)	107.4(4)	C(5')-C(6')-C(12)	127.6(13)
C(14)-C(12)-C(13)	108.1(4)	C(7')-C(6')-C(12)	114.7(13)
C(15)-C(12)-C(6')	105.9(6)	O(1')-C(7')-C(2')	120.3(9)
C(14)-C(12)-C(6')	106.9(12)	O(1')-C(7')-C(6')	120.2(11)
C(13)-C(12)-C(6')	119.7(11)	C(2')-C(7')-C(6')	119.3(11)
C(15)-C(12)-C(6)	114.5(4)	C(22)-O(2)-V(1)	128.8(3)
C(14)-C(12)-C(6)	110.6(5)	C(17)-C(16)-N(1)	112.1(4)
C(13)-C(12)-C(6)	107.7(5)	C(17)-C(16)-H(16A)	109.2
C(12)-C(13)-H(13A)	109.5	N(1)-C(16)-H(16A)	109.2
C(12)-C(13)-H(13B)	109.5	C(17)-C(16)-H(16B)	109.2
H(13A)-C(13)-H(13B)	109.5	N(1)-C(16)-H(16B)	109.2
C(12)-C(13)-H(13C)	109.5	H(16A)-C(16)-H(16B)	107.9
H(13A)-C(13)-H(13C)	109.5	C(22)-C(17)-C(18)	120.8(4)
H(13B)-C(13)-H(13C)	109.5	C(22)-C(17)-C(16)	119.5(4)
C(12)-C(14)-H(14A)	109.5	C(18)-C(17)-C(16)	119.6(4)
C(12)-C(14)-H(14B)	109.5	C(19)-C(18)-C(17)	121.3(5)
H(14A)-C(14)-H(14B)	109.5	C(19)-C(18)-H(18)	119.4
C(12)-C(14)-H(14C)	109.5	C(17)-C(18)-H(18)	119.4
H(14A)-C(14)-H(14C)	109.5	C(20)-C(19)-C(18)	116.1(6)
H(14B)-C(14)-H(14C)	109.5	C(20)-C(19)-C(23)	123.4(6)
C(12)-C(15)-H(15A)	109.5	C(18)-C(19)-C(23)	120.5(5)
C(12)-C(15)-H(15B)	109.5	C(19)-C(20)-C(21)	124.8(7)
H(15A)-C(15)-H(15B)	109.5	C(19)-C(20)-H(20)	117.6
C(12)-C(15)-H(15C)	109.5	C(21)-C(20)-H(20)	117.6
H(15A)-C(15)-H(15C)	109.5	C(20)-C(21)-C(22)	116.8(6)
H(15B)-C(15)-H(15C)	109.5	C(20)-C(21)-C(27)	121.8(6)
C(7')-O(1')-V(1)	131.2(7)	C(22)-C(21)-C(27)	121.4(5)
C(2')-C(1')-N(1)	117.6(8)	O(2)-C(22)-C(17)	119.1(4)
C(2')-C(1')-H(1'1)	107.9	O(2)-C(22)-C(21)	121.5(5)
N(1)-C(1')-H(1'1)	107.9	C(17)-C(22)-C(21)	119.4(5)
C(2')-C(1')-H(1'2)	107.9	C(19')-C(23)-C(25)	121.3(9)
N(1)-C(1')-H(1'2)	107.9	C(19')-C(23)-C(24)	110.5(7)
H(1'1)-C(1')-H(1'2)	107.2	C(25)-C(23)-C(24)	109.3(4)
C(3')-C(2')-C(7')	120.9(9)	C(19')-C(23)-C(26)	96.9(9)
C(3')-C(2')-C(1')	119.4(9)	C(25)-C(23)-C(26)	108.9(4)
C(7')-C(2')-C(1')	119.6(8)	C(24)-C(23)-C(26)	108.9(4)
C(2')-C(3')-C(4')	120.9(12)	C(25)-C(23)-C(19)	106.5(4)
C(2')-C(3')-H(3')	119.5	C(24)-C(23)-C(19)	112.2(4)
C(4')-C(3')-H(3')	119.5	C(26)-C(23)-C(19)	111.0(4)
C(3')-C(4')-C(5')	117.1(16)	C(23)-C(24)-H(24A)	109.5

C(23)-C(24)-H(24B)	109.5	C(17')-C(16')-H(16C)	109.3
H(24A)-C(24)-H(24B)	109.5	N(1)-C(16')-H(16C)	109.3
C(23)-C(24)-H(24C)	109.5	C(17')-C(16')-H(16D)	109.3
H(24A)-C(24)-H(24C)	109.5	N(1)-C(16')-H(16D)	109.3
H(24B)-C(24)-H(24C)	109.5	H(16C)-C(16')-H(16D)	107.9
C(23)-C(25)-H(25A)	109.5	C(22')-C(17')-C(18')	120.4(9)
C(23)-C(25)-H(25B)	109.5	C(22')-C(17')-C(16')	120.9(9)
H(25A)-C(25)-H(25B)	109.5	C(18')-C(17')-C(16')	118.1(9)
C(23)-C(25)-H(25C)	109.5	C(17')-C(18')-C(19')	121.5(11)
H(25A)-C(25)-H(25C)	109.5	C(17')-C(18')-H(18')	119.2
H(25B)-C(25)-H(25C)	109.5	C(19')-C(18')-H(18')	119.2
C(23)-C(26)-H(26A)	109.5	C(20')-C(19')-C(18')	116.0(15)
C(23)-C(26)-H(26B)	109.5	C(20')-C(19')-C(23)	127.0(13)
H(26A)-C(26)-H(26B)	109.5	C(18')-C(19')-C(23)	117.0(13)
C(23)-C(26)-H(26C)	109.5	C(19')-C(20')-C(21')	125.4(16)
H(26A)-C(26)-H(26C)	109.5	C(19')-C(20')-H(20')	117.3
H(26B)-C(26)-H(26C)	109.5	C(21')-C(20')-H(20')	117.3
C(21)-C(27)-C(28)	114.3(4)	C(20')-C(21')-C(22')	115.8(14)
C(21)-C(27)-C(30)	112.1(4)	C(20')-C(21')-C(27)	123.1(12)
C(28)-C(27)-C(30)	108.5(4)	C(22')-C(21')-C(27)	120.9(12)
C(21)-C(27)-C(29)	106.7(5)	O(2')-C(22')-C(17')	119.8(9)
C(28)-C(27)-C(29)	108.6(4)	O(2')-C(22')-C(21')	120.3(11)
C(30)-C(27)-C(29)	106.3(4)	C(17')-C(22')-C(21')	119.9(11)
C(28)-C(27)-C(21')	103.7(9)	C(37)-O(3)-V(1)	133.4(3)
C(30)-C(27)-C(21')	110.0(6)	N(1)-C(31)-C(32)	116.3(4)
C(29)-C(27)-C(21')	119.4(9)	N(1)-C(31)-H(31A)	108.2
C(27)-C(28)-H(28A)	109.5	C(32)-C(31)-H(31A)	108.2
C(27)-C(28)-H(28B)	109.5	N(1)-C(31)-H(31B)	108.2
H(28A)-C(28)-H(28B)	109.5	C(32)-C(31)-H(31B)	108.2
C(27)-C(28)-H(28C)	109.5	H(31A)-C(31)-H(31B)	107.4
H(28A)-C(28)-H(28C)	109.5	C(33)-C(32)-C(37)	120.5(4)
H(28B)-C(28)-H(28C)	109.5	C(33)-C(32)-C(31)	119.4(4)
C(27)-C(29)-H(29A)	109.5	C(37)-C(32)-C(31)	119.7(4)
C(27)-C(29)-H(29B)	109.5	C(32)-C(33)-C(34)	120.7(5)
H(29A)-C(29)-H(29B)	109.5	C(32)-C(33)-H(33)	119.7
C(27)-C(29)-H(29C)	109.5	C(34)-C(33)-H(33)	119.7
H(29A)-C(29)-H(29C)	109.5	C(35)-C(34)-C(33)	117.0(7)
H(29B)-C(29)-H(29C)	109.5	C(35)-C(34)-C(38)	122.7(6)
C(27)-C(30)-H(30A)	109.5	C(33)-C(34)-C(38)	120.3(6)
C(27)-C(30)-H(30B)	109.5	C(34)-C(35)-C(36)	125.0(7)
H(30A)-C(30)-H(30B)	109.5	C(34)-C(35)-H(35)	117.5
C(27)-C(30)-H(30C)	109.5	C(36)-C(35)-H(35)	117.5
H(30A)-C(30)-H(30C)	109.5	C(35)-C(36)-C(37)	116.4(6)
H(30B)-C(30)-H(30C)	109.5	C(35)-C(36)-C(42)	123.3(6)
C(22')-O(2')-V(1)	132.7(7)	C(37)-C(36)-C(42)	120.3(6)
C(17')-C(16')-N(1)	111.7(9)	O(3)-C(37)-C(32)	120.2(4)

O(3)-C(37)-C(36)	119.6(5)	C(42)-C(43)-H(43C)	109.5
C(32)-C(37)-C(36)	120.2(5)	H(43A)-C(43)-H(43C)	109.5
C(41)-C(38)-C(34)	114.2(4)	H(43B)-C(43)-H(43C)	109.5
C(41)-C(38)-C(39)	108.0(4)	C(42)-C(44)-H(44A)	109.5
C(34)-C(38)-C(39)	110.9(5)	C(42)-C(44)-H(44B)	109.5
C(41)-C(38)-C(40)	107.8(4)	H(44A)-C(44)-H(44B)	109.5
C(34)-C(38)-C(40)	106.8(5)	C(42)-C(44)-H(44C)	109.5
C(39)-C(38)-C(40)	109.0(4)	H(44A)-C(44)-H(44C)	109.5
C(41)-C(38)-C(34')	110.0(7)	H(44B)-C(44)-H(44C)	109.5
C(39)-C(38)-C(34')	103.3(9)	C(42)-C(45)-H(45A)	109.5
C(40)-C(38)-C(34')	118.3(9)	C(42)-C(45)-H(45B)	109.5
C(38)-C(39)-H(39A)	109.5	H(45A)-C(45)-H(45B)	109.5
C(38)-C(39)-H(39B)	109.5	C(42)-C(45)-H(45C)	109.5
H(39A)-C(39)-H(39B)	109.5	H(45A)-C(45)-H(45C)	109.5
C(38)-C(39)-H(39C)	109.5	H(45B)-C(45)-H(45C)	109.5
H(39A)-C(39)-H(39C)	109.5	C(37')-O(3')-V(1)	130.9(7)
H(39B)-C(39)-H(39C)	109.5	N(1)-C(31')-C(32')	113.8(9)
C(38)-C(40)-H(40A)	109.5	N(1)-C(31')-H(31C)	108.8
C(38)-C(40)-H(40B)	109.5	C(32')-C(31')-H(31C)	108.8
H(40A)-C(40)-H(40B)	109.5	N(1)-C(31')-H(31D)	108.8
C(38)-C(40)-H(40C)	109.5	C(32')-C(31')-H(31D)	108.8
H(40A)-C(40)-H(40C)	109.5	H(31C)-C(31')-H(31D)	107.7
H(40B)-C(40)-H(40C)	109.5	C(33')-C(32')-C(37')	119.5(9)
C(38)-C(41)-H(41A)	109.5	C(33')-C(32')-C(31')	120.5(9)
C(38)-C(41)-H(41B)	109.5	C(37')-C(32')-C(31')	120.0(9)
H(41A)-C(41)-H(41B)	109.5	C(32')-C(33')-C(34')	122.5(12)
C(38)-C(41)-H(41C)	109.5	C(32')-C(33')-H(33')	118.8
H(41A)-C(41)-H(41C)	109.5	C(34')-C(33')-H(33')	118.8
H(41B)-C(41)-H(41C)	109.5	C(33')-C(34')-C(35')	116.1(15)
C(36)-C(42)-C(44)	108.0(5)	C(33')-C(34')-C(38)	127.0(15)
C(36)-C(42)-C(45)	114.4(4)	C(35')-C(34')-C(38)	116.8(13)
C(44)-C(42)-C(45)	109.7(3)	C(36')-C(35')-C(34')	124.4(17)
C(36)-C(42)-C(43)	110.5(4)	C(36')-C(35')-H(35')	117.8
C(44)-C(42)-C(43)	107.1(3)	C(34')-C(35')-H(35')	117.8
C(45)-C(42)-C(43)	106.9(3)	C(35')-C(36')-C(37')	117.2(14)
C(44)-C(42)-C(36')	116.1(10)	C(35')-C(36')-C(42)	118.5(13)
C(45)-C(42)-C(36')	102.4(9)	C(37')-C(36')-C(42)	124.1(13)
C(43)-C(42)-C(36')	114.2(7)	O(3')-C(37')-C(32')	120.0(9)
C(42)-C(43)-H(43A)	109.5	O(3')-C(37')-C(36')	119.8(11)
C(42)-C(43)-H(43B)	109.5	C(32')-C(37')-C(36')	120.1(11)
H(43A)-C(43)-H(43B)	109.5		

Table A22. Atomic coordinates (x 10^4) for **TA9**.

	x	y	z
V(1)	7614(1)	2826(1)	7461(1)
N(1)	6640(1)	2792(1)	6468(1)
O(1)	7888(1)	3714(1)	7225(1)
C(2)	7630(1)	4120(1)	6598(1)
C(3)	8199(1)	4664(1)	6385(1)
C(4)	7907(2)	5037(1)	5714(1)
C(5)	7098(1)	4911(1)	5231(1)
C(6)	6551(1)	4386(1)	5470(1)
C(7)	6794(1)	4001(1)	6146(1)
C(8)	6162(1)	3448(1)	6390(1)
C(9)	9122(2)	4818(1)	6867(2)
C(10)	9802(2)	4249(2)	6727(2)
C(11)	8961(2)	4894(2)	7773(2)
C(12)	9562(2)	5471(2)	6583(2)
C(13)	6839(2)	5349(1)	4493(1)
C(14)	6506(2)	6031(1)	4785(2)
C(15)	7684(2)	5452(2)	3978(2)
C(16)	6056(2)	5046(1)	3949(2)
O(17)	8295(1)	2141(1)	7005(1)
C(18)	8102(1)	1729(1)	6373(1)
C(19)	8455(1)	1076(1)	6369(1)
C(20)	8301(1)	703(1)	5665(1)
C(21)	7789(1)	932(1)	4980(1)
C(22)	7388(1)	1557(1)	5028(1)
C(23)	7541(1)	1956(1)	5707(1)
C(24)	7135(1)	2646(1)	5718(1)
C(25)	9036(2)	785(1)	7095(1)
C(26)	9181(2)	31(1)	7011(2)
C(27)	8561(2)	890(1)	7892(1)
C(28)	9993(2)	1127(1)	7134(2)
C(29)	7707(2)	522(1)	4196(2)
C(30)	8085(5)	-183(2)	4298(3)
C(31)	6751(5)	533(5)	3791(6)
C(32)	8382(4)	862(3)	3592(3)
C(30')	7277(10)	-167(5)	4492(6)
C(31')	6927(11)	767(10)	3621(12)
C(32')	8583(7)	419(8)	3850(8)
O(33)	6687(1)	2607(1)	8177(1)
C(34)	5755(1)	2495(1)	8079(1)
C(35)	5182(1)	2503(1)	8745(1)
C(36)	4237(1)	2356(1)	8601(1)
C(37)	3832(1)	2207(1)	7842(1)

C(38)	4410(1)	2220(1)	7198(1)
C(39)	5356(1)	2350(1)	7305(1)
C(40)	5950(1)	2254(1)	6591(1)
C(41)	5587(1)	2627(1)	9611(1)
C(42)	6275(2)	2068(1)	9842(1)
C(43)	4844(2)	2620(2)	10237(1)
C(44)	6053(2)	3311(1)	9669(2)
C(45)	2814(6)	1977(7)	7699(8)
C(46)	2812(9)	1249(5)	7409(8)
C(47)	2315(10)	2424(5)	7078(8)
C(48)	2243(9)	2037(7)	8445(7)
C(45')	2783(9)	2062(12)	7710(14)
C(46')	2677(15)	1434(8)	7205(12)
C(47')	2294(18)	2632(9)	7237(15)
C(48')	2381(15)	1874(13)	8545(13)
C(45")	2816(14)	1970(20)	7719(13)
C(46")	2460(20)	2000(20)	6822(17)
C(47")	2780(20)	1225(17)	7970(20)
C(48")	2170(20)	2390(20)	8110(20)
C(49)	9652(2)	2830(2)	8252(2)
O(50)	8682(1)	2842(1)	8432(1)
C(51)	8550(2)	2776(2)	9276(2)
C(52)	8751(2)	3388(2)	9742(2)
O(53)	9724(1)	3454(1)	9926(1)
C(54)	9945(2)	4045(1)	10357(2)

Table A23. Bond lengths (Å) for **TA9**.

V(1)-O(17)	1.8674(14)	C(16)-H(16C)	0.9800
V(1)-O(1)	1.8718(15)	O(17)-C(18)	1.350(2)
V(1)-O(33)	1.8780(14)	C(18)-C(23)	1.404(3)
V(1)-N(1)	2.0993(16)	C(18)-C(19)	1.404(3)
V(1)-O(50)	2.1589(15)	C(19)-C(20)	1.391(3)
N(1)-C(40)	1.486(2)	C(19)-C(25)	1.539(3)
N(1)-C(8)	1.488(2)	C(20)-C(21)	1.395(3)
N(1)-C(24)	1.489(2)	C(20)-H(20)	0.9500
O(1)-C(2)	1.354(3)	C(21)-C(22)	1.384(3)
C(2)-C(7)	1.401(3)	C(21)-C(29)	1.532(3)
C(2)-C(3)	1.417(3)	C(22)-C(23)	1.387(3)
C(3)-C(4)	1.384(3)	C(22)-H(22)	0.9500
C(3)-C(9)	1.541(3)	C(23)-C(24)	1.501(3)
C(4)-C(5)	1.396(3)	C(24)-H(24A)	0.9900
C(4)-H(4)	0.9500	C(24)-H(24B)	0.9900
C(5)-C(6)	1.383(3)	C(25)-C(27)	1.530(3)
C(5)-C(13)	1.532(3)	C(25)-C(28)	1.534(3)
C(6)-C(7)	1.387(3)	C(25)-C(26)	1.535(3)
C(6)-H(6)	0.9500	C(26)-H(26A)	0.9800
C(7)-C(8)	1.501(3)	C(26)-H(26B)	0.9800
C(8)-H(8A)	0.9900	C(26)-H(26C)	0.9800
C(8)-H(8B)	0.9900	C(27)-H(27A)	0.9800
C(9)-C(10)	1.527(4)	C(27)-H(27B)	0.9800
C(9)-C(11)	1.534(4)	C(27)-H(27C)	0.9800
C(9)-C(12)	1.539(4)	C(28)-H(28A)	0.9800
C(10)-H(10A)	0.9800	C(28)-H(28B)	0.9800
C(10)-H(10B)	0.9800	C(28)-H(28C)	0.9800
C(10)-H(10C)	0.9800	C(29)-C(32')	1.425(9)
C(11)-H(11A)	0.9800	C(29)-C(31)	1.494(6)
C(11)-H(11B)	0.9800	C(29)-C(31')	1.511(11)
C(11)-H(11C)	0.9800	C(29)-C(30)	1.520(5)
C(12)-H(12A)	0.9800	C(29)-C(32)	1.583(5)
C(12)-H(12B)	0.9800	C(29)-C(30')	1.601(9)
C(12)-H(12C)	0.9800	C(30)-H(30A)	0.9800
C(13)-C(16)	1.529(3)	C(30)-H(30B)	0.9800
C(13)-C(15)	1.532(3)	C(30)-H(30C)	0.9800
C(13)-C(14)	1.535(3)	C(31)-H(31A)	0.9800
C(14)-H(14A)	0.9800	C(31)-H(31B)	0.9800
C(14)-H(14B)	0.9800	C(31)-H(31C)	0.9800
C(14)-H(14C)	0.9800	C(32)-H(32A)	0.9800
C(15)-H(15A)	0.9800	C(32)-H(32B)	0.9800
C(15)-H(15B)	0.9800	C(32)-H(32C)	0.9800
C(15)-H(15C)	0.9800	C(30')-H(30D)	0.9800
C(16)-H(16A)	0.9800	C(30')-H(30E)	0.9800
C(16)-H(16B)	0.9800	C(30')-H(30F)	0.9800

C(31')-H(31D)	0.9800	C(48)-H(48A)	0.9800
C(31')-H(31E)	0.9800	C(48)-H(48B)	0.9800
C(31')-H(31F)	0.9800	C(48)-H(48C)	0.9800
C(32')-H(32D)	0.9800	C(45')-C(46')	1.516(13)
C(32')-H(32E)	0.9800	C(45')-C(47')	1.534(18)
C(32')-H(32F)	0.9800	C(45')-C(48')	1.57(3)
O(33)-C(34)	1.359(2)	C(46')-H(46D)	0.9800
C(34)-C(39)	1.402(3)	C(46')-H(46E)	0.9800
C(34)-C(35)	1.408(3)	C(46')-H(46F)	0.9800
C(35)-C(36)	1.396(3)	C(47')-H(47D)	0.9800
C(35)-C(41)	1.536(3)	C(47')-H(47E)	0.9800
C(36)-C(37)	1.386(3)	C(47')-H(47F)	0.9800
C(36)-H(36)	0.9500	C(48')-H(48D)	0.9800
C(37)-C(38)	1.383(3)	C(48')-H(48E)	0.9800
C(37)-C(45')	1.538(12)	C(48')-H(48F)	0.9800
C(37)-C(45)	1.539(8)	C(45")-C(48")	1.44(5)
C(37)-C(45")	1.540(17)	C(45")-C(46")	1.541(19)
C(38)-C(39)	1.386(3)	C(45")-C(47")	1.54(2)
C(38)-H(38)	0.9500	C(46")-H(46G)	0.9800
C(39)-C(40)	1.504(3)	C(46")-H(46H)	0.9800
C(40)-H(40A)	0.9900	C(46")-H(46I)	0.9800
C(40)-H(40B)	0.9900	C(47")-H(47G)	0.9800
C(41)-C(43)	1.525(3)	C(47")-H(47H)	0.9800
C(41)-C(44)	1.528(3)	C(47")-H(47I)	0.9800
C(41)-C(42)	1.528(3)	C(48")-H(48G)	0.9800
C(42)-H(42A)	0.9800	C(48")-H(48H)	0.9800
C(42)-H(42B)	0.9800	C(48")-H(48I)	0.9800
C(42)-H(42C)	0.9800	C(49)-O(50)	1.439(3)
C(43)-H(43A)	0.9800	C(49)-H(49A)	0.9800
C(43)-H(43B)	0.9800	C(49)-H(49B)	0.9800
C(43)-H(43C)	0.9800	C(49)-H(49C)	0.9800
C(44)-H(44A)	0.9800	O(50)-C(51)	1.424(3)
C(44)-H(44B)	0.9800	C(51)-C(52)	1.469(4)
C(44)-H(44C)	0.9800	C(51)-H(51A)	0.9900
C(45)-C(47)	1.513(11)	C(51)-H(51B)	0.9900
C(45)-C(48)	1.521(13)	C(52)-O(53)	1.421(3)
C(45)-C(46)	1.539(9)	C(52)-H(52A)	0.9900
C(46)-H(46A)	0.9800	C(52)-H(52B)	0.9900
C(46)-H(46B)	0.9800	O(53)-C(54)	1.409(3)
C(46)-H(46C)	0.9800	C(54)-H(54A)	0.9800
C(47)-H(47A)	0.9800	C(54)-H(54B)	0.9800
C(47)-H(47B)	0.9800	C(54)-H(54C)	0.9800
C(47)-H(47C)	0.9800		

Table A24. Bond angles (deg) for **TA9**.

O(17)-V(1)-O(1)	119.72(6)	C(11)-C(9)-C(3)	110.7(2)
O(17)-V(1)-O(33)	119.05(7)	C(12)-C(9)-C(3)	111.7(2)
O(1)-V(1)-O(33)	121.20(7)	C(9)-C(10)-H(10A)	109.5
O(17)-V(1)-N(1)	90.12(6)	C(9)-C(10)-H(10B)	109.5
O(1)-V(1)-N(1)	90.40(6)	H(10A)-C(10)-H(10B)	109.5
O(33)-V(1)-N(1)	91.17(6)	C(9)-C(10)-H(10C)	109.5
O(17)-V(1)-O(50)	86.78(6)	H(10A)-C(10)-H(10C)	109.5
O(1)-V(1)-O(50)	89.49(6)	H(10B)-C(10)-H(10C)	109.5
O(33)-V(1)-O(50)	91.99(6)	C(9)-C(11)-H(11A)	109.5
N(1)-V(1)-O(50)	176.36(6)	C(9)-C(11)-H(11B)	109.5
C(40)-N(1)-C(8)	110.28(14)	H(11A)-C(11)-H(11B)	109.5
C(40)-N(1)-C(24)	108.83(14)	C(9)-C(11)-H(11C)	109.5
C(8)-N(1)-C(24)	109.97(15)	H(11A)-C(11)-H(11C)	109.5
C(40)-N(1)-V(1)	109.70(12)	H(11B)-C(11)-H(11C)	109.5
C(8)-N(1)-V(1)	108.86(12)	C(9)-C(12)-H(12A)	109.5
C(24)-N(1)-V(1)	109.18(11)	C(9)-C(12)-H(12B)	109.5
C(2)-O(1)-V(1)	132.90(12)	H(12A)-C(12)-H(12B)	109.5
O(1)-C(2)-C(7)	119.78(18)	C(9)-C(12)-H(12C)	109.5
O(1)-C(2)-C(3)	120.99(18)	H(12A)-C(12)-H(12C)	109.5
C(7)-C(2)-C(3)	119.2(2)	H(12B)-C(12)-H(12C)	109.5
C(4)-C(3)-C(2)	117.44(19)	C(16)-C(13)-C(15)	107.9(2)
C(4)-C(3)-C(9)	121.4(2)	C(16)-C(13)-C(5)	112.25(19)
C(2)-C(3)-C(9)	121.2(2)	C(15)-C(13)-C(5)	110.70(19)
C(3)-C(4)-C(5)	124.5(2)	C(16)-C(13)-C(14)	107.9(2)
C(3)-C(4)-H(4)	117.7	C(15)-C(13)-C(14)	108.8(2)
C(5)-C(4)-H(4)	117.7	C(5)-C(13)-C(14)	109.15(19)
C(6)-C(5)-C(4)	116.3(2)	C(13)-C(14)-H(14A)	109.5
C(6)-C(5)-C(13)	123.08(18)	C(13)-C(14)-H(14B)	109.5
C(4)-C(5)-C(13)	120.63(19)	H(14A)-C(14)-H(14B)	109.5
C(5)-C(6)-C(7)	122.11(19)	C(13)-C(14)-H(14C)	109.5
C(5)-C(6)-H(6)	118.9	H(14A)-C(14)-H(14C)	109.5
C(7)-C(6)-H(6)	118.9	H(14B)-C(14)-H(14C)	109.5
C(6)-C(7)-C(2)	120.34(19)	C(13)-C(15)-H(15A)	109.5
C(6)-C(7)-C(8)	119.92(17)	C(13)-C(15)-H(15B)	109.5
C(2)-C(7)-C(8)	119.75(19)	H(15A)-C(15)-H(15B)	109.5
N(1)-C(8)-C(7)	113.23(15)	C(13)-C(15)-H(15C)	109.5
N(1)-C(8)-H(8A)	108.9	H(15A)-C(15)-H(15C)	109.5
C(7)-C(8)-H(8A)	108.9	H(15B)-C(15)-H(15C)	109.5
N(1)-C(8)-H(8B)	108.9	C(13)-C(16)-H(16A)	109.5
C(7)-C(8)-H(8B)	108.9	C(13)-C(16)-H(16B)	109.5
H(8A)-C(8)-H(8B)	107.7	H(16A)-C(16)-H(16B)	109.5
C(10)-C(9)-C(11)	110.7(2)	C(13)-C(16)-H(16C)	109.5
C(10)-C(9)-C(12)	108.3(3)	H(16A)-C(16)-H(16C)	109.5
C(11)-C(9)-C(12)	107.3(2)	H(16B)-C(16)-H(16C)	109.5
C(10)-C(9)-C(3)	108.1(2)	C(18)-O(17)-V(1)	132.27(12)

O(17)-C(18)-C(23)	119.45(17)	H(28A)-C(28)-H(28C)	109.5
O(17)-C(18)-C(19)	121.05(17)	H(28B)-C(28)-H(28C)	109.5
C(23)-C(18)-C(19)	119.50(18)	C(32')-C(29)-C(31')	115.8(11)
C(20)-C(19)-C(18)	117.64(18)	C(31)-C(29)-C(30)	112.2(5)
C(20)-C(19)-C(25)	120.15(18)	C(32')-C(29)-C(21)	112.7(5)
C(18)-C(19)-C(25)	122.14(18)	C(31)-C(29)-C(21)	113.5(5)
C(19)-C(20)-C(21)	123.70(19)	C(31')-C(29)-C(21)	112.2(10)
C(19)-C(20)-H(20)	118.1	C(30)-C(29)-C(21)	113.3(3)
C(21)-C(20)-H(20)	118.1	C(31)-C(29)-C(32)	106.8(4)
C(22)-C(21)-C(20)	117.05(19)	C(30)-C(29)-C(32)	104.1(4)
C(22)-C(21)-C(29)	121.41(19)	C(21)-C(29)-C(32)	106.2(2)
C(20)-C(21)-C(29)	121.49(19)	C(32')-C(29)-C(30')	111.1(7)
C(21)-C(22)-C(23)	121.42(19)	C(31')-C(29)-C(30')	100.8(8)
C(21)-C(22)-H(22)	119.3	C(21)-C(29)-C(30')	102.7(4)
C(23)-C(22)-H(22)	119.3	C(29)-C(30)-H(30A)	109.5
C(22)-C(23)-C(18)	120.36(18)	C(29)-C(30)-H(30B)	109.5
C(22)-C(23)-C(24)	119.81(18)	H(30A)-C(30)-H(30B)	109.5
C(18)-C(23)-C(24)	119.79(18)	C(29)-C(30)-H(30C)	109.5
N(1)-C(24)-C(23)	113.21(16)	H(30A)-C(30)-H(30C)	109.5
N(1)-C(24)-H(24A)	108.9	H(30B)-C(30)-H(30C)	109.5
C(23)-C(24)-H(24A)	108.9	C(29)-C(31)-H(31A)	109.5
N(1)-C(24)-H(24B)	108.9	C(29)-C(31)-H(31B)	109.5
C(23)-C(24)-H(24B)	108.9	H(31A)-C(31)-H(31B)	109.5
H(24A)-C(24)-H(24B)	107.7	C(29)-C(31)-H(31C)	109.5
C(27)-C(25)-C(28)	109.9(2)	H(31A)-C(31)-H(31C)	109.5
C(27)-C(25)-C(26)	106.4(2)	H(31B)-C(31)-H(31C)	109.5
C(28)-C(25)-C(26)	108.6(2)	C(29)-C(32)-H(32A)	109.5
C(27)-C(25)-C(19)	111.73(18)	C(29)-C(32)-H(32B)	109.5
C(28)-C(25)-C(19)	108.06(17)	H(32A)-C(32)-H(32B)	109.5
C(26)-C(25)-C(19)	112.00(19)	C(29)-C(32)-H(32C)	109.5
C(25)-C(26)-H(26A)	109.5	H(32A)-C(32)-H(32C)	109.5
C(25)-C(26)-H(26B)	109.5	H(32B)-C(32)-H(32C)	109.5
H(26A)-C(26)-H(26B)	109.5	C(29)-C(30')-H(30D)	109.5
C(25)-C(26)-H(26C)	109.5	C(29)-C(30')-H(30E)	109.5
H(26A)-C(26)-H(26C)	109.5	H(30D)-C(30')-H(30E)	109.5
H(26B)-C(26)-H(26C)	109.5	C(29)-C(30')-H(30F)	109.5
C(25)-C(27)-H(27A)	109.5	H(30D)-C(30')-H(30F)	109.5
C(25)-C(27)-H(27B)	109.5	H(30E)-C(30')-H(30F)	109.5
H(27A)-C(27)-H(27B)	109.5	C(29)-C(31')-H(31D)	109.5
C(25)-C(27)-H(27C)	109.5	C(29)-C(31')-H(31E)	109.5
H(27A)-C(27)-H(27C)	109.5	H(31D)-C(31')-H(31E)	109.5
H(27B)-C(27)-H(27C)	109.5	C(29)-C(31')-H(31F)	109.5
C(25)-C(28)-H(28A)	109.5	H(31D)-C(31')-H(31F)	109.5
C(25)-C(28)-H(28B)	109.5	H(31E)-C(31')-H(31F)	109.5
H(28A)-C(28)-H(28B)	109.5	C(29)-C(32')-H(32D)	109.5
C(25)-C(28)-H(28C)	109.5	C(29)-C(32')-H(32E)	109.5

H(32D)-C(32')-H(32E)	109.5	C(41)-C(43)-H(43B)	109.5
C(29)-C(32')-H(32F)	109.5	H(43A)-C(43)-H(43B)	109.5
H(32D)-C(32')-H(32F)	109.5	C(41)-C(43)-H(43C)	109.5
H(32E)-C(32')-H(32F)	109.5	H(43A)-C(43)-H(43C)	109.5
C(34)-O(33)-V(1)	133.58(13)	H(43B)-C(43)-H(43C)	109.5
O(33)-C(34)-C(39)	119.65(17)	C(41)-C(44)-H(44A)	109.5
O(33)-C(34)-C(35)	121.18(17)	C(41)-C(44)-H(44B)	109.5
C(39)-C(34)-C(35)	119.14(17)	H(44A)-C(44)-H(44B)	109.5
C(36)-C(35)-C(34)	117.87(18)	C(41)-C(44)-H(44C)	109.5
C(36)-C(35)-C(41)	120.61(17)	H(44A)-C(44)-H(44C)	109.5
C(34)-C(35)-C(41)	121.43(17)	H(44B)-C(44)-H(44C)	109.5
C(37)-C(36)-C(35)	123.84(19)	C(47)-C(45)-C(48)	104.2(10)
C(37)-C(36)-H(36)	118.1	C(47)-C(45)-C(46)	111.1(8)
C(35)-C(36)-H(36)	118.1	C(48)-C(45)-C(46)	109.6(12)
C(38)-C(37)-C(36)	116.80(18)	C(47)-C(45)-C(37)	109.8(10)
C(38)-C(37)-C(45')	121.2(8)	C(48)-C(45)-C(37)	113.6(9)
C(36)-C(37)-C(45')	122.0(8)	C(46)-C(45)-C(37)	108.6(9)
C(38)-C(37)-C(45)	119.4(5)	C(45)-C(46)-H(46A)	109.5
C(36)-C(37)-C(45)	123.6(5)	C(45)-C(46)-H(46B)	109.5
C(38)-C(37)-C(45")	120.5(9)	H(46A)-C(46)-H(46B)	109.5
C(36)-C(37)-C(45")	122.4(9)	C(45)-C(46)-H(46C)	109.5
C(37)-C(38)-C(39)	121.98(18)	H(46A)-C(46)-H(46C)	109.5
C(37)-C(38)-H(38)	119.0	H(46B)-C(46)-H(46C)	109.5
C(39)-C(38)-H(38)	119.0	C(45)-C(47)-H(47A)	109.5
C(38)-C(39)-C(34)	120.33(18)	C(45)-C(47)-H(47B)	109.5
C(38)-C(39)-C(40)	117.95(17)	H(47A)-C(47)-H(47B)	109.5
C(34)-C(39)-C(40)	121.36(17)	C(45)-C(47)-H(47C)	109.5
N(1)-C(40)-C(39)	115.14(16)	H(47A)-C(47)-H(47C)	109.5
N(1)-C(40)-H(40A)	108.5	H(47B)-C(47)-H(47C)	109.5
C(39)-C(40)-H(40A)	108.5	C(45)-C(48)-H(48A)	109.5
N(1)-C(40)-H(40B)	108.5	C(45)-C(48)-H(48B)	109.5
C(39)-C(40)-H(40B)	108.5	H(48A)-C(48)-H(48B)	109.5
H(40A)-C(40)-H(40B)	107.5	C(45)-C(48)-H(48C)	109.5
C(43)-C(41)-C(44)	106.58(19)	H(48A)-C(48)-H(48C)	109.5
C(43)-C(41)-C(42)	106.9(2)	H(48B)-C(48)-H(48C)	109.5
C(44)-C(41)-C(42)	111.57(18)	C(46')-C(45')-C(47')	108.1(14)
C(43)-C(41)-C(35)	112.74(17)	C(46')-C(45')-C(37)	107.7(14)
C(44)-C(41)-C(35)	110.29(18)	C(47')-C(45')-C(37)	110.5(17)
C(42)-C(41)-C(35)	108.76(17)	C(46')-C(45')-C(48')	105(2)
C(41)-C(42)-H(42A)	109.5	C(47')-C(45')-C(48')	116.6(18)
C(41)-C(42)-H(42B)	109.5	C(37)-C(45')-C(48')	108.9(15)
H(42A)-C(42)-H(42B)	109.5	C(45')-C(46')-H(46D)	109.5
C(41)-C(42)-H(42C)	109.5	C(45')-C(46')-H(46E)	109.5
H(42A)-C(42)-H(42C)	109.5	H(46D)-C(46')-H(46E)	109.5
H(42B)-C(42)-H(42C)	109.5	C(45')-C(46')-H(46F)	109.5
C(41)-C(43)-H(43A)	109.5	H(46D)-C(46')-H(46F)	109.5

H(46E)-C(46')-H(46F)	109.5	H(48G)-C(48")-H(48H)	109.5
C(45')-C(47')-H(47D)	109.5	C(45")-C(48")-H(48I)	109.5
C(45')-C(47')-H(47E)	109.5	H(48G)-C(48")-H(48I)	109.5
H(47D)-C(47')-H(47E)	109.5	H(48H)-C(48")-H(48I)	109.5
C(45')-C(47')-H(47F)	109.5	O(50)-C(49)-H(49A)	109.5
H(47D)-C(47')-H(47F)	109.5	O(50)-C(49)-H(49B)	109.5
H(47E)-C(47')-H(47F)	109.5	H(49A)-C(49)-H(49B)	109.5
C(45')-C(48')-H(48D)	109.5	O(50)-C(49)-H(49C)	109.5
C(45')-C(48')-H(48E)	109.5	H(49A)-C(49)-H(49C)	109.5
H(48D)-C(48')-H(48E)	109.5	H(49B)-C(49)-H(49C)	109.5
C(45')-C(48')-H(48F)	109.5	C(51)-O(50)-C(49)	112.38(19)
H(48D)-C(48')-H(48F)	109.5	C(51)-O(50)-V(1)	126.84(14)
H(48E)-C(48')-H(48F)	109.5	C(49)-O(50)-V(1)	120.27(15)
C(48")-C(45")-C(37)	112(3)	O(50)-C(51)-C(52)	113.8(2)
C(48")-C(45")-C(46")	103(3)	O(50)-C(51)-H(51A)	108.8
C(37)-C(45")-C(46")	111.8(15)	C(52)-C(51)-H(51A)	108.8
C(48")-C(45")-C(47")	115(3)	O(50)-C(51)-H(51B)	108.8
C(37)-C(45")-C(47")	108(2)	C(52)-C(51)-H(51B)	108.8
C(46")-C(45")-C(47")	107(3)	H(51A)-C(51)-H(51B)	107.7
C(45")-C(46")-H(46G)	109.5	O(53)-C(52)-C(51)	110.7(2)
C(45")-C(46")-H(46H)	109.5	O(53)-C(52)-H(52A)	109.5
H(46G)-C(46")-H(46H)	109.5	C(51)-C(52)-H(52A)	109.5
C(45")-C(46")-H(46I)	109.5	O(53)-C(52)-H(52B)	109.5
H(46G)-C(46")-H(46I)	109.5	C(51)-C(52)-H(52B)	109.5
H(46H)-C(46")-H(46I)	109.5	H(52A)-C(52)-H(52B)	108.1
C(45")-C(47")-H(47G)	109.5	C(54)-O(53)-C(52)	112.3(2)
C(45")-C(47")-H(47H)	109.5	O(53)-C(54)-H(54A)	109.5
H(47G)-C(47")-H(47H)	109.5	O(53)-C(54)-H(54B)	109.5
C(45")-C(47")-H(47I)	109.5	H(54A)-C(54)-H(54B)	109.5
H(47G)-C(47")-H(47I)	109.5	O(53)-C(54)-H(54C)	109.5
H(47H)-C(47")-H(47I)	109.5	H(54A)-C(54)-H(54C)	109.5
C(45")-C(48")-H(48G)	109.5	H(54B)-C(54)-H(54C)	109.5
C(45")-C(48")-H(48H)	109.5		

Computational Data

Computational Parameters for Coodination of Ethanediol to TA1 : Absolute electronic energies E (au), Gibbs free energies G (au) at 298K, and Cartesian coordinates (Å) from DFT calculations in the gas phase and in water (PCM)

CH_2OH-CH_2OH, gas phase

No imaginary frequencies
E= -230.348100 a.u., G= -230.290151 a.u.

H	-2.169958	-0.696927	0.258087
C	0.729695	0.567242	-0.273478
H	1.274032	1.450582	0.064616
H	0.693502	0.587935	-1.370526
C	-0.684234	0.600775	0.268719
H	-0.656498	0.605552	1.364153
H	-1.194335	1.508097	-0.078717
O	1.450485	-0.564583	0.191412
H	0.909871	-1.338435	-0.011466
O	-1.341657	-0.576031	-0.216111

CH_2OH-CH_2OH, in water

No imaginary frequencies
E= -230.356567 a.u., G= -230.299110 a.u.

H	2.161725	-0.703945	-0.274757
C	-0.728099	0.573054	0.271856
H	-1.270538	1.454859	-0.070556
H	-0.699017	0.593145	1.368037
C	0.683883	0.599610	-0.270041
H	0.663128	0.597981	-1.364458
H	1.192682	1.508038	0.071421
O	-1.455734	-0.568099	-0.188222
H	-0.903616	-1.339328	-0.003642
O	1.345851	-0.575243	0.221106

[V(O)L], gas phase

No imaginary frequencies
E= -1535.8721684 a.u., G= -1535.713849 a.u.

23	0.000000	0.000000	1.170735
8	0.000000	0.000000	2.755026
8	-0.228572	1.737537	0.718065
8	-1.390465	-1.066718	0.718065
8	1.619037	-0.670819	0.718065
7	0.000000	0.000000	-1.360710
6	0.000000	2.302038	-0.553459
6	-0.465945	1.354809	-1.662042
6	-1.993624	-1.151019	-0.553459
6	-0.940327	-1.080925	-1.662042
6	1.993624	-1.151019	-0.553459
6	1.406272	-0.273884	-1.662042
1	1.068235	2.528370	-0.658370
1	-0.540465	3.251814	-0.619680
1	-1.556536	1.341748	-1.675048

1	-0.127718	1.708935	-2.645793
1	-2.723750	-0.339066	-0.658370
1	-2.545921	-2.093963	-0.619680
1	-0.383720	-2.018873	-1.675048
1	-1.416122	-0.965074	-2.645793
1	1.655515	-2.189304	-0.658370
1	3.086386	-1.157850	-0.619680
1	1.940256	0.677125	-1.675048
1	1.543840	-0.743861	-2.645793

[V(O)L], in water

No imaginary frequencies

E= -1535.892309 a.u., G= -1535.734760 a.u.

V	1.138355	-0.000982	0.002014
O	2.745319	0.000469	0.002824
O	0.729941	1.233155	-1.252697
O	0.723053	0.469206	1.697645
O	0.726526	-1.704231	-0.440573
N	-1.299719	0.000691	-0.002158
C	-0.561336	1.451334	-1.809760
C	-1.638436	1.218373	-0.754055
C	-0.569948	0.841482	2.160038
C	-1.643636	0.042692	1.426941
C	-0.566488	-2.292045	-0.352086
C	-1.639612	-1.258701	-0.681300
H	-0.689261	0.780465	-2.665125
H	-0.609499	2.477304	-2.183219
H	-1.641582	2.057417	-0.058531
H	-2.632042	1.162779	-1.212743
H	-0.698532	1.917157	2.004519
H	-0.622375	0.653469	3.235331
H	-1.647449	-0.979336	1.805363
H	-2.638475	0.466368	1.605107
H	-0.696635	-2.695071	0.657211
H	-0.616320	-3.129387	-1.052651
H	-1.638678	-1.076158	-1.755733
H	-2.635271	-1.624856	-0.407002

$[V(O)LH]^+$, structure A, gas phase

No imaginary frequencies

E= -1536.2209936 a.u., G= -1536.051033 a.u.

23	1.127875	-0.125650	-0.012276
8	2.687444	0.106771	-0.046964
8	0.708601	-0.866741	-1.560894
8	0.664738	1.846044	0.077964
8	0.756063	-0.917786	1.517188
7	-1.249281	0.002315	0.007441
6	-0.594759	-1.301576	-1.950597
6	-1.628334	-0.326223	-1.387231
6	-0.683882	2.387657	-0.114159
6	-1.644902	1.353544	0.449212
6	-0.540805	-1.146498	2.067698
6	-1.603554	-1.070144	0.973447
1	-0.743043	-2.322529	-1.590545
1	-0.628265	-1.326309	-3.041094
1	-1.604023	0.591904	-1.974342

1	-2.641683	-0.735500	-1.451892
1	-0.820886	2.567412	-1.180349
1	-0.756322	3.329620	0.427603
1	-1.598924	1.382583	1.537936
1	-2.669040	1.607483	0.155195
1	-0.689705	-0.396929	2.850223
1	-0.543593	-2.127057	2.547260
1	-1.620918	-2.012545	0.427443
1	-2.600833	-0.921893	1.399556
1	1.363728	2.510639	-0.005310

$[V(O)LH]^+$, structure A, in water

No imaginary frequencies

E= -1536.3080938 a.u., G= -1536.138823 a.u.

V	-1.119999	-0.092012	0.016365
O	-2.700742	0.099573	0.041605
O	-0.721526	-0.847866	1.570040
O	-0.633121	1.848595	-0.072006
O	-0.776467	-0.897893	-1.519199
N	1.234840	-0.022447	-0.011483
C	0.584052	-1.292182	1.960188
C	1.623847	-0.338690	1.382163
C	0.730390	2.369294	0.099560
C	1.661207	1.317022	-0.468104
C	0.522316	-1.155703	-2.065499
C	1.574320	-1.108067	-0.964837
H	0.715083	-2.317157	1.607693
H	0.622163	-1.300080	3.050207
H	1.620037	0.585584	1.957507
H	2.629384	-0.764832	1.437042
H	0.877572	2.553505	1.162015
H	0.804285	3.303356	-0.452268
H	1.608042	1.340345	-1.555411
H	2.691971	1.541486	-0.179778
H	0.692196	-0.405261	-2.841114
H	0.503471	-2.136567	-2.542591
H	1.561404	-2.048857	-0.417185
H	2.576796	-0.981923	-1.382236
H	-1.308243	2.534504	0.035759

$[V(O)LH]^+$, structure B, gas phase

No imaginary frequencies

E= -1536.203633 a.u., G= -1536.032685 a.u.

V	-1.436537	0.001041	0.000099
O	-3.008672	0.003732	-0.000443
O	-0.710451	1.572694	-0.445340
O	-0.714823	-1.173011	-1.138461
O	-0.714092	-0.401596	1.584805
N	2.066286	-0.000157	0.000632
C	0.483882	2.119612	0.054767
C	1.766488	1.453494	-0.430441
C	0.480349	-1.013485	-1.861245
C	1.763803	-1.100103	-1.042324
C	0.480355	-1.109085	1.803918
C	1.762849	-0.354227	1.474260
H	0.447898	2.151345	1.148318

H	0.555233	3.156008	-0.291680
H	1.822052	1.460644	-1.517296
H	2.601003	2.040683	-0.043885
H	0.444483	-0.083283	-2.437058
H	0.552125	-1.832599	-2.584544
H	1.819778	-2.044665	-0.504556
H	2.597558	-1.059853	-1.745094
H	0.444624	-2.069054	1.279453
H	0.551827	-1.332723	2.873587
H	1.816325	0.582710	2.025472
H	2.596773	-0.982597	1.791054
H	3.084610	-0.001258	0.001450

$[V(O)LH]^+$, structure B, in water

No imaginary frequencies

E= -1536.304160 a.u., G= -1536.132743 a.u.

V	-1.438368	0.001626	0.001251
O	-3.034500	-0.005541	-0.002544
O	-0.720965	1.283477	-1.002480
O	-0.720605	-1.508126	-0.602067
O	-0.717085	0.231754	1.610714
N	2.074495	-0.000865	-0.003923
C	0.494205	1.971232	-0.742758
C	1.765624	1.168490	-0.957055
C	0.491735	-1.634336	-1.330631
C	1.767732	-1.411749	-0.536372
C	0.496925	-0.338428	2.078434
C	1.770890	0.240309	1.485434
H	0.456556	2.398774	0.261716
H	0.558181	2.803807	-1.447450
H	1.812430	0.762790	-1.963962
H	2.598190	1.860234	-0.837700
H	0.449433	-0.986619	-2.209448
H	0.553211	-2.664139	-1.690416
H	1.823877	-2.079915	0.319124
H	2.594956	-1.653714	-1.201707
H	0.454382	-1.422638	1.953001
H	0.563068	-0.138125	3.150512
H	1.824085	1.314913	1.638188
H	2.601251	-0.215389	2.022914
H	3.093941	0.003055	-0.007384

$[V(O)LH]^+$, structure C, gas phase

No imaginary frequencies

E= -1536.191029 a.u., G= -1536.020930 a.u.

V	-1.409602	-0.000344	0.003797
O	-2.980529	-0.001474	0.011031
O	-0.642947	-1.507485	0.627720
O	-0.640243	1.297331	0.990394
O	-0.656310	0.211614	-1.619123
N	1.584207	-0.001363	-0.002642
C	0.564956	-2.216673	0.409108
C	1.813152	-1.338396	0.666526
C	0.569859	1.468915	1.708663
C	1.815919	1.248584	0.816686
C	0.553239	0.753759	-2.122224

C	1.800821	0.085345	-1.497189
H	0.564029	-2.600783	-0.615719
H	0.596279	-3.070856	1.087511
H	1.932543	-1.146387	1.731136
H	2.721547	-1.796808	0.280039
H	0.572577	0.778781	2.558253
H	0.601037	2.486095	2.102543
H	1.935574	2.072482	0.115813
H	2.725290	1.143996	1.405574
H	0.555983	1.832496	-1.936959
H	0.582423	0.598748	-3.202050
H	1.912879	-0.933276	-1.863484
H	2.710660	0.644389	-1.708318
H	0.573143	-0.000530	0.007232

[V(O)LH]$^{+}$, structure C, in water

No imaginary frequencies

E= -1536.280392 a.u., G= -1536.110307 a.u.

V	-1.416092	0.010827	0.014229
O	-2.987986	-0.005585	-0.022634
O	-0.643836	1.533683	-0.541370
O	-0.656264	-1.264521	-1.045768
O	-0.641513	-0.289919	1.600826
N	1.587457	-0.004236	-0.010621
C	0.566365	2.211882	-0.335385
C	1.810318	1.362181	-0.630934
C	0.566755	-1.391976	-1.758572
C	1.811648	-1.216460	-0.859992
C	0.574019	-0.837837	2.082118
C	1.814540	-0.124861	1.484687
H	0.570089	2.574391	0.703278
H	0.596586	3.097811	-0.982896
H	1.919857	1.190302	-1.703261
H	2.716961	1.802523	-0.234459
H	0.569953	-0.672545	-2.583315
H	0.595236	-2.399755	-2.191739
H	1.929923	-2.074989	-0.198720
H	2.716974	-1.101129	-1.454086
H	0.577942	-1.905024	1.868749
H	0.610559	-0.703630	3.169121
H	1.935403	0.863104	1.878767
H	2.718801	-0.700306	1.662218
H	0.574553	0.003040	-0.006542

[V(O)L] with CH_2OH-CH_2OH, structure A, gas phase

No imaginary frequencies

E= -1766.234694 a.u., G= -1765.998627 a.u.

V	0.185285	-1.485278	-0.041345
O	-1.335208	-0.540568	0.135486
O	1.032702	-1.178072	-1.581656
O	1.249556	-1.343710	1.389350
O	-1.295763	2.149688	-0.376127
N	1.559725	1.167572	0.037147
C	1.652287	-0.020439	-2.110531
C	2.451177	0.714997	-1.039404
C	2.315876	-0.494166	1.744038

C	2.073227	0.972810	1.394685
C	-0.297993	2.842198	0.356445
C	1.097696	2.551946	-0.180354
H	0.884652	0.636042	-2.534216
H	2.313057	-0.338356	-2.923279
H	3.196351	0.025901	-0.641394
H	3.000957	1.550239	-1.493735
H	3.228449	-0.868125	1.266760
H	2.470244	-0.573174	2.825014
H	1.329090	1.375293	2.083258
H	3.011226	1.527810	1.570143
H	-0.367976	2.612811	1.426753
H	-0.500084	3.908625	0.239207
H	1.068209	2.734632	-1.255452
H	1.815092	3.268252	0.252382
C	-3.710744	-0.101144	-0.285650
H	-4.672791	-0.615693	-0.213305
H	-3.467683	-0.003276	-1.351701
C	-2.675051	-0.993121	0.385778
H	-2.837823	-0.984619	1.467315
H	-2.771698	-2.019930	0.019646
O	-3.879776	1.160339	0.332195
H	-3.119734	1.723579	0.109164
O	-0.276171	-2.997897	-0.088261
H	-1.160725	1.191649	-0.233584

[V(O)L] with CH_2OH-CH_2OH, structure A, in water

No imaginary frequencies

E= -1766.253209 a.u., G= -1766.017739

V	-0.252627	-1.450946	0.062242
O	1.311660	-0.566020	-0.075470
O	-1.126330	-1.147361	1.586673
O	-1.246819	-1.318789	-1.415285
O	1.402576	2.107732	0.469087
N	-1.479685	1.169245	-0.063427
C	-1.792264	0.014261	2.074302
C	-2.478166	0.760654	0.940325
C	-2.238214	-0.397766	-1.847253
C	-1.929488	1.042063	-1.455738
C	0.420357	2.825467	-0.279418
C	-0.988188	2.537890	0.215982
H	-1.059218	0.651394	2.577796
H	-2.526851	-0.311704	2.815234
H	-3.210925	0.094254	0.486867
H	-3.032055	1.618304	1.340081
H	-3.200295	-0.726369	-1.444159
H	-2.305812	-0.462002	-2.936434
H	-1.127771	1.415207	-2.092989
H	-2.821549	1.653826	-1.660928
H	0.521961	2.611700	-1.348562
H	0.628231	3.886459	-0.135776
H	-0.987775	2.683712	1.296834
H	-1.678903	3.279797	-0.210875
C	3.709465	-0.211924	0.265788
H	4.654906	-0.747338	0.153809
H	3.517032	-0.096436	1.339037

C	2.623105	-1.077664	-0.353097
H	2.753313	-1.112126	-1.438574
H	2.699133	-2.094765	0.042618
O	3.876887	1.053024	-0.366004
H	3.111968	1.612632	-0.135077
O	0.164915	-2.988864	0.130835
H	1.210077	1.154843	0.359493

[V(O)L] with CH_2OH-CH_2OH, structure B, gas phase

No imaginary frequencies

E= -1766.230547 a.u., G= -1765.996050 a.u.

V	0.735296	-0.886616	-0.002787
O	1.154518	0.846053	-0.075939
O	-0.086591	-1.328580	1.511293
O	-0.164811	-1.433110	-1.444598
O	-0.826050	2.827870	0.298678
N	-2.150363	0.052639	0.002442
C	-1.290945	-0.879143	2.107345
C	-2.432364	-0.885084	1.095690
C	-1.531840	-1.647906	-1.718024
C	-2.417704	-0.463522	-1.339969
C	-2.032754	2.545553	-0.379943
C	-2.784722	1.365655	0.225693
H	-1.141184	0.128355	2.509179
H	-1.515956	-1.550900	2.941451
H	-2.533428	-1.898493	0.705295
H	-3.375613	-0.646541	1.604764
H	-1.849178	-2.561684	-1.203770
H	-1.636806	-1.835172	-2.791367
H	-2.229704	0.347331	-2.044328
H	-3.471305	-0.767191	-1.470057
H	-1.860458	2.389939	-1.453374
H	-2.661592	3.433738	-0.284351
H	-2.830710	1.540167	1.301700
H	-3.822238	1.356687	-0.148235
C	3.601824	1.010928	-0.541691
H	4.324233	1.802029	-0.761198
H	3.443359	0.443209	-1.466890
C	2.306040	1.696370	-0.133632
H	2.429862	2.149837	0.853667
H	2.071154	2.487871	-0.852611
O	4.172739	0.207572	0.474258
H	3.707781	-0.641045	0.479568
O	2.102089	-1.704937	-0.007541
H	-0.227847	2.069498	0.185536

[V(O)L] with CH_2OH-CH_2OH, structure B, in water

No imaginary frequencies

E= -1766.249061 a.u., G= -1766.014938 a.u.

V	0.683920	-0.875165	0.068236
O	1.133744	0.853337	-0.049942
O	-0.161802	-1.288426	1.576705
O	-0.107447	-1.494269	-1.402475
O	-0.772959	2.841280	0.450411
N	-2.070377	0.058257	-0.075784
C	-1.459950	-0.960129	2.063413

C	-2.470827	-0.942239	0.926709
C	-1.452233	-1.570445	-1.855060
C	-2.282269	-0.353078	-1.467867
C	-1.952834	2.580201	-0.300914
C	-2.712929	1.362052	0.203169
H	-1.410880	0.012738	2.560830
H	-1.732815	-1.712416	2.807861
H	-2.499065	-1.934002	0.476876
H	-3.473253	-0.745531	1.325438
H	-1.884200	-2.494919	-1.461831
H	-1.435244	-1.658610	-2.944381
H	-1.995968	0.484909	-2.103205
H	-3.339445	-0.576523	-1.679780
H	-1.722318	2.491097	-1.368746
H	-2.598076	3.452754	-0.182831
H	-2.807979	1.467135	1.284705
H	-3.731306	1.372538	-0.213859
C	3.569820	0.958007	-0.596633
H	4.301989	1.727204	-0.851336
H	3.373120	0.373139	-1.502146
C	2.302261	1.674879	-0.161186
H	2.466645	2.150649	0.809967
H	2.069143	2.453348	-0.893708
O	4.159469	0.151764	0.419205
H	3.622514	-0.652475	0.494207
O	2.059456	-1.697777	0.157616
H	-0.170293	2.087201	0.321051

[V(O)L] with CH_2OH-CH_2OH, structure C, gas phase

No imaginary frequencies

E= -1766.168178 a.u., G= -1765.930641 a.u.

V	-0.454263	-0.781061	0.394143
O	-1.147531	-1.691907	1.488334
O	-0.430806	1.162232	0.463217
O	0.634997	-1.532191	-0.949969
O	1.283894	-0.626604	1.461717
N	2.181012	0.719524	-0.485462
C	0.571692	2.086241	0.773683
C	1.630013	2.113274	-0.353212
C	0.926222	-0.732911	-2.069296
C	2.228769	0.071346	-1.841586
C	2.617612	-0.913962	1.222516
C	3.254666	0.309874	0.487469
H	1.051215	1.857285	1.732207
H	0.134954	3.088606	0.845756
H	1.148092	2.366305	-1.296720
H	2.443325	2.814013	-0.160832
H	0.095689	-0.055514	-2.303046
H	1.082630	-1.371148	-2.946218
H	3.081849	-0.604608	-1.842048
H	2.381004	0.833576	-2.606414
H	2.736550	-1.809308	0.594509
H	3.159245	-1.081864	2.159719
H	3.407529	1.135012	1.180555
H	4.183702	0.094804	-0.038286
C	-3.807629	0.760322	-0.503026

H	-4.889975	0.700201	-0.360022
H	-3.621349	1.230925	-1.478638
C	-3.232601	-0.654189	-0.528736
H	-3.436380	-1.167147	0.418344
H	-3.692245	-1.219194	-1.349334
O	-3.290689	1.543029	0.554445
H	-2.317849	1.538242	0.494380
O	-1.841439	-0.585649	-0.749753
H	1.433099	0.186298	0.018229

[V(O)L] with CH_2OH-CH_2OH, structure C, in water

No imaginary frequencies

E= -1766.198620 a.u., G= -1765.960196 a.u.

V	0.427397	-0.785034	-0.412953
O	1.214237	-1.675619	-1.487350
O	0.466538	1.124311	-0.562250
O	-0.663243	-1.506395	0.954750
O	-1.244563	-0.749655	-1.488665
N	-2.131292	0.751493	0.492152
C	-0.543248	2.079218	-0.815872
C	-1.550726	2.132579	0.348273
C	-0.981500	-0.735161	2.101589
C	-2.247325	0.123233	1.858862
C	-2.605006	-0.910485	-1.199098
C	-3.175877	0.360189	-0.521835
H	-1.060086	1.860816	-1.755715
H	-0.081078	3.065541	-0.907116
H	-1.038993	2.374442	1.277784
H	-2.350933	2.849633	0.176410
H	-0.136955	-0.098242	2.384557
H	-1.188719	-1.403508	2.941315
H	-3.136496	-0.501923	1.851236
H	-2.365269	0.899878	2.611367
H	-2.752843	-1.767529	-0.528922
H	-3.169831	-1.095687	-2.117451
H	-3.269680	1.176065	-1.234226
H	-4.131584	0.197265	-0.030163
C	3.739888	0.778421	0.546904
H	4.827390	0.731724	0.451561
H	3.504040	1.292879	1.486922
C	3.185900	-0.641166	0.607083
H	3.425690	-1.175911	-0.320672
H	3.655441	-1.167398	1.447383
O	3.252355	1.513355	-0.570563
H	2.274798	1.504757	-0.537608
O	1.790453	-0.613811	0.805837
H	-1.374840	0.194078	0.086696